Mechano-Chemical Modelling of Boundary Lubrication

By

Ali Ghanbarzadeh

Submitted in accordance with the requirements for the degree of
Doctor of Philosophy

The University of Leeds
School of Mechanical Engineering
Leeds, UK

March, 2016

The candidate confirms that the work submitted is his own, except where work which has formed part of jointly-authored publications has been included. The candidate confirms that appropriate credit has been given within the thesis where reference has been made to the work of others.

In all the papers listed below, Ali Ghanbarzadeh completed all the numerical work. Pourya Parsaeian has carried out the wear and MTM/SLIM measurements and Elio Piras has conducted the experiments to validate the surface topography predictions. All authors contributed to proof reading of the articles prior to publication.

Papers contributing to this thesis:

- Ghanbarzadeh, A., Wilson, M., Morina, A., Dowson, D., & Neville, A. (2016). **Development of a new mechano-chemical model in boundary lubrication**. Tribology International, 93, 573-582.
- Ghanbarzadeh, A., Parsaeian, P., Morina, A., Wilson, M. C., van Eijk, M. C., Nedelcu, I.. & Neville, A. (2016). **A Semi-deterministic Wear Model Considering the Effect of Zinc Dialkyl Dithiophosphate Tribofilm**. Tribology Letters, 61(1), 1-15.
- Ghanbarzadeh, A., Piras, E., Nedelcu, I., Wilson, M., Morina, A., Dowson, D., Neville, A. **Zinc Dialkyl Dithiophosphate Antiwear Tribofilm and its Effect on the Topography Evolution of Surfaces: A Numerical and Experimental Study**. Submitted to Wear.
- Ghanbarzadeh, A., Wilson, M., Morina, A., Dowson, D., & Neville, A., **A New Boundary Element Method for Contact Mechanics of Moving Rough Surfaces**, Submitted to European Journal of Computational Mechanics

Conferences presented:

- Ali Ghanbarzadeh *et al*. Mechano-Chemical Numerical Modelling of Boundary Lubrication, 41st Leeds-Lyon Symposium on Tribology, Leeds 2014.
- Ali Ghanbarzadeh *et al*. Chemo-Mechanical Numerical Modelling of Boundary Lubrication, STLE 69th Annual Meeting, Orlando Florida, USA 2014.
- Ali Ghanbarzadeh *et al*, Analytical and Experimental Study of Tribofilm Growth Generated by Zinc Dialkyl Dithiophosphate and its Effect on Wear 42st Leeds-Lyon Symposium on Tribology, Lyon 2015
- Ghanbarzadeh A *et al*, A Semi-deterministic Wear Model Considering the Effect of Zinc Dialkyl Dithiophosphate Tribofilm, TurkeyTrib 2015

Assertion of moral rights:

Acknowledgements

First of all, I would like to express my sincere gratitude and special appreciation to my great supervisors Dr Mark Wilson, Professor Ardian Morina and Professor Anne Neville for their help, guidance and also being supportive and encouraging through my PhD. They have been tremendous mentors and this work would not have been possible without their support. I would also show my appreciation to ENTICE consortium which gave a great opportunity to interact with experts in the field of tribology/tribochemistry.

I would like to thank Professor Duncan Dowson for the time he has put on sharing his knowledge, experience and passion on my PhD. His advice and guidance have been invaluable.

I am also thankful to the members of iFS research group, especially to Ali, Thibaut, Michael, Filippo, Erfan, Abdullah, James, Earle, Evan, Doris, Vishal, Shahriar, Joe, Pourya, Fredrick, Siavash, John, Rick, Fiona, Lukman, Mohsen, Zahra, Farnaz, Macdonald, Elio, Nadia and Wassim. I would also like to thank my friends, especially Pouya, Ali, Neda, Mostafa and Reza.

I especially thank my mom (Roshanak Oliyaei), dad (Mehdi Ghanbarzadeh), brother (Khashayar) and grandparents (Fatemeh, Ehteram and Ramzanali) for their continuous support, encouragement and love. I am also thankful to Nasser and Nassim, my cousins, who gave me the opportunity to travel to UK and helped me with finding the suitable PhD.

ABSTRACT

Boundary lubrication is known to be significantly important in the design of machine parts. The decrease in the efficiency of the system as well as its durability when operating in boundary lubrication conditions highlights the importance of this regime. Boundary lubrication involves many different physical, chemical and mechanical phenomena which make it difficult to understand the real mechanisms of friction, wear and lubrication. Tribochemistry is undoubtedly one of the most important processes occurring in boundary lubrication. Modelling such a complicated process needs a robust physical and chemical modelling framework that is capable of capturing different phenomena.

The majority of the modelling attempts in boundary lubrication covers the contact mechanics of rough surfaces with different numerical approaches. Despite the importance of the tribochemistry and its effect in reducing friction and wear of boundary lubricated contacts, there is no comprehensive modelling framework that considers tribochemistry into the boundary lubrication models.

In this work, tribochemistry was implemented into the deterministic contact mechanics simulation for elastic-perfectly plastic contact of rough surfaces. A tribochemical model for the growth of the ZDDP antiwear additive was developed based on the thermodynamics of interfaces that combines formation and removal of the tribofilm. The tribochemical model was then coupled with the contact mechanics model which was developed based on potential energy principles. A modification to Archard's wear equation was proposed which accounts for the role of ZDDP tribofilm

in reducing the wear. This model was proposed based on the experimental observations of ZDDP in reducing wear.

The numerical framework was then validated against experiments. The wear prediction capability of the model was validated against experiments from Mini-Traction Machine in a rolling/sliding contact. The model is able to predict changes in the topography of the surfaces and this was validated with experiments on a Micro Pitting Rig (MPR).

The model shows a good potential in capturing the behaviours in boundary lubrication and opens new ways for further developments and testing the effect of different parameters in tribochemistry and wear. It can give insights in better understanding the real mechanisms of tribochemistry and also help in optimizing boundary lubricated contacts.

Table of Contents

Acknowledgements ..... **IV**

ABSTRACT ..... **V**

Table of Figures ..... **XIII**

List of Tables ..... **XX**

Chapter 1. Introduction **1**

1.1 Motivation for Research 1

1.2 Literature Gaps, Aims and Objectives 3

1.3 Structure of Thesis 3

Chapter 2. Fundamentals of Tribology, Lubrication and Wear **5**

2.1 Introduction 5

2.2 What is Tribology? 5

2.3 Lubrication, Friction and Wear 6

2.3.1 Wear Mechanisms 11

2.3.1.1 Adhesive Wear 12

2.3.1.2 Abrasive Wear 13

2.3.1.3 Corrosive Wear 14

2.3.1.4 Fatigue Wear 14

2.3.1.5 Erosive Wear 15

2.3.2 Friction Mechanisms 15

2.3.3 Running-in 16

2.3.3.1 Friction 17

2.3.3.2 Wear 17

2.3.3.3 Surface Roughness 18

2.3.3.4 Attempts at Modelling Running-in 19

2.3.4 Boundary Lubrication 19

2.3.4.1 Antiwear Additives 21

2.3.4.2 Friction Modifiers 21

2.4 Summary 21

Chapter 3. ZDDP as an Antiwear Additive: A Review of the Literature. **23**

3.1 Mechanical Properties 25

3.2 Tribofilm Growth 28

3.3 Tribochemistry of ZDDP 31

3.4 Stability of ZDDP 34
3.5 ZDDP on Non-Ferrous Surfaces 35
3.6 Summary 36
Chapter 4. Boundary Lubrication Modelling: A Review of the Literature ……..... 38
4.1 Introduction 38
4.2 Modelling Methods in Boundary Lubrication 43
4.2.1 Molecular Dynamics 43
4.2.1.1 Simulation of Atomic Friction 44
4.2.1.2 Simulation of Contact Mechanics 47
4.2.1.3 Tribochemical Aspects 49
4.2.2 Finite Element Method (FEM) 53
4.2.3 Discrete Element Method (DEM) 57
4.2.4 Boundary Element Method (BEM) 58
4.2.5 Surface Generation 60
4.3 Contact Mechanics 61
4.3.1 Variational Principle 65
4.3.2 Boussinesq Potential Solution 67
4.3.3 Tribofilm Properties 71
4.3.4 Numerical Implementation 75
4.3.5 Contact Mechanics Numerical Implementations 76
4.3.6 Fast Fourier Transformation (FFT) 79
4.3.7 Frictional Heating and Flash Temperature 80
4.3.8 Implementation of Wear Equation 82
4.4 Tribochemistry and the Film Formation/Removal Effect on Wear and Friction 84
4.4.1 Tribofilm Growth 85
4.5 Tribofilm Formation and Removal Models 89
4.5.1 Spikes' Model 90
4.5.2 Andersson's Model: 92
4.5.3 Diffusion Model: 93
4.5.4 Turing (Diffusion-Reaction) Systems: 95
4.6 Thermodynamics of Friction and Wear: 98
4.6.1 Thermodynamic Analysis of Tribofilm Growth: 98
4.6.2 Tribo-activation: 101

4.7 Summary 103
Chapter 5. Development of the Contact Mechanics Model 105
5.1 Boundary Lubrication Modelling and Tribochemistry 105
5.2 Introduction to the Contact Mechanics Model 109
5.3 Rough Surface Generation 110
5.4 Contact of Rough Surfaces 114
5.5 Direct Quadratic Mathematical Programming 119
5.6 Elastic-Perfectly Plastic Contact Model 122
5.7 Movement of the Contacting Surfaces 123
5.8 New Surface Movement Strategy 123
5.9 Fast Fourier Transform (FFT) Implication 128
5.10 Tribofilm Mechanical Properties 129
5.11 Flash Temperature Calculation 131
5.12 Results 133
5.12.1 Influence Matrix 133
5.12.2 Contact Pressure for Static Contact 134
5.12.3 Movement of the Surfaces 134
5.12.4 Plastic Deformations 135
5.12.5 Flash Temperature 136
5.13 Summary 136
Chapter 6. Tribofilm Growth Model Development 140
6.1 Introduction 140
6.2 Thermodynamics of Interfaces 141
6.3 The Tribochemical Reaction Kinetics Model 142
6.4 Tribofilm Formation Model 148
6.5 Tribofilm Removal 150
6.6 Results 152
6.6.1 Calibration 153
6.6.1.1 Effect of ZDDP Concentration on x_{tribo} 155
6.6.1.2 Effect of Temperature on x_{tribo} 159
6.6.2 Tribofilm Growth 161
6.6.3 Inhomogeneity of the Tribofilm 163
6.6.4 Tribofilm Coverage 164
6.6.5 Effect of Load 166

6.6.6 Effect of Surface Roughness 168
6.6.7 Effect of Sample Sizes 170
6.7 Discussion and Summary 173
Chapter 7. Wear Modelling 176
7.1 Introduction 176
7.2 Archard's Wear Equation 178
7.3 Tribochemical Wear Calculation 180
7.4 Effect of Input Parameters on Wear Prediction 185
7.4.1 Real Time Wear Calculation 185
7.4.2 Effect of Coefficient of Wear 187
7.4.3 Effect of Load 187
7.5 Model Validation 190
7.5.1 Experimental Procedure 190
7.5.1.1 Tribo-Test Set-up 190
7.5.1.2 Materials and Lubricating Oil 191
7.5.1.3 Wear Measurement 193
7.5.2 Experimental Results 193
7.5.2.1 Tribofilm Thickness Results 193
7.5.2.2 Wear Results 194
7.5.3 Numerical Results and Discussion 198
7.6 Summary 207
Chapter 8. Surface Topography Prediction 210
8.1 Introduction 210
8.2 Surface Roughness 214
8.2.1 Centre Line Average Roughness 215
8.2.2 Root Mean Square Roughness 215
8.3 Effect of Parameters on Topography of Surfaces 216
8.3.1 Effect of Wear Coefficient 217
8.3.2 Effect of Load 219
8.3.3 Effect of the Initial Surface Roughness 221
8.3.4 Effect of Material Hardness 223
8.4 Model Validation 224
8.4.1 Experimental Setup 224
8.4.2 Numerical Results and Discussion 230

8.4.3 Experimental Results 237
8.5 Summary 244
Chapter 9. Discussions 246
9.1 Overall Discussion 246
9.1.1 Contact Mechanics Model 248
9.1.2 Tribofilm Growth Model 249
9.1.3 Coupling Growth Model with Contact Mechanics 251
9.1.4 Wear Model 252
9.1.5 Prediction of Surface Topography 255
9.2 Limitations of This Study 256
Chapter 10. Conclusions and Future Work 258
10.1 Conclusions 258
10.2 Future Work 260
Chapter 11. References 262

Table of Figures

Figure 1-1 Boundary lubrication and the asperity-asperity contact (4) 1

Figure 2-1 Hydrodynamic lubrication (19, 20) 7

Figure 2-2 Elastohydrodynamic lubrication schematic (20) 7

Figure 2-3 Stribeck diagram showing the relation between specific film thickness and lubrication regimes (22) 9

Figure 2-4 Schematic of the different lubrication regimes (23) 10

Figure 2-5 Different possible modes of two body abrasion (27) 13

Figure 2-6 3rd body abrasive particles between contacting surfaces (27) 14

Figure 2-7 Running-in and steady state wear versus time (28) 18

Figure 2-8 Surface topography variations during the running-in period (31) 19

Figure 3-1. Structure of zinc dialkyldithiophosphate tribofilm (35) 24

Figure 3-2 Changes in the chemical structure of zinc phosphates by cross-linking due to increasing load (51) 26

Figure 3-3 Schematic of mechanical properties of the ZDDP tribofilm reported in (45) a) Full antiwear film formed from ZDDP solution. b) The same film after being washed by the solvent. 27

Figure 3-4 Schematic of the spacer layer interferometry mounted on the mini traction machine 29

Figure 3-5 Spacer layer images at different time for ZDDP tribofilm (15) 30

Figure 3-6 Single-asperity tribofilm growth results (60) 32

Figure 3-7. Illustration of the stability of a ZDDP tribofilm: when the lubricant in the tribotest is replaced with ZDDP-free base oil, the tribofilm's thickness is maintained, and is only reduced by the addition of a dispersant under rubbing conditions (15). 36

Figure 4-1 Boundary lubrication showing: surfaces, lubricants and adsorbed films (17) 39

Figure 4-2 Schematic for modelling oxide layer formation and its effect on oxidational wear in boundary lubrication (76) 41

Figure 4-3 Time history of micro-contact for (a) contact probabilities (b) shear stress and contact pressure (c) contact temperature (79). 45

Figure 4-4 An example of model set up in molecular dynamics for friction studies (87) 46

Figure 4-5 System configuration for coupling FEM and MD to generate real rough surfaces (96) 48

Figure 4-6 The coupling between atomistic and the continuum zones in a combined FEM-MD method (96) 49

Figure 4-7 Molecular dynamics simulation for an abrasive iron oxide particle in a glassy phosphate tribofilm formed on steel surfaces considering load and sliding speed and molecular contents of particle and tribofilm (13). 52

Figure 4-8 Molecular dynamics model for phosphate glass tribofilm between two steel surfaces considering load from 0 to 500 ps without considering sliding (13)..... 52

Figure 4-9 Molecular dynamics model for phosphate glass tribofilm for two steel surfaces considering load and sliding speed from 0 to 300 ps (13). 53

Figure 4-10 Finite element configuration of two contacting bodies (sphere on flat). Very fine mesh has been used for the area in contact. (105) 54

Figure 4-11 Finite element model using remeshing for deformed geometry (114) 56

Figure 4-12 Discretised surface of a contacting body in BEM (156) 59

Figure 4-13 Finite element model for the influence coefficient calculation in a combined FEM/BEM model (156)..... 60

Figure 4-14 Three dimensional digital rough surface generated using low pass filter and random Gaussian numbers A) View of the surface B) height distribution of the generated surface C) autocorrelation function of the generated surfaces (160)..... 61

Figure 4-15 Definition of strain energy and complementary potential energy (145) 66

Figure 4-16 Point forces on the surface point ($\xi 1, \xi 2$) and surface deformation of the point ($x1, x2, x3$) (174) 68

Figure 4-17 Zinc dialkyldithiophosphate tribofilm structure and its mechanical properties in various regions (45). 72

Figure 4-18 Variation of elastic modulus with hardness for ZDDP tribofilm (52)..... 73

Figure 4-19 Hardness model for two surfaces with tribofilms in contact with three different possible cases. (1) The thicker tribofilm with lower hardness plastically deforms (2) both tribofilms deform plastically (3) the tribofilm plastically deforms to the point that it reaches the underlying material, the underlying material will also be plastically deformed in this case. (176)..... 75

Figure 4-20 Schematic figure of surface mesh in the boundary element method in 2 dimensions a) front view of two surfaces b) top view of a surface (145). 77

Figure 4-21 Schematic flowchart of contact mechanics simulation model used for capturing the contact mechanics of rough surfaces 78

Figure 4-22 Schematic of the wear track and the pressure distribution for the calculation of wear depth (139) 84

Figure 4-23. Growth of the ZDDP tribofilm by time for $\lambda = 0.5$ (39)..... 86

Figure 4-24 Images of the tribofilm formation during the time for different lambda ratios (39). 86

Figure 4-25 Tribofilm thickness variations by sliding speed and contact load (195). 87

Figure 4-26 Running in time variation by sliding velocity and applied load (195). 88

Figure 4-27 Coefficient of friction variations by sliding speed and load (195). 88

Figure 4-28 Spacer layer interferometry making 3D image of the tribofilm (38). 89

Figure 4-29 Evolution of mean film thickness in time for base oil and ZDDP, dispersant, GMO, detergents added to it (41). 90

Figure 4-30 Pattern formation of dissipative structures at interfaces due to frictional energy dissipations with periodic pattern 1 (199)..... 97

Figure 4-31 Pattern formation of dissipative structures at interfaces due to frictional energy dissipations with periodic pattern 2 (199)..... 97

Figure 5-1 Thin layer of the tribofilm covering the contacting asperities..... 105

Figure 5-2 Boundary lubrication modelling framework and its constituents..... 106

Figure 5-3 Schematic of the numerical approach in this thesis for modelling boundary lubrication considering tribochemistry 108

Figure 5-4 Filter coefficient for a circular digital low pass filter 112

Figure 5-5 Three dimensional digital rough surface generated using low pass filter and random Gaussian numbers a) $Ra = 250\ nm$ b) $Ra = 25\ nm$..... 112

Figure 5-6 Three dimensional rough surfaces with $Ra = 25nm$ and different asperity lateral sizes a) $\alpha = 0.08$ b) $\alpha = 0.2$ 113

Figure 5-7 Surface discretization in Boundary Element Method (145) 116

Figure 5-8 Single asperity model – Schematics of rigid body movement..... 121

Figure 5-9 Discretized surface and schematic of two point. The point which is deformed (k) because of the load applied on another point (p)..... 125

Figure 5-10 Movement of surfaces in contact. The shaded area shows the area of contact between two surfaces. The red dotted lines shows the area of the upper surface that enters the contact from the left. 126

Figure 5-11 Influence matrix selection in the case of moving surfaces 127

Figure 5-12 Influence matrix element values 133

Figure 5-13 The deformation of surface due to load applied in the centre 134

Figure 5-14 Contours of contact pressure for the contact of two rough surfaces 135

Figure 5-15 Contact area and pressure evolution for a ball loaded on the flat in an elastic-perfectly plastic model. Load increases from (a) 50 MPa (b) 200 MPa (c) 600 MPa (d) 900 MPa (e) 1.2 GPa (f) 1.6 GPa 137

Figure 5-16 Contour of contact pressure showing the asperity contact pressures in surface movement. The upper surface enters the contact from the left (a) and exits from the right (f). The contour is indicating the pressures on the lower body..... 138

Figure 5-17 Plastic deformation due to contact of ball (b) on flat (a)..... 139

Figure 5-18 Flash temperature rise at the contacting asperities 139

Figure 6-1 Schematic of the step by step mechanical and thermal activation of the tribochemical reaction 146

Figure 6-2 Schematic of the tribofilm removal occurring at the same time with formation 152

Figure 6-3 Tribofilm growth model calibration; goodness of the fitting. Experimental results are extracted from Ref (1) 154

Figure 6-4 The tribofilm growth for different secondary ZDDP concentrations of in oil measured experimentally (15)..... 156

Figure 6-5 The tribofilm growth for different primary ZDDP concentrations of in oil measured experimentally (15)..... 156

Figure 6-6 Fitting examples for different concentrations of ZDDP..... 158

Figure 6-7 Variation of $xtribo$ with concentration of ZDDP for (a) primary (b) secondary ZDDP 159

Figure 6-8 The tribofilm growth for secondary ZDDP at different temperatures measured experimentally (15) 160

Figure 6-9 The tribofilm growth for primary ZDDP at different temperatures measured experimentally (15) 160

Figure 6-10 Variation of $xtribo$ for both a) secondary and b) primary ZDDP at different temperatures 162

Figure 6-11 Formation of a tribofilm on rough surface- the original rough surface is shown on top and only the mesh of the tribofilm is shown in the bottom..... 162

Figure 6-12 Mean tribofilm thickness calculation on the rough surface 163

Figure 6-13 Evolution of surface coverage by ZDDP tribofilm. The surface patch is 20µm×20µm. 165

Figure 6-14 ZDDP tribofilm coverage of the surfaces from the calculations (corresponding to the tribofilm growth in Figure 6-13) 166

Figure 6-15 Effect of load on the mean tribofilm thickness calculated by the model 167

Figure 6-16 Effect of load on the tribofilm coverage percentage on a rough surface calculated by the model 167

Figure 6-17 Tribofilm growth for different Ra values of rough surface..... 168

Figure 6-18 The tribofilm area coverage percentage for different Ra values 169

Figure 6-19 Different sample sizes as inputs of the numerical model, ... 171

Figure 6-20 Growth of the tribofilm for different sample sizes..... 171

Figure 6-21 Coverage of the surface by tribofilm for different sample sizes . 172

Figure 7-1 Illustration of the wear hypothesis 183

Figure 7-2 Schematic of coefficient of wear variation with tribofilm thickness. 184

Figure 7-3 Real time wear calculation in the case of ZDDP on steel surfaces for a ball on disk configuration. The tribofilm growth model has been calibrated based on the experimental results from Ref (1). Wear calculation is qualitative because the wear model was not calibrated. 186

Figure 7-4 Wear depth calculation for different dimensional *initial* coefficients of wear ($CoWsteel$) 188

Figure 7-5 Wear depth calculation for different loads 188

Figure 7-6 Linear behaviour of the final wear depth calculation with respect to the applied load 189

Figure 7-7 Experimental set up for MTM SLIM 191

Figure 7-8 Tribofilm thickness measurements for 100℃ at different times .. 194

Figure 7-9 Tribofilm thickness measurements for 60℃ at different times 195

Figure 7-10 Tribofilm thickness measurements at different temperatures for 1Wt% ZDDP in oil 195

Figure 7-11 Tribofilm thickness measurements at different temperatures for 0.5 Wt% ZDDP in oil..... 196

Figure 7-12 2D and 3D images of wear track taken by white light interferometry 196

Figure 7-13 2D wear track image and the image profile of the surface after the experiment..... 197

Figure 7-14 Wear measurements for different temperatures and different times for 1 Wt% ZDDP in oil 199

Figure 7-15 Wear measurements for different temperatures for 1 Wt% ZDDP in oil at 2 hours..... 200

Figure 7-16 Example of numerical and experimental tribofilm growth for 1 Wt% ZDDP in oil at three different temperatures..... 200

Figure 7-17 Simulation of wear for different temperatures over 2 hours for 1 wt% ZDDP in oil 202

Figure 7-18 Simulation of wear for different temperatures over 2 hours for 0.5wt% ZDDP in oil..... 203

Figure 7-19 Variation of the predicted average coefficient of wear with time for different temperatures for 1 Wt% ZDDP in oil..... 204

Figure 7-20 An example of two experimental cases with different tribofilm growth rates and different tribofilm steady-state thickness 207

Figure 8-1 Prediction of wear on the bearing using the Archard wear equation. Reprinted from Ref (242) 212

Figure 8-2 Surface profile of a rough surface from numerical simulation 214

Figure 8-3 Surface roughness evolution for rough and smooth surface at different *initial* wear coefficients..... 218

Figure 8-4 Surface roughness evolution for rough surface at different loads 219

Figure 8-5 Final surface topography after 5 minutes at different loads 221

Figure 8-6 Effect of initial roughness on the Surface topography evolution of the rougher surface 222

Figure 8-7 Total roughness modification for different initial R_q values 223

Figure 8-8 Roughness evolution of rings for different material hardness 224

Figure 8-9 The load unit of the MicroPitting Rig (MPR) 225

Figure 8-10. Example of Wyko roughness measurements (all values are in microns)..... 229

Figure 8-11 (Left) roughness evolutions and (Right) tribofilm growth for the (a) rougher (ring) (b) smoother (roller) body as predicted by the model 234

Figure 8-12 The comparison of the topography evolution between the cases when a tribofilm growth is considered in the model and the case that there is no tribofilm being formed on the surfaces. 235

Figure 8-13 Surface topography evolution predicted by the model (a) surface of the ring before the experiment point 0 (b) surface of the ring at point 1 (c) surface of the ring at point 2 (d) surface of the roller before the experiment point 0 (e) surface of the roller at point 1 (f) surface of the roller at point 2..... 236

Figure 8-14 Tribofilm growth on the contacting asperities (a) at point 1 for rough surface (ring) (b) at point 2 for rough surface (ring) (c) at point 1 for smooth surface (d) at point 2 for smooth surface..... 237

Figure 8-15 Experimental results on different roughness of rings 239

Figure 8-16 Roughness measurement experimental results for both ring and roller 241

Figure 8-17 SEM image of the tribofilm uniformly formed on the wear track 243

Figure 8-18 XPS depth profile of the tribofilm formed on the surface of the ring 243

Figure 8-19. Ratio of BO/NBO for the two lubricating conditions 244

List of Tables

Table 4-1 Expressions for maximum flash temperature rise for various heat source distributions (179)..... 82

Table 6-1 The calibration parameters for the growth model..... 154

Table 6-2 Calibration parameters for primary ZDDP at different concentrations..... 158

Table 6-3 Calibration parameters for secondary ZDDP at different concentrations..... 159

Table 6-4 Calibration parameters for primary ZDDP at different temperatures..... 161

Table 6-5 Calibration parameters for secondary ZDDP at different temperatures..... 161

Table 7-1 Material properties used in the MTM..... 192

Table 7-2 Working parameters..... 192

Table 7-3 Numerical inputs and calibrated parameters..... 201

Table 7-4 Comparison between experimental measurements and numerical wear depth calculations..... 206

Table 7-5 Wear depth results for different cases in Figure 7-20..... 206

Table 8-1 Working conditions..... 217

Table 8-2 Material properties..... 217

Table 8-3. List of experimental test conditions for MicroPitting Rig..... 226

Table 8-4 Properties of base oil and additive used for experiments. 227

Table 8-5 Chemical properties of steel AISI 52100 in %..... 230

Table 8-6 The calibration parameters..... 240

Chapter 1. Introduction

1.1 Motivation for Research

Boundary lubrication is the lubrication regime where the combination of high loads and relatively small sliding speeds can lead to direct solid-solid contact. In this situation, interface behaviour is dominated by chemical reactions that happen at the surfaces due to the presence of lubricant additives. In those regions tribofilm formation occurs and the load is carried by the asperities. In the boundary lubrication regime the asperity-to-asperity contacts (Figure 1-1) may lead to elastic or plastic deformation or even fracture and can generate frictional heat which will be accompanied by chemical reactions to produce organic and inorganic surface films. A wide range of studies regarding many aspects of tribofilm formation and removal and their roles in reducing friction and wear have been conducted (2, 3)

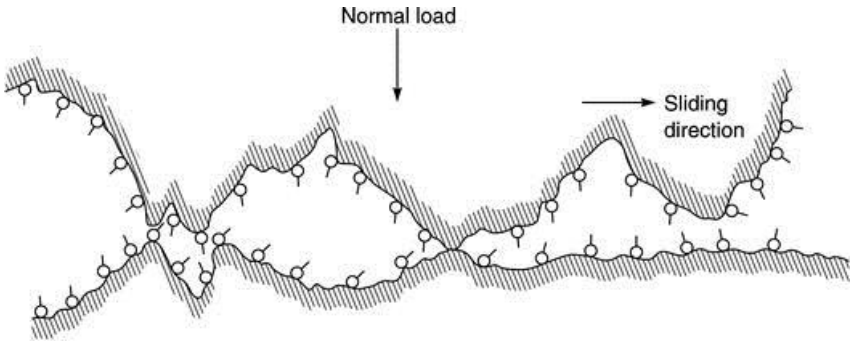

Figure 1-1 Boundary lubrication and the asperity-asperity contact (4)

The effectiveness of boundary lubrication has been considered for a long time as a necessity for modern designs of machines with reliable operations. Because of the need for more energy efficiency, availability of new materials and machine part downsizing, the need for understanding true interactions in this regime is of great

importance. The boundary lubrication regime has been the subject of many studies for more than 70 years (5-12) and the majority of these studies are experimental investigations into the nature of what happens in this regime. Many of the studies cover the boundary film chemical (13, 14), physical (15) and mechanical (16) properties and their effects on wear and friction reduction. The subject of many works has been to investigate different kinds of additives in oils and their effects on various aspects of tribological performance. As the boundary lubrication regime is mainly related to interactions of two surfaces and the additive-containing oils between them, the analytical studies of surfaces including topography measurements, chemical analyses, mechanical and physical studies are considerable. All these experiments give good insight into different chemical and physical characteristics covering various aspects of boundary lubrication systems.

It is clear from the wealth of experimental literature in this area that the phenomena happening in this regime are very complicated. Studying the entire problem needs a multiscale understanding ranging from component scale down to the micro-scale and also molecular interactions of films and lubricant additives. Experimentation across such scales is challenging and hence it is important to complement such studies with the ability to predict the friction and wear of a working system without running experiments. It is also important to analyse the system and optimise its performance in order to design cost-effective experiments. Many modelling attempts have been made in the past years but a comprehensive multiscale model of boundary lubrication considering tribochemistry phenomena in order to predict friction and wear of the system is still lacking.

1.2 Literature Gaps, Aims and Objectives

At the time of start of the project, there was no comprehensive modelling framework that included tribochemistry into the boundary lubrication modelling. Andersson *et al*. (17) used a semi-deterministic chemo-mechanical model to predict the growth of the Zinc dialkyldithiophosphate (ZDDP) tribofilm in the boundary lubricated condition. There was no removal of the tribofilm in the model and the effect of the tribofilm in reducing the wear was not included. In another work Bosman *et al*. (18) included the effect of an antiwear additive in reducing the wear of the system. Although these works opened new insights into modelling of boundary lubrication, the consideration of some necessary parameters were still lacking. In this thesis, the main aim was to **initiate** a comprehensive modelling framework to consider tribofilm formation, removal and mechanical properties into the deterministic contact mechanics simulations in order to predict wear in the boundary lubrication regime. The main components of the developed modelling framework are listed as follows:

- A flexible contact mechanics simulation to consider the elastic-perfectly plastic contact of rough surfaces in boundary lubrication
- A tribofilm growth model that considers both formation and removal concepts of the tribofilm
- A new modification to Archard's wear equation employing a spatially resolved coefficient of wear that considers the effect of antiwear additive in reducing the wear in the boundary lubrication.

1.3 Structure of Thesis

An introduction to the science of tribology is reported in **Chapter 2** of this thesis which includes fundamentals of lubrication, friction, wear and boundary lubrication.

A review into the literature about the zinc dialkyldithiophosphate (ZDDP) antiwear additive and its tribofilm is reported in **Chapter 3**. A comprehensive review in the literature about the boundary lubrication modelling is included in **Chapter 4**. In that chapter, literature about different numerical approaches applicable in modelling of boundary lubrication are reported. Modelling attempts in contact mechanics have been included as well as different mathematical approaches for capturing the tribofilm growth on the contacting asperities. **Chapter 5** presents the development of the contact mechanics simulation. Step-by-step development of the contact mechanics model is represented and results for the contacts of rough surfaces, their elastic plastic pressure distribution and surface deformations are reported. **Chapter 6** shows the development of a tribofilm growth model that includes both formation and removal of the tribofilm. This tribofilm growth model is implemented into the contact mechanics model of Chapter 5 to predict the growth of the tribofilm based on the local contact properties of the surfaces. **Chapter 7** reports the development of a mild wear model that considers the effect of ZDDP antiwear additive tribofilm in reducing wear by modifying Archard's wear equation. A mechanism for wear in the presence of the antiwear additive is proposed, and wear predictions are validated against experimental results. Changes in the surface topography can be predicted via the model and this aspect is covered in **Chapter 8**. The topography evolution predicted is then validated against experimental results. The overall discussion of the thesis is presented in **Chapter 9.** The conclusions of the work as well as recommendations for future studies are presented in **Chapter 10**.

Chapter 2. Fundamentals of Tribology, Lubrication and Wear

2.1 Introduction

In the current chapter, the basics of tribology science will be introduced and properties of different lubrication regimes will be briefly discussed. More focus will be on boundary lubrication and its fundamentals. In addition, a definition of various mechanisms of wear is presented in this chapter.

2.2 What is Tribology?

Tribology is defined as the science and technology that deals with interacting surfaces in relative motion. This interaction is characterised by many physical and chemical parameters such as materials, load, temperature, surface roughness and lubricating oil properties etc. The behaviour of a tribo-contact is dependent on all these parameters in combination. Therefore a thorough understanding of the real mechanisms needs coverage of all the above mentioned phenomena.

Important aspects of tribology have been friction, wear and lubrication since the introduction of this science. Friction is defined as the resistance to motion once two surfaces are moving tangentially to each other. Wear is defined as the damage to surfaces due to contact and relative motion. The term lubrication is used for the process or techniques employed to reduce friction and wear between contacting surfaces in relative motion by interposing a substance called a lubricant between them.

2.3 Lubrication, Friction and Wear

Lubricants are added to the system of the two surfaces in contact to reduce friction and wear. The amount of friction and wear in the system is characterised by many parameters as mentioned above. Lubrication regimes are defined to distinguish between different phenomena that possibly happen due to different severities of the contact between surfaces.

In the situation that a liquid lubricant film is between two interacting surfaces the friction force generated is significantly decreased and the wear is almost eliminated. In this situation the applied load is sustained by the liquid film and this regime of lubrication is called hydrodynamic lubrication. Generally, the lubricants used for this purpose are oils such as petroleum oils. The equations that describe this lubrication regime are basic equations of fluid mechanics. In this case, bulk properties of the lubricant are of great importance and define the behaviour of the tribosystem. A schematic representation of this regime is illustrated in Figure 2-1 where the oil is completely separating the surfaces.

When the load increases or the speed decreases, a form of hydrodynamic lubrication happens in which pressure is large and can deform the lubricated surface elastically. This regime is called elastohydrodynamic lubrication (EHL). There are some considerable differences between hydrodynamic and elastohydrodynamic regimes such as the importance of material hardness, conformation of contacting surfaces and viscosity increase under pressure. A schematic representation of the surfaces and the lubricant between them is illustrated in Figure 2-2. Extensive studies have been carried out to capture the behaviour of tribosystems in the elastohydrodynamic regime since a wide range of machine element lubrications occur in this regime.

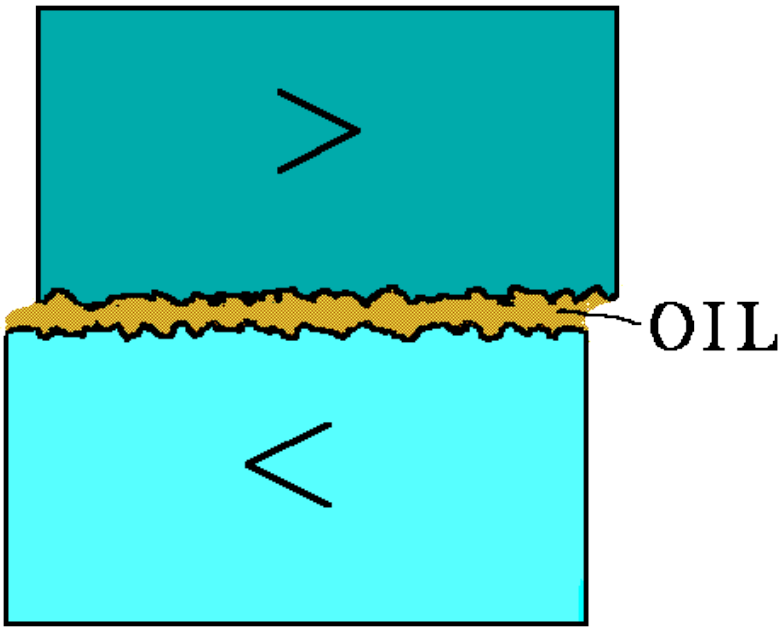

Figure 2-1 Hydrodynamic lubrication (19, 20)

Experimental techniques such as optical interferometers and transducers have made it possible to measure lubricant film thickness, contact pressures and temperature in EHL.

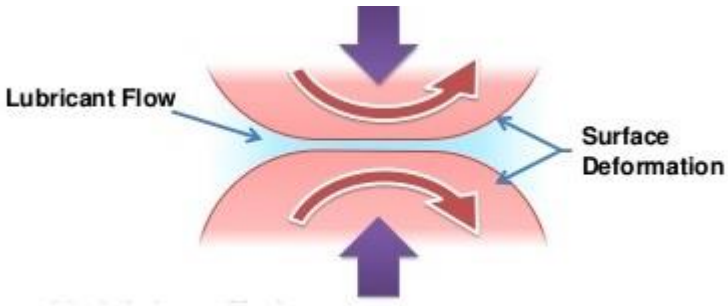

Figure 2-2 Elastohydrodynamic lubrication schematic (20)

One very important quantity in elastohydrodynamic lubrication is the lubricant film thickness. Lubricant film thickness is defined as the value of the separation of the centre lines of the two surfaces in a tribological system. Attention has been put on calculation and measuring film thickness for several decades. A well-known

mathematical formulation was developed by Hamrock and Dowson (21) for general elliptical contacts as follows:

$$h_{min} = 3.63R_x U^{0.68} G^{0.49} W^{-0.073}(1 - e^{-0.68k}) \quad \text{Equation 2-1}$$

h_{min} is the minimum lubricant film thickness between contacting surfaces and *U, W, G* and *k* are the non-dimensional forms of speed, load, material properties and the geometry.

Calculating the minimum film thickness between contacting surfaces is important because it can give insight into the severity of the contact when compared to the roughness of the surfaces. In light of this, a parameter is defined as the ratio of the minimum film thickness and the composite root mean square roughness of the surfaces R_q and is showed by λ.

$$\lambda = \frac{h_{min}}{\sqrt{R_{q1}^2 + R_{q2}^2}} \quad \text{Equation 2-2}$$

Lubrication regimes can be theoretically defined by the value of the λ ratio. If the value is greater than 3 it is widely accepted that the lubricant film thickness is significantly greater than the composite roughness of the surfaces leading to a full film lubrication regime.

In this respect, lubrication regimes can be distinguished by the above mentioned parameter. There is a famous curve of lubrication regimes categorized by λ ratio showing the changes in friction of the tribosystem. The diagram is called Stribeck

curve. The Stribeck curve is plotted based on the Stribeck number which includes the three important parameters of load, speed and the viscosity of the oil. All these three physical parameters are somehow related to the severity of the contact and the λ ratio which can be clearly understood from a comparison by Equation 2-1. The curve is demonstrated in Figure 2-3:

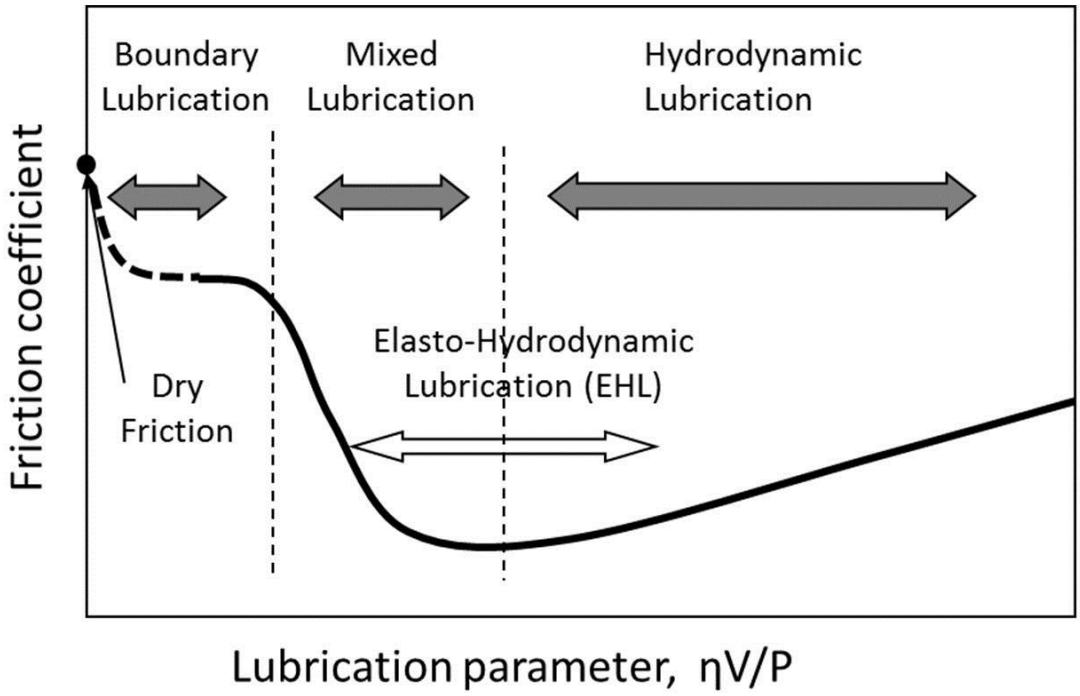

Figure 2-3 Stribeck diagram showing the relation between specific film thickness and lubrication regimes (22)

Changes in the coefficient of friction with respect to different lubrication regimes are indicated in Figure 2-3. It can be seen that shifting from full film lubrication to elastohydrodynamic and mixed lubrication the coefficient of friction will decrease. Transition from elastohydrodynamic lubrication to mixed and boundary lubrication will result in an increase in the friction of the system. The terms boundary and mixed lubrication are defined here.

When the severity of contact increases for example when the load is high and/or the speed is low, the hydrodynamic regime might not be the dominant lubrication regime and the lubricant fluid film cannot support the load, thus the surfaces may contact each other. This contact may occur at surface asperities which includes peaks and hills. There are some parameters that affect the amount and severity of this contact such as surface roughness, normal load, hardness and elastic properties of asperities etc. When the contact pressure increases and it goes beyond the EHL conditions, it makes the asperities contact each other more severely and therefore deform plastically. Also the number of asperities in contact will be increased due to increased contact severity. When the two surfaces come into direct contact the probability of adhesion, abrasion and fatigue and therefore wear will be increased. In this situation, frictional heating and rubbing of surfaces will induce chemical reactions between substrate material and the lubricant liquid and the result is the formation of a very thin film on the substrate called a tribofilm. The λ ratio in the boundary lubrication regime is less than 1. It means that the minimum film thickness is less than the roughness of the surfaces and the possibility of contact between surface asperities is higher. It is reasonable that smaller λ ratios correspond to more severe conditions in the boundary lubrication regime. The schematic of lubrication regimes is indicated in Figure 2-4.

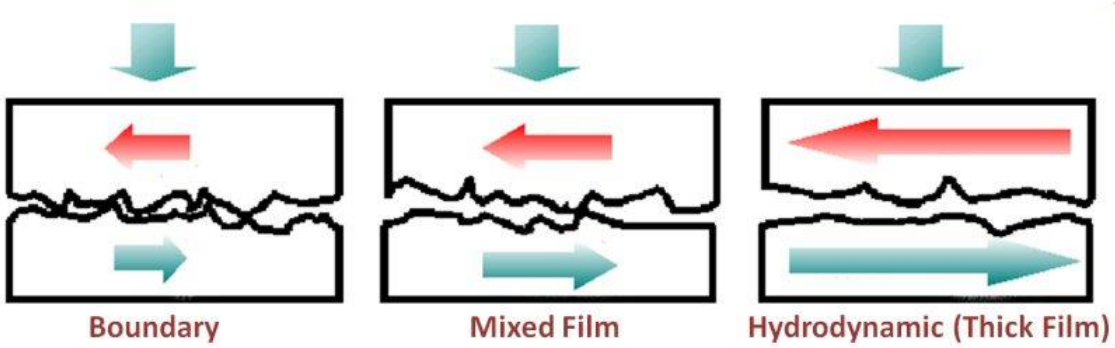

Figure 2-4 Schematic of the different lubrication regimes (23)

Boundary lubrication is the lubrication regime in which chemical reactions happen at the surface and tribofilm is formed as a result. The load is almost exclusively carried by the asperities. In the boundary lubrication regime the asperity-to-asperity contacts may lead to elastic or plastic deformation or even fracture and can generate frictional heat. Chemical reactions accompany these contacts and produce organic and inorganic surface films. There are a wide range of studies regarding many aspects of tribofilm formation and removal and their roles in reducing friction and wear which will be discussed later.

Boundary lubrication and hydrodynamic lubrication are two extremes of the lubrication regimes and in many cases a combination of these two regimes occur. This lubrication regime is called mixed lubrication in which part of the load is carried by the surface asperities and the rest is carried by lubricant between surfaces.

2.3.1 Wear Mechanisms

There is a need to understand the real mechanisms of wear in tribology. Scientific studies of wear emerged in the mid twentieth century (24, 25). It is well accepted that some parameters are very important in the wear of materials. This resulted in the following general trends of wear:

- Wear increases as the sliding contact increases
- Wear increases with normal load between rubbing surfaces
- Wear decreases with the hardness of the material in contact

These three laws for wear are not applicable for all materials and working conditions; however they can be supported by a wide range of experimental reports.

The above observations lead to extraction of the conventional Archard wear equation. Archard (25) found a correlation between wear and the above parameters with the pool of experimental results. He proposed a model for material loss in the sliding condition. Archard's model is formulated as the following:

$$W = K\frac{F_N}{H}S \qquad \text{Equation 2-3}$$

in which W is the wear volume and K, F_N, S and H are the wear coefficient, normal load, sliding distance and the hardness of the material respectively.

Wear in real applications occurs due to several mechanisms and understanding the whole mechanism is complicated. Here a few important mechanisms of wear are introduced.

- Adhesive wear
- Abrasive wear
- Corrosive wear
- Fatigue wear
- Erosive wear

A brief discussion of the mechanisms is presented in this chapter.

2.3.1.1 Adhesive Wear

Adhesive wear occurs once the material of one surface at contacting asperities is welded to the counter body and is removed due to sliding. This is the most common mechanism of wear and results in a very unstable coefficient of friction (26). It has been hypothesised that adhesion between metals is because of electron transfer between the surfaces in contact. The amount of adhesion depends on properties of

both surfaces. It is reported that hardness and roughness of surfaces can significantly affect the adhesion between surfaces (27).

2.3.1.2 Abrasive Wear

Abrasive wear occurs when a harder material ploughs into the surface of a relatively softer material. There are different modes of abrasive wear that can possibly occur and are shown in Figure 2-5.

Apart from the two-body abrasive mechanism which happens when two surfaces are in contact, there is another mechanism of abrasive wear and is called three body abrasion. When hard third body particles are confined between surfaces, plough into the contacting surfaces because of high load and can result in high wear. (See Figure 2-6).

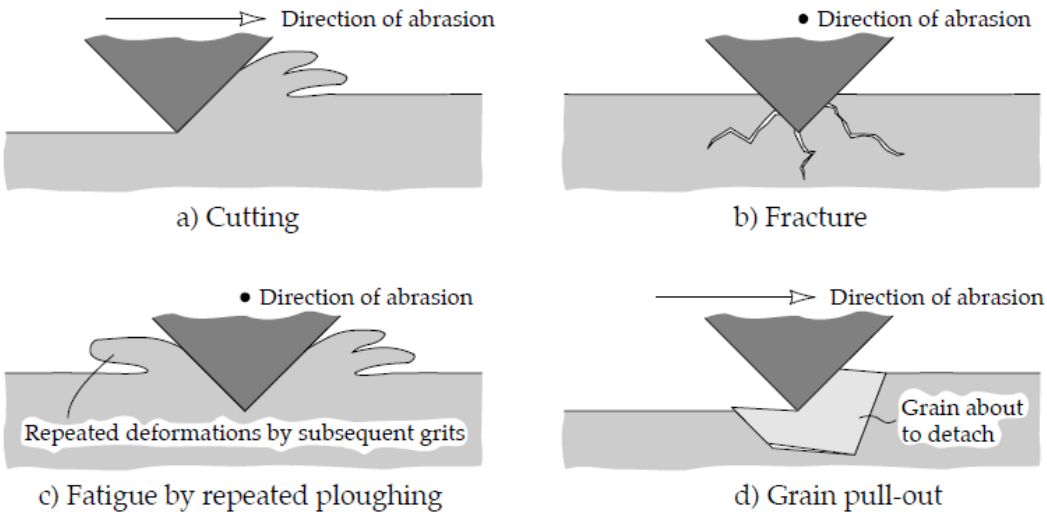

Figure 2-5 Different possible modes of two body abrasion (27)

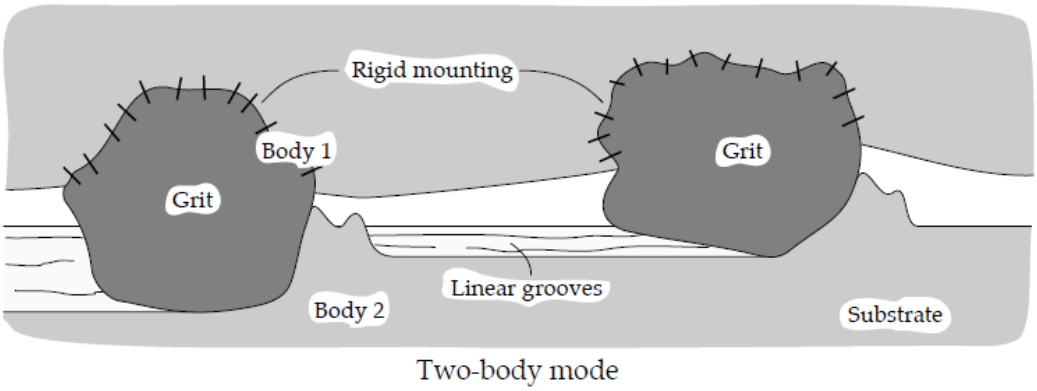

Figure 2-6 3rd body abrasive particles between contacting surfaces (27)

2.3.1.3 Corrosive Wear

Corrosive wear can occur in any corrosive environment. In tribology, corrosion rate increases when surfaces are in direct contact since rubbing can mechanically initiate the chemical corrosive reactions. Rubbing can also depassivate the corrosion product on the surface hence the surfaces become nascent and more willing to be corroded. The formation and removal of the oxide layer is a good example of corrosive wear in tribologically loaded contacts. This mechanism is similar to the formation and removal of the tribofilm on contacting asperities that leads to the tribochemical wear of the boundary lubricated contacts. Both tribochemical and tribocorrosive wear mechanisms are chemical mechanisms induced by rubbing action. Therefore the similarities in the physics and chemistry of the problems suggests similar approaches to be employed for studying them.

2.3.1.4 Fatigue Wear

This kind of wear can happen even if there are no direct solid contacts between surfaces. If there is a cyclic stress between surfaces of rolling elements, fatigue can occur and large amount of material can be removed from the surface. The inclusion, porosity or micro-cracks in the surfaces can initiate the fatigue.

2.3.1.5 Erosive Wear

Erosive wear happens if a hard worn particle is carried by the lubricating fluid and impacts the surfaces. Such impacts and their severity can induce different forms of damage on the surface ranging from partial wear to initiation of cracks and contact fatigue. The wear in this case is found to be proportional to kinetic energy of the particles.

2.3.2 Friction Mechanisms

The concept of friction goes back to the early human times as they used stones and wood to make fire. The friction force is the force that resists the motion of a surface when is rubbed against another surface. The coefficient of friction is probably the most important parameter that describes the friction intensity. The ratio of the friction force and the normal load between contacting surfaces is defined as the coefficient of friction and is formulated as Equation 2-4.

$$\mu = \frac{f}{W}$$ Equation 2-4

Friction is one of the biggest technology challenges to be optimized and there are still big difficulties in predicting its behaviour. However engineers could reduce friction in tribological contacts by designing new materials and lubricants. There are three main laws for friction:

- Friction force is proportional to the applied load
- Friction force is independent of the nominal contacting area

- Friction force is independent of speed

The friction arises from the rough nature of real surfaces. Both adhesion and abrasion can be important in frictional behaviour of the system. If the asperities come into contact and adhesion occurs between them, this adhesion can lead to an increase in the friction force. In addition, if a surface ploughs into another surface, there is a resistance to motion that can increase the friction force.

Friction and wear are two very important subjects in tribology and there are numerous parameters affecting them in boundary lubrication conditions. The friction and wear in boundary lubrication should be studied more carefully considering complicated physical, chemical and mechanical mechanisms. Different lubricant chemistries can lead to different wear and friction results for the same set of working conditions which supports the assertion that boundary lubrication mechanisms should be studied separately. A brief introduction to boundary lubrication and friction and wear in this regime is given in this chapter.

2.3.3 Running-in

Running-in occurs when two bodies start to contact and are in relative sliding/rolling motion. This process involves significant changes in the chemical, physical and mechanical properties of the interfaces including surface topography changes, tribofilm formation, bulk material and lubricant changes. This phenomenon will lead to steady state conditions that can modify the load characteristics of the tribosystems (28).

Due to complexity of phenomena happening during running-in, the exact behaviours of materials and lubricants is not known in this region. Because of this, it is difficult

to get reliable experimental results during the running-in period; this makes it very important to model the physics of the problem.

There are four important aspects that should be studied during running-in including wear, friction, tribofilm formation and surface roughness variations. All these variations should be studied as a function of the time because changes in these properties can be significant during the time and will affect the performance of the tribosystems.

2.3.3.1 Friction

According to literature, there are different types of friction curves (trends) during running-in (28-30). This is the result of different basic phenomena and even their combinations; therefore, it cannot be a representative of a single simple process.

However, these results can give a good insight into what happens at the interfaces due to changes in mechanical and chemical properties of the surfaces.

2.3.3.2 Wear

Figure 2-7 shows the real-time wear against the time of rubbing. The wear rate is higher during the running-in period (Figure 2-7) than the steady state due to numerous physical and chemical processes occurring. The reason could be significant changes in mechanical and chemical properties of interfaces and also wear due to asperity-asperity interactions. The tribofilm is not fully formed on the contacting asperities which can result in low load carrying capacity of the surfaces.

Furthermore, in the running-in stage, the asperities are not well smoothened and their sizes have not been subjected to a significant change. The modification to the asperity sizes (due to high load) can increase the load-carrying capacity of the surfaces. This

is the main reason that the wear rate is higher in the running-in stage in comparison to the steady-state condition.

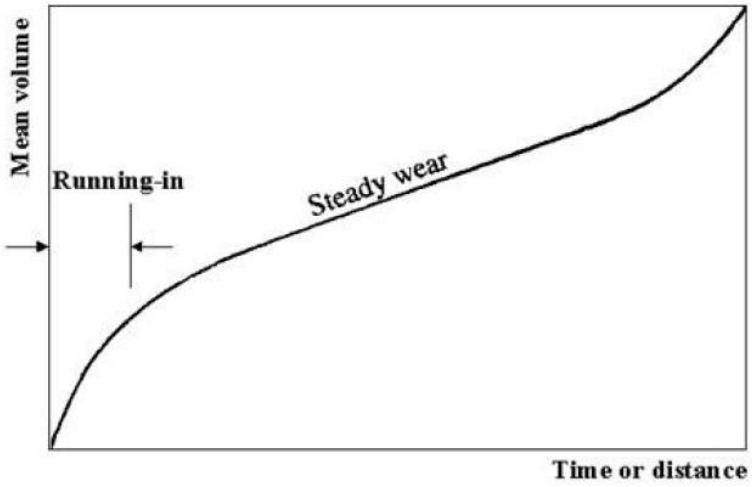

Figure 2-7 Running-in and steady state wear versus time (28)

2.3.3.3 Surface Roughness

Changes in surface roughness are dramatic during the running-in period. Several attempts have been made at characterizing the surface roughness variations during the running-in period (31, 32). The evolution of surface roughness seems to be different for different combinations of roughness between contacting bodies. In general, the roughness of the rougher surface starts to decrease to a steady state point (Figure 2-8).

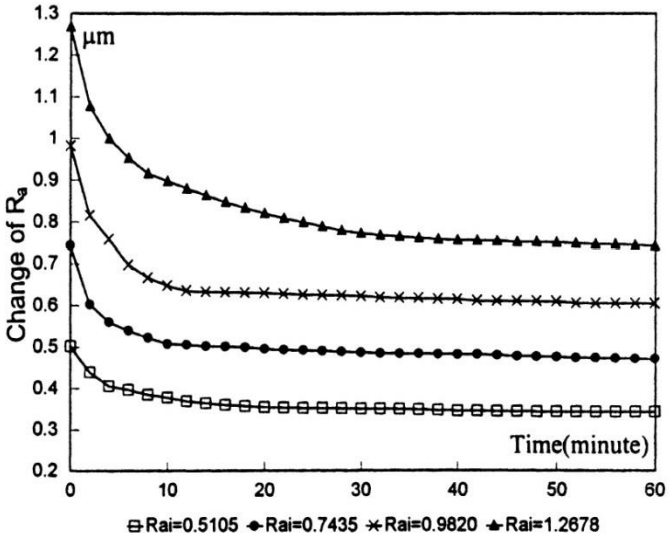

Figure 2-8 Surface topography variations during the running-in period (31)

2.3.3.4 Attempts at Modelling Running-in

Blau (29) modelled the friction during running-in based on his experiments and considered the effects of lubricant flow and solid materials.

Some works considered elasto-plastic contact of rough surfaces in order to model the behaviour in the running-in and predict surface topography and wear (31-34)

All these models and experimental results give us a good insight of how chemical, physical and mechanical properties of interfaces change during running-in and help us use the appropriate method for modelling the fundamental physics of the problem. The model results of Chapter 8 of this thesis which are a prediction of surface topography evolution of surfaces are compared to the above mentioned results in the literature.

2.3.4 Boundary Lubrication

A comprehensive theory which fully describes the physical and chemical processes occurring in boundary lubrication is still lacking. However, there are some

explanations for the chemistry of lubricants and their additives and also contact between interacting surfaces.

In the boundary regime, surface materials and tribofilms from lubricant additives determine the friction and wear behaviour at the interfaces. In this case, the contact characteristics are governed by both physical and chemical properties of tribofilms and the properties of the bulk fluid lubricant have less importance. Boundary lubricants can be classified by the type of surface actions that attaches them to the surface or results in their tribofilm formation. Some types of action in which the tribofilms form are listed below:

- Formation of a layer of molecules adsorbed by Van der Waals forces.
- Formation of high viscosity layers by reaction of oil components in the presence of rubbed metal surfaces.
- Thin reacted layer plus smoothing (oil components chemically attack exposed clean metal surfaces to give a thin chemically altered layer).
- Thick reacted inorganic layers (reactions between active oil components and metal surfaces forms thick reacted low shear strength inorganic films e.g. sulphides).

A variety of lubricant additives have been developed over the past years that give different properties to the boundary lubricating oils. There are major classes of additives such as: antiwear additives, friction modifiers, extreme pressure additives, detergents, dispersants, antioxidants, corrosion inhibitors etc. All these additives have their specific mechanisms in improving one aspect of boundary lubricated contacts.

Two most commonly used and important lubricant additives are friction modifiers and antiwear additives. Because of the importance of these two, a brief introduction into

the mechanism of them is introduced here. Then recent advances in understanding the mechanisms of the most commonly used antiwear additive are then reported in Chapter 3.

2.3.4.1 Antiwear Additives

These additives are used to significantly reduce wear in boundary lubrication. The most widely used lubricant additive for this purpose is zinc dialkyldithiophosphate known as ZDDP and tricresyl phosphate. The antiwear additives generally function by adsorbing and/or reacting with the substrate to form a solid-like tribofilm that acts as a protective layer thus reducing wear. The real mechanisms in which antiwear additives like ZDDP reduce wear are still not clear. However, there are a wide range of studies covering different chemical, physical and mechanical processes (See Chapter 3).

2.3.4.2 Friction Modifiers

These additives are used to modify the frictional behaviour of the system by forming a reactive chemical layer on top of the surface that has low shear strength and that can be easily removed. One well-known friction modifier is molybdenum dialkyldithiocarbamate known as MoDTC that reacts with the contacting surface and forms MoS_2 which has a lattice structure as well as very low shear strength that once formed, reduces friction in the contact.

2.4 Summary

Fundamentals of the science of tribology were introduced in this chapter. The main definition of terms and the important mechanisms in which friction and wear occur have been presented. Since the focus of this thesis is on the boundary lubrication and

its modelling, a brief introduction to this regime has been made. The importance of lubricant additives such as friction modifiers and antiwear additives has been mentioned. ZDDP as an antiwear additive will be the subject of the next chapter of this thesis.

Chapter 3. ZDDP as an Antiwear Additive: A Review of the Literature

ZDDP has been known as one of the most effective and successful lubricant additives and have been used in engine oils for 70 years. It was originally developed as an antioxidant but very soon after was recognized to have antiwear capabilities. Based on the new regulations of the fuel industry, using ZDDP in lubricant oils is restricted. This fact necessitates finding new alternatives for ZDDP that can act as an antiwear additive. Therefore understanding the true mechanisms in which ZDDP acts as an antiwear additive is essential. Recently, most researches conducted on ZDDP has focused on tribofilm formation, the chemistry and mechanical properties on the sliding surfaces (35).

It is reported that the diffusion or adsorption of the ZDDP molecules on the substrate is necessary prior to the formation of any surface films (36). ZDDP films form on the surfaces as thermal and tribo-films. There are studies that introduce thermal films which are different from tribofilms (37). It has been reported that tribofilms unlike thermal films need asperity-asperity contact and sliding to be formed on the surface. The tribofilms form only on sliding tracks (35, 38, 39). This tribofilm forms at even ambient temperatures and there are many experiments that show that with increasing temperature, the rate of ZDDP film formation will be increased (15). The ZDDP tribofilms can form and grow to a thickness of 50-150nm (15, 40). The films initially form as separate pads at the rubbing surfaces and then will grow laterally until they form a almost continuous form of tribofilm. The tribofilm consists of iron sulphide and zinc sulphide or iron oxide and zinc oxide near the substrate in the case of steel

surfaces with a thicker layer of glassy phosphates and a thin outer layer of zinc polyphosphates (Figure 3-1) (41).

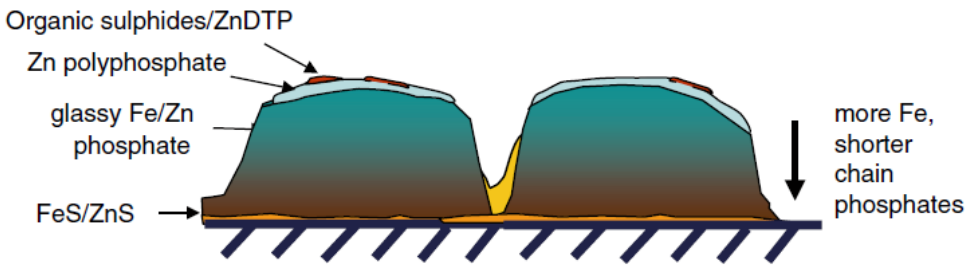

Figure 3-1. Structure of zinc dialkyldithiophosphate tribofilm (35)

Because of the complex nature of tribofilm formation and the way it reduces wear, there are several theories that explain the mechanisms:

(i) forming a tribofilm which is softer than the substrate and it acts as a barrier to decrease the amount of direct asperity-asperity contact (3),

(ii) digestion of the oxide particles and therefore reducing the three body abrasion and

(iii) formation of glassy phosphates which can act as a viscous lubricant in sliding conditions (42). There is another theory that assumes the glassy phosphates can prevent thermo-oxidative reactions and thus reduce wear (35).

Beside the effects of ZDDP on reducing wear, the influence of this widely used additive on friction should also be considered. It was shown that ZDDP increases the friction not only in the boundary lubrication regime but also in mixed lubrication (43). Some authors suggested that this behaviour is because of the pad-like structure of

ZDDP films and therefore the rough nature of these films but later it was shown that ZDDP films increase friction even in the mixed lubrication regime by inhibiting the entrainment of the fluid lubricant into the rubbing contact (44).

3.1 Mechanical Properties

There are several works which study the mechanical properties of ZDDP tribofilms formed in boundary-lubricated contacts and many techniques are used to understand what behaviour leads to these properties (16, 45-50). They found that the properties of the tribofilm layers are dependent on applied loads and can be adapted to different conditions. They also showed that the mechanical properties of tribofilms vary from surface to substrate (45). This is used to develop the contact mechanics of the ZDDP tribofilm reported in Section 5.10.

Mosey *et al.* (51) developed a new theory for the functionality of ZDDP tribofilms at the molecular level. They suggested that pressure-induced cross-linking is the reason for chemically-connected networks and many experimentally-validated behaviours of ZDDP can be explained by this theory (Figure 3-2). It was reported that the high pressure at the surface of the film will lead to higher cross-linking and result in longer chain phosphates. They have reported that shorter chain polyphosphates are harder than the longer chain ones. Figure 3-2-(a) shows the initial structure of the tribofilm. Once loaded, Figure 3-2-(b) shows the structure with hexa-coordinate Zn observed above 17 GPa and Figure 3-2-(c) indicates the final structure of the ZDDP tribofilm after high load.

The effect of the steel substrate in changing the nano-indentation results of tribofilms has been reported and different models for extracting the tribofilm properties were

developed (45, 52). All these studies give good insights into the mechanical characteristics of ZDDP tribofilm under severe conditions that might explain some of the experimentally observed behaviours that the ZDDP tribofilm can act as a smart material in tribologically loaded contacts (35).

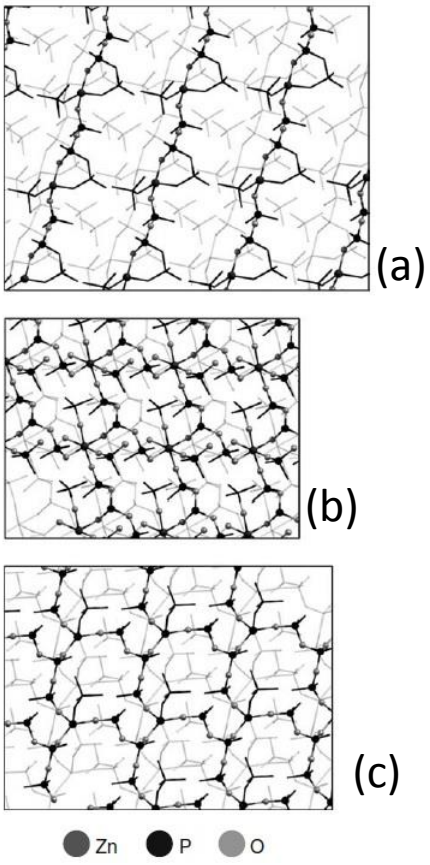

Figure 3-2 Changes in the chemical structure of zinc phosphates by cross-linking due to increasing load (51)

The composition of ZDDP tribofilms in boundary lubrication condition on steel surfaces has been characterized widely. It has been reported that ZDDP tribofilm has a layered structure with different chain length at different positions in the layer (53, 54). It is reported that there is a viscous layer of physically-adsorbed additive on the top layer of the tribofilm which can be easily removed by means of solvents and washing (see Figure 3-3). Underneath this viscous layer, there is a chemically

adsorbed layer of amorphous zinc and iron polyphosphates with different chain length (35, 41, 53, 54). Shorter chain polyphosphate layers are present at the bottom interlinked with the iron oxide. The top layer is thinner consisting of mainly longer chain polyphosphates. It is not shown experimentally that the layers can be distinguished by an interface; it is most likely to be gradual changes in the structure of the tribofilm.

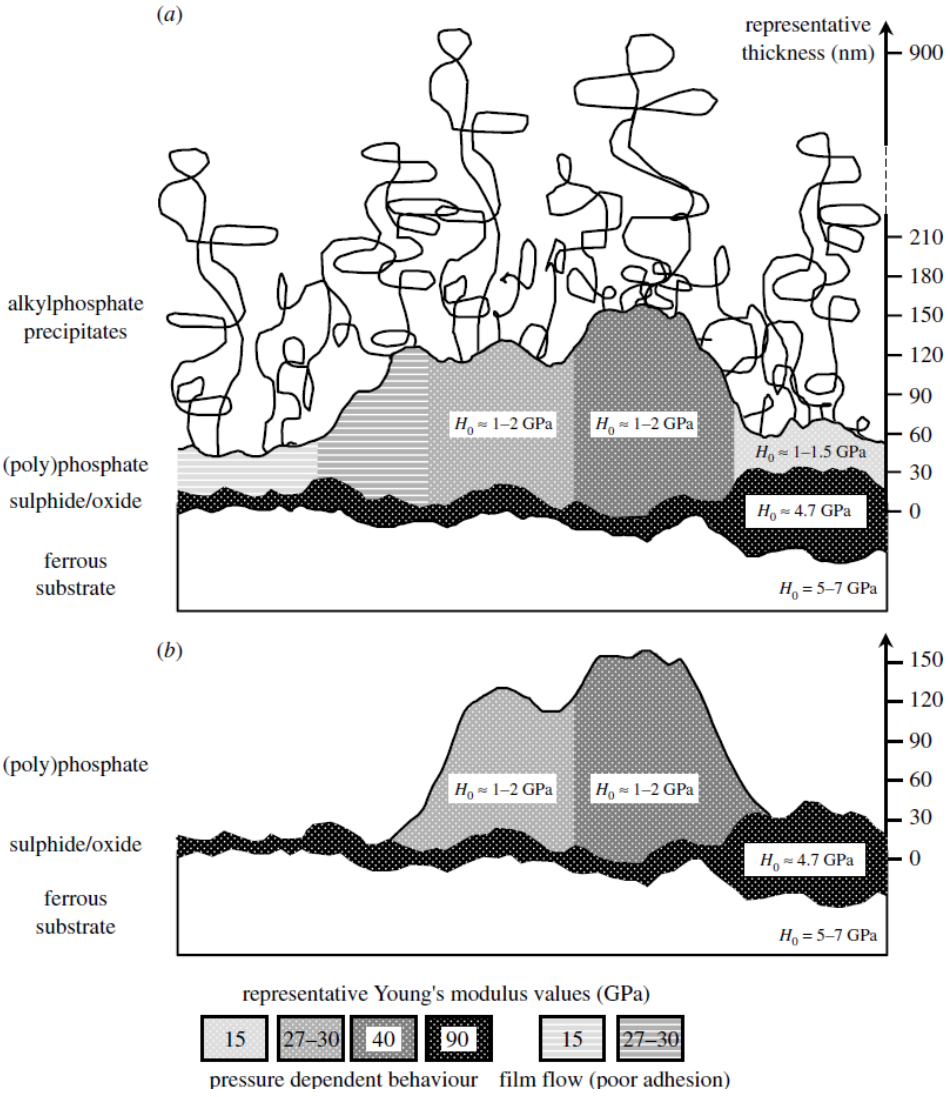

Figure 3-3 Schematic of mechanical properties of the ZDDP tribofilm reported in (45) a) Full antiwear film formed from ZDDP solution. b) The same film after being washed by the solvent.

In summary, the mechanical properties of the ZDDP tribofilm can be referred to the chain length of the glassy polyphosphates in general. Shorter chains are present in the bulk of the tribofilm close to the substrate/tribofilm interface and longer chain polyphosphates are present on top close to the body interfaces (16, 47, 48, 54, 55). The hardness at the surface is lower than the bulk hardness; as the penetration depth increases the hardness increases linearly (56).

The value of surface tribofilm hardness and tribofilm hardness near the substrate can be obtained from experimental results but the variations can be assumed to be between 2 to 6 GPa. In addition, elastic properties of the tribofilm also vary from the surface to the bulk and this variation is related to the hardness variation of the tribofilm as previously explained.

3.2 Tribofilm Growth

There are many investigations into the growth of ZDDP tribofilm with different experimental approaches (1, 16, 50, 57-59). Almost all of the works report the same pattern of ZDDP tribofilm growth on steel surfaces with the reported thickness of 50-150 nm. Fujita *et al*. (15) studied the growth of ZDDP tribofilm using a Mini Traction Machine (MTM) and Spacer Layer Interferometry Method (SLIM) (Figure 3-4).

Spacer layer interferometry is an imaging method enabling the measurement of tribofilm thickness across an area of few millimetre square. The wear track of the ball in a mini traction machine is loaded on an RGB camera and a colour image of the wear track is taken. Based on the calibration of the instrument, a thickness of the tribofilm is calculated. This method has the advantage of the measuring the tribofilm thickness at different times of experiments without removing the loaded parts. It

should be noted that an average thickness of the tribofilm can be measured over a relatively big area of the wear track without considering the roughness parameters of the contacting surfaces.

Fujita *et al*. (15) investigated the effect of temperature and concentration of both primary and secondary ZDDPs on the growth of the tribofilm on the surface. They generally concluded that higher temperature will lead to faster growth and thicker tribofilm. The same pattern was observed for different concentrations of ZDDP in the oil. Higher concentrations result in faster rate of growth for the ZDDP tribofilm. The experimental results were then used to extract semi-empirical relationships for the formation of the tribofilm. It should be noted that the growth of the tribofilm was considered as only the formation of the film. The concept of tribofilm removal was introduced in that work but it was not mentioned that tribofilm can be formed and removed at the same time.

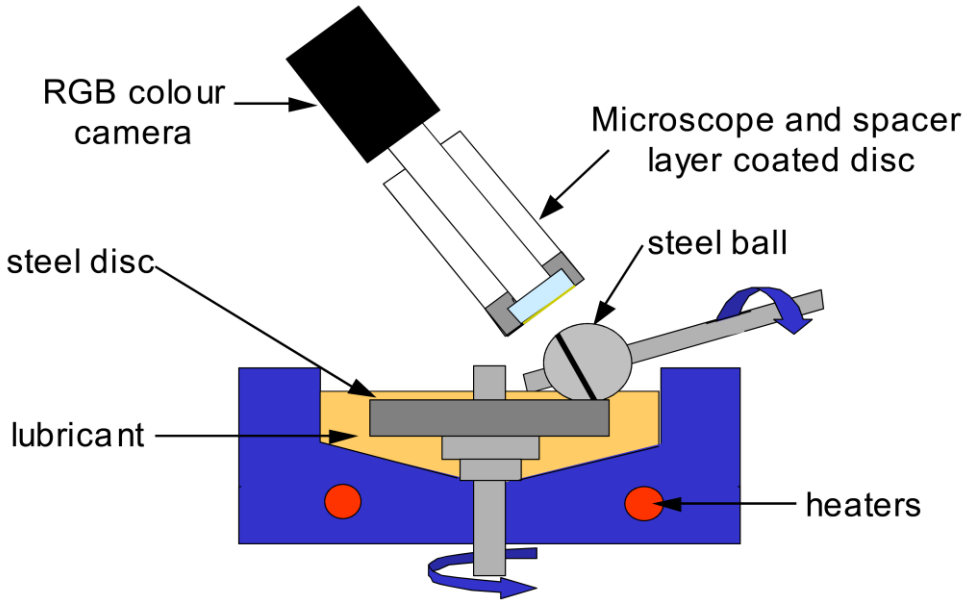

Figure 3-4 Schematic of the spacer layer interferometry mounted on the mini traction machine

The Spacer Layer images that are used to monitor the tribofilm growth are shown in Figure 3-5.

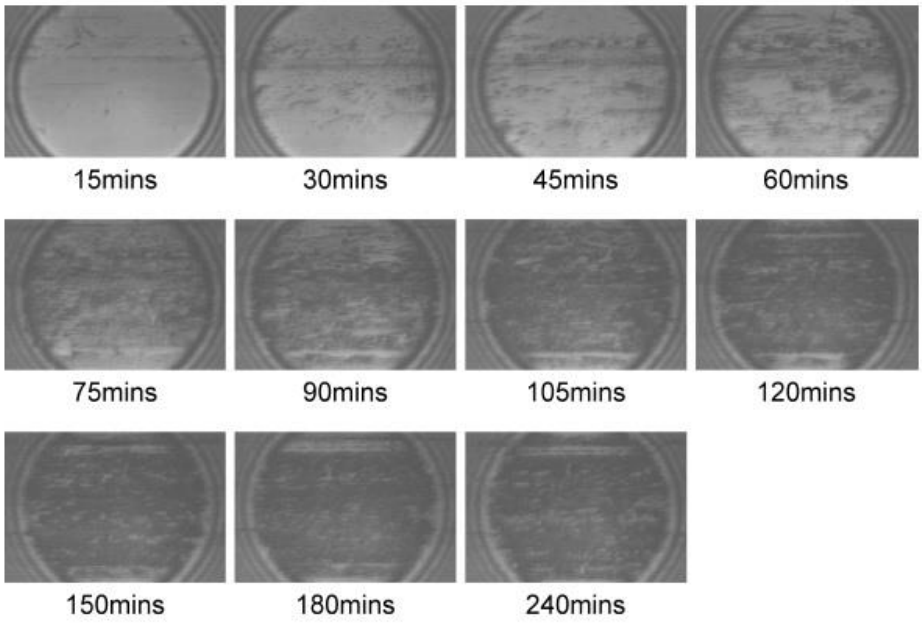

Figure 3-5 Spacer layer images at different time for ZDDP tribofilm (15)

Recently Gosvami *et al*. (60) designed an experiment to monitor the growth of the ZDDP tribofilm formed by a single asperity contact. They used an Atomic Force Microscope to generate the tribofilm and monitor the growth *in-situ*. It was reported that temperature and stress play significant roles in tribochemical reaction occurrence. They also claimed that there is no need for a reactive substrate such as iron to form the tribofilm. The reason for experimentally observing a difference in the formation of the tribofilm on the inert surfaces such as Diamond-Like Carbon (DLC) with the tribofilm formed on steel surfaces was reported to be the durability of the tribofilm formed. An example of the tribofilm growth results can be found in Figure 3-6.

They have fitted different kinetic curves to the experimental results (shown in Figure 3-6) and indicated that a power law with the order of 0.22 fits their

experimental results best. Power law of 0.22 in an Arrhenius-type kinetics model suggests a complicated path of reaction. These findings might be in line with the macroscopic growth kinetics previously reported (61). However, for a full comparison to be made, there would be a need for more sliding cycles on the single asperity case.

Although it is observed experimentally that the tribofilm can be removed at the same time as it is formed, no comprehensive study on the removal aspect has been carried out. The removal of the tribofilm due to the mechanical action of rubbing should be quantified by means of experiments both at the asperity level and at the macroscale in order to develop insights into the understanding of the real mechanism.

In summary, tribofilm thickness can be an important parameter in the boundary lubricated systems. However this thickness does not fully characterise the behaviour of the system. It should be studied carefully while considering different aspects of tribofilm such as chemical and mechanical properties too as complementary information.

3.3 Tribochemistry of ZDDP

Tribochemistry is the study of chemistry and chemical reactions happening during tribological conditions. Tribofilms generally form not only when the additives are present near the surface, but when the sliding takes place. Therefore, in the boundary lubrication regime, both the sliding and presence of additives near the surface cause the protective layer formation. It is useful to consider the ZDDP reactions during the tribological conditions but because of the complicated nature of boundary lubrication, the exact chemical reactions occurring at interfaces are not known yet.

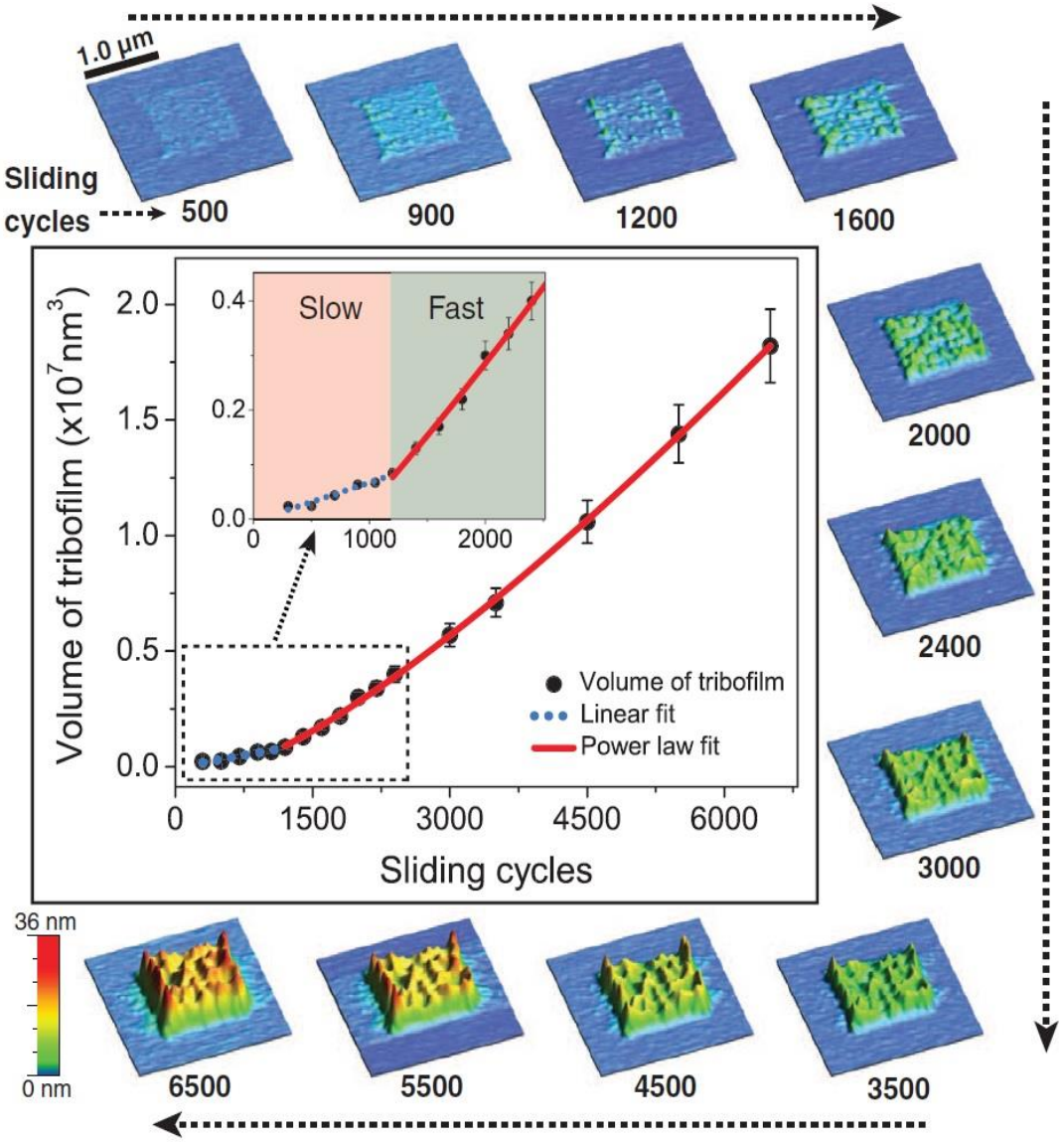

Figure 3-6 Single-asperity tribofilm growth results (60)

Fuller *et al*. (62) suggested some chemical reactions for ZDDP happening during tribological conditions and forming tribofilms on the surfaces. They used S K- and L-edge X-ray absorption near edge structure (XANES) spectroscopies and also NMR spectroscopy to monitor the chemistry.

At first, ZDDP is adsorbed on the rubbing surfaces as follows:

$$Zn[(RO)_2PS_2]_2(solution) \longrightarrow Zn[(RO)_2PS_2]_2(absorbed) \quad (1)$$

Then ZDDP becomes a Linkage Isomer ZDDP LI-ZDDP in solution form;

$$Zn[(RO)_2PS_2]_2(solution) \longrightarrow Zn[O_2P(SR)_2]_2\ (LI-ZDDP\ in\ solution) \quad (2)$$

After some time LI-ZDDP adsorb to the surface like ZDDP;

$$Zn[O_2P(SR)_2]_2(LI-ZDDP\ in\ solution) \longrightarrow Zn[O_2P(SR)_2]_2\ (absorbed) \quad (3)$$

Then some thermal activated oxidation reactions happen and polyphosphate chains are produced:

$$Zn(RO)_4P_2S_4 + O_2 \longrightarrow Zn(PO_3)_2 + sulphur\ species \quad (4)$$

When the rubbing Continues long chains react with water and the results are shorter chain polyphosphates;

$$Zn(RO)_4P_2S_4 + O_2 \longrightarrow Zn(PO_3)_2 + sulphur\ species \quad (5)$$

$$7Zn(PO_3)_2 + 6H_2O \longrightarrow Zn_7(P_5O_{16})_2 + 4H_3PO_4 \quad (6)$$

$$2Zn(PO_3)_2 + 3H_2O \longrightarrow Zn_2P_2O_7 + 2H_3PO_4 \quad (7)$$

In addition there are other chemical reactions have been suggested considering the digestion of abrasive oxide particles by phosphate tribofilms which is one of the possible mechanisms of reducing wear by ZDDP tribofilm (13, 63).

$$5Zn(PO_3)_2 + Fe_2O_3 \longrightarrow Fe_2Zn_3P_{10}O_{31} + 2ZnO \quad (8)$$

As discussed before, the full understanding of chemical reactions happening during sliding in boundary lubrication conditions is very difficult to achieve. However the chemical reactions (1-8) mentioned in this section give some directions into better understanding of the real tribochemical process.

3.4 Stability of ZDDP

Tribofilm can be formed and removed at the same time (64). Experiments show that ZDDP film is very stable after forming. When the oil containing ZDDP was replaced by ZDDP-free base oil, the film thickness was stable even after rubbing (3) (Figure 3-7). The results show that the film thickness is reduced under rubbing conditions only once the dispersant is added to the oil. This durable tribofilm can be the reason of good performance of the ZDDP to act as an antiwear additive (15).

In general, the good performance of an antiwear additive occured when the film formation rate is higher than the film removal. However, because of good stability and durability of ZDDP tribofilm, it has a superior role and is widely used in the lubrication of important parts in IC Engines.

To understand the removal behaviour of the ZDDP tribofilm and its effect on the wear behaviour of the tribosystem, experiments should be carefully designed to quantify this aspect. The removal of the tribofilm should then be somehow implemented into

the computational models which can help to capture a more accurate physical model and also understand the real mechanism in which ZDDP act as an antiwear.

3.5 ZDDP on Non-Ferrous Surfaces

ZDDP as an antiwear additive can form tribofilms on various materials including steel, diamond-like carbon (DLC) and Si/Al alloys (49, 65-73). Though extensively studied, the specific processes involved in formation and removal of tribofilms in these different systems are not yet fully understood. In the case of inert surfaces such as DLCs, tribofilms do form, but some reports indicate that they can be easily removed from the surface (60, 72). The tribofilm has negligible effect on the wear (72), with wear resistance properties being dominated by those of the DLC itself, and with the type of DLC having an important influence (71). In contrast, ZDDP tribofilms formed on steel surfaces have been shown to contain iron in the bulk (74), indicating a significant interaction between the ZDDP and the substrate.

This can be due to several reasons: (i) chemical reaction resulting from cation exchange in the polyphosphate (Fe^{3+} in place of Zn^{2+}); (ii) mechanical mixing in the process of high load and shear stress; and (iii) digestion of the iron oxide abrasive particles in the bulk of the tribofilm. There are different wear reduction scenarios reported for ZDDP but the most accepted one is coverage of the surface, prevention of direct asperity-asperity contact and increasing the load carrying capacity of surfaces.

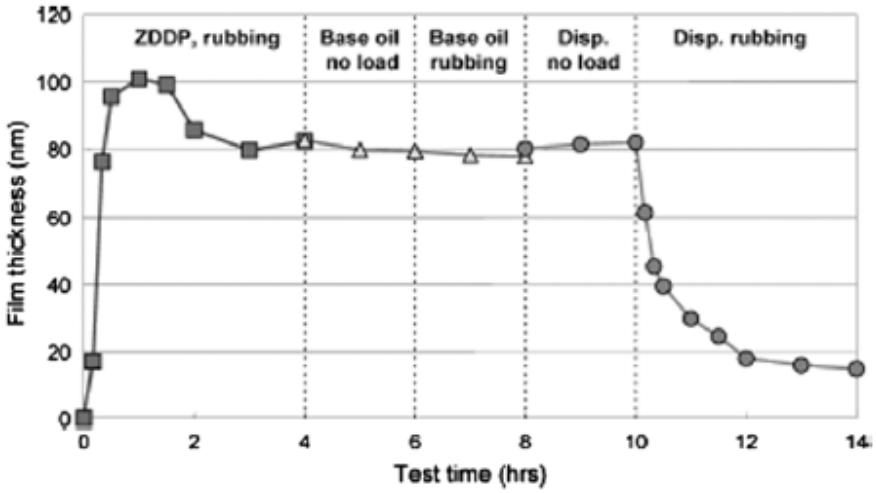

Figure 3-7. Illustration of the stability of a ZDDP tribofilm: when the lubricant in the tribotest is replaced with ZDDP-free base oil, the tribofilm's thickness is maintained, and is only reduced by the addition of a dispersant under rubbing conditions (15).

3.6 Summary

ZDDP is an antiwear additive mostly used in the lubricant industry because of its remarkable antiwear performance. The mechanism in which ZDDP reduces wear is still not clear but there are few proposed mechanisms in the literature. ZDDP forms a tribofilm on the contacting asperities that has a different mechanical properties form the surface. This tribofilm is inhomogeneous and its thickness differs from point to point on the surface and depends on the inhomogeneity of many physical parameters on the surface such as temperature and load. The mechanical properties of the tribofilm are interlinked with the chemical characteristics of the film. A smart behaviour was observed when the tribofilm was exposed to higher loads. It was proposed that a change in the structure of the tribofilm occurs while is subjected to higher loads. ZDDP has a complicated tribochemistry as there are plenty of chemical

reactions involved at the same time in the formation of the tribofilm. ZDDP tribofilm can form on various surfaces such as DLCs , Al/Si alloys and steel but the mechanisms in which ZDDP reduces wear is different on different surfaces. The stability of the ZDDP tribofilm on the surfaces of contacting bodies is reported to be very important in characterizing the wear behaviour of the tribosystems. Quantifying such an important parameter needs robust and careful experimental design. In the next section, an overall overview of the boundary lubrication modelling based on the literature studies is presented. It is shown that what important parameters should be considered in modelling boundary lubrication with respect to tribochemistry.

Chapter 4. Boundary Lubrication Modelling: A Review of the Literature

4.1 Introduction

In the previous chapters an introduction to tribology, lubrication, friction and wear was presented with a focus on boundary lubrication and previous studies on the antiwear performance of ZDDP as an antiwear additive were presented. The effectiveness of boundary lubrication has been considered for a long time as a necessity for modern designs of machines with reliable operations. Because of the need for more energy efficiency, availability of new materials and machine part downsizing, the need for understanding true interactions in this regime is of great importance. The boundary lubrication regime has been the subject of many studies for more than 70 years (5, 6) and the majority of these studies are experimental investigations into the nature of what happens in this regime.

Many of the studies cover the boundary film chemical (13, 14), physical and mechanical properties (16, 45-47) and their effects on wear and friction reduction. The subject of many works has been to investigate different kinds of additives in oils and their effects on various aspects of tribological performance (2, 64, 75). As the boundary lubrication regime is mainly related to interactions of two surfaces and the oils containing additives between them (Figure 4-1), the analytical studies of surfaces including topography measurements, chemical analyses, mechanical and physical studies are considerable.

All these experiments give good insight into different chemical and physical characteristics covering various aspects of boundary lubrication systems.

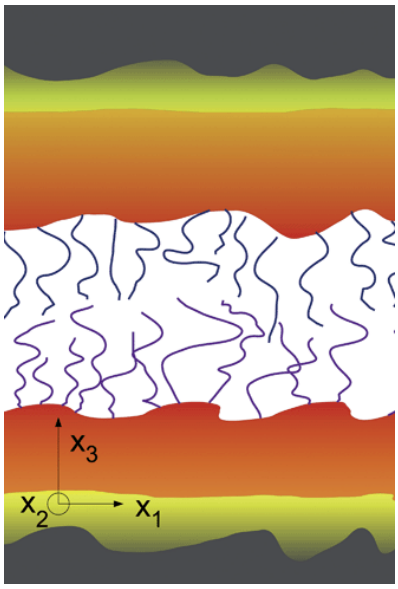

Figure 4-1 Boundary lubrication showing: surfaces, lubricants and adsorbed films (17)

However, it is clear from the wealth of experimental literature in this area that the nature of the phenomena happening in this regime is very complicated. Studying the entire problem needs a multiscale understanding ranging from component scale down to the micro-scale and also molecular interactions of films and lubricant additives. Experimentation across such scales is challenging and hence it is important to complement such studies with the ability to predict the friction and wear of a working system without running experiments. It is also important to analyse the system and optimise its performance in order to design cost effective experiments. Many modelling attempts have been made recently (17, 18) but a comprehensive multiscale model of boundary lubrication considering tribochemistry phenomena in order to predict friction and wear of the system is still lacking.

In this chapter firstly some interesting attempts for boundary lubrication modelling are introduced. Secondly, different numerical techniques applicable in boundary lubrication are discussed as well as examples in the literature. The Boundary Element Method (BEM), which is a commonly-used approach for capturing the system behaviour in boundary lubrication, is discussed in more detail and the contact mechanics formulation corresponding to that is reported. Literature reporting the calculation of contact pressures as well as flash temperature is also included. At the end, some tribochemical modelling attempts in the literature will be reviewed.

Despite the complexity, there are some examples of boundary lubrication models that will be referred in this section.

Sullivan (76) developed a model for oxidational wear under boundary lubrication (See Figure 4-2). He proposed a mathematical model which relates the wear to applied load and pressure and involves many other factors that together can be assumed as Archard's wear equation coefficient. He found a relationship for the wear as a function of the load. The calculation of the contact temperature was one of the abilities of the model. The model was one of the pioneering modelling attempts in boundary lubrication that considers not only the contact but the effect of lubricant additives and surface layers.

Stolarski (77) developed a model for wear prediction in boundary lubricated contacts both in dry contact and contact with lubricants between sliding surfaces. He used statistical models and probability functions to predict the asperity-asperity contact and determining probability of elastic or plastic contact and thus calculating the wear. The wear prediction model was capable of distinguishing between lubrication regimes and it was assumed that only boundary and mixed lubrication regimes are responsible for

adhesive wear calculations. The plasticity index was calculated to see the probability of elastic and plastic deformations in that model as well as the fractional film defect. It used Greenwood and Williamson model of contact mechanics (78).

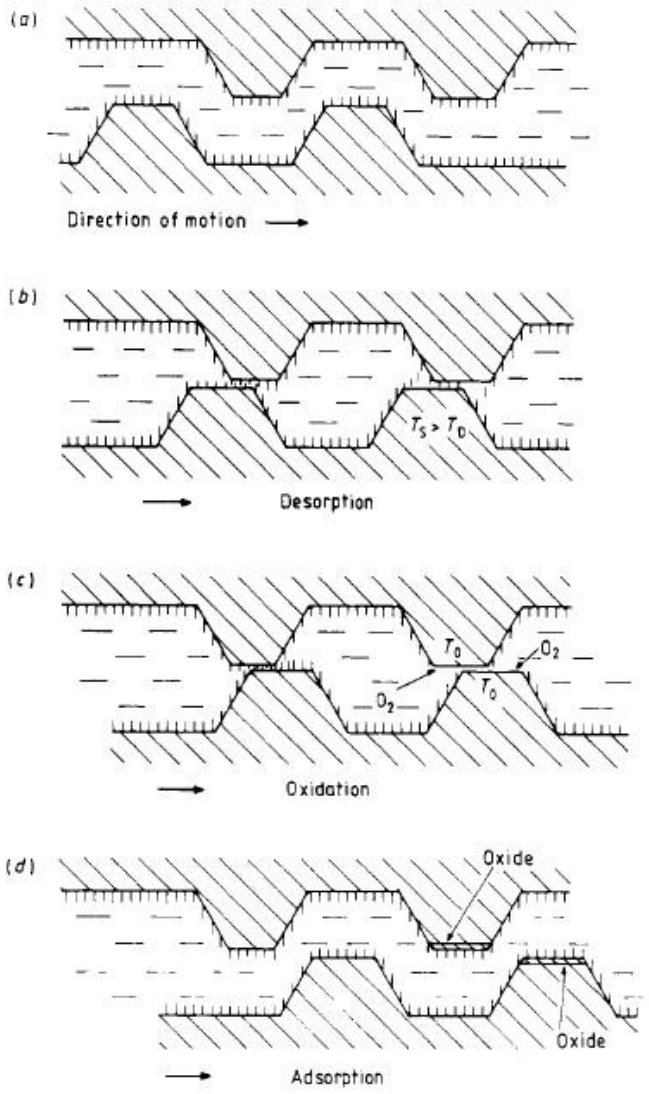

Figure 4-2 Schematic for modelling oxide layer formation and its effect on oxidational wear in boundary lubrication (76)

Zhang *et al*. (79) derived a model for micro contacts. The deformation of asperities in this model can be elastic, elasto-plastic or even fully plastic and the possibility of

contact is determined by a contact probability equation. They used the Jaeger equation over the contact area in order to calculate the asperity flash temperature. Then the classical wear theories were used for calculating the probability of contact covered by oxide layer and also probability of contact covered by physically and chemically adsorbed layers were studied. Flash temperatures, real area of contact and friction force were also calculated by the model. An example of the model results are shown in Figure 4-3. In the figure, S_a is the probability of the micro-contact to be covered by an adsorbed film, S_o is the probability of the contact being protected by an oxide layer and S_n is the probability of contact with no boundary protections. The model suggests that higher lubricant/surface reactivity or substrate hardness enhance the micro-contact behaviour therefore affecting the wear of the system.

There are some modelling attempts that used commercial software like ABAQUS to simulate wear in boundary lubricated contacts. Hegadekatte *et al*. (80) developed a multi time-scale model for wear prediction. They used commercial codes for determining their contact pressure and deformations and then used Archard's wear equation for calculating wear. There are more examples of such models that incorporated the Finite Element Method for the contact problem and they are reported later in this chapter.

These modelling attempts are general examples of boundary lubrication modelling from different aspects of view at the problem. Here different modelling approaches in the literature will be reported and their drawbacks and advantages will be discussed as well as some examples of such models in the literature.

4.2 Modelling Methods in Boundary Lubrication

There have been various methods in modelling different aspects of boundary lubrication in the literature ranging from molecular scale simulations to large scale computations. Mostly used methods of modelling and examples of each approach are listed below and will be discussed in this chapter.

4.2.1 Molecular Dynamics

A computer simulation of physical movement of atoms and molecules is called Molecular Dynamics (MD). Atoms and molecules can interact with each other and their trajectories are calculated numerically by solving Newton's equations of motion. In this case, forces and potential energy between atoms and molecules are defined by molecular mechanics forces.

With present knowledge, contact mechanics, chemistry and thermodynamics are three major important bases of boundary lubrication. The contact mechanics simulations have been developed by many scientists but still need more investigations for the tribofilm mechanical properties.

The other two bases have been less studied and that is where tribochemistry comes in to account. Molecular dynamics is a way to consider the chemical aspect of boundary lubrication and is able to give very good insights of this phenomenon by investigating molecular scale interaction of additive molecules and substrate atoms. There have been so many studies on MD simulations of boundary lubrication in recent years due to development of computational facilities. Some examples of MD simulations in boundary lubrication are reported in this chapter.

4.2.1.1 Simulation of Atomic Friction

It has been reported by Dong *et al*. (81) that atomic friction simulations in molecular dynamics is significantly affected by many parameters such as materials, surfaces, compliances, contact area, load, temperature and velocity. They showed that one of the most significant limitations of the molecular dynamics is the time scale of the simulations. This limitation restricts the direct validation of simulations with experimental data and makes it almost impossible for extracting data useful for understanding the real phenomena in tribological applications.

Because of the limitations in timescale, the small scales in size are also a restriction for the molecular dynamics framework. Since a very small scale of real experiments needs a massive number of molecules, validation and comparison with experimental data is cumbersome.

A very important part of any molecular dynamics simulation is the potential formulation between atoms. There is no fixed formulation for potential between atoms in MD simulations and these relationships come from empirical equations to match the material behaviour. The reliability of molecular dynamics simulations is highly dependent on accuracy of the potential defined. Because of the variety of the materials used nowadays, more flexible and general formulations for potential can be very useful. Literature still lacks a comprehensive formulation and it can be good area of physical science research.

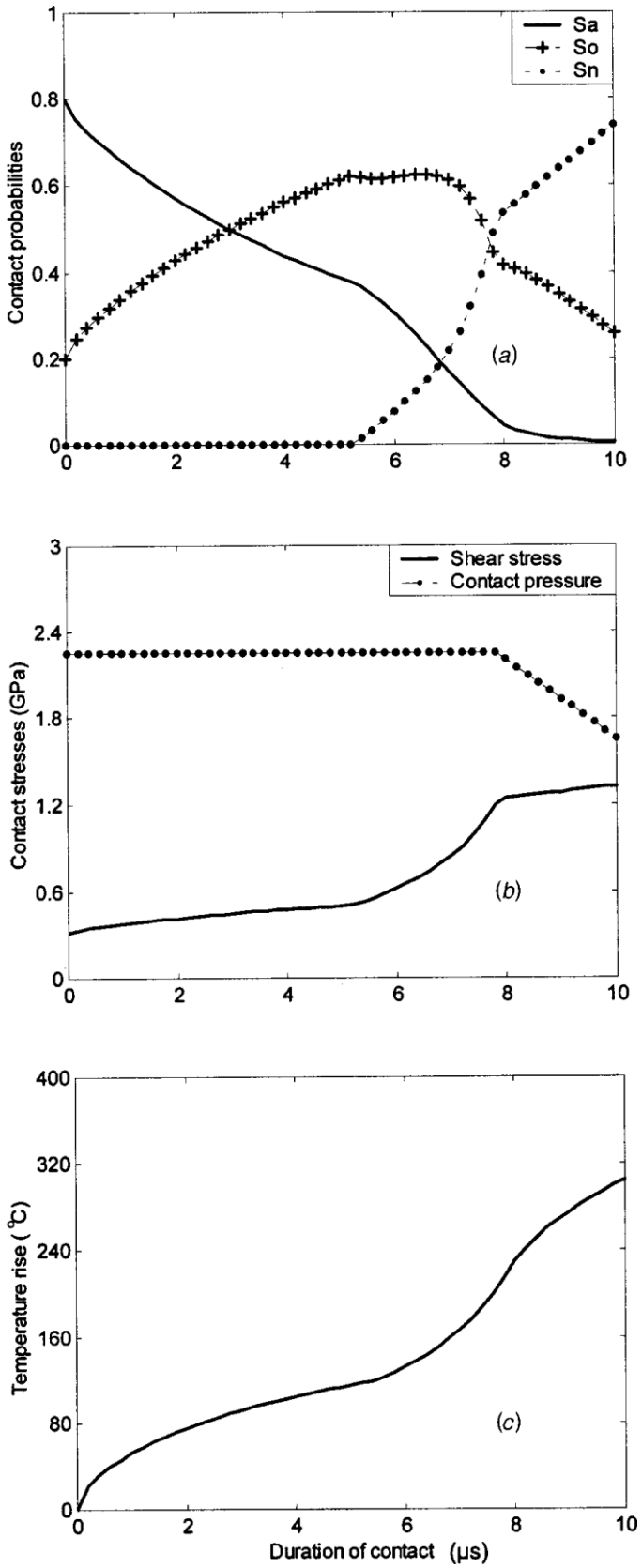

Figure 4-3 Time history of micro-contact for (a) contact probabilities (b) shear stress and contact pressure (c) contact temperature (79).

Li *et al*. (82) showed that atomic stick-slip is thermally activated at low speeds. They stated that comparison between molecular dynamics and AFM measurements are very tricky due to the high speeds in simulations that leads to dynamic effects. They showed that MD simulation data can be used for interpreting AFM data if the speed is low enough. The atomic friction simulations in molecular dynamics have been the subject of several studies (83-93). An example of the model is shown in Figure 4-4. Substrates are made from a number of atoms and are bonded to each other. The contact problem is then simulated using a load and applying sliding velocity to the bodies. The friction force is then calculated and coefficient of friction is obtained by dividing that by the normal load.

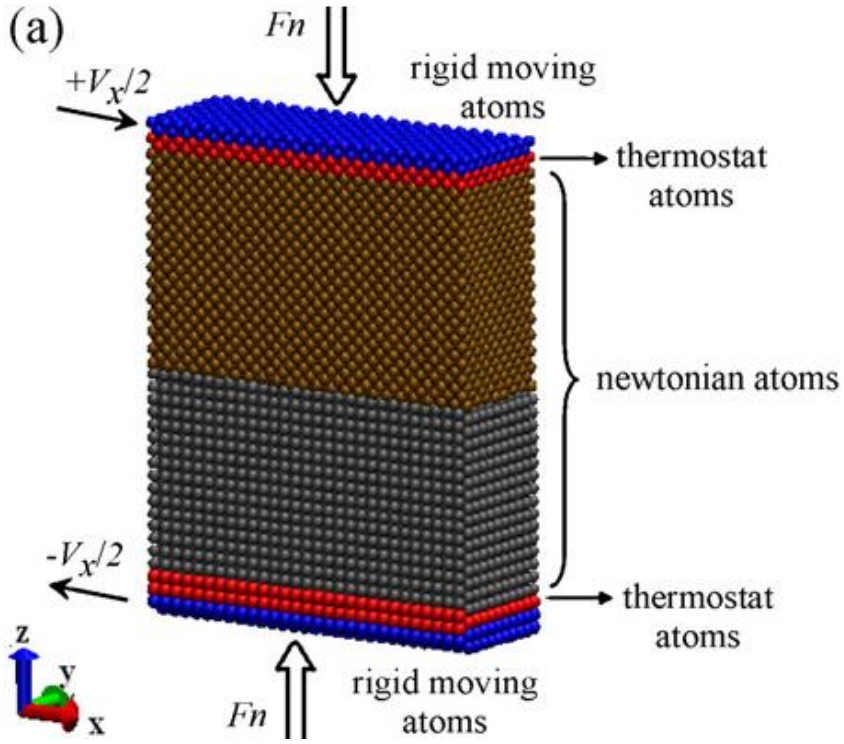

Figure 4-4 An example of model set up in molecular dynamics for friction studies (87)

4.2.1.2 Simulation of Contact Mechanics

Contact mechanics calculations have been the subject of molecular dynamics simulations recently because of the ability to study the local physics of the phenomena. Solar *et al*. (94) simulated a nano-indentation test with molecular dynamics and compared their results with experimental nano-indentation tests. They could show good agreement between simulations and experiments for loading and unloading curves. In another work, Zheng *et al*. (95) incorporated contact mechanics to simulate the contact of 3D rough surfaces in mixed lubrication. They calculated the contact area and pressure distribution for various lubricated conditions.

One approach of simulating contact mechanics is using combined molecular dynamics and finite element analysis. This multiscale approach allows the local calculation of contact on the surface as well as robust features of the finite element method and bulk material properties. Anciaux *et al*. (96) used a multiscale approach consisting of a finite element simulator and a molecular dynamics engine and also a coupling scheme. The results were validated for Hertzian contact and also for contact of rough surfaces. It can be seen in Figure 4-5 how a real rough surface was generated by coupling molecular dynamics and finite element analysis. The bulk of the material is modelled by a rigid body and is meshed like conventional FEM simulations. The boundary of the solid which is the surface, is simulated by small atoms. These two parts are named continuum and atomistic zones.

For linking the two zones, a numerical approach was suggested. A bridging zone was defined to be link between atomistic and continuum parts. The data was then transferred between the two zones via the bridging section. The schematic representation of the coupling configuration is demonstrated in Figure 4-6.

In another study, Yang *et al*. (97) used a multiscale molecular dynamics simulation to calculate the real area of contact and compared the calculations with analytical contact mechanics models based on continuum mechanics. They showed that the real area of contact is best defined by studying the interfacial pressure distribution and fitting an analytical formulation to that.

In summary, molecular dynamics seems to be a good approach for contact of rough surfaces (98). However the simulations are very time-consuming and more time-efficient approaches will be favourable for calculating contact pressures and surface deformations.

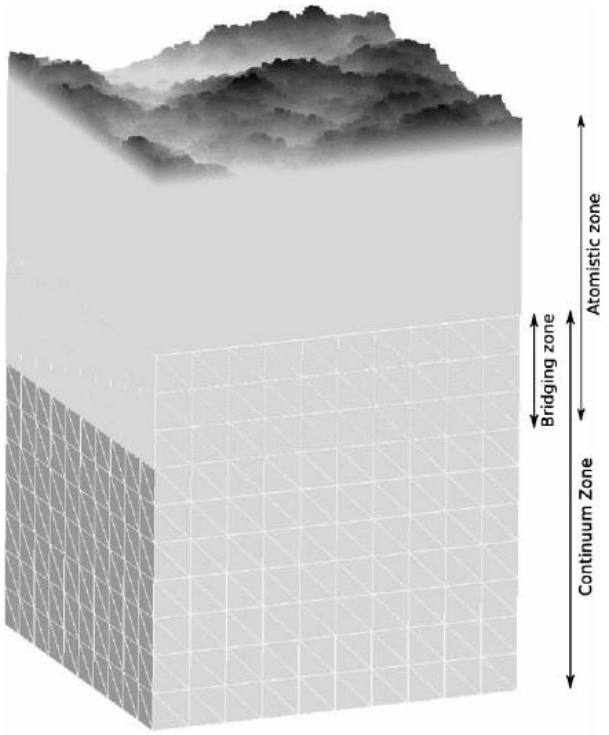

Figure 4-5 System configuration for coupling FEM and MD to generate real rough surfaces (96)

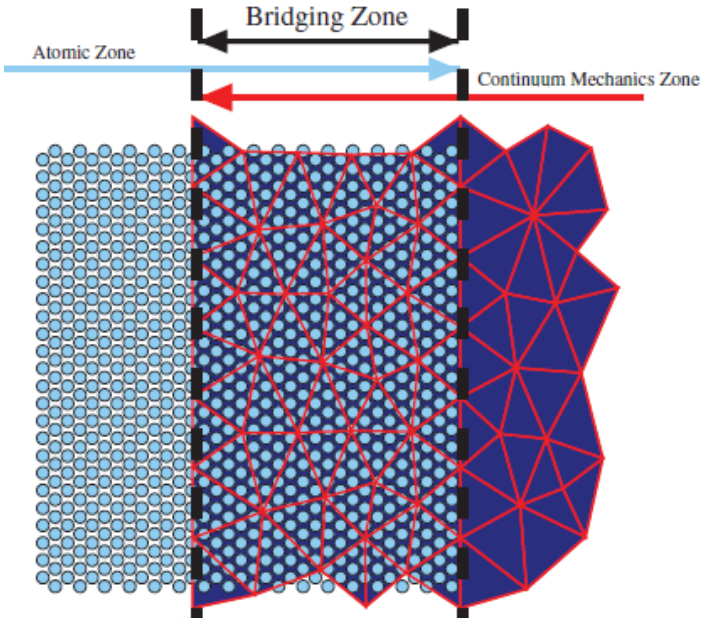

Figure 4-6 The coupling between atomistic and the continuum zones in a combined FEM-MD method (96)

4.2.1.3 Tribochemical Aspects

Attempts have been made to study the molecular interactions in the tribochemical processes using molecular dynamics. Molecular dynamics was then combined with chemistry calculations to study whether a chemical reaction is likely to happen or not. These reactions might be the reaction between substrate atoms and the additives or the particles and the tribofilm.

One of the most well-known tribochemical studies in molecular dynamics is the investigation of the tribochemical reaction of zinc-phosphates with iron oxides. It has been the subject of several studies (13, 42, 63, 99, 100) to study this tribochemical reaction. It was reported that iron oxide particles react with zinc polyphosphates and are digested inside this tribofilm (see Figure 4-7, Figure 4-8 and Figure 4-9). This process only occurs when the combined effect of normal load and shear stress is present. It was also reported that this digestion does not occur for all substrate

materials like Al/Si Alloys. It was shown that aluminium particles can hardly be digested and why the presence of Si can help the performance. They concluded that zinc metaphosphates are more chemically reactive to iron oxides than the orthophosphates. They also proposed a path for the tribochemical reaction of the digestion of iron oxide inside the glassy polyphosphates based on HSAB principle as the following:

$$5Zn(PO_3)_2 + Fe_2O_3 \longrightarrow Fe_2Zn_3P_{10}O_{31} + 2ZnO \quad (1)$$

They suggested that the above equation is the main reaction for digestion of abrasive particles inside the tribofilm.

Martin *et al*. (101) studied an alternative antiwear additive for ZDDP with better friction performance but less efficiency in antiwear. The molecular dynamics simulation in that work showed that the combination of both borate and phosphate additives can compromise both performances depending on the P:B ratio in the oil.

Onodera (100) explained how theoretically a molecular dynamics simulation can deal with studying a tribochemical reaction. They numerically tested the abrasive wear prevention of two different phosphate glasses as a tribofilm. They showed that $Zn(PS_{0.5}O_{2.5})_2$ can digest the Fe_2O_3 wear particles in the friction process. They also found that $Zn(PO_3)_2$ is also capable of digesting the Fe_2O_3 abrasive particles and had an even better antiwear performance than $Zn(PS_{0.5}O_{2.5})_2$. They concluded that $Zn(PO_3)_2$ was better in both wear prevention and environmental issues.

The work was continued in another work by Martin *et al*. (102). They found that the combined effect of pressure and sliding (shear) is essential for this reaction to happen. By analysing the set of their results they concluded that the driving force of this tribochemical reaction is not only the flash temperature but the combined effect of temperature, pressure and sliding induces the reactions. By other means, the increase in the entropy of the system will cause the tribochemical reaction happening. In this case, the free Gibbs' energy can be taken into account as well as thermodynamics equations of free Gibbs' energy to examine whether which reaction happens or not.

$$\Delta G = \Delta H - T\Delta S \qquad \text{Equation 4-1}$$

in which ΔH, T and ΔS are enthalpy change, absolute temperature and entropy change, repectively.

Yue *et al*. (103) studied the occurrence of tribochemical reactions of phosphoric acid at different temperatures and hypothesized the reason for different friction behaviour of their system. In another work, Hayashi *et al*. (104)used molecular dynamics to study the contact of DLC-DLC and reported the effect of hydrogen in chemical bonding of atoms that results in lower friction.

Overall, a molecular dynamics simulation might potentially answer fundamental questions in tribochemistry if it overcomes its important shortcomings. It needs to be adapted to larger scales (at least asperity scale). It also needs to be more efficient in terms of time to be able to cover longer time of the tribological systems. The non-equilibrium thermodynamics with its complicated formulations must be adapted to MD simulations in order to capture the behaviour in boundary lubrication.

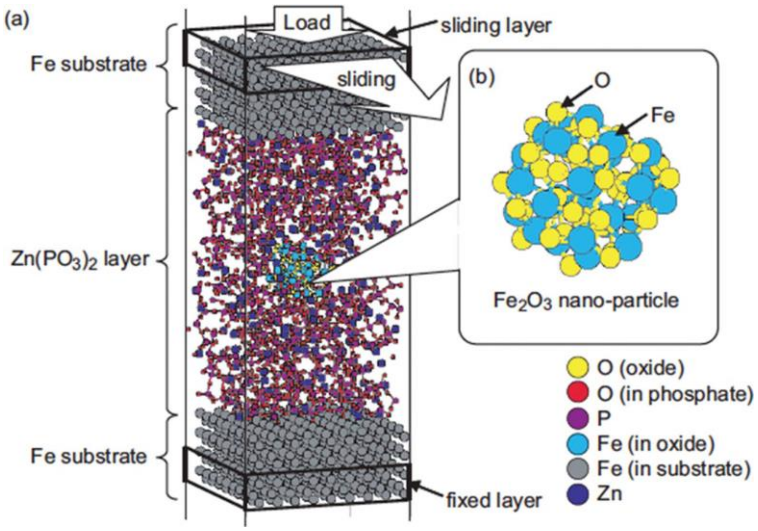

Figure 4-7 Molecular dynamics simulation for an abrasive iron oxide particle in a glassy phosphate tribofilm formed on steel surfaces considering load and sliding speed and molecular contents of particle and tribofilm (13).

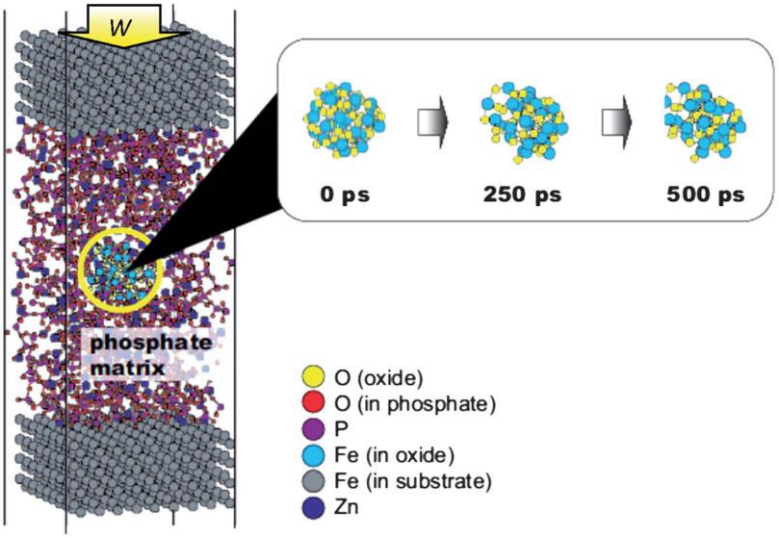

Figure 4-8 Molecular dynamics model for phosphate glass tribofilm between two steel surfaces considering load from 0 to 500 ps without considering sliding (13).

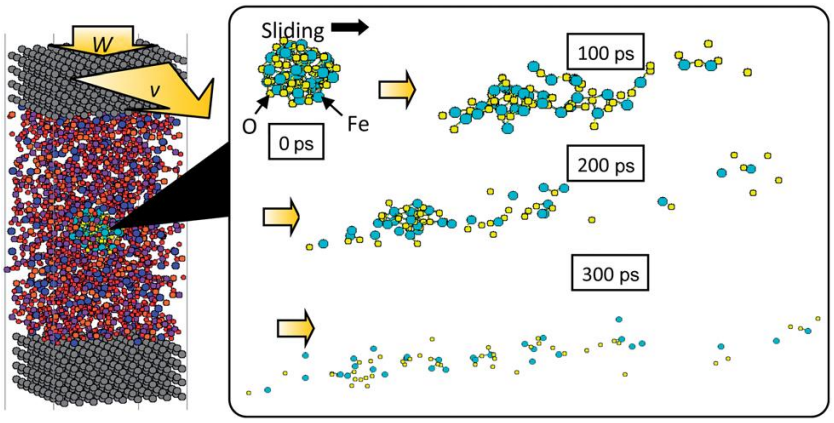

Figure 4-9 Molecular dynamics model for phosphate glass tribofilm for two steel surfaces considering load and sliding speed from 0 to 300 ps (13).

4.2.2 Finite Element Method (FEM)

There have been so many attempts to model wear and also friction in dry contacts by using finite element analysis (80, 105-116).

The Finite Element Method is a very robust way for studying continuum mechanics. Despite all FEM advantages in solid mechanics simulations, it has significant drawbacks in modelling the boundary lubrication problems.

In the case of contact mechanics in boundary lubrication, because two surfaces are in cyclic contact, the concept of wear comes in to account and geometries should be changed due to loss of material. In addition, due to different surface phenomena and tribochemical reactions in boundary lubrication, mechanical and chemical properties of the surfaces are constantly changing as well as their surface topography.

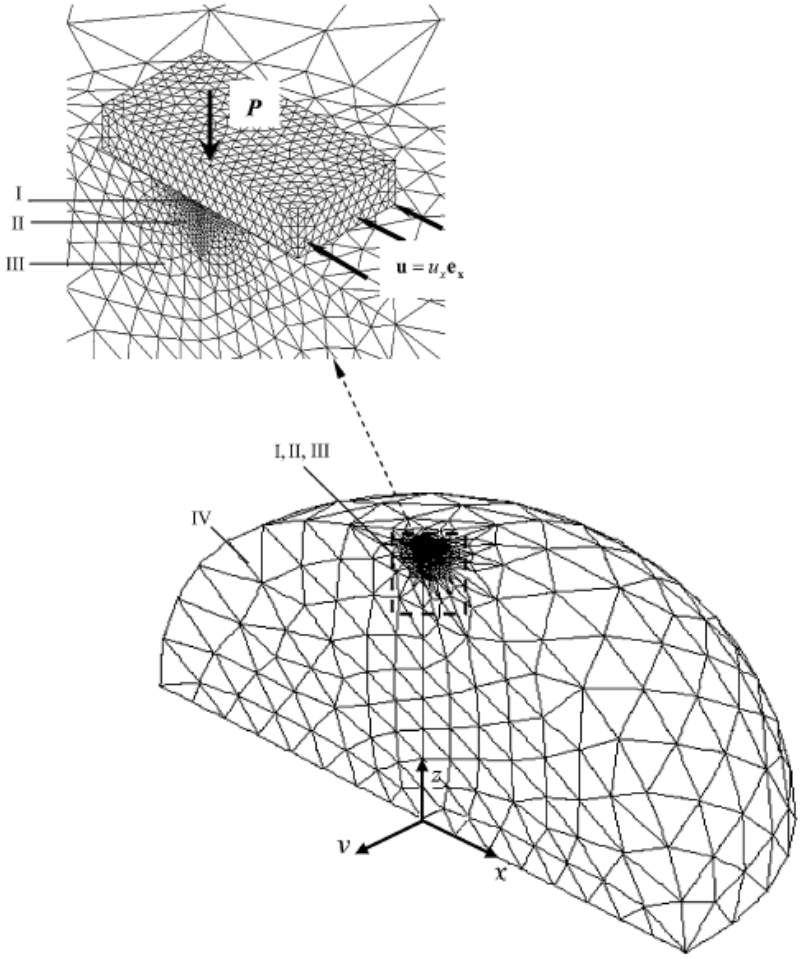

Figure 4-10 Finite element configuration of two contacting bodies (sphere on flat). Very fine mesh has been used for the area in contact. (105)

Wear of materials, plastic deformation and tribochemical reactions are the main reasons that affect the topography variations of the surfaces in boundary lubrication. Therefore a robust Finite Element Analysis needs a constant variation of meshing near the surfaces that will increase the computational time significantly. In addition, due to the difference in scale size of the surface roughness with the contacting body, simulating surface roughness is difficult in FEM. Because of these problems, attempts have been made to calculate wear and eventually ignore the changing geometry. Some

of more robust studies tried to change the geometry for each time step and used some new methods of changing the mesh or remeshing the geometry (80, 114, 115).

Figure 4-10 shows and example of the Finite Element Method model configuration for capturing boundary lubrication. They proposed a theoretical wear model for approximation for the volume of a potential wear particle that can be detached from an elastic-plastic sphere. The novelty of the work was that they did not use any empirical coefficient of wear for the calculations. They also proposed an empirical relationship for predicting the coefficient wear.

Hegadekatte *et al*. (114) introduced a numerical method to simulate wear via the Finite Element Method (see Figure 4-11) . They used a post-processing FE package along with the commercial software, ABAQUS, to calculate the contact pressures and surface deformations of two contacting bodies and then employed Archard's wear equation to calculate wear. A new method for refining mesh on the surfaces was introduced which enabled a good discretization across the contacting surfaces.

These methods are very time consuming and computationally expensive. It should be remembered that all these attempts were for simulating wear or friction only for dry contacts. Boundary lubrication and the processes going on at the surfaces of tribological contacts are heavily influenced by microscopic and nanoscopic properties of both surface and lubricant additives. Real surfaces are rough and the roughnesses have to be captured on the nanometre or micrometre scale.

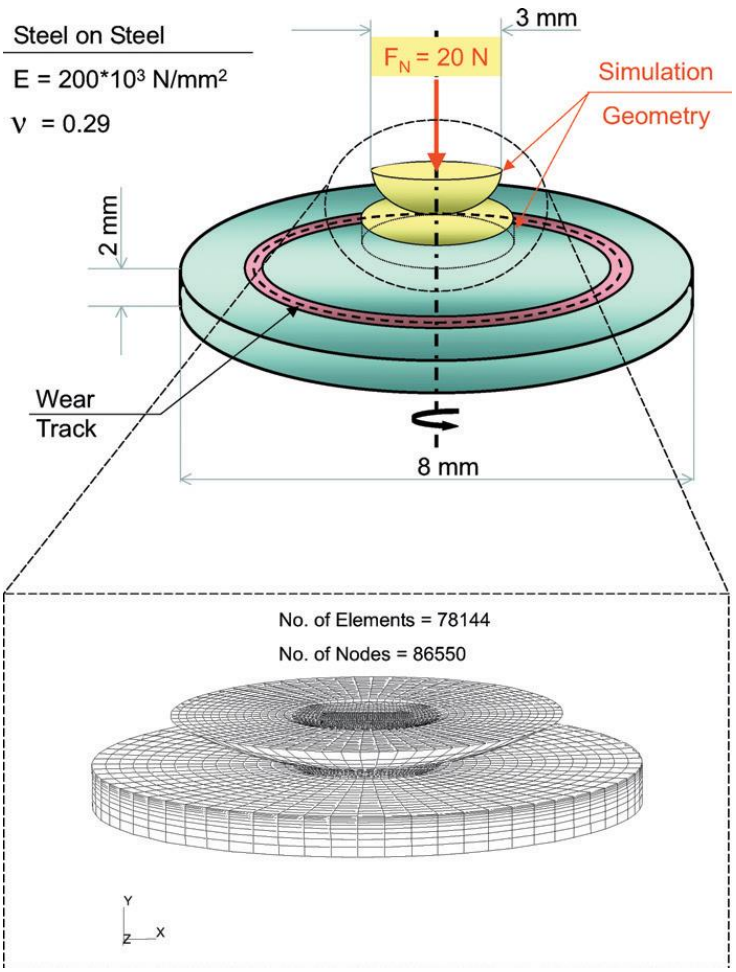

Figure 4-11 Finite element model using remeshing for deformed geometry (114)

This is very difficult in FEM because of the requirements for very fine mesh size. In addition, wear is a phenomenon which happens at local asperities and the geometry of local surface points has to change at a very small scale. It is also very difficult to capture in FEM because the geometry has to change continuously and the body should therefore be remeshed. These are only the complexities allocated with capturing wear and the moving boundaries allocated with that. In boundary lubrication the tribofilm is formed and at the same time removed (64, 117) while the sliding happens. Therefore the geometry of bodies at the surfaces is changed not only because of wear but also due to tribofilm growth.

4.2.3 Discrete Element Method (DEM)

Understanding the behaviour of particles is of great importance in many systems such as granulation, compaction and fluidisation systems. The common problems encountered in studying such systems are parameters which can not be easily measured or quantified experimentally, unavailability of materials, expensive experimentations and difficulty in sensitive analysis. For these reasons, modelling of small particles in such systems gives a very good understanding of the processes.

The macroscopic behaviour of bulk is governed by microscopic behaviour of small particles. The principle of DEM was introduced by Cundall *et al*. (118). In this technique the Newton's law is used to show the particle motion and interaction of particles in an assembly. It is assumed that in each time step the velocity of the particles is constant and the position of the particle is updated in each step. A good review of application and formulations of DEM is available in (119, 120).

Recently only very few works have been done on contact of rough surfaces by DEM and to the best of author's knowledge there is no work done on tribochemistry of rough surfaces using DEM (121).

Study of boundary lubrication is mainly focused on interactions at the interfaces. These interactions can be asperity-asperity or asperity-additive interactions therefore microscopic scale behaviours are of great importance. DEM is an efficient way of capturing complicated geometries in small scales and also in capable of adapting to deformations in very small scales. Thus small asperity deformations as well as wear particles and tribofilm formation can be captured in DEM. There are some literatures about crack propagations in solids using DEM simulations (122-127). Recently some authors used DEM to calculate wear in a tribosystem for solid dry contacts (128).

They used mass balance principles to find the amount of detached particles from the surfaces. The particles were bonded together using physical bonds in a commercial software package. The idea behind these models is the ability of DEM to simulate real solid behaviours by bonding small particles (123-126, 129-133).

There has been some research effort focused on modelling contact problems using combined DEM-FEM by capturing the areas near the contact or force using DEM and areas far from that by FEM (134).

In summary, Discrete Element Method is a rapidly growing approach to model interfaces with different scales. It has advantages of small scale calculations of contact force and deformations. Roughness of surfaces can be ideally simulated by discrete particles and wear of materials can be directly calculated by detachment of particles from the bonds. On the other hand, similar to molecular dynamics, DEM is limitted with time and length scale and capturing the macroscale behvaiour of tribosystems is cumbersome via DEM. In addition, employing tribochemistry in DEM is complicated but not impossible. It can be a good area of study for boundary lubrication models if tribochemistry and its effects would be covered.

4.2.4 Boundary Element Method (BEM)

There is another alternative method for modelling boundary lubrication problems called the Boundary Element Method (BEM). The advantage of BEM compared to FEM is that BEM just considers the boundary of the systems and solving the problems only for a discretized boundary. Therefore the computational time for solving a boundary element problem is much less than finite element study of that continuum. In this case boundary of system is discretised into small elements which show the surface of the material. An example of the discretization is shown in Figure 4-12.

There are many studies in which BEM is used to capture contact mechanics of surfaces. They tried to investigate various parameters such as surface deformation, contact pressures, wear etc (17, 18, 56, 135-158)

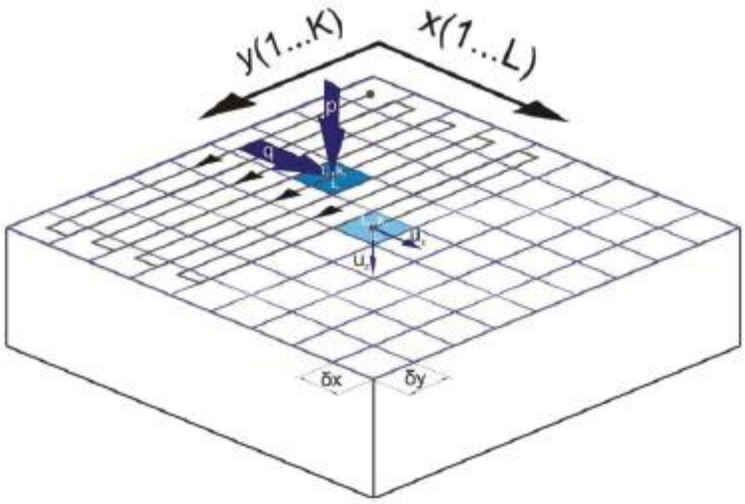

Figure 4-12 Discretised surface of a contacting body in BEM (156)

Some work has been reported on combining BEM and FEM to investigate some specific applications (156, 159). They mainly used FEM for calculation of the effect of tangential forces to extract the accurate influence matrix for contact mechanics simulations. An example of the FEM analysis in this combined approach to extract the tangential part of the influence matrix is shown in Figure 4-13.

BEM is a good and efficient method of calculating local contact properties of rough surfaces which is of great importance for studying boundary lubrication problems. Boundary Element Method will be employed in this thesis bacause of its efficiencies in solving the contact problem and its flexibilities to implement different physical

parameters. Various aspects of Boundary Element Method and the previous literature are reported in this chapter.

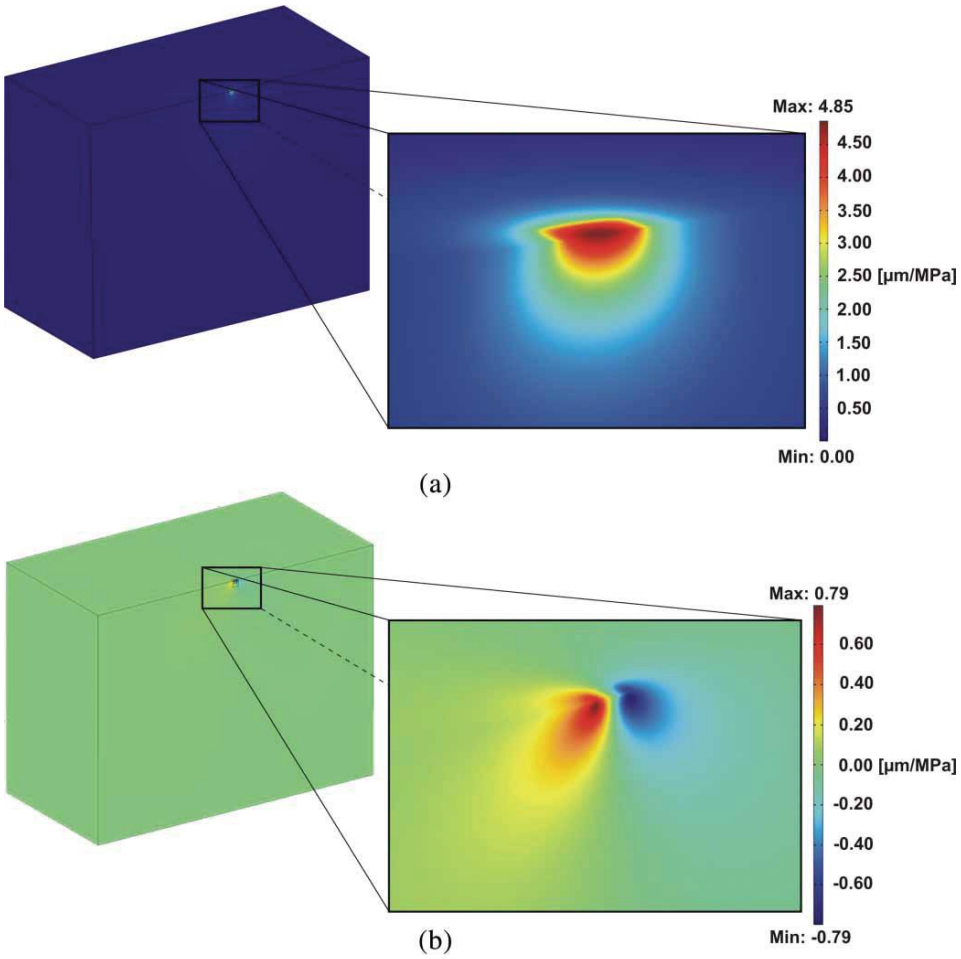

Figure 4-13 Finite element model for the influence coefficient calculation in a combined FEM/BEM model (156)

4.2.5 Surface Generation

For starting the contact mechanics simulations it is necessary to define surfaces with specific surface topographies. Therefore there are some choices to input the surfaces to the model. There are surface analytical instruments that measure the topography of surfaces and are able to produce a digitized topography map such as Atomic Force Microscope or Interferometers. A real surface can be put inside the instrument and surface maps can be obtained in 2D or 3D for further investigations. Another way of

generating the rough surfaces is to simulate the surfaces with mathematical methods such as employment of digital filters and random numbers. The advantage of the latter is that it enables the generating surfaces with defined topographical characteristics (160-165). An example of the digitized surface generated by means of digital filters using a low pass filter is shown in Figure 4-14.

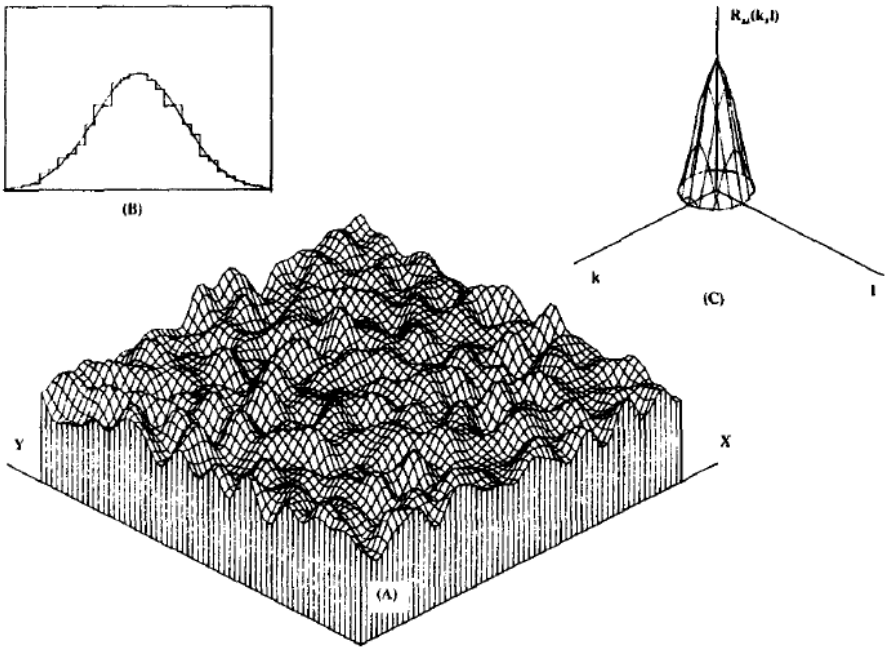

Figure 4-14 Three dimensional digital rough surface generated using low pass filter and random Gaussian numbers A) View of the surface B) height distribution of the generated surface C) autocorrelation function of the generated surfaces (160)

4.3 Contact Mechanics

As was discussed earlier, the boundary lubrication regime is a condition in which dry solid contact happens and asperities in both surfaces come in to direct contact. Therefore, study of forces and deformation in this condition is in the territory of contact mechanics. Contact mechanics is the mathematical description of what

happens in dry contacts. Contact mechanics studies go back to 19th century when Hertz developed a model for a simple elastic contact (166).

Hertz calculated contact pressure and deformation of an elastic contact. For this purpose a load was applied to surfaces and contact mechanics analysis started. As a result of load, each surface is deformed by $u_i(x_1, x_2)$. A gap between surfaces was considered and Equation 4-2 should be satisfied in the contact:

$$u_1(x_1, x_2) + u_2(x_1, x_2) + g(x_1, x_2) = \delta_1 + \delta_2 \qquad \text{Equation 4-2}$$

g is the gap between surfaces and $u_1$and $u_2$are the deformations of body 1 and 2. $\delta_1$and δ_2 are rigid body movements of surfaces 1 and 2.

Hertz calculated the contact pressure of $p(x_1, x_2)$ in the case of satisfying the above equation.

Greenwood and Williamson (78) developed a contact mechanics model for real rough surfaces. Their model was a mathematical modelling of contact mechanics based on probability functions using Hertzian contact equations for an individual asperity and generalised it to the whole contact. They considered the contact radius, area and load in terms of a single asperity radius and a compliance which was defined as the distance which points outside the deforming zone move together. They calculated the number of contact spots, total real contact area and load in terms of separation of surfaces mean planes. They proposed that the separation is proportional to nominal pressure and the number of contact spots and real area of contact only depend on load. Their

model was good for considering surface roughness in contact mechanics but it was mainly based on probability functions.

Later on, Stolarski (77) used a similar probability based approach in contact mechanics simulation for wear prediction. He used Archard's wear equation and proposed that probability of surface asperity contact is very important in probability of wear happening during sliding. Therefore the probability of asperity contact was the necessary condition for wear happening. He classified the asperity contacts into elastic and plastic contacts and mentioned that the adhesive wear only happens when the plastic contacts occurs. The real area of contact (A_r) was divided into area of elastic (A_e) and area of plastic (A_p) contact as follows:

$$A_r = A_p + A_e \qquad \text{Equation 4-3}$$

The adhesive wear in lubricated contact was modelled by Stolarski and two additional parameters were added to the model. The first parameter was fractional film defect which explains the metal to metal contact as the wear only happens where the asperities are in direct contact.

$$\beta = \frac{A_m}{A_r} \qquad \text{Equation 4-4}$$

in which A_m is the area of metal to metal contact.

The second parameter is to find a way to share the total load between the lubricant and the asperities in the contact. It was proposed that the only load contributing in wear is the part of load carried by asperities. The solution to this model was based on combining the contact between two rough surfaces and elastohydrodynamic model.

One of the interesting parts of this model was the ability to predict severe wear or scuffing. It was based on calculation of specific film thickness and plasticity index and then calculating the probability of scuffing by comparing the surface contact temperature T_s with critical lubricant temperature T_{cr}.

These contact mechanics models give very good insight of what happens during contact between two rough surfaces but as mentioned earlier they are not able to calculate the real behaviour of engineering surfaces deterministically.

In the case of real application analysis, we need to model a real 3 dimensional rough surface in contact. With the developments in computing systems and computational facilities a measured surface topography can be digitized and used in computer simulations as inputs (167).

Several numerical approaches have been used to computationally solve the contact of rough surfaces. The most widely used approaches are based on boundary element methods to solve elastic and elastic/plastic contacts both in 2 dimensional and 3 dimensional contacts. For small and moderate amounts of asperities in contact in 3 dimensional models finite element methods were used to calculate deformation of all contact points, contact geometry of rough surfaces and the pressure both in elastic and elastic/plastic contacts (168). For larger areas of contact in 3 dimensional conditions, the requirement of large amount of meshes makes the model complicated and difficult to calculate. Therefore some researchers used moving grid methods for reducing the amount of data storage and optimizing the calculation procedure (155). Their works were based on using the conventional inverse matrix solution for convergence of results so they had a large influence matrix and dealt a large amount of time for convergence.

Other works used the variational principle for the purpose of modelling 3 dimensional rough surfaces in contact. In the variational model, the real area of contact and contact pressure distributions for both elastic and elastic/plastic contacts are calculated from minimising the potential energy. Early works using variational principles were reported by Conry and Kalker (169, 170) but it was difficult for them to search the amount of minimum potential energy for all of the contact points.

Other researchers used variational principle by a quadratic mathematical programming which leads to a unique solution for 3 dimensional rough surfaces contact mechanics problems and also enables the researcher to consider larger amount of input points as contact points (145).

4.3.1 Variational Principle

As explained before, contact area is a very small fraction of nominal area of contact and it can be assumed that the asperity of the contacting bodies are in an elastic half space and the linear theory of elasticity is used in contacting areas. Contact mechanics problems are always described by differential equations. Finding the solution for boundary values of differential equations is similar to solving the minimum value of an integral equation. In solving contact mechanics problems and using a variational approach, there are two minimum integrals; one is the total elastic strain energy and the other one is the total complementary potential energy (171).

There are some reports using the latter one because it is suitable for solving problems of unknown contact pressure (170). When the problem is finding the unknown contact pressure and also the real area of contact for rough surfaces, it can be solved by minimizing the total complementary potential energy of the system. The diagram for the complementary potential energy is shown in Figure 4-15.

The complementary potential energy is given as Equation 4-5:

$$V^* = \int_D U_0^* \, \sigma dA - \int_\Omega u_i^* T_i dA \qquad \text{Equation 4-5}$$

Where U_0^* is the internal complementary energy density, D is the domain of deformation, Ω is the domain in which traction forces happen, T_i is the surface traction force and is a function of location. σ is the stress and the u_i^* is the prescribed displacement and are both the function of location. It should be noted that σ, $u_i^*$and $T_i$are scalars and function of location, $\sigma(x,y), u_i^*(x,y), T_i(x,y)$ respectively.

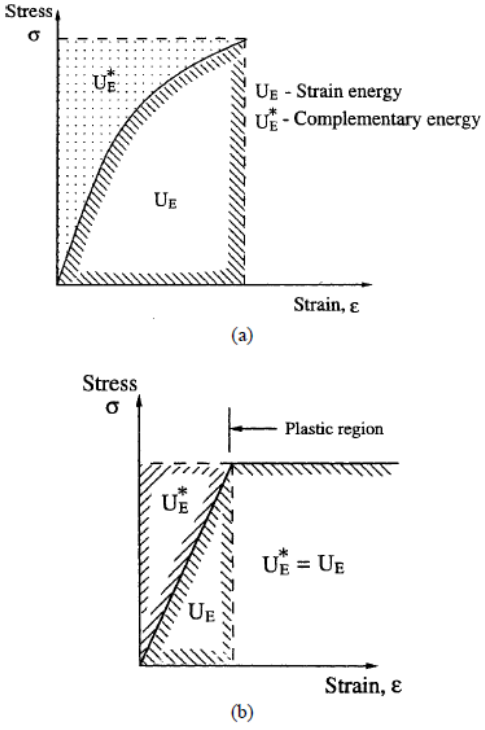

Figure 4-15 Definition of strain energy and complementary potential energy

(145)

For two rough surfaces the expression is given as Equation 4-6:

$$V^* = U_E^* - \int p(u_{z_1}^* + u_{z_2}^*)d\Omega \qquad \text{Equation 4-6}$$

$$= U_E^* - \int p\,\overline{u_z^*}d\Omega$$

In Equation 4-6, U_E^* is the internal complementary energy of two rough surfaces and the terms $u_{z_1}^*$ and $u_{z_2}^*$ are prescribed displacements of the two surfaces. In the case of two rough surfaces the linear elasticity assumption is made and the total complementary potential energy is equal to the elastic strain energy U_E and is calculated from the relation given as the following:

$$U_E = \frac{1}{2}\int p(u_{z_1} + u_{z_2})\,d\Omega = \frac{1}{2}\int p\,\overline{u_z}d\Omega \qquad \text{Equation 4-7}$$

Here $\overline{u_z}$ is the composite surface displacement and is equal to two rough surfaces deformation. So the total complementary potential energy converts to the following Equation 4-8:

$$V^* = \frac{1}{2}\iint p\overline{u_z}\,dxdy - \iint p\,\overline{u^*}\,dxdy \qquad \text{Equation 4-8}$$

Now for solving Equation 4-8 and finding the answers we need to have a relation between contact pressures and the deformations. This was solved and reported by Boussinesq (172, 173).

4.3.2 Boussinesq Potential Solution

The Boussinesq solution is for a half plane under a load distribution with traction forces. The solution will be given here and some expressions will be introduced. Indices q=1, 2, 3 show the directions in the axes x_q in Figure 4-16.

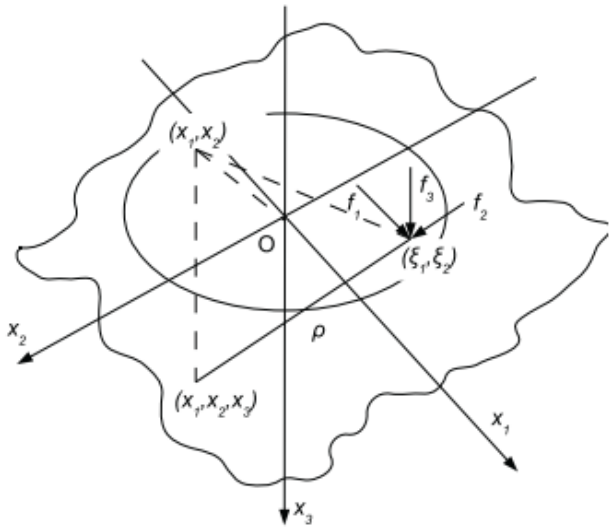

Figure 4-16 Point forces on the surface point (ξ_1, ξ_2) and surface deformation of the point (x_1, x_2, x_3) (174)

$$F_{1q} = \iint f_q(\xi_1, \xi_2)\Omega \, d\xi_1 \, d\xi_2 \qquad \text{Equation 4-9}$$

$$\Omega = x_3 \ln(\rho + x_3) - \rho \qquad \text{Equation 4-10}$$

$$\rho = ((x_1 - \xi_1)^2 + (x_2 - \xi_2)^2 + x_3^2)^{1/2} \qquad \text{Equation 4-11}$$

where F_{1q} is a potential function of the load f_q.

The elastic displacement component of each point of contact can be calculated from Love's equations (175):

$$u_1 = \frac{1}{4\pi\bar{G}}\left(2\frac{\partial F_1}{\partial x_3} - \frac{\partial F_3}{\partial x_1} + 2\nu\frac{\partial \Psi_1}{\partial x_1} - x_3\frac{\partial \Psi}{\partial x_1}\right) \qquad \text{Equation 4-12}$$

$$u_3 = \frac{1}{4\pi\bar{G}}\left(2\frac{\partial F_3}{\partial x_3} - \frac{\partial F_3}{\partial x_3} + (1-2\nu)\frac{\partial \Psi_1}{\partial x_3} - x_3\frac{\partial \Psi}{\partial x_3}\right)$$

The above equations can be solved if the traction forces are known. In order to simplify the problem tangential traction are assumed to be zero and the load becomes only P_3:

$$P_3 = \iint f_3(\xi_1, \xi_2)d\xi_1 d\xi_2 \qquad \text{Equation 4-13}$$

To calculate the potentials (normal load is the only load so $f_1 = f_2 = F_1 = F_2 = 0$) then:

$$\Psi_1 = \frac{\partial F_{1q}}{\partial x_q} = \frac{\partial F_{13}}{\partial x_3} = F_3 = \iint f_3(\xi_1, \xi_2)\ln(\rho + x_3)\, d\xi_1 d\xi_2 \qquad \text{Equation 4-14}$$

$$\Psi = \frac{\partial \Psi_1}{\partial x_3} = P_3\frac{\partial}{\partial x_3}\ln(\rho + x_3) = \frac{P_3}{\rho} \qquad \text{Equation 4-15}$$

$$\frac{\partial \Psi}{\partial x_3} = P_3\frac{\partial}{\partial x_3}\frac{1}{\rho} = -P_3\frac{x_3}{\rho^3} \qquad \text{Equation 4-16}$$

By substituting these equations into deformation equations, deformation at each point is calculated as:

$$u(x_1, x_2, x_3) = \frac{1}{4\pi\bar{G}}\left(\frac{\partial F_3}{\partial x_3} + (1-2\nu)\Psi - x_3\frac{\partial \Psi}{\partial x_3}\right)$$

$$= \frac{1}{4\pi\bar{G}}\left(\frac{P_3}{\rho} + (1-2\nu)\frac{P_3}{\rho} + P_3\frac{x_3^2}{\rho^3}\right) \qquad \text{Equation 4-17}$$

$$= \frac{P_3}{2\pi\bar{G}}\left((1-\nu)\frac{1}{\rho} + \frac{x_3^2}{2\rho^3}\right)$$

Considering the Hertz assumptions, x_3 is very small in comparison to x_1 and x_2 , therefore the deformation becomes:

$$u(x_1, x_2) = \frac{P_3(1-\nu)}{2\pi\bar{G}\rho_{x_3=0}} = \frac{P_3(1-\nu^2)}{\pi E}\frac{1}{\sqrt{(x_1^2 + x_2^2)}} \qquad \text{Equation 4-18}$$

By the assumption of distributed load $p(x_1, x_2)$ on the surfaces, the total deformation of the surfaces due to the load is as follows:

$$u(x_1, x_2) = \frac{(1-\nu^2)}{\pi E}\iint_{-\infty}^{\infty}\frac{p(s_1, s_2)}{\sqrt{(x_1 - s_1)^2 + (x_2 - s_2)^2}}ds_1 ds_2 \qquad \text{Equation 4-19}$$

Equation 4-19 relates the contact pressure to surface displacement and enables the contact mechanics problems of two rough surfaces with distributed load to be solved. In addition the composite displacement of two contacting surfaces is given by:

$$u(x_1, x_2) = \frac{1}{\pi E^*}\iint_{-\infty}^{\infty}\frac{p(s_1, s_2)}{\sqrt{(x_1 - s_1)^2 + (x_2 - s_2)^2}}ds_1 ds_2 \qquad \text{Equation 4-20}$$

$$\frac{1}{E^*} = \frac{(1-{\nu_1}^2)}{E_1} + \frac{(1-{\nu_2}^2)}{E_2} \qquad \text{Equation 4-21}$$

In a more accurate approach, the tangential forces can also be considered in the solution as the following:

$$\begin{aligned} & u(x_1, x_2) \\ & = \frac{1}{\pi E^*} \iint_{-\infty}^{\infty} \frac{p(s_1, s_2)}{\sqrt{(x_1 - s_1)^2 + (x_2 - s_2)^2}} ds_1 ds_2 \\ & + \frac{1}{\pi G^*} \iint_{-\infty}^{\infty} \frac{q(s_1, s_2)(x_1 - s_1)}{(x_1 - s_1)^2 + (x_2 - s_2)^2} ds_1 ds_2 \end{aligned} \qquad \text{Equation 4-22}$$

in which q is the tangential force in the contact spots. Therefore solving the problem of minimum complementary energy converts to solving the problem of unknown contact pressure.

As discussed earlier, many contact mechanics models studied the contact of two rough surfaces but not considering the tribofilm properties. Boundary lubrication modelling is greatly involved with tribofilm properties since the tribofilm formation and removal and its properties are significantly influencing the contact which has big effects on wear and friction reduction. Therefore tribofilm mechanical properties and the approach how to implement it into the contact mechanics will be discussed.

4.3.3 Tribofilm Properties

As explained in the previous chapter, the mechanical properties of the ZDDP tribofilm are difficult to define. Usually mechanical and chemical properties are linked and the

nano-mechanical properties of the ZDDP tribofilm are being referred to different behaviours of the short and long chain polyphosphates.

Bec *et al*. (45) suggested that tribofilms formed from ZDDP additives behave like smart materials. They found that the properties of the tribofilms layers are dependant of applied load and can adapt to conditions. They also showed that the mechanical properties of tribofilms vary from surface to substrate as shown in Figure 4-17.

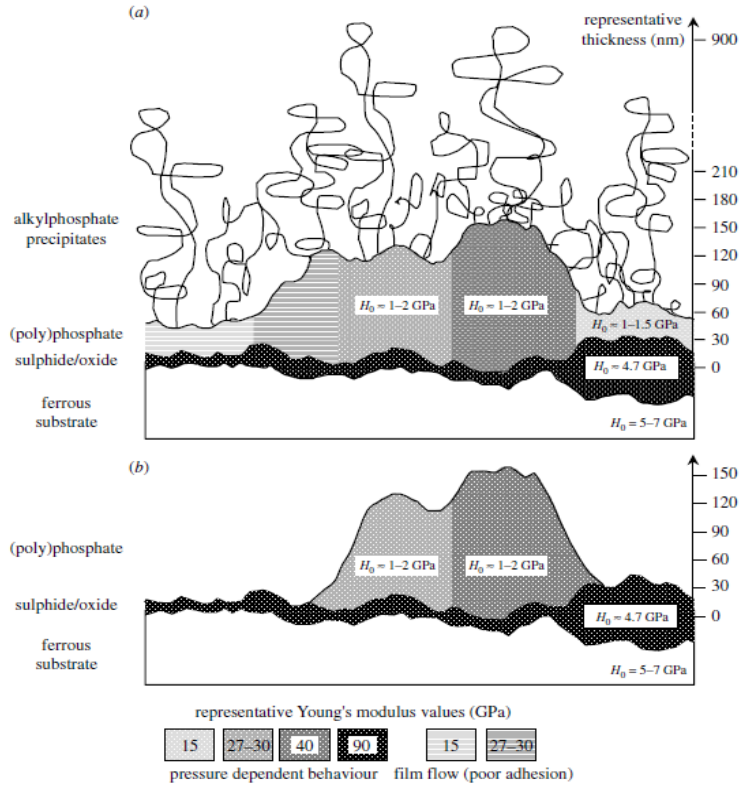

Figure 4-17 Zinc dialkyldithiophosphate tribofilm structure and its mechanical properties in various regions (45).

Demmou *et al*. (52) found that the pressure affects the elastic properties of the tribofilm and it will happen when the pressure exceeds a threshold amount of H_0. So for contact pressures below H_0 the elastic modulus is constant and after that it will

change by variation of hardness. The linear function of this relation is given as

$$E_f^* = \frac{E_{f_0}^*}{H_0} H \qquad \text{Equation 4-23}$$

Equation 4-23:

E_f^* is the film reduced modulus and $E_{f_0}^*$ is the constant elastic modulus before threshold pressure. $E_{f_0}^*$ was almost the same for all temperatures and equal to 39$\pm$4Gpa. H_0 was found to be dependant to temperature.

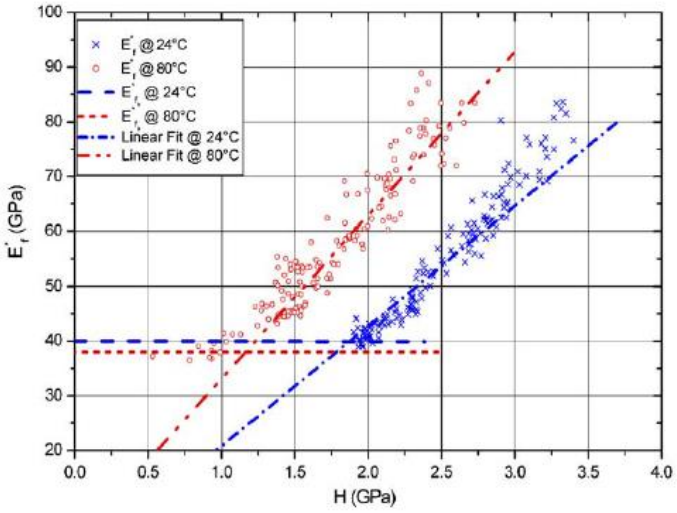

Figure 4-18 Variation of elastic modulus with hardness for ZDDP tribofilm (52).

In summary, assumptions for mechanical properties of tribofilm are obtained based on the previous studies of ZDDP or ZDDP/MoDTC tribofilm properties. ZDDP tribofilms have thickness values of 50-150nm and the mechanical properties change from surface of the film to bulk. The hardness at the surface is lower than the bulk hardness as when the penetration depth increases the hardness increases linearly. The

value of surface tribofilm hardness and tribofilm hardness near the substrate can be obtained from experimental results but the variations can be assumed to be between 1 to 4 GPa. In addition elastic properties of the tribofilm are also varying from surface to bulk and its variation is related to hardness variation of tribofilm as explained before (Figure 4-18). Variation of both elastic properties and hardness of tribofilm can be implemented in the numerical models using mathematical formulations.

In work by Andersson *et al*. (17, 176) variation of the hardness in depth of the ZDDP tribofilm has been numerically implemented into the contact mechanics model.

Variation of hardness from surface to bulk of tribofilm is assumed to be linear and is formulated as follow:

$$H(h) = H_{max} - (H_{max} - H_{min})\frac{h}{h_{max}} \qquad \text{Equation 4-24}$$

For considering the plastic deformation, a mathematical formulation should be used in order to consider the tribofilm hardness variations when the tribofilm deforms plastically. This model considers the two surfaces and their deformations and shows how the hardness is calculated in different deformation conditions. (See Figure 4-19).

$$\begin{cases} H_s - \dfrac{H_s - H_t}{h_{max}}\left(h' - U_p\right) & U_p < |h_1 - h_2| \\ H_s - \dfrac{H_s - H_t}{2h_{max}}\left(h_1 + h_2 - U_p\right) & |h_1 - h_2| \le U_p \le h_1 + h_2 \\ H_s & h_1 + h_2 \le U_p \end{cases} \qquad \text{Equation 4-25}$$

where H_s , H_t, h_{max} are the substrate's hardness, tribofilms surface hardness and maximum film thickness respectively. U_p is the plastic deformation and h' is the thicker of h_1 , h_2. The formulation shows that the deformation happens when the

material is softer and at the same time hardness of the tribofilm is calculated by the iteration between hardness and the thickness.

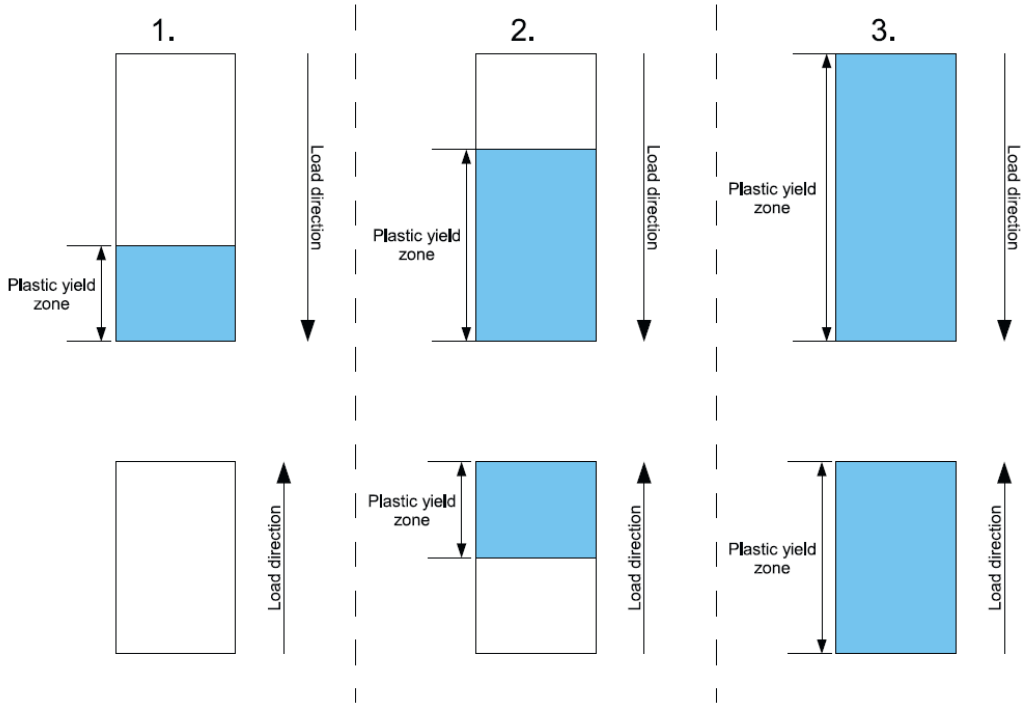

Figure 4-19 Hardness model for two surfaces with tribofilms in contact with three different possible cases. (1) The thicker tribofilm with lower hardness plastically deforms (2) both tribofilms deform plastically (3) the tribofilm plastically deforms to the point that it reaches the underlying material, the underlying material will also be plastically deformed in this case. (176)

4.3.4 Numerical Implementation

Predicting wear numerically is a very important engineering aim. Since wear mainly occurs in the boundary lubrication regime, it is important to predict different phenomena in this regime. Boundary lubrication is influenced by many factors such as temperature, sliding speed, load, surface mechanical characteristics, surface topography, oil and additives and chemistry of interfaces. Because of this complexity

in the nature, the majority of the investigations about the boundary lubrication are experimental research. However the experimental investigations in this field are of great importance, the full understanding of the mechanisms of boundary lubrication cannot be achieved only by these observations. On the other hand, analytical studies in boundary lubrication have several advantages that can in line with the experiments, help in better understanding the real mechanisms of boundary lubrication.

As many parameters are affecting the functionality of the systems in boundary lubrication, the numerical model covering the whole aspects needs to be comprehensive and is still under survey. It is also significantly important to find an efficient way to employ all the models and parameters to cover the boundary lubrication problem.

Examples of numerical implementation of different aspects of the boundary lubrication modelling in the literature are reported in the next section.

4.3.5 Contact Mechanics Numerical Implementations

In order to solve the problem of minimum complementary potential energy for contact mechanics problem (145, 173), surfaces are made in to small mesh elements as shown in Figure 4-20 and the contact pressure and deformation can be calculated for each element. As the mesh elements are small the contact pressure inside each element can be assumed as a constant. A simple flowchart of the contact mechanics algorithm is shown in the diagram of Figure 4-21. G is dimensionless gap and U is the dimensionless surface deformations.

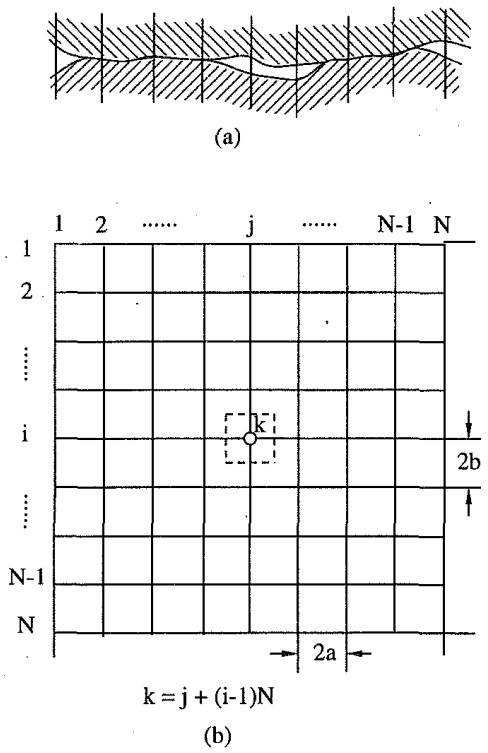

Figure 4-20 Schematic figure of surface mesh in the boundary element method in 2 dimensions a) front view of two surfaces b) top view of a surface (145).

In another work, Sahlin *et al*. (141) used an elastic-perfectly plastic algorithm for solving the contact problem. They used the same contact mechanics formulation for contact of rough surfaces but proposed a new approach for calculating the plastic pressures and the corresponding plastic deformations. Their numerical approach contained several steps as the following:

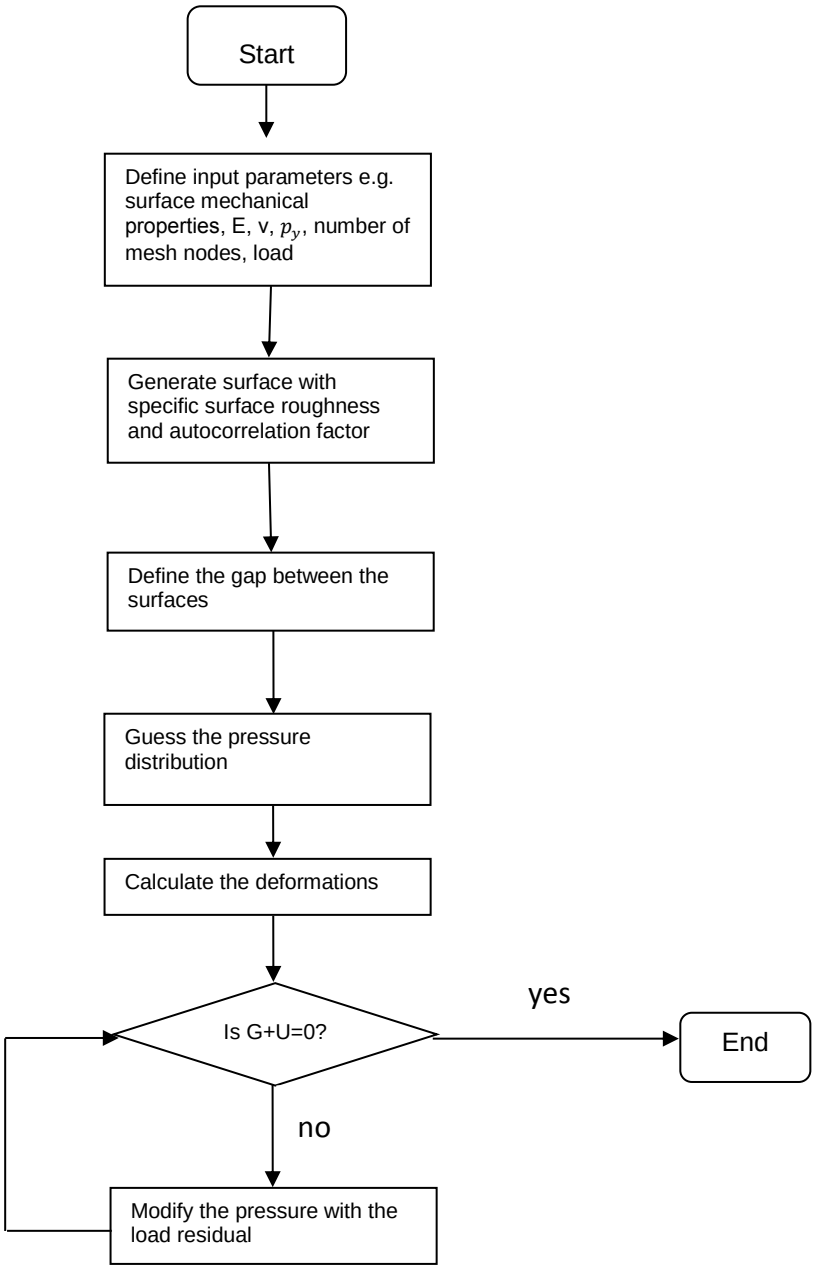

Figure 4-21 Schematic flowchart of contact mechanics simulation model used for capturing the contact mechanics of rough surfaces

1- Starting the contact pressure iteration by guessing a pressure distribution which fullfils the citeria for the load applied on the surface (summation of contact pressures is equal to the applied load)

2- Adjust the pressure by the elastically deformed roughness function

3- Update the pressure distribution by assigning $P_e = 0$ for negative pressures and $P_p = H$ for values more than the hardness of the material (it should be noted that the pressure distribution is not truncated at this stage)
4- Check if the new pressure distribution satisfies the load (see number 1)
5- Truncate the pressures $P_e = 0$ and $P_p = H$
6- Calculate the elastic deformations
7- Calculate the rigid body interference. It is very important to note that in this stage they assumed that only the points which experience the elastic deformation are included in the calculation. The points experiencing the elastic perfectly plastic deformations are not included because they freely float inside the contact plane)
8- Checking if the elastic deformations are the same as the rigid body interferences for the points that only experience elastic deformation
9- Calculate the plastic deformations by substratcting the elastic deformations from the rigid body interference.

4.3.6 Fast Fourier Transformation (FFT)

It has been reported in the literature that solving the contact mechanics problem using the matrix multiplications is computationally expensive especially for large amount of contact points. Using Fast Fourier Transforms helps to reduce the computational sampling points from $N^2 \times N^2$ down to $N^2 \log N^2$ (141). Stanley and Kato (177) employed an FFT based model for elastic contact of periodic random surfaces. They showed that because of the high numerical efficiency of FFT, their model is suitable for contact mechanics of rough surfaces especially when the number of sample points is large.

Later Liu *et al*. (148) studied the error source for utilizing FFT in contact mechanics problems and suggested that using discrete convolution and FFT should be used to avoid additional error. They studied different numerical approaches for employing FFT in contact mechanics calculations and showed number of methods that can be efficient for contact mechanics simulations.

In another work by Liu (178), they studied the issues corresponding to accurate calculation of contact problems using FFT. They showed that DC-FFT is very efficient for non-periodic contact problems and CC-FFT (Cyclic Convolution FFT) is more appropriate for periodic contact problems. Later, Almqvist *et al*. (140) used FFT for calculation of elastic-perfectly plastic contact of rough surfaces.

In summary, contact mechanics of rough surfaces can be calculated much faster by employing FFT for large amounts of surface points. There are some errors in using FFT for contact problems but using DC-FFT combined with variational principle reduces the error reasonably.

4.3.7 Frictional Heating and Flash Temperature

Friction occurs when two solid bodies slide against each other which can be due to various mechanisms at the real area of contact on both surfaces. During these processes the mechanical kinetic energy is converted to the internal energy of the solids and heat is dissipated at the interfaces. This heat can result in the temperature increase of the surfaces of the bodies. This produced heat which is known as frictional heating and the corresponding temperature increase in the contact can have significant effects on the tribological performance of the solids in the contact. The raised temperature can affect the chemical, physical and mechanical properties of the boundary films both in terms of their formation and their durability. Since the focus

of this study is on the boundary lubrication, calculation of surface temperature is important at local and global scales.

Considering two surfaces in contact, the rate of total energy dissipated in the contact is determined by the following equation:

$$q_{total} = \mu PV \qquad \text{Equation 4-26}$$

In which μ, P and V are the coefficient of friction, contact pressure and the relative sliding speed between surfaces respectively (179).

The maximum flash temperature rise for different shapes of contact areas with different pressure distributions have been studied by Blok (180), Jaeger (181), Archard (182), Kuhlmann-Wilsdorf (183), Greenwood (184), Tian and Kennedy (185) and Bos and Moes (186). In all of the theoretical studies, the temperature rise is calculated using the single heat source on a stationary or moving surface. The summary of all the expressions is reported in Table 4-1:

Table 4-1 Expressions for maximum flash temperature rise for various heat source distributions (179)

Shape of Heat Source	Heat Flux Distribution	Figure No.	Maximum Flash Temperature Rise (Steady State) Stationary or Low Speed Pe < 0.1	High Speed Pe > 10	Approximate Expression for All Velocities
Band	Uniform	6.7	$\frac{2qb}{k\sqrt{\pi}}$	$\frac{2qb}{k\sqrt{\pi Pe}}$	$\frac{2qb}{k\sqrt{\pi(1+Pe)}}$
Square	Uniform	6.10a	$\frac{1.122qb}{k}$	$\frac{2qb}{k\sqrt{\pi Pe}}$	$\frac{2qb}{k\sqrt{\pi(1.011+Pe)}}$
Circular	Uniform	6.5	$\frac{qa}{k}$	$\frac{2qa}{k\sqrt{\pi Pe}}$	$\frac{2qa}{k\sqrt{\pi(1.273+Pe)}}$
Circular	Parabolic	6.10b	$\frac{3\pi\bar{q}a}{8k}$	$\frac{2.32\bar{q}a}{k\sqrt{\pi Pe}}$	$\frac{2.32\bar{q}a}{k\sqrt{\pi(1.234+Pe)}}$
Elliptical	Uniform	6.10c	$\frac{qa}{k\sqrt{Se}}$	$\frac{2qa}{k\sqrt{\pi Pe}}$	$\frac{2qa}{k\sqrt{\pi(1.273Se+Pe)}}$
Elliptical	Semi-ellipsoidal	6.10d	$\frac{3\pi\bar{q}a}{8k\sqrt{Se}}$	$\frac{2.32\bar{q}a}{k\sqrt{\pi Pe}}$	$\frac{2.32\bar{q}a}{k\sqrt{\pi(1.234Se+Pe)}}$

In Table 4-1, b is the width of the area of the contact and q is the frictional heating. Pe is the Peclet number and k is the thermal diffusivity.

4.3.8 Implementation of Wear Equation

Because of the importance of the prediction of the wear for the efficient running of many tribological systems there have been numerous attempts to model wear. There are almost 300 equations for wear/friction in the literature which are for different conditions and materials pairs but none of them can fully predict the wear based on first principles including the whole physics of the problem (187, 188). This is primarily due to the fact that in most wear processes there are multi factor effects and models struggle to capture all of the appropriate physics.

When sliding speed is low and load is limited such that seizure does not happen in the contact, it leads to delamination wear. Well known Archard's wear equation is used to describe this kind of wear (24, 25, 189, 190).

Archard's wear equation is based on the fact that wear volume is proportional to applied load and sliding distance and is developed for global conditions in a tribosystem. The coefficient of wear in this equation depends on the working conditions and is different for different experiments; therefore makes it difficult to fully predict the tribological applications.

Many works have used Archard's wear equation in different methods of numerical calculations such as FEM and BEM. There are some works that use Archard's wear equation in local calculations and try to calculate local wear in FEM (108, 109, 116, 191-193).

As the problem of wear is mainly related to surfaces of materials, using boundary element method is a reasonable approach for modelling the contact. There are several developed contact models using BEM and implementing Archard's wear equation as a local model in order to capture the surface topography changes in solid-solid contact and trying to calculate wear in local scales. As an example, implementation of Archard's wear equation in a contact mechanics model developed by Andersson *et al*. (139) is explained here.

They used a localized version of Archard's wear equation and calculated the wear depth using Equation 4-27:

$$\Delta h(y) = k.\frac{1}{M.\Delta x}\int_0^L P(x,y)dx.\Delta t.v \qquad \text{Equation 4-27}$$

In which L shows the length of the entire contact, M is the amount of grid nodes, Δx is the length of one grid in the direction x (Figure 4-22). Δh represents the amount of wear depth at every point over the time step of Δt at a speed of v and P is the contact pressure.

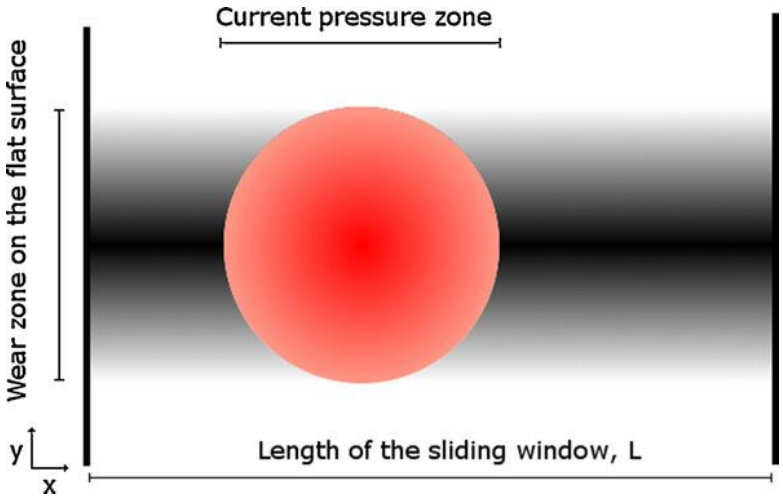

Figure 4-22 Schematic of the wear track and the pressure distribution for the calculation of wear depth (139)

4.4 Tribochemistry and the Film Formation/Removal Effect on Wear and Friction

The previous models in the boundary lubrication regime cover contact mechanics aspects. They calculate contact pressure and deformation of each point of asperity contact either in elastic or plastic contact. The models are able to calculate the real area of contact which is very important in the case of contact pressure and separating the elastic and plastic contact. These models do not consider the tribofilm properties which have a large influence on reducing friction and wear. One of the most important parts of the predictive models of wear and friction in boundary lubrication regime

which considers the tribochemistry phenomenon is the tribofilm formation/removal rate, the tribofilm thickness, its mechanical properties and the roughness of surface before and after the film formation. Therefore, contact mechanics models considering the tribofilm mechanical properties should be used for covering the contact simulation of surfaces in the boundary lubrication regime. The tribofilm properties are related to film thickness so the film growth models are of significant importance in the prediction model.

There is no developed local tribofilm growth model based on local mechanical, chemical and physical properties of contact in tribosystems so far but there are some studies that have tried to model tribofilm formation and removal. These studies and their results give some good insights of this complicated phenomenon.

4.4.1 Tribofilm Growth

There have been many investigations on tribofilm formation in boundary lubrication conditions for various additives added to the base oil. Both *in-situ* and *ex-situ* measurements have been carried out to investigate the various aspects of the tribofilm and especially its thickness.

One of the *in-situ* techniques for measurement of tribofilm thickness is Spacer Layer Interferometry Method (SLIM) (194) which can measure the tribofilm thickness during the time. Fujita and Spikes *et al*. (39) used this method to measure the ZDDP tribofilm thickness on steel surfaces. Their results show that tribofilm thickness will grow in overall during the time and it will reach a constant value after about 1 hour running. They also showed that specific film thickness which is an indicator of the severity of the contact plays an important role in tribofilm formation. They demonstrated that tribofilms are formed only in boundary regime when the specific

film thickness is low enough. Examples of these results are shown in Figure 4-23. Examples of images taken from the Spacer Layer Interferometer are also shown in Figure 4-24.

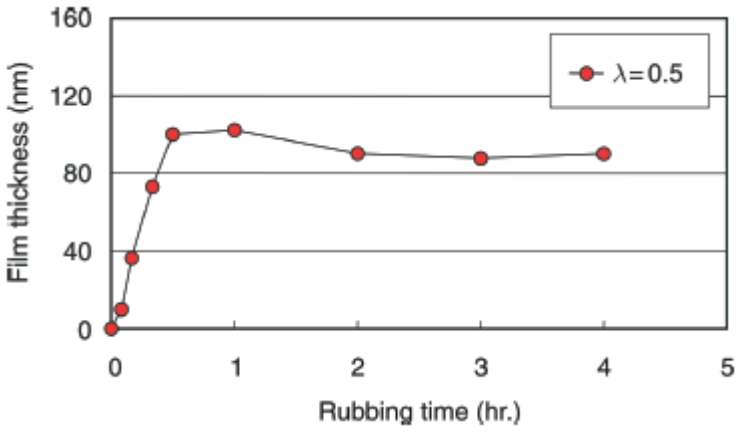

Figure 4-23. Growth of the ZDDP tribofilm by time for $\lambda = 0.5$ (39).

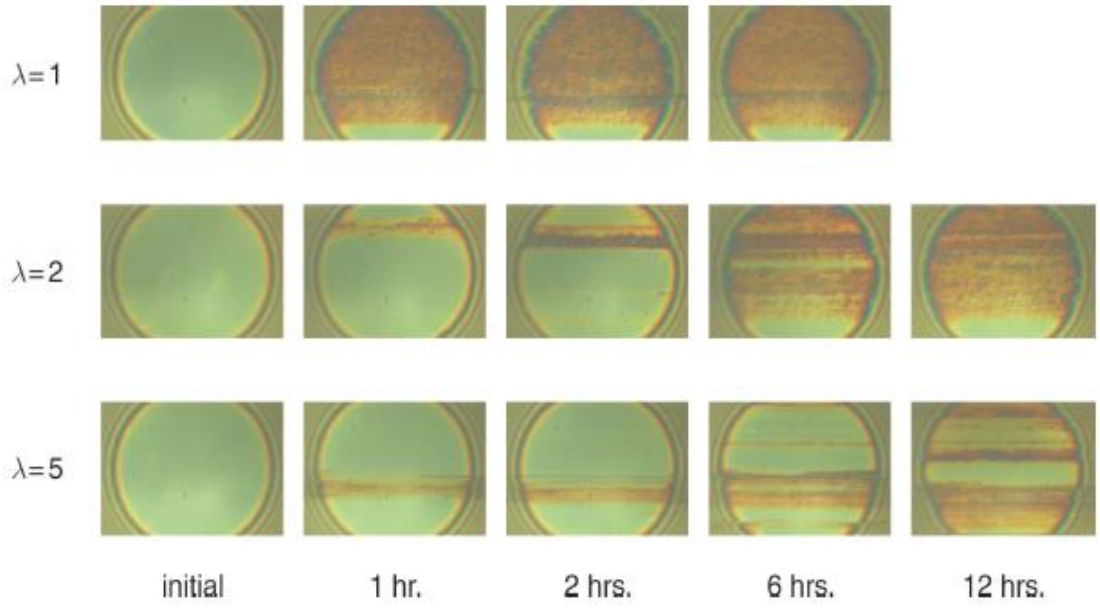

Figure 4-24 Images of the tribofilm formation during the time for different lambda ratios (39).

Naveira-Suarez et.al investigated *in-situ* film thickness by SLIM and then analysed the surfaces by AFM. They measured the tribofilm thickness, wear track width and average friction coefficient for four different types of ZDDPs during the time (1, 57).

Ji *et al*. (195) performed various wear tests of ZDDP additive in lubricant oil on cast iron surfaces. They investigated the changes of coefficient of friction, time of running in, final film thickness and amount of energy dissipation at rubbing contacts. The wear surfaces were then analysed using X-ray Adsorption Near Edge structures Spectroscopy (XANES) and AFM. They showed that the tribofilm thickness will vary with load and sliding speed. They also indicated that coefficient of friction, power dissipation and running-in time are varying with sliding speed and load. Some of the results are shown in Figure 4-25, Figure 4-26 and Figure 4-27.

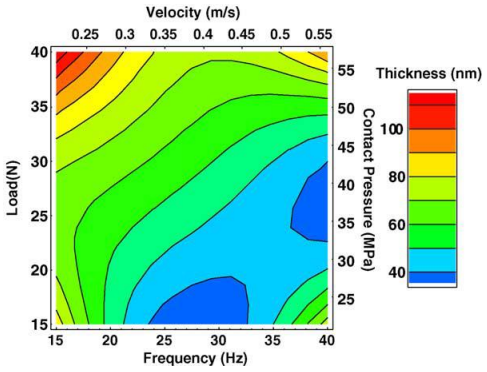

Figure 4-25 Tribofilm thickness variations by sliding speed and contact load (195).

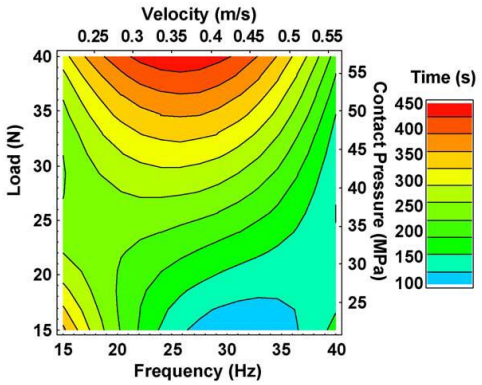

Figure 4-26 Running in time variation by sliding velocity and applied load (195).

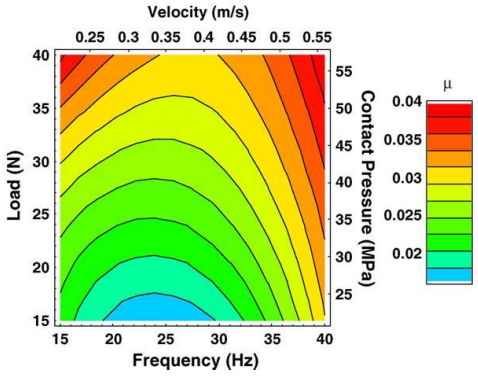

Figure 4-27 Coefficient of friction variations by sliding speed and load (195).

Taylor *et al*. (38, 44) investigated the ZDDP tribofilm formation on rubbing surfaces. They obtained a 3D map of the tribofilm formed on sliding surfaces by SLIM and investigated the morphology of tribofilm during rubbing (See Figure 4-28). They showed that how ZDDP affect the coefficient of friction during mixed and boundary lubrication regime. They proved that the tribofilm is only formed on sliding tracks by setting up an experiment with ZDDP solution in 150^0 C with ball and disc in stationary contact. They reported that almost no tribofilm was formed on surfaces (38).

Yin *et al*. (41) investigated the chemical nature of ZDDP films formed on the steel surfaces. They demonstrated that rubbing time affects the chemical composition of antiwear films. Also concentration of ZDDP, temperature, load and surface characteristics affect the tribofilm formation and its chemical composition (Figure 4-29).

4.5 Tribofilm Formation and Removal Models

There are a few models showing the tribofilm formation as a function of the time. Some of these models are introduced and a detailed discussion is presented in order to see the advantages and disadvantages of each model for comparison reasons.

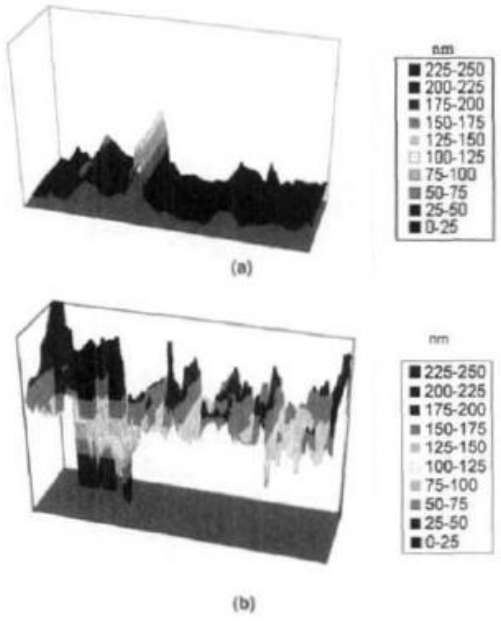

Figure 4-28 Spacer layer interferometry making 3D image of the tribofilm (38).

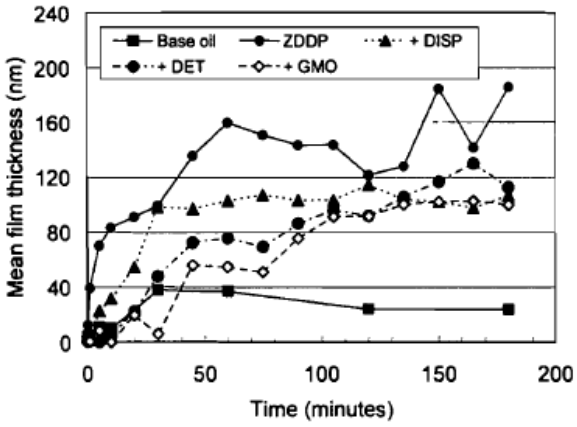

Figure 4-29 Evolution of mean film thickness in time for base oil and ZDDP, dispersant, GMO, detergents added to it (41).

4.5.1 Fujita's Model

In Fujita's model, the tribofilm formation and removal is modelled in terms of temperature and time and the constants of the equations are calculated by fitting the experimental results in to their model (196). The temperature used in Fujita's model is the lubricant bulk temperature and this is one of the significant differences between this model and Andersson's.

Spikes assumed that ZDDP film formation is due to gradual coverage of the surface by the individual pads. They proposed four different models for film formation and considered an induction time for the initiation of the film formation. The strength of these models is the good agreement with their experimental results of film formation and also considering film removal as a result of rubbing.

Their simplest model which assumes that the rate of film formation is proportional to the area of surface that is not covered with tribofilm is as follows:

$$h_{mean} = h_{max}(1 - e^{-k_1(t-t_i)})$$ Equation 4-28

Where h_{mean} is the tribofilm height at each time and h_{max} is the maximum film thickness. k_1 is the equation constant and should be determined from fitting to experimental results. In their model, the constant and also the maximum film thickness are determined from their own experimental results and the curves had very good agreement with experimental results. It was found that maximum film thickness ($h_{\max}$) changes with the temperature (T) as follows:

$$h_{max} = 0.87T - 210$$ Equation 4-29

And k_1 is related to the ZDDP concentration; the rate will increase by increasing the concentration and it has the relation to $(concentration)^{0.5}$. Considering the film removal and the relationship for film removal, the model for kinetics of this process can be obtained. The relationship for film removal is proposed as follow:

$$h_{mean.r} = h_{max}(X_0 + \left(\frac{k_5 t}{n-1} + \frac{1}{(1-X_0)^{n-1}}\right)^{\frac{-1}{n-1}})$$ Equation 4-30

Equation 4-30 is very close to the experimental results when the n=4. The values of k_5 and X_0 are in tables provided by author which are calculated by fitting the experimental results. The net film formation rate will be achieved by adding the two equations of formation and removal.

4.5.2 Andersson's Model:

Andersson *et al*. (17) used an Arrhenius type equation for their model and assumed that the tribofilm is formed as a result of chemical reaction between substrate and the lubricant fluid (17). The tribofilm is assumed to grow only in sliding contact areas. The film growth equation is defined as follows:

$$\left(\frac{dh}{dt}\right)_{growth} = C_4(h_{max} - h)k(T) \qquad \text{Equation 4-31}$$

$$k(T) = C_1 e^{\frac{-C_2}{T}} \qquad \text{Equation 4-32}$$

where the left hand side of Equation 4-31 shows the film growth. C_1, C_4, C_2 are the equation constants and h_{max} is the maximum film thickness during sliding. The temperature in this equation is the reaction temperature which is the asperity-asperity contact temperature. Therefore, the temperature would be a combination of flash temperature and bulk temperature as follows:

$$T = T_{flash} + T_{bulk} \qquad \text{Equation 4-33}$$

The flash temperature can be proportional to the local friction heating (17).

$$T_{flash} = D(\mu pv)^r \qquad \text{Equation 4-34}$$

where D is the equation constant and r is the exponent and for Peclet numbers below 5, r can be assumed as 1.

The tribofilm formation of Equation 4-31 can be converted into a finite difference equation in order to allow using this formula in the finite element analysis. Finite difference form of the equation is as follows:

$$h_{n+1}(i,j) = h_n(i,j) + \Delta t C_6 (h_{max} - h_n(i,j)) e^{\frac{-C_5}{\mu v p_{n(i,j)}}} \quad \text{Equation 4-35}$$

Equation 4-35 allows calculating the film thickness of each point of the sliding contact under boundary lubrication continuously during the sliding time.

The constants of Equation 4-35 should be extracted from experiments. So the first part of this work is to collect the experimental data to find h_{max}, C_5, C_6 for the above equation. The experiment needed for calculating these constants is an experiment in which the *in-situ* measurement of film thickness is carried out. The advantage of that model is the ability of implementing the formation model for local scale studies. The local properties of the contact between rough surfaces can result in local formation of the tribofilm on the asperities. One of the aspects that was not included to their model was the removal of the tribofilm.

4.5.3 Diffusion Model:

So *et.al* (197) modelled a theory for ZDDP and its antiwear mechanism at elevated temperatures in boundary lubrication conditions. The theory consists of physical and mechanical models. There was an elastic model for prediction of run-in and the critical thickness of the chemical film. The growth of the tribofilm was predicted with a diffusion model after the formation of the chemical film.

The effect of various parameters such as temperature, surface characteristics and kind of ZDDP on the growth of tribofilm was modelled.

It was suggested that based on experimental results the formation of chemical tribofilm consists of three main processes. Firstly, when the temperature reaches a specific value, ZDDP starts to decompose. Secondly, the decomposed ZDDPs are chemically adsorbed to the rubbing surfaces. Eventually these chemically-adsorbed species react with the surface and form tribofilms.

They suggested that because of complexity of chemical reactions happening during sliding, the compounds cannot be identified separately. The author described the chemical reactions by physical concepts and models of diffusion. In this diffusion model they considered the diffusion concentration of all elements instead of considering each element individually. The diffusion model used in this paper is based on moving boundary diffusion models proposed by Danckwerts and Booth (198). The equation for film thickness of chemical reaction film is as follows:

$$h = kC_r \exp\left(\frac{-Q}{RT}\right) k_d t^{\frac{1}{2}} \qquad \text{Equation 4-36}$$

in which k and Q are expressing the concentration of ZDDP as Arrhenius equation and C_r is the surface characteristics coefficient and the expression for k_d is:

$$k_d = (\frac{2DC}{W\rho})^{\frac{1}{2}} \qquad \text{Equation 4-37}$$

where W is the mass fraction of diffusion substances, ρ is the density of compounds, D is the diffusion coefficient and C is the concentration of diffusion substances at time t and $h = 0$.

The coefficient of diffusion can be expressed in terms of temperature:

$$D = D_0 \exp\left(\frac{-E}{RT}\right)$$ Equation 4-38

where D_0 and E are frequency factor and activation energy of diffusion respectively.

The constants of Equation 4-36 are calculated from curve fitting results. k_d is calculated from the diagram of thickness versus $t^{\frac{1}{2}}$. In addition, Q and C_r will be calculated from writing the logarithmic equation of:

$$\ln\left(\frac{k_d t_c^{\frac{1}{2}}}{h_c}\right) = \frac{Q}{RT} - \ln(kC_r)$$ Equation 4-39

By plotting the $\ln\left(\frac{k_d t_c^{\frac{1}{2}}}{h_c}\right)$ versus $\frac{1}{T}$ the constants can be calculated from the slope of the line.

All these diffusion equations for calculating the film thickness should be discretized to be used in the numerical models.

4.5.4 Turing (Diffusion-Reaction) Systems:

Friction in sliding contacts will results in irreversible energy dissipation. In certain conditions, this friction can induce self-organisation or formation of some patterns. These self-organised patterns are called secondary structures which include many phenomena such as *in-situ* tribofilms and some surface topography changes or some interfacial patterns such as propagating stick-slip zones. Friction generates heat and heat can result in thermal expansion and it would lead to thermo-elastic instabilities. However friction is coupled with other effects like wear. In these cases the coefficient of friction can be dependent on various parameters such as load, sliding speed, temperature and surface characteristics.

Some studies investigated the possibility of occurrence of this Turing type patterns (199). Turing or diffusion-reaction systems show the changes in concentration of some chemical species with time because of some local chemical reaction coupled with diffusion. The patterns can be formed at interfaces during friction because of various parameters such as heat transfer, mass transfer, various tribochemical reactions and also wear. They considered two major things:

- Heat flow and corresponding matter flow
- Abrasion and corresponding flow of ions

It is applicable for flow of solvent and the temperature and pressure gradient are considered. They used the simulation data for showing the possibility of these pattern formations and calculated the pattern results and their figures.

It is obvious that in these mathematical models there is no contact mechanics involved or there is no way to involve contact mechanics. Investigation of Turing systems in this case only results in a general pattern of tribofilm formation at interfaces which is resulted from mathematical equations.

Results of pattern formation for two cases in which the Turing systems are justified by frictional heating and heat and mass transfer are represented in Figure 4-30 and Figure 4-31.

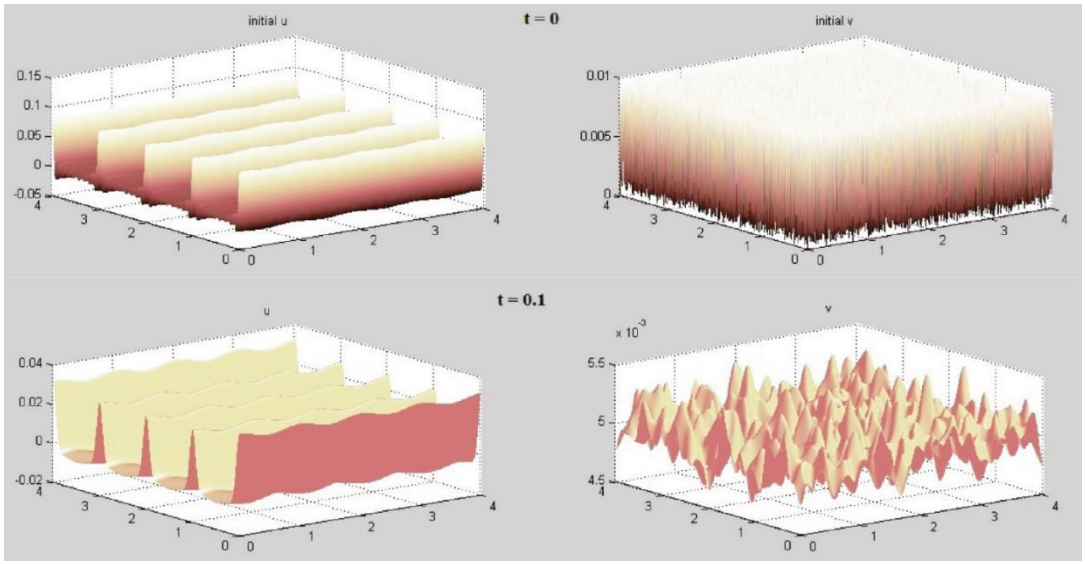

Figure 4-30 Pattern formation of dissipative structures at interfaces due to frictional energy dissipations with periodic pattern 1 (199).

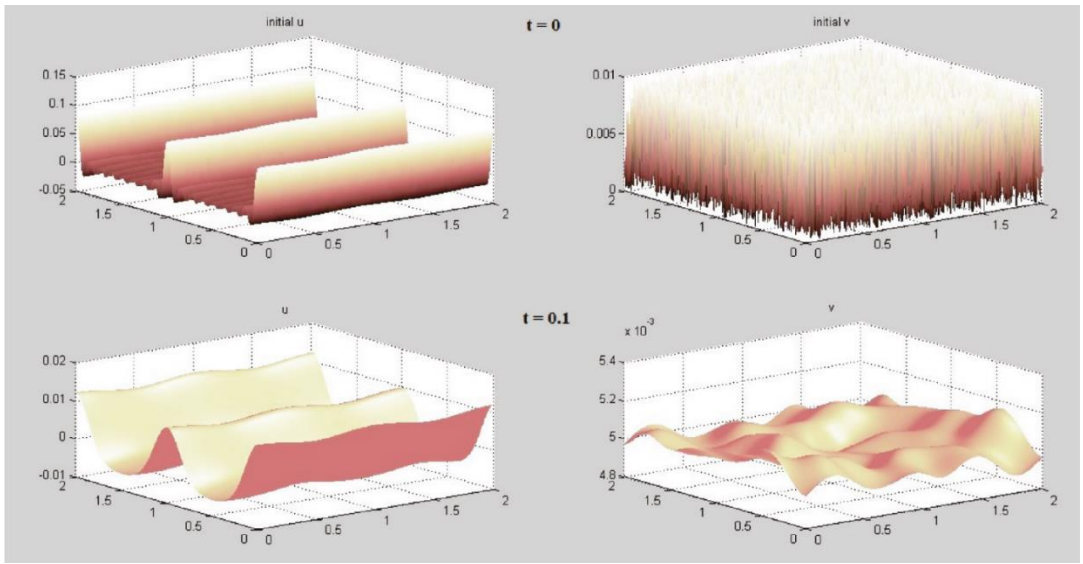

Figure 4-31 Pattern formation of dissipative structures at interfaces due to frictional energy dissipations with periodic pattern 2 (199).

4.6 Thermodynamics of Friction and Wear:

Friction is an irreversible process because of energy dissipation at interfaces. It is shown that this process changes and develops its own characteristics during the time. Energy is transferred during the friction process; therefore systems with friction can be regarded as thermodynamic systems. Friction is a non-equilibrium process which should be considered in non-equilibrium thermodynamics (200-202).

The main concept of irreversible thermodynamics is entropy and its generation. Changes in entropy production characterise the changes in process. Hence, friction and wear can be characterised by material and heat transfer –entropy change- of the systems. There are some structures formed in the interfaces during energy dissipation and material and energy transfer which are called secondary structures. These structures that form in non-equilibrium conditions of thermodynamics are also called dissipative structures and the process is called self-organization. The energy which would be spent on damaging the surfaces will be spent on forming these dissipative structures and that is why the wear rate drops significantly. Formation of surface tribofilms (secondary structures) is essential for energy dispersion. To obtain the minimum wear rate, the dissipation of energy should occur in the lowest entropy growth rate (203). It is shown that surface tribofilms store about 90% of total frictional energy.

4.6.1 Thermodynamic Analysis of Tribofilm Growth:

Some attempts have been made (204) for expressing the non-spontaneous chemical reactions($\Delta G > 0$) happening by friction induction and modelling the tribofilm formation and its growth from the thermodynamics point of view. In irreversible

thermodynamics, the dissipative function of $(\frac{dS}{dt})$ shows the entropy production of system due to internal sources in the system and is expressed as:

$$\frac{dS}{dt} = \sum_k J_k X_k > 0 \qquad \text{Equation 4-40}$$

Where X_k is the generalized force and J_k is the generalized flow resulted from the generalized force. For open thermodynamic systems with friction considering the tribochemical reactions occurring, the dissipative function can be expressed as:

$$\frac{dS}{dt} = -\frac{\overrightarrow{F_{fr}}\vec{V}}{T} + \frac{1}{T} A\dot{\varepsilon} \qquad \text{Equation 4-41}$$

In Equation 4-41 F_{fr} is the friction force, V is the sliding velocity, T is the temperature, A is the chemical affinity and $\dot{\varepsilon}$ is the rate of chemical reaction happening.

It can be shown that the rate of tribochemical reaction is independent of time in the case that tribo-activation is enough and it is governed by the sliding speed of surfaces. For expressing the dependency of rate of chemical reaction on moving speed, the theory of activated complex was used.

The activated complex is a system of destroying the old bonds and forming the new bonds in molecular level. For thermally activated chemical reactions the following expression is valid:

$$-\frac{dC}{dt} = k\vartheta[A^{\ddagger}] = k\frac{KT}{h}[A^{\ddagger}] \qquad \text{Equation 4-42}$$

C is the concentration of one of the original substances, $k$is the transmission coefficient, h is the Plank constant, $K$is the Boltzmann constant and $[A^{\ddagger}]$ is the concentration of activated complex.

For mechano-activated reactions passing through the surface of potential energy of these processes are independent of temperature. Therefore the rate of the tribochemical reaction is as follow:

$$-\frac{dC}{dt} = [A^{\ddagger}]\frac{V}{d} \qquad \text{Equation 4-43}$$

$$\dot{\varepsilon} = [A^{\ddagger}]V'\frac{V}{d} \qquad \text{Equation 4-44}$$

Where $[A^{\ddagger}]V' = n$ is the number of activated complex moles in the volume V'.

It can be easily understood that in these thermodynamic expressions for tribochemical reaction rates, the author tried to express tribochemical reaction rate in term of sliding speed and mechano-activation instead of temperature. They generally tried to investigate the tendency of tribochemical reactions (chemical affinity) in tribological systems based on thermodynamics principles.

As it is reported in many experimental and theoretical works, thermodynamics plays an important role in studying tribochemistry. Many results show that not only the flash temperature but also the entropy changes at interfaces are very important in occurring tribochemical reactions. Hence the tribochemical reaction and the tribochemical film growth models should consider entropy and the factors affecting the entropy of the system.

Recently there are some studies investigating the effect of mechanical rubbing on tribochemical reactions and they proposed a parameter to account for the effect of mechanical activation on the tribochemical reaction rate. The theory is discussed below.

4.6.2 Tribo-activation:

Bulgarevich et.al (205) presented a thermodynamic analysis of chemical reactions happening by friction in the interfaces based on energy, temperature and pressure. They showed that the adsorption films form on the rubbing surfaces by mechano-activated reactions rather than thermo-activated ones. They also demonstrated that heavy pressures in the contacts will affect the equilibrium absorption of low molecular weight additives and some high molecular weight additives to lubricants.

They considered endothermic and exothermic chemical reactions and investigated their reaction coefficients in various temperatures regarding their time of adsorption and Gibbs energy.

They indicated that even in high temperatures the effect of thermo-activation for chemical reactions is very low and Tribo-activation is mostly affecting the reactions.

They supposed that one of the most important parts of mechano-activation reactions in the contact zones is the dependency of population of transition state of the chemical reaction to mechano-activation process (206). In which, friction is shown to be a unique natural phenomenon that affect the happening of highly inverse transition states in chemical reactions. They also showed the expressions for thermo-activation and Tribo-activation which is as follow:

$$x_{tribo} = \frac{\sigma^2 d N_A V_m}{N_A V_m V_h}$$ Equation 4-45

$$x_{tribo} = \frac{3d}{16\pi\sigma}$$ Equation 4-46

$$x_{thermo} = exp\left(\frac{\Delta E}{RT}\right)$$ Equation 4-47

$$k_{thermo} = \frac{kT}{h} exp\left(\frac{\Delta E}{RT}\right)$$ Equation 4-48

In which σ, d, N_A, V_m and V_h are contact area diameter, thickness of monatomic layer, Avogadro number, mole material volume and half-sphere volume. Here, x_{tribo} and x_{thermo} are the effects of mechanoactivation and thermoactivation respectively. The terms x_{tribo} and x_{thermo} can be interpreted as the role of mechanoactivation and thermoactivation in inducing the tribochemical reactions. k and h are the Boltzmann and Plank's constant and ΔE, R and T are activation energy, gas universal constant and the temperature respectively.

They suggested a new chemical reaction constant based on both *tribo* and *thermo*-activation:

$$k_{tribo-thermo} = \frac{x_{tribo}}{x_{thermo}} k_{thermo}$$ Equation 4-49

Where x_{tribo} and x_{thermo} are the population of transition states of mechano-activation and thermo-activation. In the theory of activated complex they substituted all the equations in Equation 4-49:

$$k_{thermo} = \frac{kT}{h} exp\left(\frac{\Delta E}{RT}\right) \quad \text{Equation 4-50}$$

$$x_{thermo} = exp\left(\frac{\Delta E}{RT}\right) \quad \text{Equation 4-51}$$

$$k_{tribo-thermo} = \frac{kT}{h} x_{tribo} \quad \text{Equation 4-52}$$

It can be clearly seen that the rate constant of chemical reaction in this case is independent of activation energy and depends only on temperature. This equation can be discretised and used for numerical simulations.

As discussed before the tribochemical reaction rate is dependent on entropy change of the system and the term x_{tribo} can be used semi-analytically to extract information from the experiment. Therefore x_{tribo} should be a parameter which is affected by some other parameters that can change the entropy of the system. A study of this hypothesis and utilisation of the term x_{tribo} to develop a semi-analytical tribofilm growth model is used in this thesis and is reported in chapter 6.

4.7 Summary

Boundary lubrication is a complicated regime of lubrication concerned with multiscale physical, chemical and mechanical characteristics of interfaces. Therefore a full understanding of processes and interactions of surfaces and lubricants is very

difficult to achieve. A comprehensive modelling of boundary lubrication considering all these complexities is of great importance for engineers.

Different attempts for modelling boundary lubrication are reported in this chapter as well as different possible approaches to capture these models. The advantages and disadvantages of these approaches is also reported. It seems that Molecular Dynamics is a good approach to study the molecular interactions between lubricant additives and substrates at a very small scale. The biggest disadvantage of molecular studies is the limited computational efficiency and limitted time and length scales. Tribological applications are mainly dealing with long times and large amounts of loading cycles and such small scale investigations can not cover this important parameter. Finite Element Method is a robust method of calculating contact problems. It is limitted with surface roughness characteristics and implementation of wear equations due to small changes in the geometries. Because of the importance of small changes in the surfaces of contacting boddies due to wear, plastic deformation and tribofilm formation, FEM becomes inefficient in modelling boundary lubrication.

One suitable approach for boundary lubrication modelling is the Boundary Element Method. This method has the advantage of fast convergence for boundary problems. The wear, plastic deformation and tribofilm formation can be modelled by BEM as well as the convenient way of implementing surfacae roughness.

A comprehesive model of boundary lubrication needs a chemical and physical modeling of the tribofilm growth process. This is an unavoidable part of any boundary lubrication models since the tribofilm plays the significant role in characterizing the behaviour of the tribosystem. Some of the developed tribofilm growth model reported in the literature were introduced in this chapter.

Chapter 5. Development of the Contact Mechanics Model

5.1 Boundary Lubrication Modelling and Tribochemistry

As discussed about boundary lubrication and its characteristics, the lubricant does not provide hydrodynamic support for the load but it plays an important role of carrying the lubricant additives which react with the surface and form tribofilms. Therefore above the metal substrate there is a very thin layer of tribofilm formed (Figure 5-1) which is discussed briefly earlier in Section 2.3.4. This thin film prevents the substrate's direct asperity-asperity contact. These films are worn off during the sliding contact and formed again at the same time. Working conditions will affect the removal rate and also formation rate of the tribofilms. A good design of the boundary lubricated systems happens when there is a balance between film formation and removal.

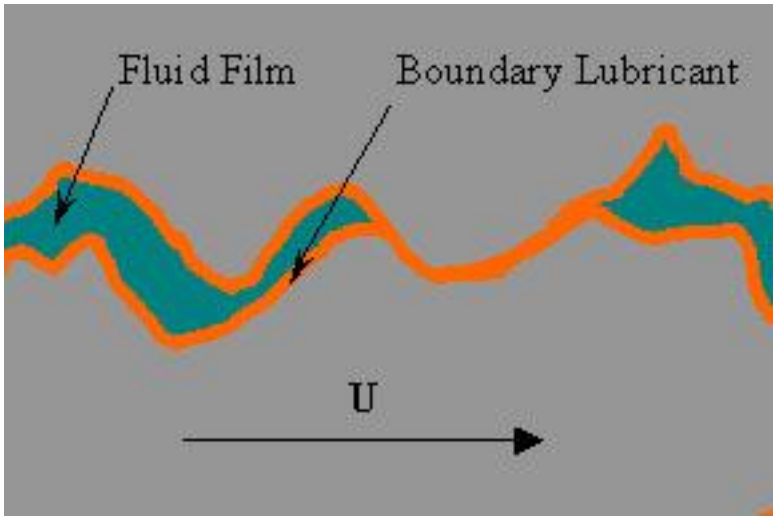

Figure 5-1 Thin layer of the tribofilm covering the contacting asperities

Therefore a robust modelling approach for boundary lubricated systems considering all of the mentioned characteristics is very difficult and is still lacking in the literature.

This framework should consider contact between rough surfaces and be able to analyse the load and deformations as well as temperature at interfaces. The model also should consider chemistry of the lubricant additives that can possibly react with the substrate to form the protective tribofilm. Consideration of the tribofilm should not be limited only to the reaction kinetics but also the chemical characterization of the tribofilm and its mechanical properties which in overall define the durability and behaviour of the tribofilm (See Figure 5-2). The removal and the durability of the tribofilm should be considered in the model which can affect the wear behaviour of the tribosystem. The mechanism in which this tribofilm forms and gets removed, should be considered in the modelling framework.

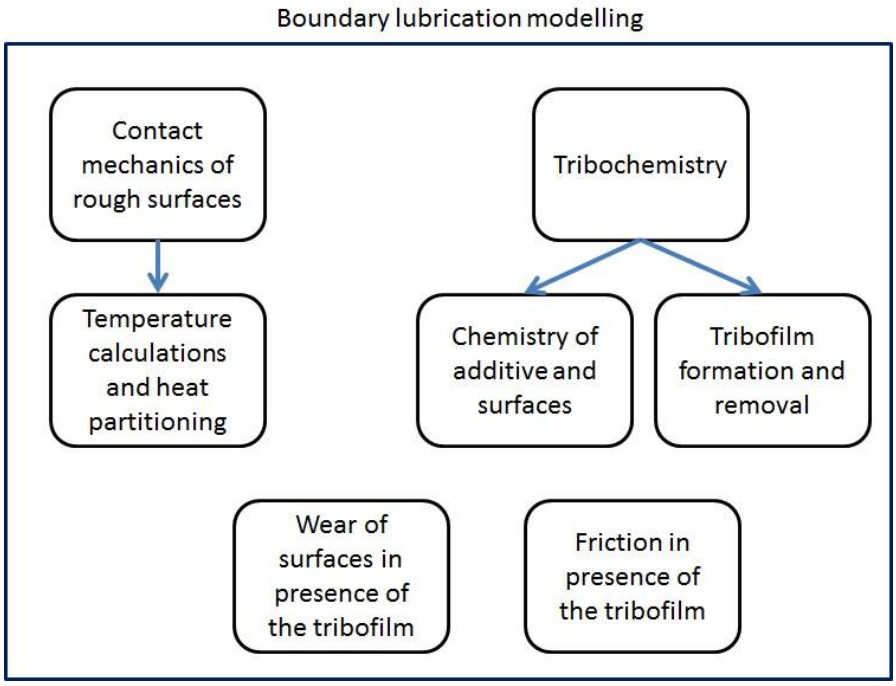

Figure 5-2 Boundary lubrication modelling framework and its constituents

Such a modelling framework needs a multiscale modelling approach ranging from *ab-initio* studies for covering the molecular interactions up to microscale interaction of

surface asperities and further up to components scale. This modelling approach will be cumbersome and analytically difficult.

In this thesis, a flexible contact mechanics model is developed which considers the elastic-perfectly plastic contact of rough surfaces. A growth model for the tribofilm is developed which considers both formation and removal of the tribofilm. The formation part of the tribofilm is based on the kinetics of the tribochemical reactions and the removal part is a phenomenological mathematical model to capture the behaviour. The local properties of the contact calculated by the contact mechanics model will be implemented into the tribochemical model to predict the growth of the tribofilm. A wear model is also proposed which can modify the local wear properties of the asperities. The whole numerical approach is schematically shown in Figure 5-3. Development of the contact mechanics, tribofilm growth and the wear model proposals are reported in Chapters 5, 6 and 7 of this thesis respectively.

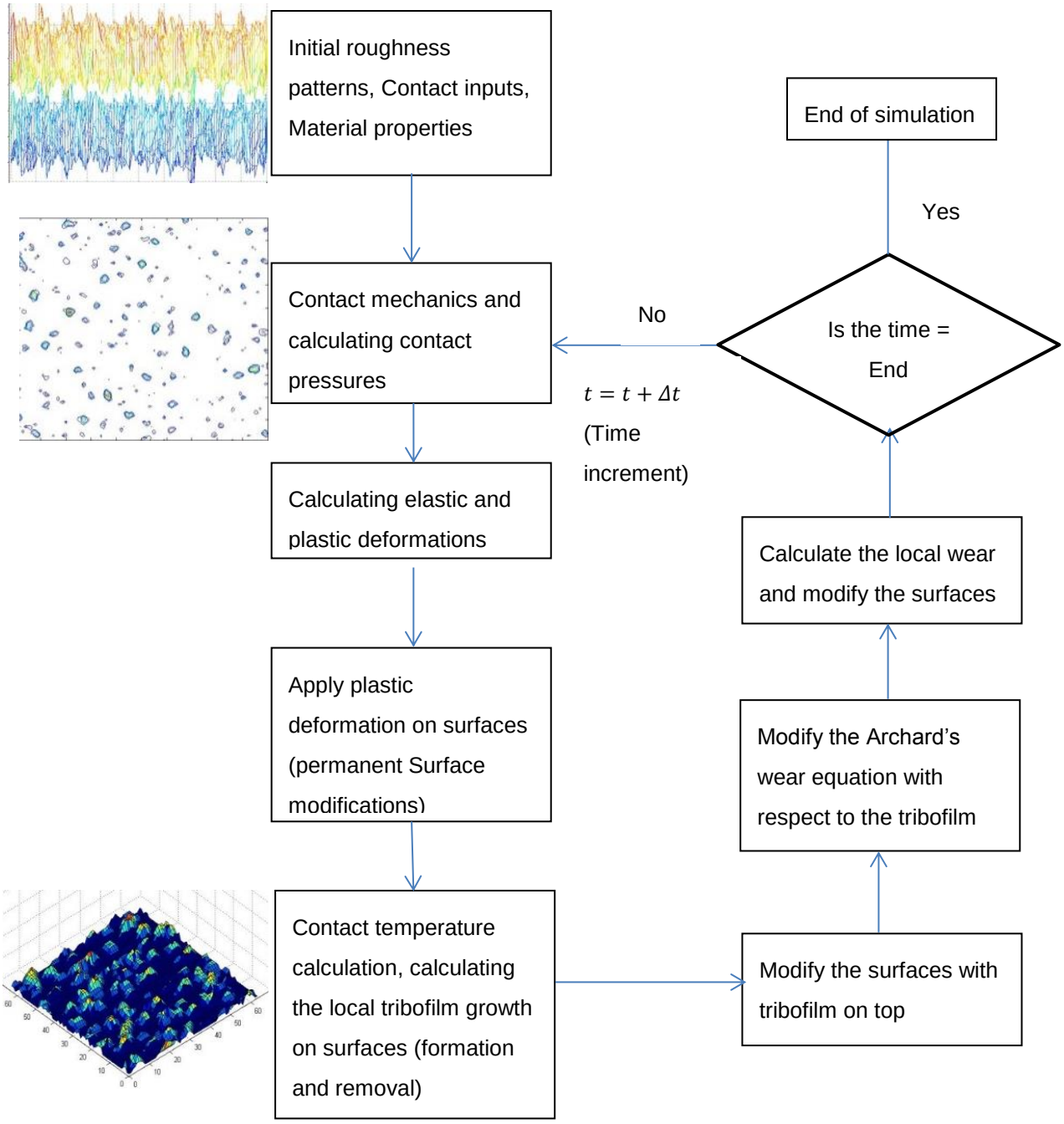

Figure 5-3 Schematic of the numerical approach in this thesis for modelling boundary lubrication considering tribochemistry

5.2 Introduction to the Contact Mechanics Model

Boundary lubrication is the lubrication regime in which direct contact of solid surfaces happens at their highest asperities and chemical reactions occur due to interactions with lubricant additives. Therefore contact mechanics is an essential area of study in modelling systems working in boundary lubrication. An extensive study of the literature on contact mechanics was discussed in the literature review of Chapter 4.

As tribochemical reactions are occurring due to asperity-asperity interactions as well as asperity-lubricant interactions, the study of contact at asperity levels is of great importance. Roughness of the interacting surfaces should be implemented into the study since roughness plays a key role in determining the severity of the contact. In order to study such problems, investigating the contact at the microscale and linking the system behaviour to macroscale is essential. The contact mechanics simulations used in this work are based on the model developed by Tian et.al (145). They used complementary potential energy method to solve the contact problem and find the true contact pressures and surface deformations. An elasto-plastic contact model is then used based on the model from Sahlin *et al*. (141). A new procedure for movement of surfaces in tribologically loaded conditions is proposed that can help in reducing the computation time.

The contact mechanics consists of four main components which are:

I. Random rough surface generation with specific characteristics
II. Elastic–perfectly plastic model of rough surfaces
III. Tribofilm properties implementation
IV. Movement of surfaces in combined rolling and sliding contact.

All these components will be explained in detail in this chapter.

5.3 Rough Surface Generation

To study the contact of rough surfaces deterministically, digitized surfaces should be used as inputs into the model. There are two different ways of digitizing surfaces. The first way is to use surface microscopes such as Atomic Force Microscope (AFM) which can give a 3D digitized map of the topography of a physical surface. Alternatively, surfaces can be generated using mathematical methods. The method used to generate surfaces is introduced by Hu *et al*. (160).

For generation of 3-dimensional rough surfaces, a specific autocorrelation function and also height distribution should be defined. Two dimensional digital filters are used for generating the 3-dimensional surfaces. By using random number generators it is possible to generate the filter inputs as Gaussian independent random numbers. The output would be obtained through the filtering operation and will give the sequence with certain autocorrelation function. It is mathematically proved that if the input numbers are Gaussian random numbers, the distribution will remain Gaussian after the filtering.

For two-dimensional systems, Finite Impulse Filters (FIR) are defined as:

$$Z(I,J) = \sum_{k=0}^{n-1} \sum_{l=0}^{m-1} h(k,l)\eta(I-k,J-l) \qquad \text{Equation 5-1}$$

In which $Z(I,J)$ is the output sequence and $\eta(I-k,J-l)$ is the input that is going to be filtered. $h(k,l)$ is the filter coefficient that is plotted in Figure 5-4. Most of engineering surfaces can be simulated using a low-pass filter in order to modify the

correlation aspects of the sequence. For generation of the isotropic surfaces, a 2-D symmetric low-pass filter is used in this work. The filter coefficient of this filter is formulated as the following:

$$h(k,l) = \alpha \frac{J_1(2\pi\alpha\sqrt{k^2+l^2})}{(K^2+l^2)^{0.5}} \qquad \text{Equation 5-2}$$

in which k and l are the lengths of the filter and J_1 is the first order Bessel function. α is the normalized frequency that can change the size of the asperities.

In this method, surfaces can be generated with different roughness (R_a or R_q) by changing the variance of the random numbers generated for the input sequence. An example of two surfaces with the same lateral asperity sizes but different R_a values is shown in Figure 5-5.

Another capability of this method is controlling the lateral asperity sizes. The α parameter in the filter coefficient is responsible for the number of grid points that can be present in a single asperity of the surface. An example of two surfaces with the same surface roughness (R_a) value and different α values (asperity lateral size) are demonstrated in Figure 5-6.

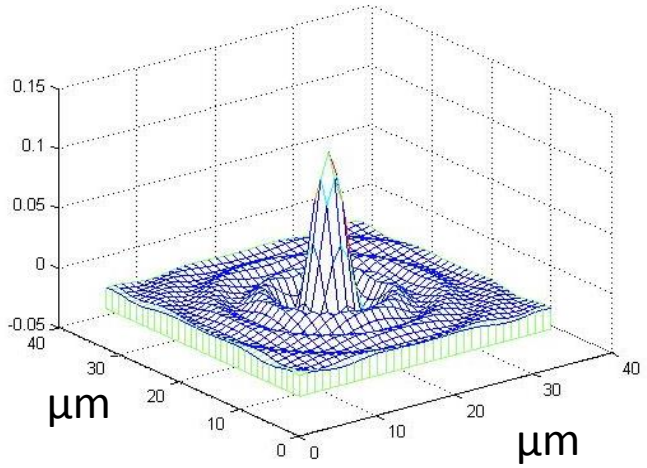

Figure 5-4 Filter coefficient for a circular digital low pass filter

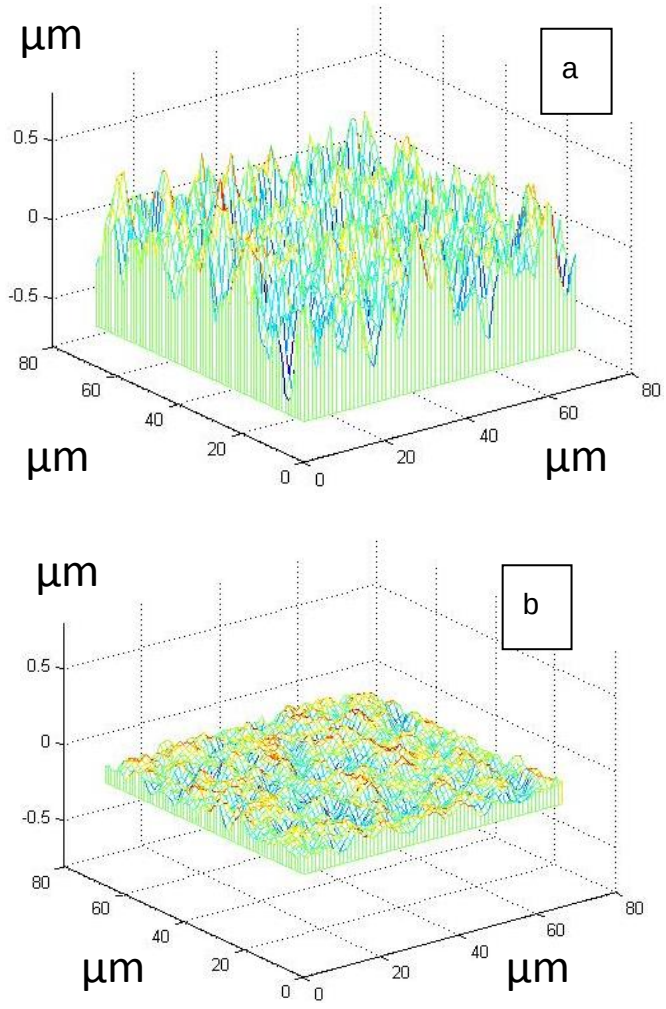

Figure 5-5 Three dimensional digital rough surface generated using low pass filter and random Gaussian numbers a) $R_a = 250\ nm$ b) $R_a = 25\ nm$

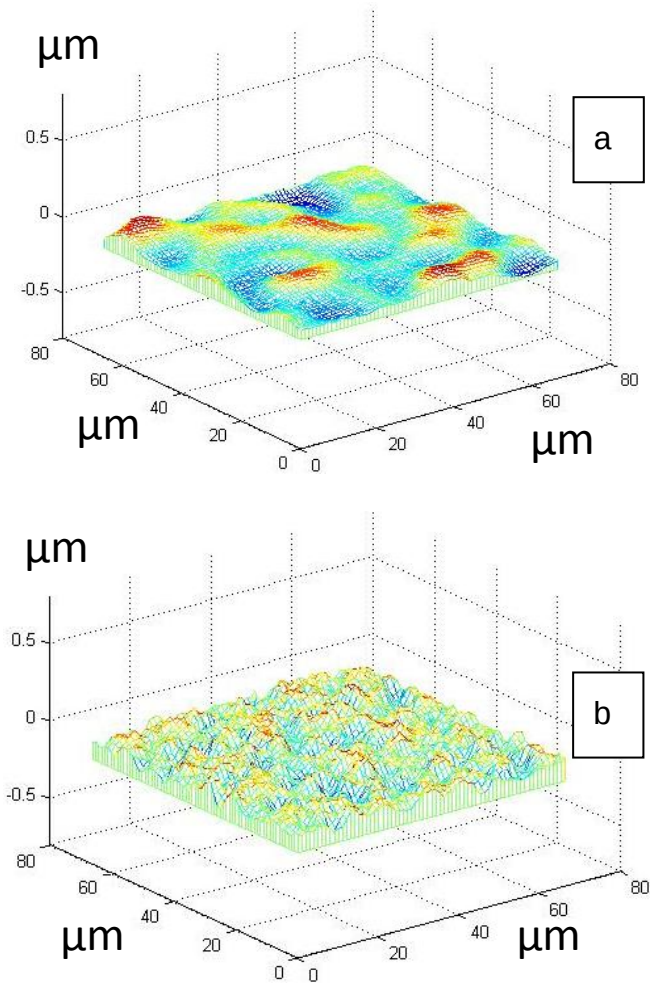

Figure 5-6 Three dimensional rough surfaces with $R_a = 25nm$ and different asperity lateral sizes a) $\alpha = 0.08$ b) $\alpha = 0.2$

This method enables varying surface roughness for studying the effect of roughness on contact of surfaces. As discussed before, surface roughness is an important parameter in the contact of surfaces in different scales, therefore this generation method gives the flexibility to generate different desired surfaces and investigating the surface effects in boundary lubrication. Surface generation is coded in MATLAB by the author.

5.4 Contact of Rough Surfaces

There have been many attempts at simulating the contact of rough surfaces in contact mechanics (140, 143, 150, 151, 154-157, 159, 169, 170, 207-209). The contact mechanics model developed by Tian and Bhushan (145) which considers the complementary potential energy will be used in this work. By applying the Boussinesq method (173) and relating the contact pressures to surface deformations, the problem would be to solve the contact mechanics only for finding contact pressures at each node and then the related contact deformations can be calculated. For this model, surfaces should be discretised into small nodes and it is assumed that the nodes are small enough and the contact pressure is constant at each node.

The problem is to minimize the complementary potential energy as follows:

$$V^* = \frac{1}{2}\iint p\overline{u_z}\,dxdy - \iint p\,\overline{u_z^*}\,dxdy \qquad \text{Equation 5-3}$$

where p is the contact pressure and V^*, $\overline{u_z}$ and $\overline{u_z^*}$ are complementary potential energy, surface deformation and prescribed displacement respectively. These are scalars and function of the location. ($p(x,y), \overline{u_z}(x,y), \overline{u_z^*}(x,y)$)

The Boussinesq solution for relating contact pressure and surface deformation usually considers only normal forces and the solution is:

$$u(x,y) = \frac{1}{\pi E^*}\iint_{-\infty}^{\infty} \frac{p(s_1,s_2)}{\sqrt{(x-s_1)^2+(y-s_2)^2}}\,ds_1 ds_2 \qquad \text{Equation 5-4}$$

in which E^* is the composite elastic modulus of two surfaces. (x, y) and (s_1, s_2) are two different surface points. It shows the relationship for the deformation of a the surface on point (x, y) when the load is applied on the point (s_1, s_2).

$$\frac{1}{E^*} = \frac{(1 - {\nu_1}^2)}{E_1} + \frac{(1 - {\nu_2}^2)}{E_2} \qquad \text{Equation 5-5}$$

$$\frac{1}{G^*} = \frac{(1 + \nu_1)(1 - 2\nu_1)}{2E_1} - \frac{(1 + \nu_2)(1 - 2\nu_2)}{2E_2} \qquad \text{Equation 5-6}$$

Here, ν_1, ν_2, E_1 and E_2 are the Poisson's ratio and Elastic Modulus of surfaces 1 and 2 respectively.

For solving the double integrals of Equation 5-4 the surfaces should be discretised into small nodes. The nodes should be small enough to assume that pressure is constant at each node. It should be noted that only boundary of solids (surfaces) are meshed in this method which can help the numerical efficiency. An example of the surface discretization is shown in Figure 5-7.

N and M are the number of nodes in two dimensions of the surface plane and a and b are the half length of each element which is the difference between the nodes. For simplicity, a and b are assumed to be equal and in this work they are set to 0.5μm. Therefore the full length of each element is 1μm which is a reasonable length for computational studies of rough surfaces (17).

The size of elemental nodes is significantly important in simulating contact mechanics of rough surfaces. It has been reported by Persson (210) that the size of nodes in a contact mechanics simulation can affect the calculation of real area of contact therefore affecting the contact pressure calculations. He stated that in order to properly describe the contact mechanics problem, it is necessary to have at least 10×10 or

100×100 grid point within one asperity contact region. This feature should be compared to the wavelength of the shortest surface roughness feature. Therefore, selection of elemental nodes for simulating a contact problem for rough surfaces is largely dependent on the features of the surface and the size of the wavelength of the smallest surface roughness feature. It was also shown that using too small number of contact nodes can lead to an overestimation of the real contact area to elimination of the true stress distribution at zero stress.

To solve the integral equation for the discretised surfaces the integral equations should first be discretised.

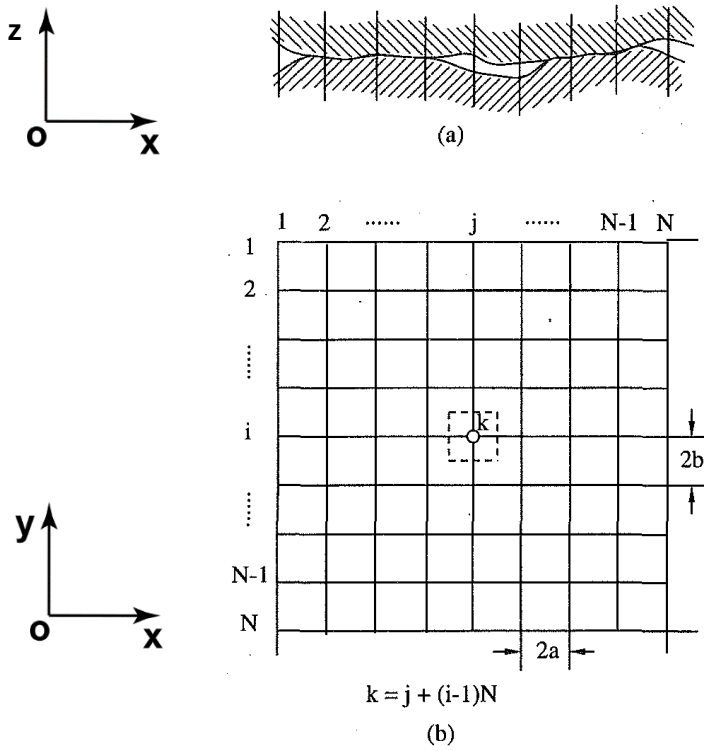

Figure 5-7 Surface discretization in Boundary Element Method (145)

$$(\overline{u_z})_l = \frac{1}{\pi E^*}\int_0^L\int_0^L \frac{p(s_1,s_2)ds_1ds_2}{\sqrt{(s_1-x)^2+(s_2-y)^2}}$$

$$= \frac{1}{\pi E^*}\sum_{k=1}^{M}\iint \frac{ds_1ds_2}{\sqrt{(s_1-x)^2+(s_1-y)^2}}p_k \quad = \sum_{k=1}^{M} C_{kl}p_k$$

Equation 5-7

C_{kl} is the influence matrix and is calculated by solving the double integral:

$$C_{kl} = \frac{1}{\pi E^*}\iint_{-\infty}^{\infty} \frac{ds_1ds_2}{\sqrt{(x-s_1)^2+(y-s_2)^2}}$$

Equation 5-8

The solution for the influence matrix in discretised form is as follows:

$$C_{kl} = \frac{1}{\pi E^*}\Bigg\{(x+a)\ln\left[\frac{(y+b)+\sqrt{(y+b)^2+(x+a)^2}}{(y-b)+\sqrt{(y-b)^2+(x+a)^2}}\right] + (y+b)\ln\left[\frac{(x+a)+\sqrt{(y+b)^2+(x+a)^2}}{(x-a)+\sqrt{(y+b)^2+(x-a)^2}}\right] + (x-a)\ln\left[\frac{(y-b)+\sqrt{(y-b)^2+(x-a)^2}}{(y+b)+\sqrt{(y+b)^2+(x-a)^2}}\right] + (y-b)\ln\left[\frac{(x-a)+\sqrt{(y-b)^2+(x-a)^2}}{(x+a)+\sqrt{(y-b)^2+(x+a)^2}}\right]\Bigg\}$$

Equation 5-9

Equation 5-3 describes the potential energy for a frictionless contact and the normal force is the only force applied on the surfaces. The potential equation for a frictional contact would be modified to the form below:

$$V^* = \frac{1}{2}\iint \boldsymbol{t}.\overline{\boldsymbol{u}}\,dxdy - \iint \boldsymbol{t}\,.\overline{\boldsymbol{u}^*}\,dxdy$$

Equation 5-10

In which t is the full surface stress vector including the in-plane tractions and u is the full surface deformation.

$$\boldsymbol{t} = q_x \boldsymbol{e_x} + q_y \boldsymbol{e_y} + p\boldsymbol{e_z} \quad \text{Equation 5-11}$$

$$\boldsymbol{u} = u_x \boldsymbol{e_x} + u_y \boldsymbol{e_y} + u_z \boldsymbol{e_z} \quad \text{Equation 5-12}$$

q_x and q_y are the in-plane traction forces and $\boldsymbol{e_x}$, $\boldsymbol{e_y}$ and $\boldsymbol{e_z}$ are the Cartesian unit basis vectors. u_x, u_y and u_z are the surface deformations in x, y and z directions respectively.

By applying the same discretising procedure, the Boussinesq solution for the fully coupled deformation-traction relationship can be expressed as:

$$u_{xk} = \sum_{l=1}^{M} \left(C_{kl}^{xx} q_{xl} + C_{kl}^{xy} q_{yl} + C_{kl}^{xz} p \right)$$

$$u_{yk} = \sum_{l=1}^{M} \left(C_{kl}^{yx} q_{xl} + C_{kl}^{yy} q_{yl} + C_{kl}^{yz} p \right) \quad \text{Equation 5-13}$$

$$u_{zk} = \sum_{l=1}^{M} \left(C_{kl}^{zx} q_{xl} + C_{kl}^{zy} q_{yl} + C_{kl}^{zz} p \right)$$

In the matrix form:

$$\begin{bmatrix} u_x \\ u_y \\ u_z \end{bmatrix} = \begin{bmatrix} C^{xx} & C^{xy} & C^{xz} \\ C^{yx} & C^{yy} & C^{yz} \\ C^{zx} & C^{zy} & C^{zz} \end{bmatrix} \begin{bmatrix} q_x \\ q_y \\ p \end{bmatrix} \quad \text{Equation 5-14}$$

The elements of the influence matrix can be obtained from the complete solution of the Boussinesq problem. Then the problem would be minimizing the potential energy for the fully coupled contact. The solution procedure is the same as frictionless contact and can be carried out by direct quadratic mathematical solution (145, 211).

Solving the quadratic form of energy for 3D problem increases the computation time by several times and it has been examined by the authors that in the case of two similar materials it does not affect the true contact pressures significantly. Therefore the

complementary potential solution was carried out only considering the normal load using the solution reported by Tian *et al*. (145). For the case of two identical materials in contact, the equivalent shear modulus of Equation 5-6 becomes zero and the Equation 5-10 reduces to Equation 5-4. As the current study considers the contact of two similar materials, only Equation 5-4 and the discretized form of that equation which is the first part of Equation 5-9 have been used for this first analysis.

5.5 Direct Quadratic Mathematical Programming

Because the total complementary potential energy is a quadratic function of the contact pressure, it can be expressed as quadratic mathematical equations. Hence the energy can be written in quadratic form of Equation 5-15:

$$V^* = \frac{1}{2}\boldsymbol{p}^T.\boldsymbol{C}.\boldsymbol{p} - \boldsymbol{p}^T\boldsymbol{u} \qquad \text{Equation 5-15}$$

Here p^T is the transpose matrix of p_k and C and u are influence matrix and gap between surfaces respectively.

$$C = \frac{1}{\pi E^*}\begin{bmatrix} C_{1,1} & \cdots & C_{1,M} \\ \vdots & \ddots & \vdots \\ C_{M,1} & \cdots & C_{M,M} \end{bmatrix} \qquad \text{Equation 5-16}$$

$$\boldsymbol{u}^T = (\overline{\boldsymbol{u}^*_{z1}}, \overline{\boldsymbol{u}^*_{z2}}, \dots, \overline{\boldsymbol{u}^*_{zk}}, \dots, \overline{\boldsymbol{u}^*_{zM}}) \qquad \text{Equation 5-17}$$

And for the complementary potential energy to have a minimum at the point $\boldsymbol{p}^*$, the solution is as:

$$\nabla V^*(\boldsymbol{p}^*) = \boldsymbol{C}.\boldsymbol{p}^* - \boldsymbol{u} = 0$$

$$\boldsymbol{p}^* = \boldsymbol{C}^{-1}.\boldsymbol{u}$$

Equation 5-18

And all the values in Equation 5-18 should satisfy the restriction criteria $p_k \geq 0$. The summation of all contact pressures must be equal to the applied load on the surfaces and the following equation should be satisfied:

$$\sum_{i,j=1}^{i,j=N} p_{i,j} = W$$

Equation 5-19

The elastic deformation is then calculated corresponding to the pressure of contacting asperity using the equation below:

$$\boldsymbol{u} = \boldsymbol{C}.\boldsymbol{p}$$

Equation 5-20

The deformation is then used to check the deformation criteria of the contact problem. It should be noted that Equation 5-19 will be valid for the whole contact. In order to find the true area of contact and the corresponding contact pressures, Equation 5-19 and Equation 5-21 should be solved at the same time iteratively.

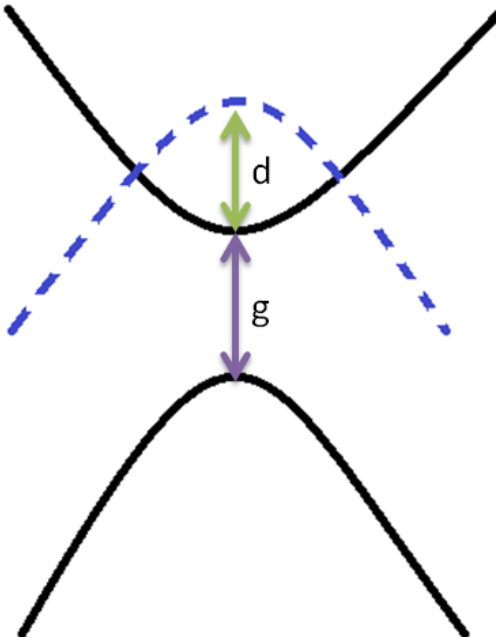

Figure 5-8 Single asperity model – Schematics of rigid body movement

The rigid body movement (r) is the movement of the bodies in normal direction of contact and is given by:

$r = (Z_2 - Z_1) + u$ & p>0 if in contact

$r < (Z_2 - Z_1) + u$ & p=0 if not in contact Equation 5-21

in which $(Z_2 - Z_1) = g$ is the gap between asperities and *u* is the elastic deformation of contacting asperities. The above formulations are valid for every single asperities in contact. Therefore they can be solved for a set of asperites and Figure 5-8 can be a representative of a single node in the contact mechanics formulation of the problem explained in Section 5.4.

5.6 Elastic-Perfectly Plastic Contact Model

The contact mechanics model used in this work is an elastic-perfectly plastic model. To consider the plastic part in the simulation, a modelling approach which was reported by Sahlin *et al*. (141) was used in this work. It is assumed that the asperities can undergo pressures between 0 and hardness of the materials:

$$0 < p(x, y) < H \qquad \text{Equation 5-22}$$

The contact pressure of the asperities that experience pressures higher than the hardness of the materials will be set to H (hardness of the material).

These asperities become plastically deformed. It is assumed that the points with pressures equal to the hardness of the material will be truncated out of the calculation for elastic deformation because they can freely float. The steps for elasto plastic contact simulation are explained as below:

- First step is to guess the initial pressure to satisfy Equation 5-19.
- Set the negative pressures to zero and the pressures above the hardness to H
- Check the calculated pressures again and compare it with Equation 5-19. If the pressure is now equal to load, pressures should be shifted up or down
- Truncate the pressures $p = 0$ and $p = H$. Then calculate the elastic deformation of Equation 5-20.
- Calculate the body interferences and check if the points of contact will satisfy Equation 5-21.
- The plastic deformation is then calculated by subtracting the elastic deformation from the body interferences.

5.7 Movement of the Contacting Surfaces

The influence matrix of Equation 5-16 shows the influence of surface points on deformation of other points in presence of load. The term g which is a two dimensional matrix of gaps between single asperities of contacting surfaces, shows the potential of asperity-asperity contact by moving surfaces in normal direction of surface planes. In this case Equation 5-21 defines the possibility of contact to happen.

In most of the tribologically loaded contacts, surfaces have relative movements tangentially, so this must be taken into account.

Conventionally, movement of surfaces are applied by shifting the matrices that contain the surface asperity height numbers. This is a very simple way to simulate the movement of surfaces. In this method controlling the shifting speed of both contacting surfaces is essential for applying the rolling-sliding condition on the tribosystem.

The influence matrix does not change in this method and the size is still $(N * M) \times (N * M)$ which in the case of square contacting area becomes $N^2 \times N^2$.

In this thesis, two ways for moving the surfaces in contact are implemented numerically. The first method is the above mentioned conventional shifting of the matrices and the second method is explained in details in the next section. For the first method, the function *circshift* from the MATLAB library is used to shift the matrix of surfaces thus simulating the movement.

5.8 New Surface Movement Strategy

It is important to know how the influence matrix works before explaining the new procedure for moving the surfaces. The elements of an influence matrix correspond

to the influence of a node of surface on other nodes of the surface if the load is applied on that point.

Imagine a surface with $N \times N$ nodes. If the load is applied to a point, it influences $N \times N$ points on the surfaces including the point itself. Therefore, a matrix of $N^2 \times N^2$ can explain the influence matrix of the whole surface. Each element of this matrix is responsible for the influence of a point on another point (Figure 5-9). If the load is applied on point *p* it will affect the deformation on point *k*.

It can be interpreted from Equation 5-9 that the elements of this matrix are dependent on the distance of the points on the surface (distance between points p and k). Therefore, this matrix would have identical values for the points that have similar distances. Now imagine two surfaces coming into rolling-sliding contact. One of the surfaces should enter the contact from one side and will exit the contact on the opposite. If the upper surface enters the contact from the left, its rightmost part would be in contact with the leftmost part of the lower surface (Figure 5-10-b).

Then the contact problem reduces to the contact of two one-dimensional matrices of two surfaces with size $(N \times 1)$. When the movement continues, more points of surfaces come into contact. For example two columns of the rightmost points of upper surface come into contact with two columns of the leftmost points on the lower surface (Figure 5-10-c). This process continues until the surfaces fully come into contact and the upper surface exits the contact from the other side. A schematic of this contact process is shown in Figure 5-10.

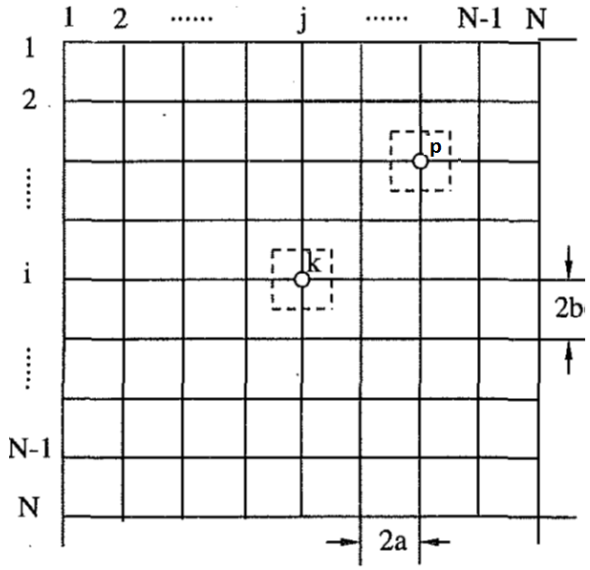

Figure 5-9 Discretized surface and schematic of two point. The point which is deformed (k) because of the load applied on another point (p).

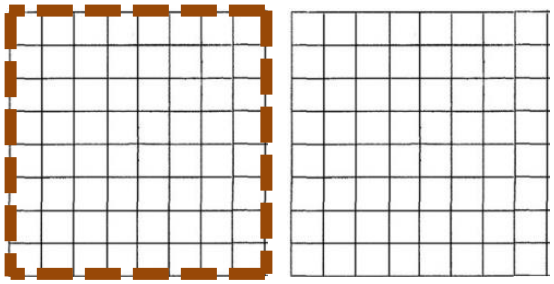

a) Two surfaces not in contact yet

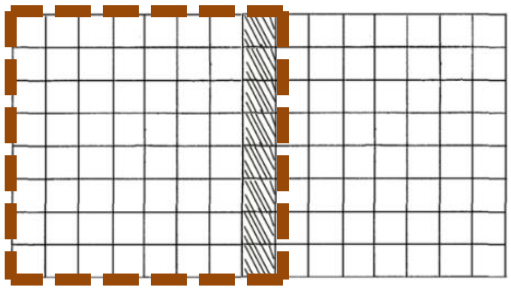

b) Start of the contact (rightmost part of a surface in contact with leftmost part of another surface)

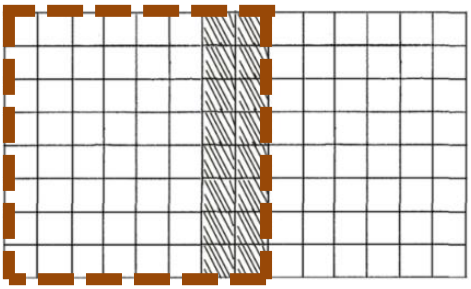

c) Two surfaces come into contact by more areas of both

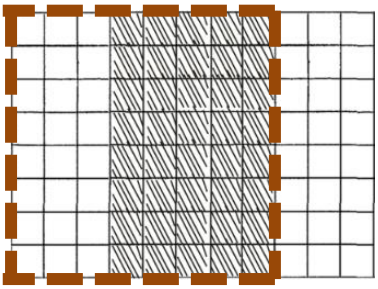

d) More evolution in the contact area of surfaces

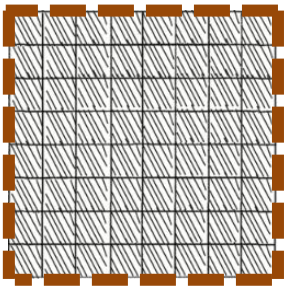

e) Entire surfaces are in contact

Figure 5-10 Movement of surfaces in contact. The shaded area shows the area of contact between two surfaces. The red dotted lines shows the area of the upper surface that enters the contact from the left.

For the beginning of the contact one column of each surface comes into contact. In this case, the influence matrix needs to cover the contact of N points on one surface with N points on another surface. Therefore the influence matrix only needs to be the first $N \times N$ matrix of the big $N^2 \times N^2$ influence matrix. It is shown in Figure 5-11 that how this $N \times N$ matrix is selected.

The true influence matrix elements should satisfy Equation 5-9. As stated before, these elements are dependent on the distance of the points of the surface so the selection shown in Figure 5-11 is valid.

If the movement continues and more points of the surfaces come into contact, the influence matrix will get bigger and becomes $2N \times 2N$, $3N \times 3N$, ... and $N^2 \times N^2$ at the end when surfaces are completely in contact.

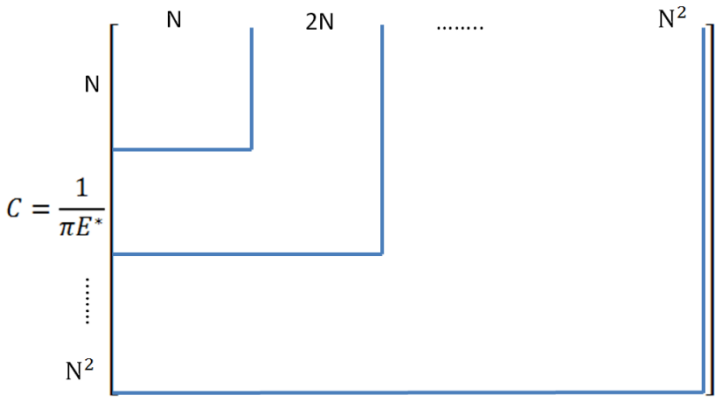

Figure 5-11 Influence matrix selection in the case of moving surfaces

The problem of contact becomes faster because the size of matrices of surfaces and influence matrices are much smaller in this case. The maximum size of the influence matrix is when two surfaces are in complete contact and it is the same size as conventional shifting of surfaces.

Then the contact pressures and surface deformations are stored for every step and can be averaged for one loading cycle.

Plastic deformations are applied to the surface asperities and the geometries of the surfaces are changed for next steps. This process of two rough surfaces coming into contact is repeated to the end of the simulation. Therefore a rolling sliding motion can

be easily modelled by this contact mechanics simulation. It should be noted that the contact mechanics model in this work is quasi-static.

5.9 Fast Fourier Transform (FFT) Implication

In general, the calculation of Equation 5-20 needs many operations especially for a large number of surface points. The calculation speed will depend on the square of the number of the grid points and the high computational cost is due to the large influence matrix. Equation 5-20 can be rewritten as a discrete convolution as the following:

$$(\boldsymbol{u_e})_{i,j} = (\boldsymbol{C} * \boldsymbol{p})_{i,j} = \sum_{k=1}^{N}\sum_{l=1}^{M} C_{i-k,j-l}p_{kl} \qquad \text{Equation 5-23}$$

N and M are the dimension sizes of the surface. The right hand side of Equation 5-23 is the same as Equation 5-20. It has been reported (141, 148, 177, 178) that the cyclic convolution of Equation 5-23 can be solved using FFT.

The influence matrix used in the convolution form is a bit different from the influence matrix introduced earlier in this chapter. The influence matrix here is a vector in the same length as the pressure vector and indicates the influence of all points on one point of the surface. The equation then transforms to the following equation:

$$(\boldsymbol{u_e})_{i,j} = (\boldsymbol{C} * \boldsymbol{p})_{i,j} = iFFT(FFT(C).FFT(p)) \qquad \text{Equation 5-24}$$

The advantage of the Equation 5-24 in comparison to Equation 5-20 is the computation demand of $N^2 \log N^2$ instead of $N^2 \times N^2$ which is a huge difference for big surfaces.

iFFT and FFT are used in this work to calculate the surface deformations in each iteration loop for satisfying the contact conditions. The FFT and iFFT built-in functions are simply used in MATLAB. It should be noted that an element by element multiplication should be used for matrices $FFT(C)$ and $FFT(p)$. The grid node numbers for the fast calculation of the problem is reported to be a power of 2 (178). In principle, the study area should cover at least several wavelengths of the surface in order to be reasonable. For the surfaces used in this work, an average wavelength of 15 to 20 µm was identified. Therefore the computation domain is selected to be a 64µm×64µm area consisting of 64 nodes of one micron size in every dimension.

5.10 Tribofilm Mechanical Properties

There are several works which study the mechanical properties of tribofilms formed in boundary lubricated contacts and many techniques are used to understand what behaviours lead to these properties (45, 46, 48, 50, 51, 212). They found that the properties of the tribofilm layers are dependent on applied loads and can be adapted to conditions. They also showed that the mechanical properties of tribofilms vary from surface to substrate.

Mosey *et al*. (51) developed a new theory for the functionality of ZDDP tribofilms at the molecular level. They suggested that pressure induced cross-linking is the reason for chemically connected networks and many experimentally validated behaviours of ZDDP can be explained by this theory. It was reported that the high pressure at the surface of the film will lead to higher cross-linking and result in longer chain phosphates. The different mechanical properties of high and short chain polyphosphates were also reported in the work. The effect of the steel substrate in

changing the nano-indentation results of tribofilm has been reported and different models for extracting the tribofilm properties were developed (45, 52). In this work the results reported for the mechanical properties of tribofilm based on those models has been used.

Demmou *et al*. (52) found that the pressure affects the elastic properties of the tribofilm and it will happen when the pressure exceeds a threshold amount of H_0. So for contact pressures below H_0 the elastic modulus is constant and after that it will change by variation of hardness. The linear function of this relation is given below:

$$E_f^* = \frac{E_{f_0}^*}{H_0} H \qquad \text{Equation 5-25}$$

E_f^* is the film reduced modulus and $E_{f_0}^*$ is the constant elastic modulus before the threshold pressure. $E_{f_0}^*$ was almost the same for all temperatures and equal to 39 ± 4GPa. H_0 was found to be dependent on temperature.

In summary, the assumptions for the mechanical properties of the tribofilm are based on previous studies of ZDDP or ZDDP/MoDTC tribofilms properties. ZDDP tribofilms have a thickness of 50-150 nm and the mechanical properties change from the surface to the bulk. The hardness at the surface is lower than the bulk hardness; as the penetration depth increases the hardness increases linearly (52, 56).

The value of surface tribofilm hardness and tribofilm hardness near the substrate can be obtained from experimental results but the variations can be assumed to be between 2 to 6 GPa. In addition, elastic properties of the tribofilm also vary from the surface to the bulk and this variation is related to hardness variation of tribofilm as previously explained.

Because of the limitations in the half space theory and the Boussinesq solution, implementation of varied elastic modulus for different local points is very complicated. Therefore a way of considering different elastic modulus values for different local points on the surface is used here in this work. The elastic modulus is the average of the modulus of all local points on the surface and the amount is used in the Boussinesq formulation.

Considering the plastic deformation, a mathematical formulation should be used in order to consider the tribofilm hardness variations when the tribofilm deforms plastically. In the initial model a linear variation of hardness value from surface to bulk of the tribofilm have been considered. The tribofilm contributes to changes in the hardness of the layer because of its thickness. This hardness contributes to the elastic-plastic contact model and gives the plastic deformation in the system.

Two surfaces are in contact and they both have tribofilms on top. Tribofilm thickness defines the hardness of the tribofilm near the surface and for simplicity an average is taken between this value and the hardness of tribofilm close to the substrate. The reason for averaging is the linear behaviour of the hardness in the tribofilm bulk. Otherwise there must be an iterative simulation for finding the tribofilm plastic deformation and its hardness which was reported in Andersson *et al*. (17). The plastic deformation is then calculated with respect to the hardness of the tribofilm.

5.11 Flash Temperature Calculation

The temperature used in the model is the temperature at the asperities. It is the summation of the flash temperature and the bulk temperature:

$$T = T_b + T_f$$ Equation 5-26

The bulk temperature is assumed to be the same as the oil bulk temperature and the flash temperature is the temperature rise due to the frictional heating resulted from asperity-asperity contacts. The frictional heating in the contact interface is reported to be (179):

$$Q = \mu . P . V$$ Equation 5-27

in which μ, P and V are the coefficient of friction, contact pressure and sliding velocity respectively. In the case of rough surfaces, contact can be discretized into small parts and the temperature rise at different locations can be calculated using the influence matrices (213).

In this work, contact pressures are already calculated using the influence matrices via the Boussinesq solution. Therefore the contact temperature can be calculated locally for each contact point considering the shape and dimensions of the single asperities. The flash temperature is calculated using the Blok's theory and the formulation that was reported by Kennedy (179).

The maximum temperature for the case of two identical bodies in contact with a square contact area is reported as following (179):

$$\Delta T_{max} \approx \frac{2Qb}{K\sqrt{\pi(1+Pe)}} \approx \frac{1.122Qb}{K}$$ Equation 5-28

where b is the width of the contact and $K = \frac{k}{\rho C}$ is the thermal diffusivity. Pe is the Peclet number and the right side of Equation 5-28 is valid for small Peclet numbers. The flash temperature calculated at every point of the surface will be added to the bulk

temperature and the value is used for the tribochemical growth model described in Chapter 6.

5.12 Results

Results for the influence matrix, contour of contact pressure for a static contact, movement of surfaces and plastic deformations are shown in this section.

5.12.1 Influence Matrix

As explained before the influence matrix is $N^2 \times N^2$ when the surfaces are represented by $N \times N$ nodes. An example of the influence matrix for a 20×20 surface is represented graphically in Figure 5-12.

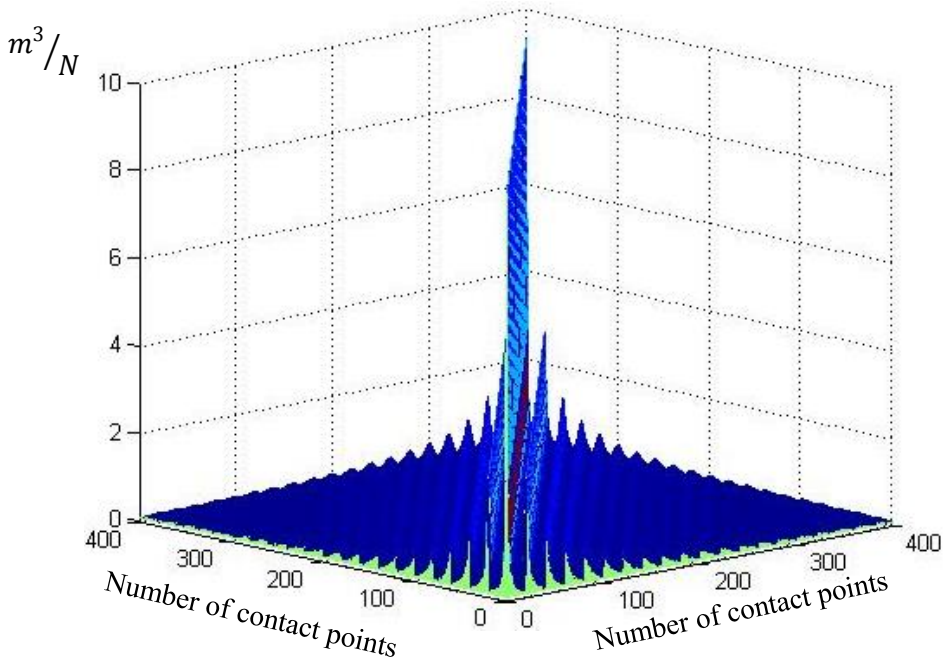

Figure 5-12 Influence matrix element values

If load is applied to a point of this surface, the deformation on all the other points is shown in Figure 5-13. It is noticeable that if a load is applied to a certain point on the

surface, the highest deformation happens at the same point and this deformation decreases as the distance from that point increases. It is in agreement with the definition of the influence matrix.

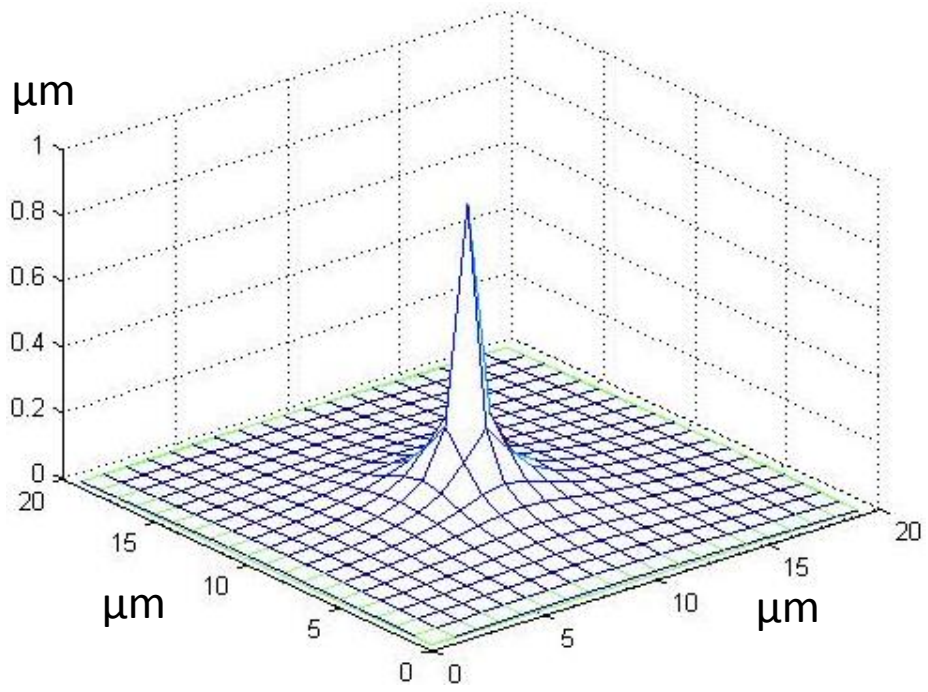

Figure 5-13 The deformation of surface due to load applied in the centre

5.12.2 Contact Pressure for Static Contact

When two surfaces are in static contact, the highest asperities of surfaces come into contact. The contour of contact pressure in this case will look like Figure 5-14.

For the case of a ball coming into contact with a flat, the contact pressure is shown in Figure 5-15.

5.12.3 Movement of the Surfaces

As explained in Section 5.7, matrices of surfaces are selected in a way that movement can be simulated. An example of this movement is shown in Figure 5-16. The contour

of contact pressure which shows the asperity-asperity interaction is demonstrated in the figure. The evolution of contacting asperities in the sliding direction can be noticed.

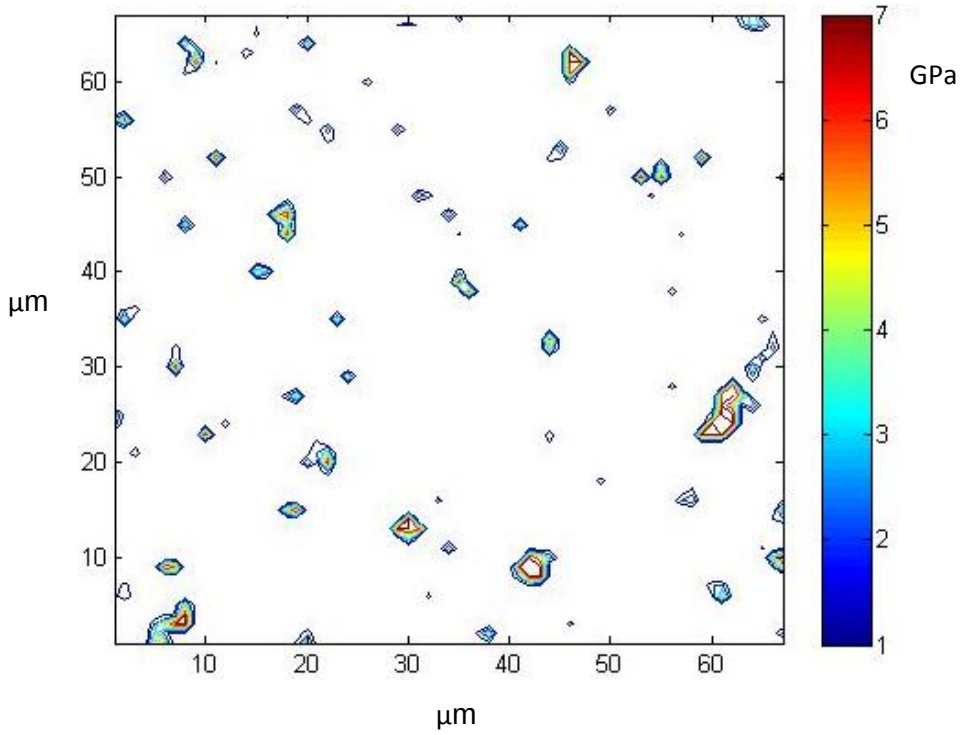

Figure 5-14 Contours of contact pressure for the contact of two rough surfaces

The upper surface comes into contact with lower surface from the left (see Figure 5-16-a) and moves towards the sliding direction. Both surfaces are entirely in contact in Figure 5-16-d. The upper surface then exits the contact from the other side (Figure 5-16-f).

5.12.4 Plastic Deformations

Calculation of elasto-plastic contact pressures and plastic deformations was formulated in Section 5.6 . An example of plastic deformation for the case of a rigid rough ball loaded on a rough surface is shown in Figure 5-17. Plastic deformations are demonstrated for both ball and the flat. In this thesis, plastic deformations are

permanent changes of surface topographies due to the applied load. If surfaces are cyclic contact, topographies are modified due to plastic deformations in each cycle and deformed surfaces are in the input of the next loading cycle.

5.12.5 Flash Temperature

The temperature calculated in this model is used for the growth model of the tribofilm. Therefore, the maximum pressures at every single asperity in contact are calculated. Flash temperature rise only happens at the asperities in contact. One example of the flash temperature calculation for a contact of ball on disc with area of 128×128 is shown in Figure 5-18. The flash temperature rise on asperities in contact is shown and the other asperities do not experience that rise.

5.13 Summary

A contact mechanics model is developed in this work which accounts for elastic-perfectly plastic contact of rough surfaces. Two different methods for movement of surfaces in tribologically-loaded contacts are introduced here. A new approach for the movement is developed and tested numerically. This approach as well as the conventional approach of shifting matrices is used in the numerical modelling of surface movements. A Fast Fourier Transform (FFT) algorithm is employed to reduce the computational time for the contact problem. FFT is very useful for simulating the contact for large surfaces.

The simulation results for contact pressures, surface plastic deformations and contact pressure contours during surface movement are reported in this chapter. The current contact model is flexible and can be adapted to different tribological system configurations. This is possible to change the geometry of the contacting surfaces and

by moving both surfaces with a specific speed. The contact mechanics model introduced in this chapter will be used as the base of the boundary lubrication framework for this thesis and other characteristics of the model will be added to it.

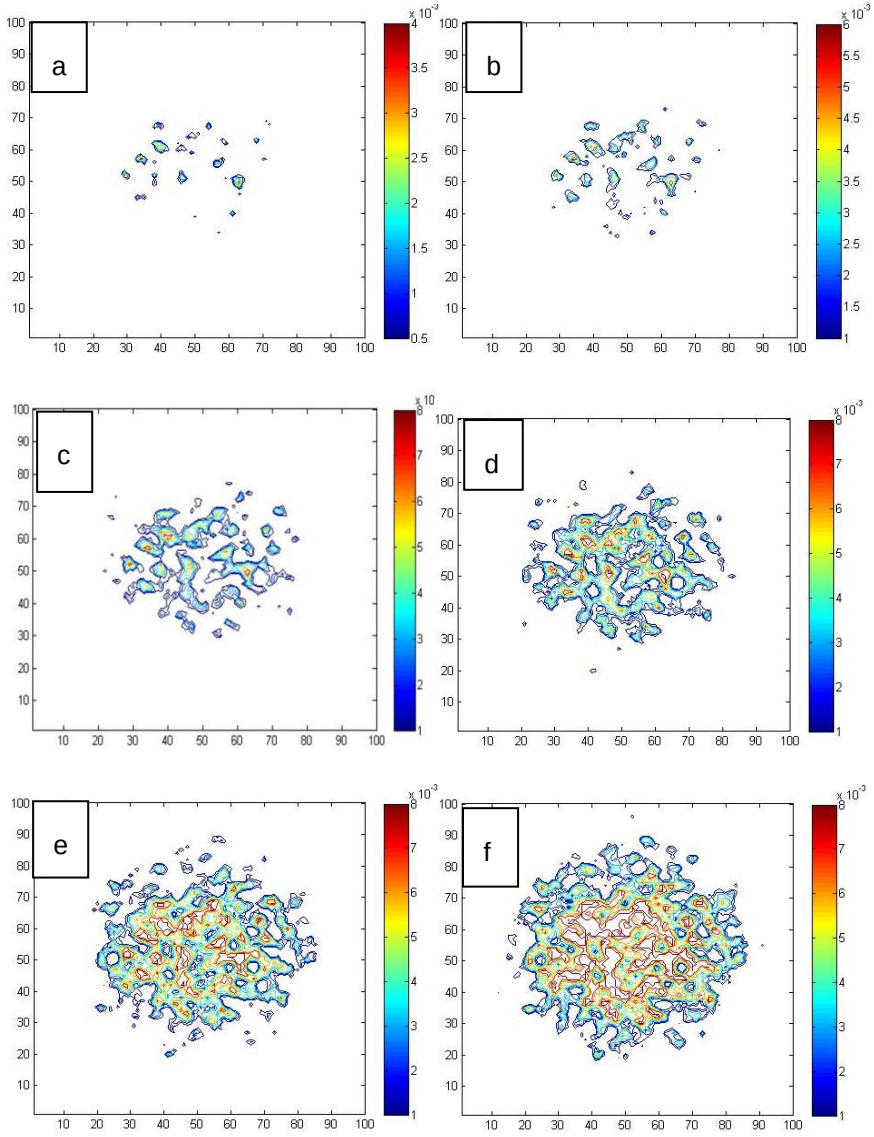

Figure 5-15 Contact area and pressure evolution for a ball loaded on the flat in an elastic-perfectly plastic model. Load increases from (a) 50 MPa (b) 200 MPa (c) 600 MPa (d) 900 MPa (e) 1.2 GPa (f) 1.6 GPa

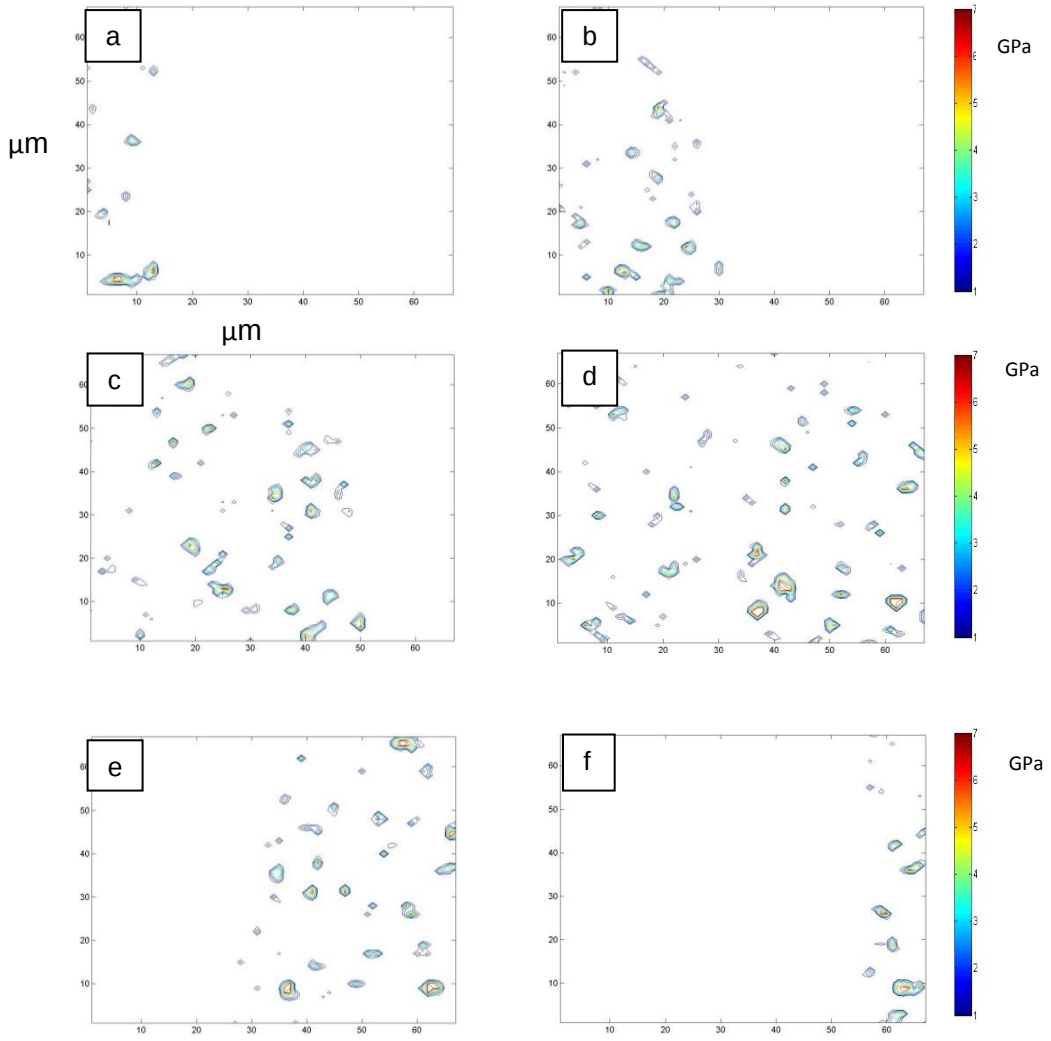

Figure 5-16 Contour of contact pressure showing the asperity contact pressures in surface movement. The upper surface enters the contact from the left (a) and exits from the right (f). The contour is indicating the pressures on the lower body.

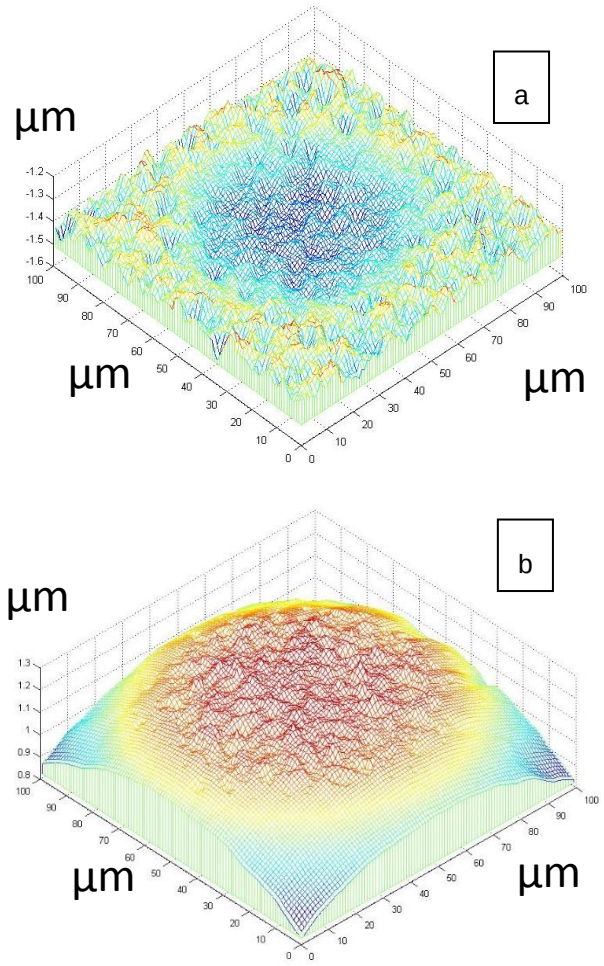

Figure 5-17 Plastic deformation due to contact of ball (b) on flat (a)

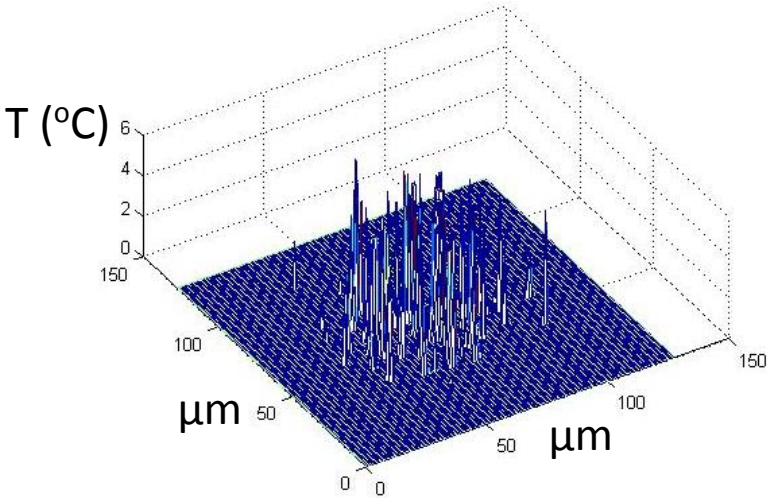

Figure 5-18 Flash temperature rise at the contacting asperities

Chapter 6. Tribofilm Growth Model Development

The development of a tribochemical growth model for the tribofilm is represented in this chapter as explained in Section 5.1. The model developed in this chapter is integrated with the contact mechanics model of Chapter 5.

6.1 Introduction

The characteristics of boundary lubrication are defined by the properties of the tribofilm formed on the surfaces. Tribofilms are the result of chemical reactions between lubricant additives and contacting surfaces. These chemical reactions happen due to a variety of physical, chemical and mechanical phenomena occurring at the asperity scale. Therefore even observation of such a complicated process is difficult experimentally. There have been a wide range of surface analytical techniques that were used to monitor the growth and properties of the tribofilm in boundary lubrication.

In the past few decades the general knowledge on the characteristics of different tribofilms has increased due to the fast development of surface characterization techniques. Despite a good general understanding, a comprehensive model explaining the physical and chemical properties of the tribofilm is still lacking in the literature (see Chapter 3). The aim of this chapter is to develop a semi-analytical tribofilm physical and mathematical growth model that can be a starting point to develop more robust analytical models. The sensitivity of the developed model is then analysed for different working parameters such as temperature, load and surface roughness.

In the next chapter, designed experiments will be addressed that will be used to develop the growth model reported in this chapter with more physical parameters. The

semi-analytical model developed in this chapter will use experimental observations to build a more robust physical-chemical growth model.

6.2 Thermodynamics of Interfaces

As explained in Section 4.6 of the literature review, the concept of thermodynamics in tribology cannot be studied by traditional equilibrium thermodynamics framework. In tribology, because of dynamic loading on the surfaces, mechanical effects on chemical reactions are important.

Friction is an irreversible process due to energy dissipation at interfaces which is a non-equilibrium process and should be studied using non-equilibrium thermodynamics. Many reports (203) suggest that mechanochemical reactions are different from those of thermochemical ones. To initiate a thermochemical reaction, only the necessary amount of heat is required. On the other hand, solid-solid interactions can result in initiation of chemical reactions at much lower activation energies compared to thermochemical ones. It has been reported (35) that tribofilms form only on areas that mechanical rubbing occurs and direct solid-solid interactions happen. This indicates that the occurrence of tribochemical reactions is not only temperature dependent but is initiated by mechanical rubbing.

There are several observations reported in the literature highlighting the fact that mechanically-activated chemical reactions should be distinguished from thermally-activated ones in tribochemistry (203). These facts are listed as follows:

- Different chemical compounds can be found after the machining process other than the ones found by heating them. For example, the difference for sodium borate is:

$$2NaBrO_3 \xrightarrow{Tribochemical} Na_2 + \frac{5}{2}O_2 + Br_2$$

$$2NaBrO_3 \xrightarrow{Thermal} NaBr + \frac{3}{2}O_2$$

- Rubbed surfaces (machined surfaces) are more reactive especially at low temperatures
- The dependency of tribochemical reactions on temperature is very different from that of thermal reactions. The Arrhenius equation is not applicable for such reactions and results in very low activation energies compared to thermal reactions. In some cases zero or negative activation energy has been reported.
- The tribochemical reactions are much less dependent on the pressure in comparison to thermal reactions.
- The value of rate constant for some tribochemical reactions is very low if is calculated through thermal theories. Even at very high temperatures, this equilibrium constant is very small but the reaction occurs fast.

Therefore the branch of thermodynamics dealing with such reactions should be non-equilibrium thermodynamics. It has been widely reported in the literature that tribosystems are open thermodynamic systems and the study of entropy change in such systems can lead to a better understanding of tribochemical reactions (202).

6.3 The Tribochemical Reaction Kinetics Model

The basis of this model comes from a recent comprehensive study of the kinetics of tribochemical reactions (205, 214). It is reported that the kinetics of tribochemical

reactions can be expressed by a modification to the conventional thermal Arrhenius equation. They used active collision theory and activated complex theory to describe the tribochemical reactions occurring in boundary lubrication. They stated that the induction force for the tribochemical reactions is mainly mechanical rubbing, or in other words the entropy change at interfaces, and not only the temperature.

The aim of the study by Bulgarevich *et al*. (205) was to evaluate the chemical process happening in a tribosystem from a thermodynamics point of view and to analyse which equilibrium condition characterizes the tribochemical process. Some important findings of that work are mentioned in this chapter since it is the basis of the current tribochemical model.

The rate of chemical reactions in simple tribochemical processes was calculated as well as the equilibria time. These calculations showed that neither endothermic nor exothermic equilibrium thermal reactions can occur in the formation of the products of a tribosystem. By analysing the times of chemical equilibria (the time that the chemical reaction reaches an equilibrium) and their affinity to occur, Bulgarevich *et al*. suggested that the chemical reactions that are responsible for the formation of the tribofilms have to be initiated by mechanical activation not thermal activation.

It is assumed that tribo- and thermal-activation of the tribochemical reaction happen at the same time to form the tribofilm. The tribochemical reaction process is simplified to be a two stage process. Firstly, surfaces rub on each other which results in mechanical activation of the surfaces:

$$A \xrightarrow{mechanical\ activation} A^*$$

This process leads to formation of a surface with high reactivity. This highly reactive surface then reacts with lubricant additives to form the tribofilm:

$$A^* + B \xrightarrow{thermomechanical\ process} C$$

In the above, *A* is the asperity before the contact and A^* is the activated asperity after rubbing, B and C are the lubricant additive molecules and the final product (tribofilm) respectively. It was reported that the population of the transition states of the chemical reaction is governed by mechanoactivation and the further movement of the activated complex to overcome the barriers and reach the products occurs thermally.

Bulgarevich *et al*. proposed that the rate of this reaction is $k_{tribo-thermo}$. The number of times that this rate exceeds the rate of the similar thermoactivated reaction k_{thermo}, is the number of times that the population of transition states of mechanoactivation reaction exceeds the population of the thermo-activated reactions. This is mathematically formulated as follows:

$$k_{tribo-thermo} = \frac{x_{tribo}}{x_{thermo}} k_{thermo} \qquad \text{Equation 6-1}$$

In which x_{tribo} and x_{thermo} are the population of the transition states for tribochemical and thermal reactions respectively.

It is known from the thermodynamics that:

$$k_{thermo} = \frac{k_1 T}{h'} exp\left(\frac{\Delta E}{RT}\right) \qquad \text{Equation 6-2}$$

$$x_{thermo} = exp\left(\frac{\Delta E}{RT}\right) \qquad \text{Equation 6-3}$$

k_1 and h' are the Boltzmann and Planck's constant and ΔE, R and T are activation energy, universal gas constant and the temperature respectively.

By substituting expressions for k_{thermo} and x_{thermo} into Equation 6-1 the tribochemical reaction rate follows:

$$k_{tribo-thermo} = \frac{k_1 T}{h'} x_{tribo} \qquad \text{Equation 6-4}$$

It shows a linear dependence of the tribochemical reaction rate on the temperature rather than an exponential one.

For the development of a tribofilm growth model, the rate of tribochemical reactions are important. These reactions include non-spontaneous chemical reactions that are not thermodynamically favourable to occur. But friction and mechanical rubbing can induce such chemical reactions. Therefore including parameters that are responsible for the mechanical activation of surfaces are essential in the tribochemical model. The term x_{tribo} is such a parameter that includes the mechanical activation of the surfaces.

In the current model, there are limitations in implementing changes in the entropy of the system from first principles. Therefore it was decided to extract this information from experiments. Hence, in practice, x_{tribo} is a calibration parameter determined from experiments that gives information about the changes in the entropy of the system due to mechanical rubbing. This calibration procedure will be discussed in detail later in this chapter.

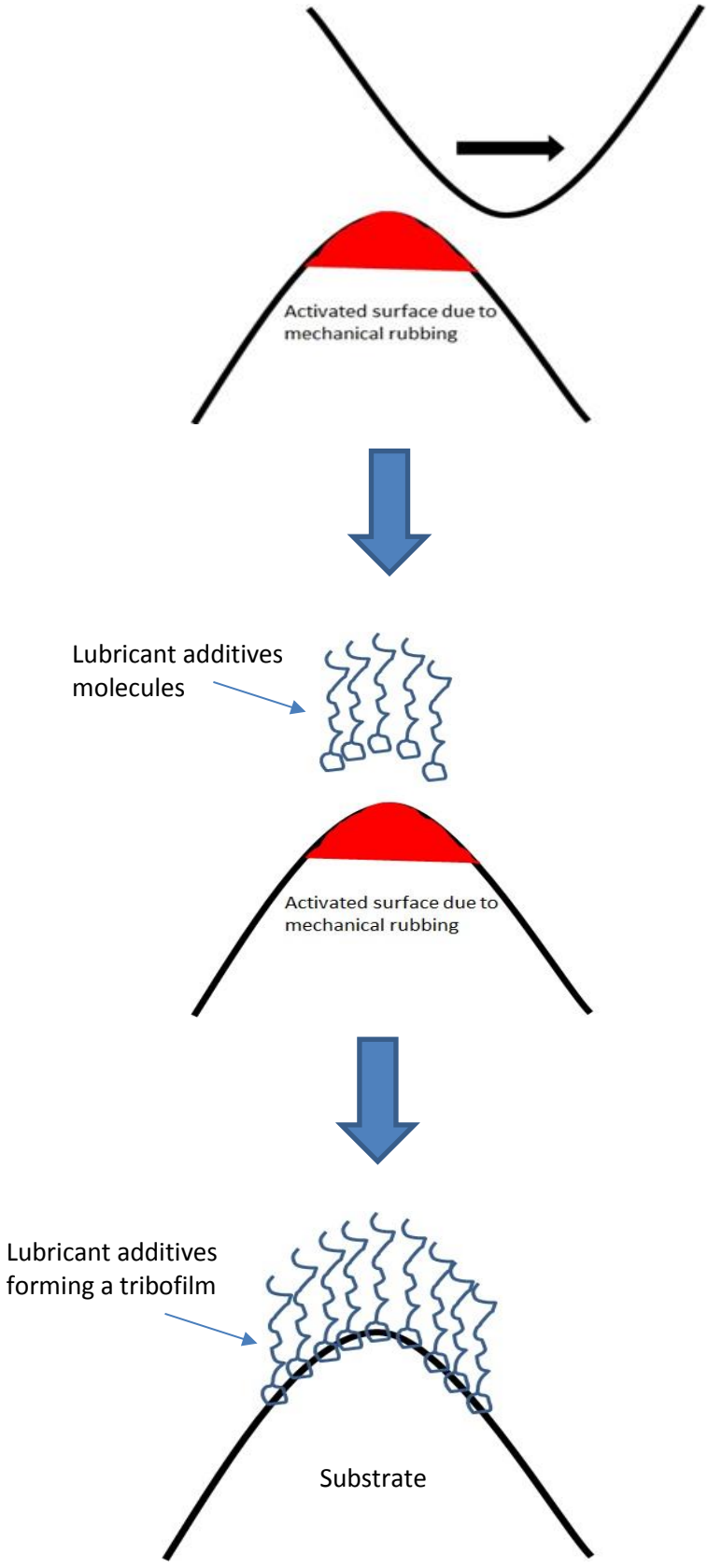

Figure 6-1 Schematic of the step by step mechanical and thermal activation of the tribochemical reaction

The temperature used in this model is the temperature at asperities which is the summation of flash temperature and bulk temperature. The flash temperature calculation is explained in Section 5.11 of the contact mechanics model. This term will be different for different applications and lubricant-substrate combinations and modifies the Arrhenius equation in a way that the effect of mechanical activation of chemical compounds is being considered. It was reported by Bulgarevich *et al*. (206, 214) that the population of transition states of activated complex due to mechanical rubbing is much more than the thermal activated ones for the tribochemical reactions. They proposed simple formulations for the term x_{tribo} for a single asperity-asperity contact.

They assumed a single asperity to be a half-sphere and the number of particles in the interacting asperity was formulated as:

$$n_a = \frac{V_h}{V_m} N_A \qquad \text{Equation 6-5}$$

where V_h is the half-sphere volume, V_m is the mole material volume and N_A is the Avogadro number. The share of particles that directly experience the mechanical activation is expressed as:

$$x_{tribo} = \frac{n_c}{n_a} \qquad \text{Equation 6-6}$$

in which n_c is the number of atoms in contact. The term was then expanded by assuming a contact area of σ^2 for the asperity experiencing elastic deformation. The formulation is as follows:

$$x_{tribo} = \frac{\sigma^2 d N_A V_m}{V_m V_h N_A} = \frac{3d}{16\pi\sigma}$$ Equation 6-7

in which d is the atomic monolayer diameter. This formula was tested for a single asperity with a radius of 10^{-6} m in that work. In this thesis, no such formulation is used and x_{tribo} is extracted from the experimental observations.

The aim of the present work was to adapt this model to the large scale observations of tribosystems in order to enable this term to be defined based on experimental results. Therefore, the model is semi-analytical and the term x_{tribo} can be calibrated from the *in-situ* tribofilm thickness measurements although it has the meaning as explained above. This term is responsible for the mechanical activation of the reactants and also rubbing effect on formation of the tribofilm. It can be a starting point to model tribofilm kinetics based on different parameters affecting the growth.

6.4 Tribofilm Formation Model

Logically, physical, chemical and mechanical properties of the contacting surfaces should be included in the model explaining the growth of the tribofilm.

The model in this work assumes that the tribofilm is a product of reaction between substrate and lubricant additives. It has been reported in the literature that the nature of such reactions are complicated (see Chapter 3). Because of this complexity, there is no clear picture of order of tribochemical reactions. It was assumed that the reaction follows a second order form and the results can be validated against experiments.

Here it is assumed that if the substance A (e.g. lubricant additive) and substance B (e.g. steel surface) form the substance C (e.g. tribofilm) due to tribochemical reaction, the reaction rate can be expressed as:

$$\frac{d[C]}{dt} = k_{tribo-thermo}\,[A].[B] \qquad \text{Equation 6-8}$$

where [A], [B] and [C] are the concentrations of substances A, B and C. It is assumed that the substance B is sufficient for the chemical reactions and only substance A is limiting the rate of reaction. When the tribofilm becomes thicker it will limit the tribochemical reaction by limiting the amount of nascent surface for forming a tribofilm. It should be noted that this model is developed for the formation of the tribofilm at asperity-scale. Therefore the concept of tribofilm coverage is irrelevant here. Hence, by assuming a maximum film thickness for the tribofilm the dependence of substance A on the tribofilm thickness can be expressed as:

$$A = A_1(h_{max} - h) \qquad \text{Equation 6-9}$$

By substituting Equation 6-9 into Equation 6-8, the tribochemical reaction rate becomes:

$$\frac{d[C]}{dt} = k_{tribo-thermo}\,A_1(h_{max} - h)[B] \qquad \text{Equation 6-10}$$

$$\frac{d[C]}{dt} = \frac{k_1 T}{h'} x_{tribo}\,.\,C_1.\,(h_{max} - h) \qquad \text{Equation 6-11}$$

In this equation C_1 is $A_1[B]$. The tribochemical reaction rate can be related to film thickness by using a relation constant as follows:

$$\frac{dh}{dt} = \frac{k_1 T}{h'} x_{tribo} \,.\, C_2 .\, (h_{max} - h)$$ Equation 6-12

Here C_2 includes C_1 and another constant.

By integrating Equation 6-12, the tribofilm thickness as a function of time can be given by:

$$h = h_{max} \left(1 - e^{\left(-\frac{k_1 T}{h'} . x_{tribo} . t\right)}\right)$$ Equation 6-13

It is noticeable that Equation 6-13 has a similar form to Spikes' proposed expression for ZDDP tribofilm growth based on the reported experimental observations (196).

The difference between this model and other attempts for capturing tribofilm growth is the ability to have local properties of surfaces.

6.5 Tribofilm Removal

The effect of tribofilm removal must also be considered in the model; it is assumed that the tribofilm both grows and is also partially removed in each time step. The wear model described later in Chapter 7 represents how the presence of a tribofilm modifies the local wear of the substrate. However the model does not predict the removal of the tribofilm itself.

In this thesis, it is suggested that the tribofilm is being removed and formed at the same time (see Figure 6-2). The process of formation and removal of the tribofilm in combination, will lead to growth of the film on the substrate. It was also reported by Lin *et al.* (64) that the tribofilm is formed and removed at the same time and the

balance between the rate of formation and removal explains the behaviour of the system. It was reported in a work by Fujita and Spikes (196) that the tribofilm removal occurs if a dispersant is added to the oil. In that work the removal was studied and an exponential form was proposed for the removal terms. So far in the literature, there is no clear picture of the removal behaviour of tribofilm. However the versatile exponential form of the removal occurs. Different functions have been tested for capturing the whole behaviour of the tribofilm and the exponential one seems to cover the behaviour in all reported experimental cases. In addition, experimental results show that a decrease in the rate of wear of tribofilm occurs with time (59). At this early stage there is no clear picture of the dominant removal process from the initial experiments.

Assuming that tribofilm removal also follows an exponential form, Equation 6-13 converts to:

$$h = h_{max}\left(1 - e^{\left(-\frac{k_1 T}{h'}.x_{tribo}.t\right)}\right) - C_3(1 - e^{-C_4 t}) \qquad \text{Equation 6-14}$$

in which C_3 and C_4 are removal constants. These removal terms are calibrated with experimental results as discussed in Section 6.6.1 and have been reported in Table 6-1. It is shown in Figure 6-3 that the model fits well with the experimental data. The single points are the Spacer Layer Interferometry Method (SLIM) tribofilm thickness results and the line is the fitted model. The fitting accuracy is shown in Figure 6-3 and the factors indicating the goodness of the fitting is included in the Table 6-1.

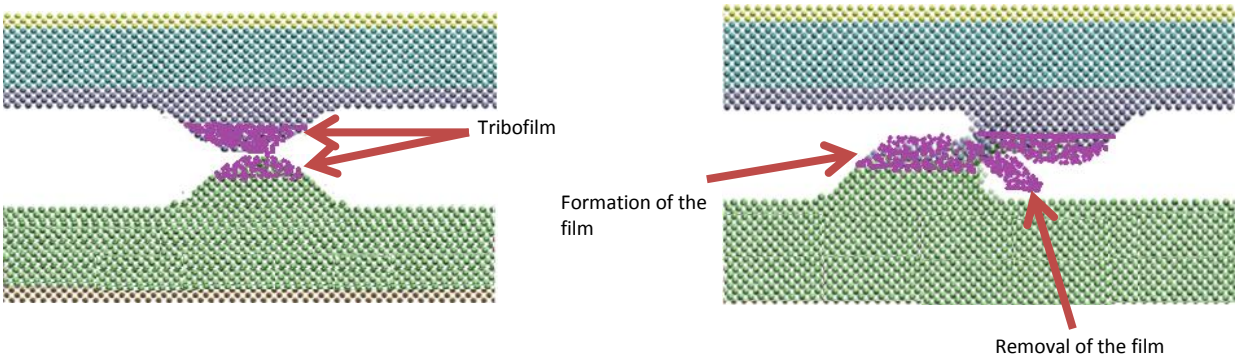

Figure 6-2 Schematic of the tribofilm removal occurring at the same time with formation

6.6 Results

The presented model in this thesis is a 'complete' model in the sense that it includes contact mechanics, tribofilm growth and a localised wear model and all components contribute to the overall prediction of the model. However, in order to focus on each aspect of the model separately, the development and the calibration of each part is discussed in separate chapters. The developed model is based on deterministic contact mechanics and includes Archard's wear equation and also a developed model for tribofilm formation. Therefore the model needs to be calibrated for both Archard's wear coefficient and also tribofilm growth formulation. The details of the wear model and its calibration procedure are presented in Chapter 7 as well as results of the wear prediction.

Model prediction of tribofilm growth, its coverage and inhomogeneity on surface asperities are discussed in this section. The growth model needs to be calibrated with experimental tribofilm growth results.

6.6.1 Calibration

The experimental results used to calibrate the model for this chapter are from the thesis of Naveira-Suarez (1) for the first set of simulations. The experiments are rolling-sliding contact for ball on ring using a Wedeven Associates Machine (WAM). The ball is steel 52100 with diameter and $R_a$value of 20mm and 10nm respectively. The ring is also steel 52100 and the R_a value is 100nm. Tribofilm thickness results for different slide to roll ratios have been used to calibrate the tribochemical model. The model calibrated for the maximum Hertzian pressure of 1.9 GPa is shown in this chapter as well as some predictive results.

In order to calibrate the model the experiment configuration should be considered in the contact mechanics simulations. Therefore two surfaces of 20µm×20µm were in contact and the rolling-sliding motion was simulated for surfaces in the way that surfaces are moved due to their speeds and one surface is moving faster than another surface depending on the SRR. The mathematical expression of Equation 6-14 was fitted to the experimental results reported in ref (1). The calibrated parameters are shown in Table 6-1.

The calibration parameters were then used in the numerical model to calculate the growth of the tribofilm on the contact asperities. An example of this calibration and the goodness of the fitting are shown in Figure 6-3.

The calibration of the tribofilm growth model is significantly important because the parameters will be used in the model to predict the wear behaviour. In essence, capturing the tribofilm behaviour is the first step of the numerical framework after the calculation of contact mechanics.

Table 6-1 The calibration parameters for the growth model

Parameter	Value	Description
h_{max}	176 nm	Maximum local tribofilm thickness in the formation process
x_{tribo}	4.13×10^{-16}	Tribofilm formation rate constant
C_3	0.1125	Tribofilm removal constant
C_4	0.0006799	Tribofilm removal exponential factor
R^2	0.9888	Goodness of the fitting by R-Square
$\bar{R}^2$	0.9805	Goodness of the fitting by adjusted R-Square

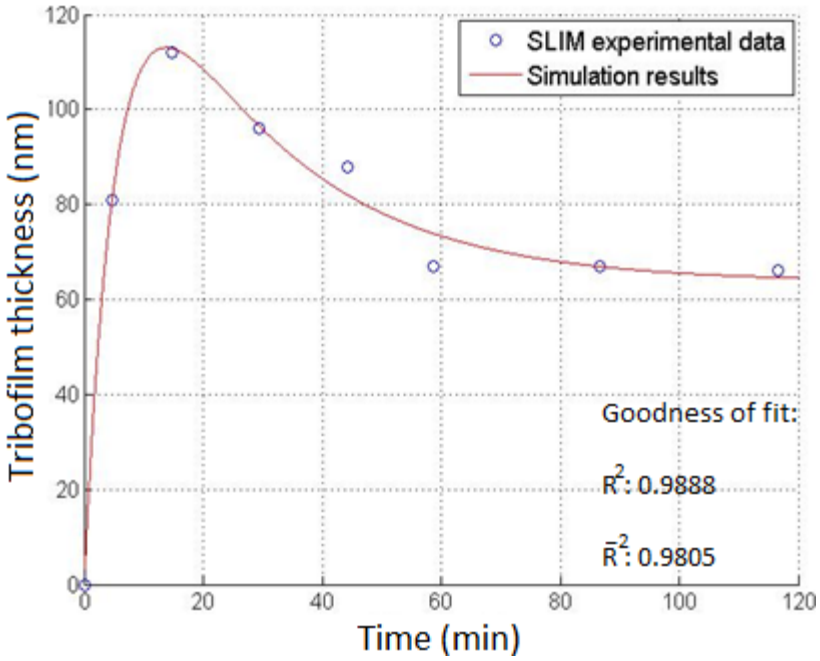

Figure 6-3 Tribofilm growth model calibration; goodness of the fitting. Experimental results are extracted from Ref (1)

Once the tribofilm behaviour is captured appropriately, its effect on the wear of the system is studied (the wear model is explained in detail in Chapter 7. The study focuses on the effect of ZDDP tribofilms on the reduction of wear on steel surfaces,

and will apply to any system that operates with the same mechanisms. Tribofilm thickness experimental results are used to capture the growth behaviour by setting the simulation values with respect to the experimental results. It is important to notice that once the tribofilm behaviour is captured, the model is able to predict the wear behaviour for the case of ZDDP on steel surfaces.

The parameters used in the tribofilm growth model such as x_{tribo}, h_{max}, C_3 and C_4 for different sets of experiments are extracted from the experimental results and can be used in the simulations. Some experimental results reported in the literature were used to investigate the above parameters (x_{tribo}, h_{max}, C_3 and C_4) and see the effect of ZDDP additive concentration and temperature on the their variations. The experiments were from a paper by Fujita *et al*. (15) which studied the growth of the ZDDP tribofilm on the contacting surfaces experimentally.

6.6.1.1 Effect of ZDDP Concentration on x_{tribo}

It was shown in the literature that ZDDP antiwear activity is dependent on the reactivity of its alkyl group (215). It was reported that secondary ZDDP (consisting of secondary alkyl) is more reactive than the primary ZDDP (containing primary alkyl). The experimental results for tribofilm growth of secondary and primary ZDDPs are reported in Figure 6-4 and Figure 6-5.

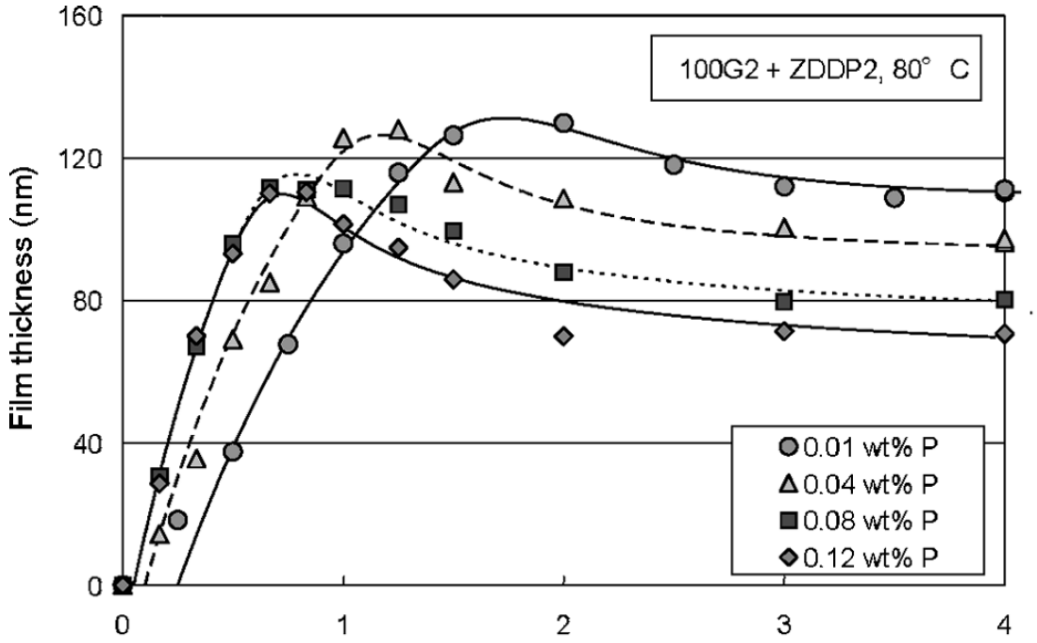

Figure 6-4 The tribofilm growth for different secondary ZDDP concentrations of in oil measured experimentally (15)

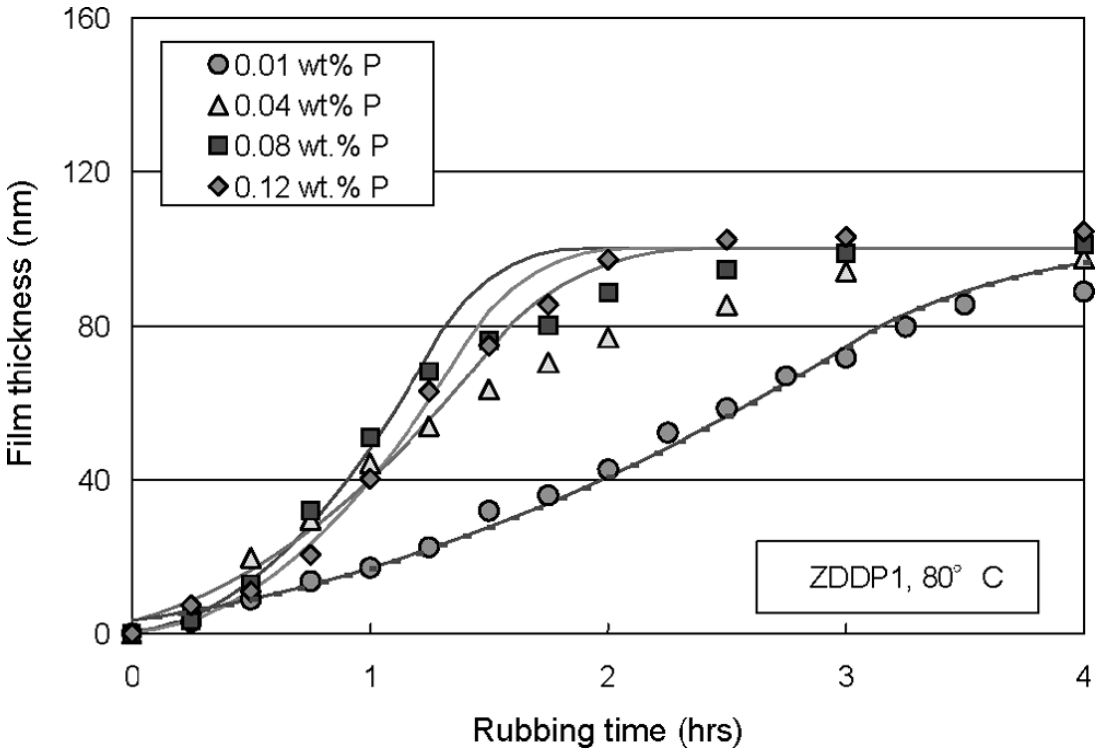

Figure 6-5 The tribofilm growth for different primary ZDDP concentrations of in oil measured experimentally (15)

Equation 6-14 was fitted to the data in Figure 6-4 and Figure 6-5 and the calibrated parameters are listed in Table 6-2 and Table 6-3 for primary and secondary ZDDP respectively. The fitting is conducted using the fitting tool in MATLAB and some examples of fitting plots are shown in Figure 6-6.

It can be seen that h_{max} is more than the maximum film thickness reported in the experiments and that is because of the combined effect of formation and removal. The tribofilm is formed and removed at the same time and if there was no removal happening at the interfaces the real formed tribofilm would be higher than what is observed in experiments.

The effect of concentration can be clearly seen on the term x_{tribo}. It is observed that concentration of ZDDP linearly changes the term x_{tribo} for both primary and secondary ZDDP. It can be interpreted in the way that the concentration of lubricant additives affects the kinetics of tribochemical reaction directly.

The variation of x_{tribo} with different ZDDP concentrations for both primary and secondary ZDDPs has been shown in Figure 6-6 and also formulated as follows:

$$x_{tribo} = (1.874 \times 10^{-16} \times x) + 2.014 \times 10^{-17} \quad \text{Equation 6-15}$$

$$x_{tribo} = (5.906 \times 10^{-16} \times x) + 2.054 \times 10^{-17} \quad \text{Equation 6-16}$$

Equation 6-15 and Equation 6-16 are for the primary and secondary ZDDPs respectively. The analysis results are in line with the hypothesis that the rate of tribochemical reaction can change with the concentration of the lubricant additive.

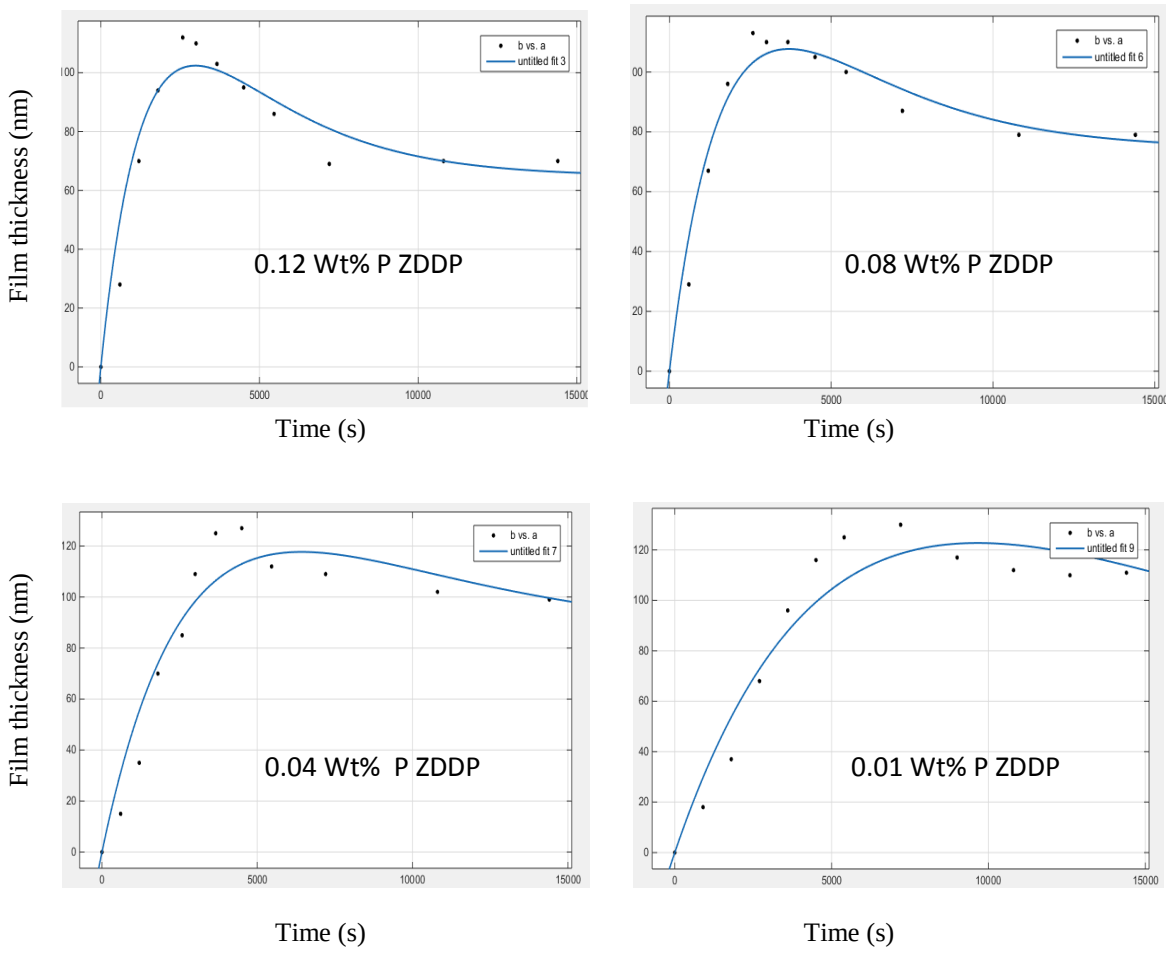

Figure 6-6 Fitting examples for different concentrations of ZDDP

Table 6-2 Calibration parameters for primary ZDDP at different concentrations

T=80^0 C	0.01%wt P	0.04%wt P	0.08%wt P	0.12%wt P
h_{max}	150 nm	150 nm	150 nm	170 nm
x_{tribo}	1.35×10^{-17}	3.57 ×10^{-17}	4.24×10^{-17}	3.58×10^{-17}
C_3	28.24 nm	50.49 nm	45.5 nm	55.94 nm
C_4	0.0006054	0.0002522	0.001571	0.001084

Table 6-3 Calibration parameters for secondary ZDDP at different concentrations

T=80^0 C	0.01%wt P	0.04%wt P	0.08%wt P	0.12%wt P
h_{max}	368.6 nm	350 nm	319.18 nm	300 nm
x_{tribo}	2.47×10^{-17}	4.45×10^{-17}	7.19×10^{-17}	8.87×10^{-17}
C_3	322.1 nm	259.9nm	246.4 nm	235.3 nm
C_4	0.00008	0.0001961	0.0002931	0.0003454

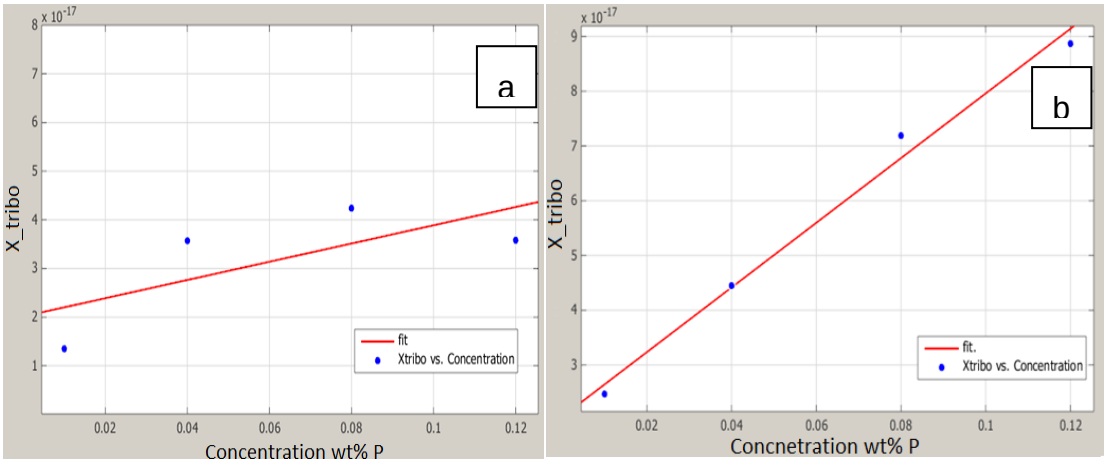

Figure 6-7 Variation of x_{tribo} with concentration of ZDDP for (a) primary (b) secondary ZDDP

6.6.1.2 Effect of Temperature on x_{tribo}

The experimental results for tribofilm growth of secondary and primary ZDDPs at different temperatures are reported in Figure 6-8 and Figure 6-9 from Ref (15) and are used for fitting Equation 6-14. The calibration data shows that the term x_{tribo} is almost independent of the temperature, which supports the fact that the mechanical activation of the tribofilm is independent of the temperature. It was suggested in Section 6.3 that the term x_{tribo} is responsible for tribo-activation of the tribochemical reaction and temperature is an independent term in the growth model.

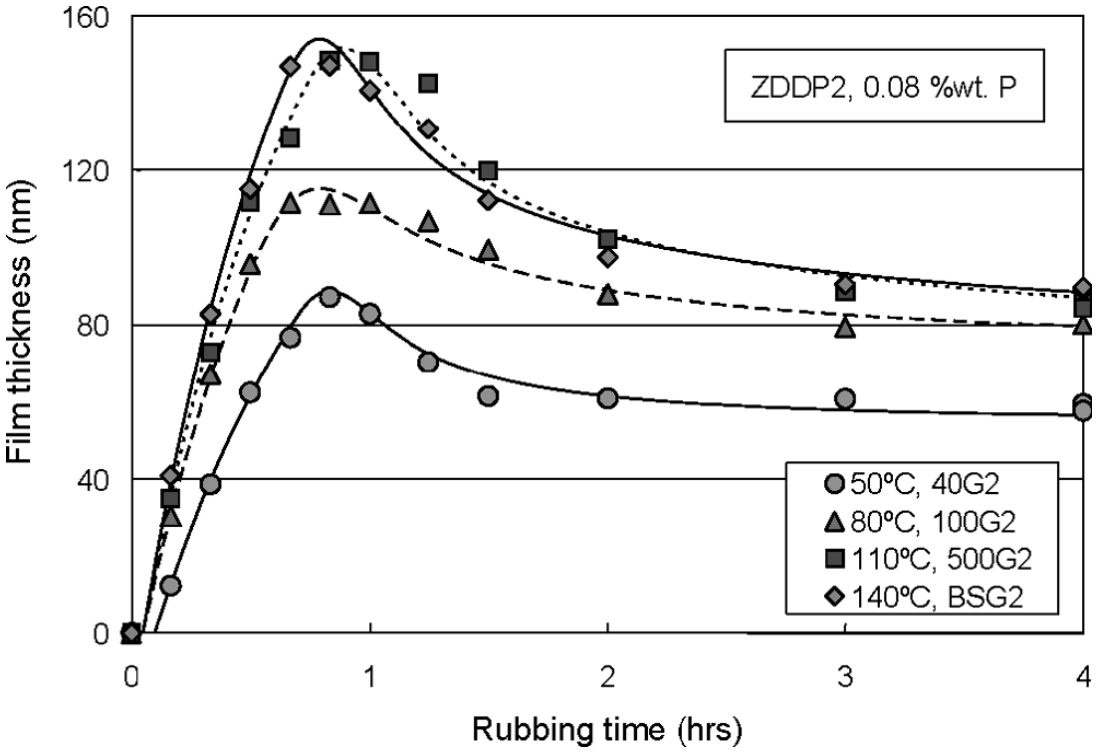

Figure 6-8 The tribofilm growth for secondary ZDDP at different temperatures measured experimentally (15)

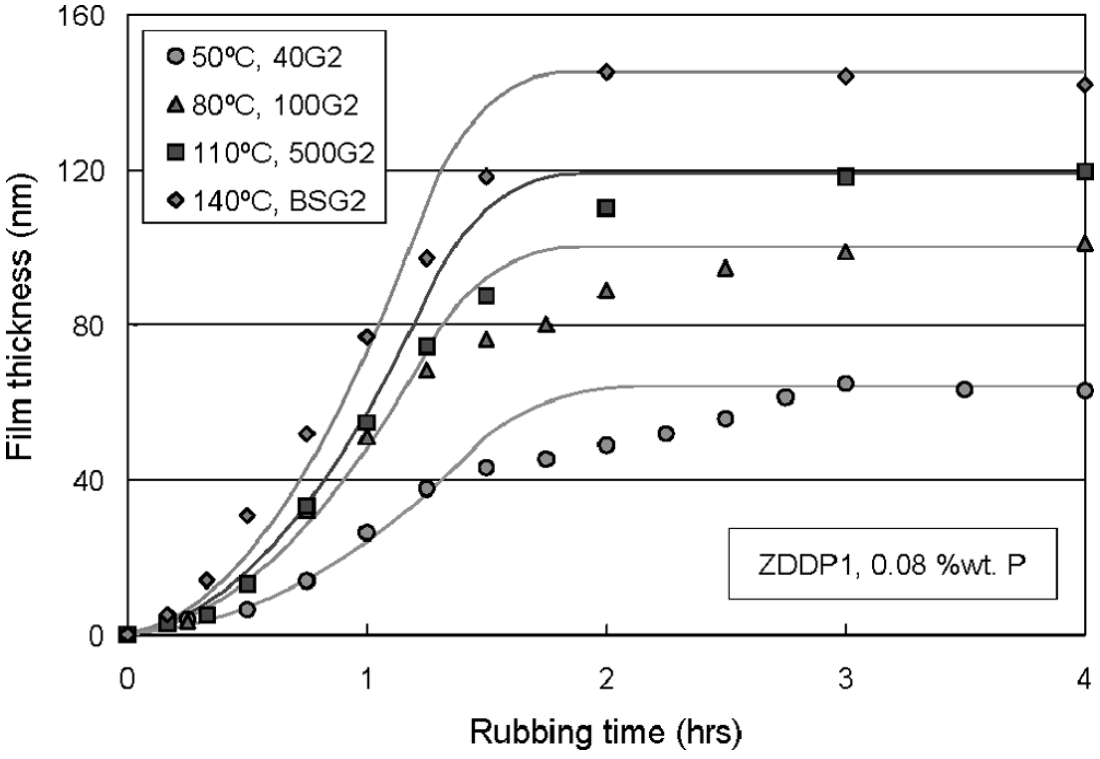

Figure 6-9 The tribofilm growth for primary ZDDP at different temperatures measured experimentally (15)

It should be noted that in this initial analysis of the proposed model, the obtained results are very encouraging and can be the starting point of any further analysis on the local tribochemical growth models.

Table 6-4 Calibration parameters for primary ZDDP at different temperatures

0.08%wt P	T=50^0 C	T=80^0 C	T=110^0 C	T=140^0 C
h_{max}	125 nm	150 nm	250 nm	250 nm
x_{tribo}	4.45×10^{-17}	4.24×10^{-17}	4.37×10^{-17}	4.25×10^{-17}
C_3	60.04 nm	47.55 nm	125 nm	101 nm
C_4	0.0006574	0.001473	0.0008284	0.001047

Table 6-5 Calibration parameters for secondary ZDDP at different temperatures

0.08%wt P	T=50^0 C	T=80^0 C	T=110^0 C	T=140^0 C
h_{max}	350 nm	319.18 nm	250 nm	300 nm
x_{tribo}	7.34×10^{-17}	7.19×10^{-17}	7.43×10^{-17}	7.11×10^{-17}
C_3	294.5 nm	246.4 nm	177.2 nm	226.7 nm
C_4	0.0003513	0.0002931	0.0001816	0.0002388

The variation of x_{tribo} for different temperatures for both secondary and primary ZDDPs is plotted in Figure 6-10.

6.6.2 Tribofilm Growth

The tribofilm is only formed on the contacting asperities. One example of the growth of the film on a rough surface is shown in Figure 6-11.

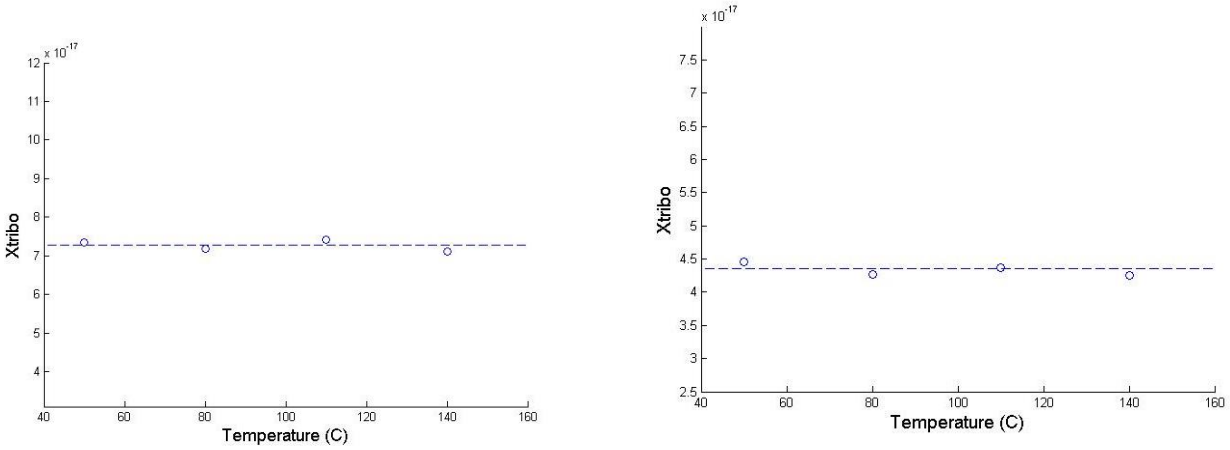

Figure 6-10 Variation of x_{tribo} for both a) secondary and b) primary ZDDP at different temperatures

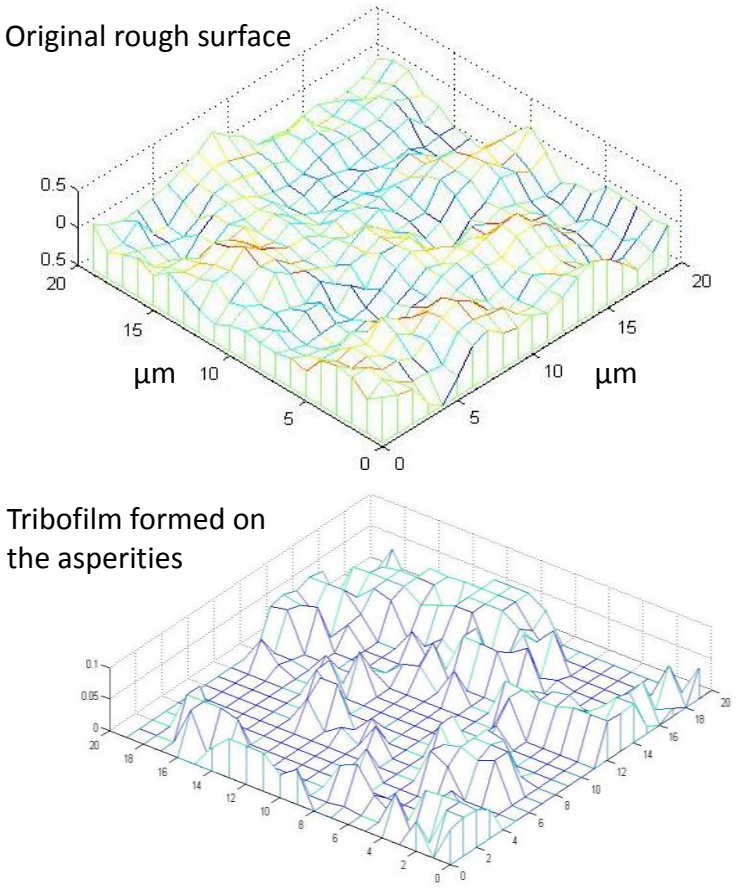

Figure 6-11 Formation of a tribofilm on rough surface- the original rough surface is shown on top and only the mesh of the tribofilm is shown in the bottom

The growth of the tribofilm can be predicted as a function of time. This is a good ability because it can monitor the film thickness at every time and any point of the surface. This helps to investigate localized effects in the tribosystems. An example of the mean tribofilm thickness calculations on the rough surface is shown in Figure 6-12. The mean tribofilm thickness is simply calculated by the average of the values of the tribofilm formed on the contacting asperities.

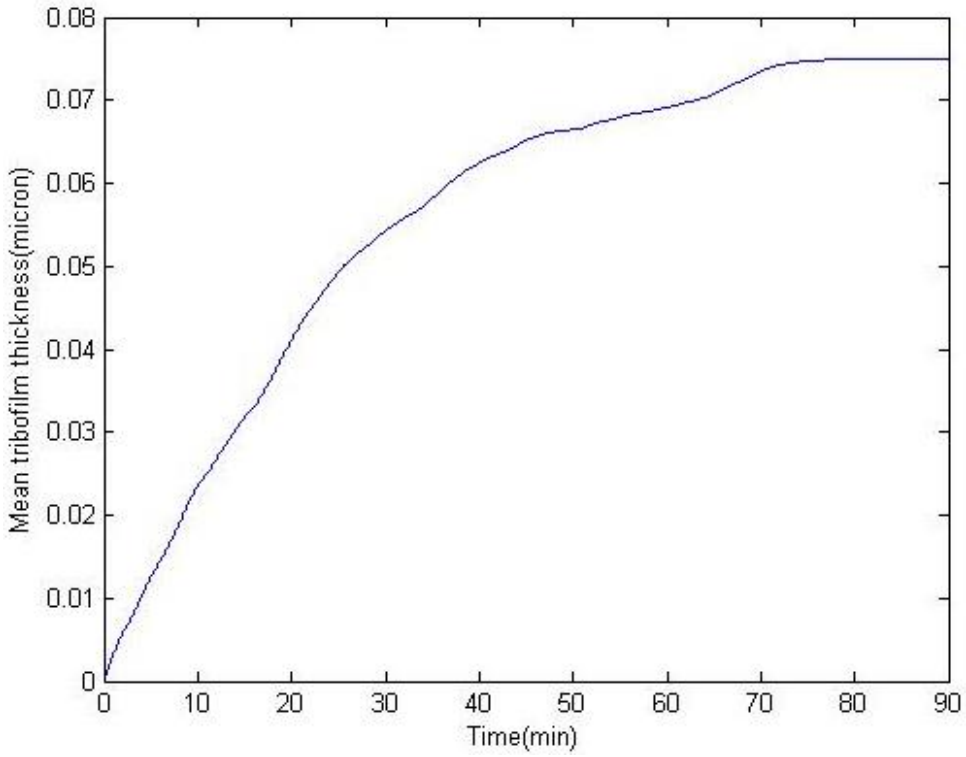

Figure 6-12 Mean tribofilm thickness calculation on the rough surface

6.6.3 Inhomogeneity of the Tribofilm

It has been reported experimentally that ZDDP tribofilms grow inhomogenously on rough surfaces. The inhomogeneity of tribological systems has, since the outset, been an important consideration in the current work. The roughness of the surfaces will lead to inhomogeneous distribution of load and also temperature on the surfaces, which will consequently result in different film formation and removal at different

parts of the surfaces. It is directly implemented into the nature of the model that the tribofilm forms differently on different areas in the surface. This inhomogeneity in the local properties of rough surfaces will result in different wear behaviours. This feature is clearly shown in Figure 6-11.

6.6.4 Tribofilm Coverage

As time increases, more asperity-asperity contact happens and the tribofilm grows over the surface. There are some experimental hypotheses that explain why the tribofilm coverage increases by time. It is suggested that the asperities become flattened due to plastic deformation and wear because of high pressures. This condition results in more asperities coming into contact therefore increasing the coverage area of the tribofilm.

In this modelling work, the hypothesis was observed numerically. Dynamic loading between surfaces in boundary-lubricated conditions results in reduction of the height of surface asperities due to plastic deformation and wear. This phenomenon then results in more asperities being in contact and the load is carried by more surface area. It can be interpreted as the load-carrying capacity of the surfaces in boundary lubrication. Increase in the number of asperities in contact results in formation of tribofilm in more contact areas that leads to more surface coverage by the tribofilm.

This behaviour is shown in Figure 6-13 which demonstrates the evolution of surface coverage by tribofilm at different times.

It can be seen in Figure 6-13 that pad-like structures of the ZDDP tribofilm form on the surfaces, as has been reported in the literature (35). This coverage behaviour in time is plotted in Figure 6-14 to show the percentage of the surface covered by the

tribofilm over the time. Once a point of the surface is in contact with the counter body, tribofilm starts to form on that asperity.

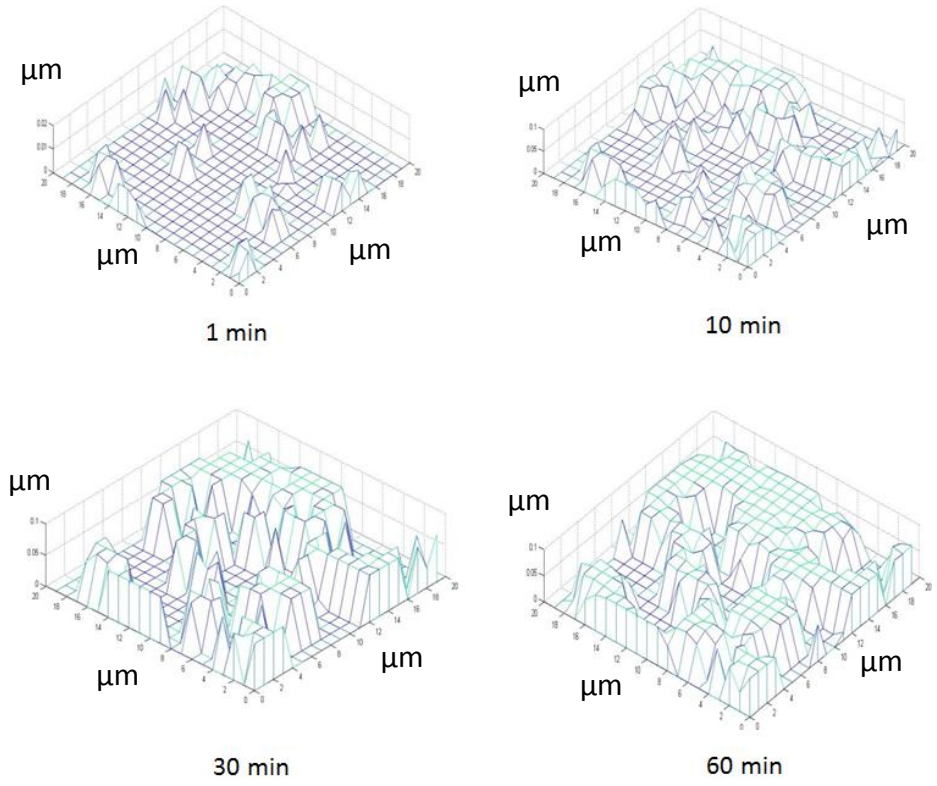

Figure 6-13 Evolution of surface coverage by ZDDP tribofilm. The surface patch is 20µm×20µm.

Therefore, any asperity after the contact is being counted as part of the surface covered by the tribofilm. This also makes sense physically since contact of the surface asperities is a starting point for the growth of the tribofilm.

With the same contact configuration, the effect of different parameters on growth and coverage of the tribofilm is investigated and reported in this chapter. The same calibration parameters were used in all the simulations in this chapter. The aim of this set of results is to show the sensitivity of the model. Experiments were designed to see the effect of these parameters on the formation and removal of the tribofilm which will help to involve more physical parameters in the growth model. All the

experimental results and the further development of the model for those parameters are reported in the next chapter.

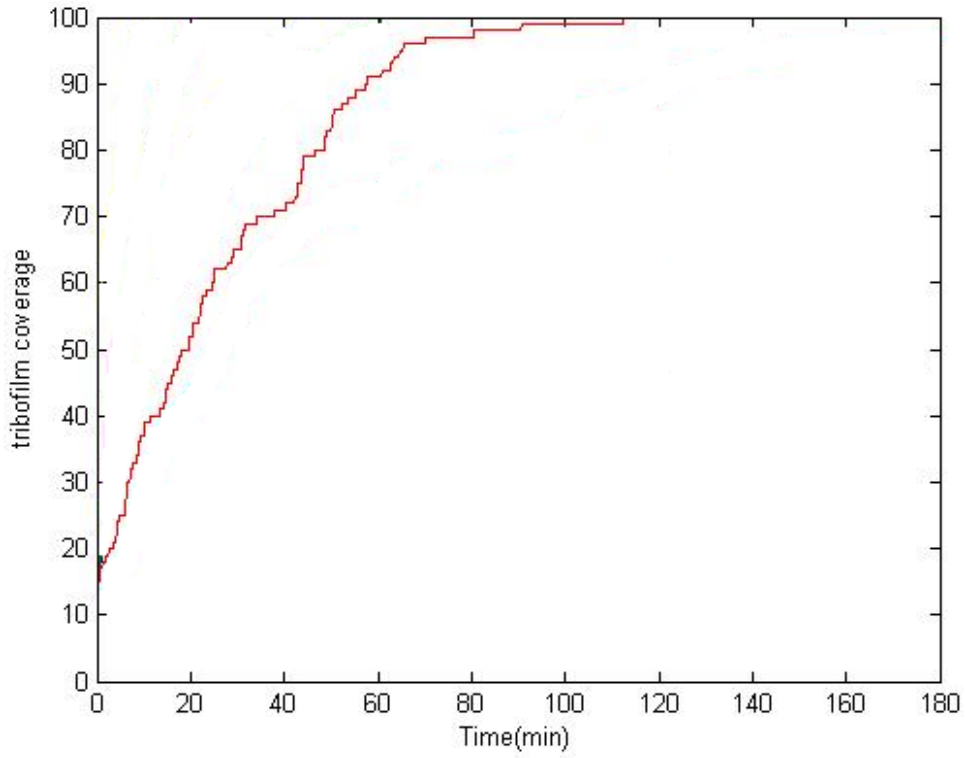

Figure 6-14 ZDDP tribofilm coverage of the surfaces from the calculations (corresponding to the tribofilm growth in Figure 6-13)

6.6.5 Effect of Load

The applied load on the surfaces in the contact mechanics simulation was changed and the tribofilm growth was calculated. The distribution of load on individual asperities was obviously different and thus resulted in different growth behaviours. The tribofilm growth results are shown in Figure 6-15. Also the predicted coverage of the tribofilm was affected by load in the simulation results, as shown in Figure 6-16.

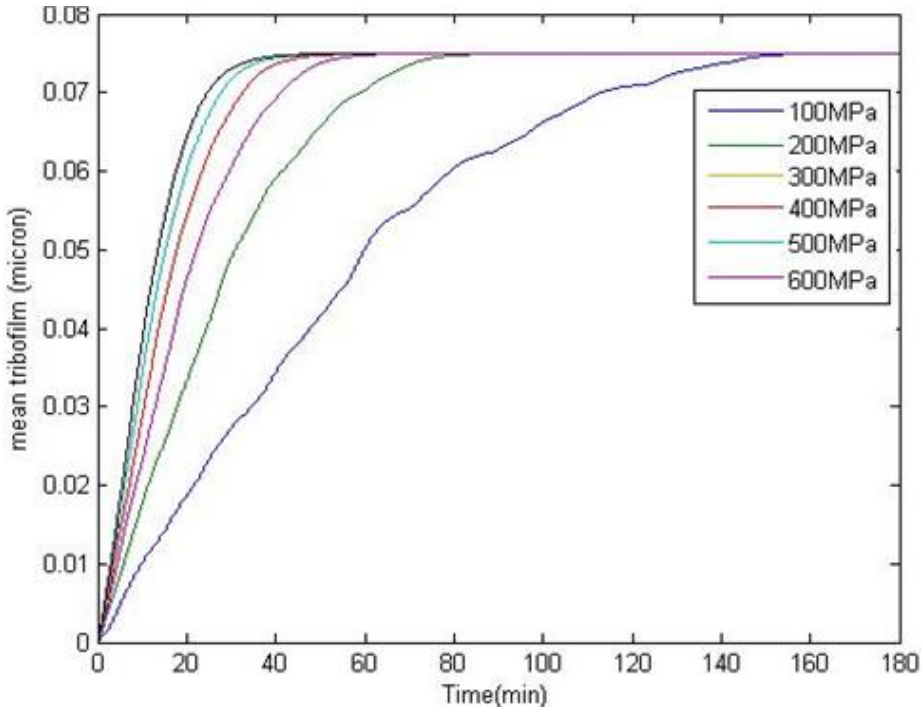

Figure 6-15 Effect of load on the mean tribofilm thickness calculated by the model

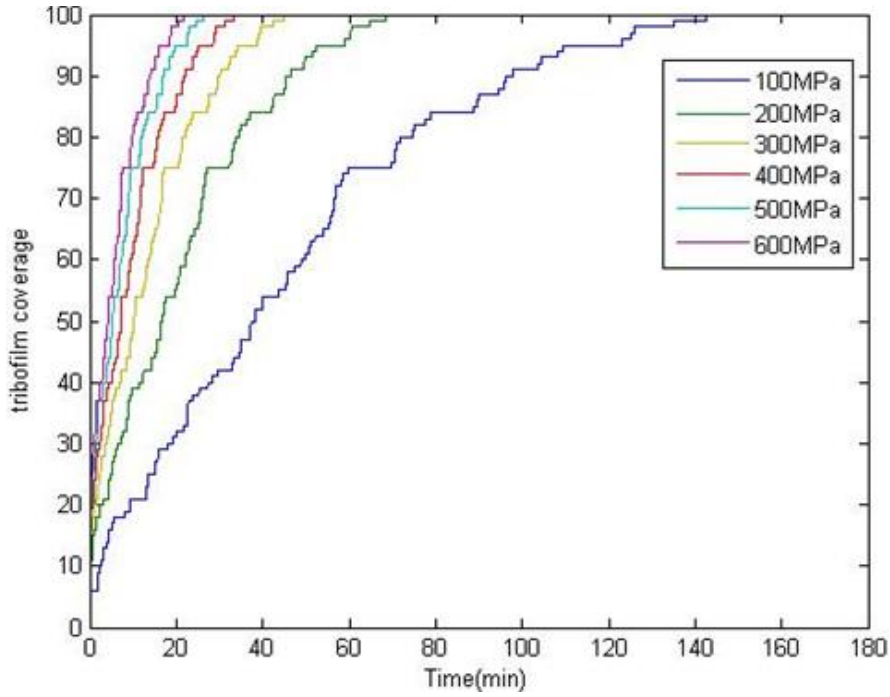

Figure 6-16 Effect of load on the tribofilm coverage percentage on a rough surface calculated by the model

It can be interpreted from the results that higher pressure leads to faster formation of the tribofilm. But this might not be true generally in the experiments. The reason is that different calibration parameters might be necessary for the model in the case of different loads.

It can also be observed that higher load results in faster coverage of the surface by the tribofilm which is reasonable. The higher load can change the topography of contacting surfaces faster which eventually results in faster coverage of the tribofilm.

6.6.6 Effect of Surface Roughness

This time the effect of initial surface roughness on the tribofilm growth is investigated. The same scenario is repeated here but the simulations were carried out only for surfaces with different Ra values. The numerical simulation results are shown in Figure 6-17.

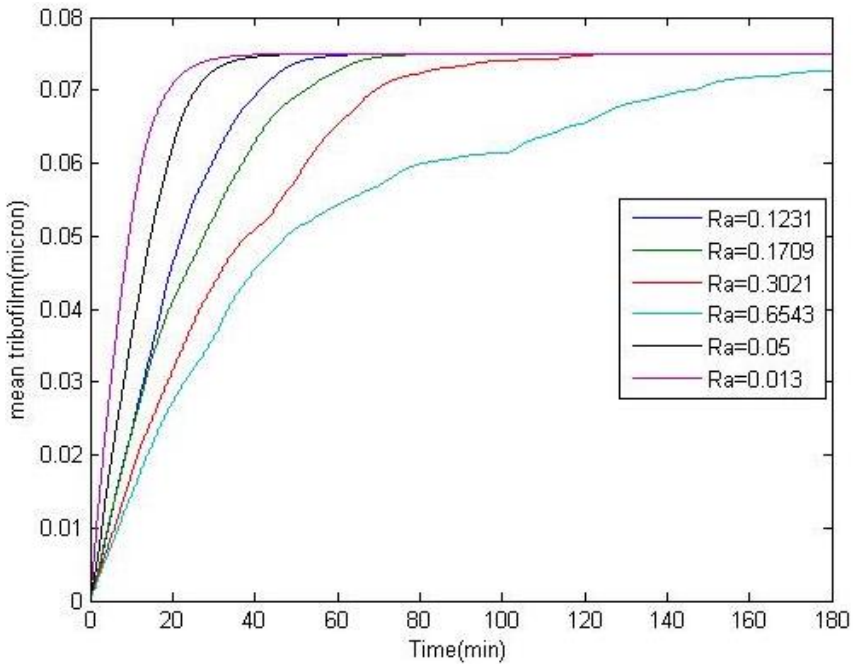

Figure 6-17 Tribofilm growth for different Ra values of rough surface

The results show that the smoother surfaces will have faster growth of the tribofilm. It can be interpreted in the way that they pass the running in process faster. The rough surfaces will take longer time to pass the running in period and one of the reasons is the longer time need for the high asperities to be flattened. This fact can be also proved by simulating the coverage area for different roughnesses. The results are shown in Figure 6-18.

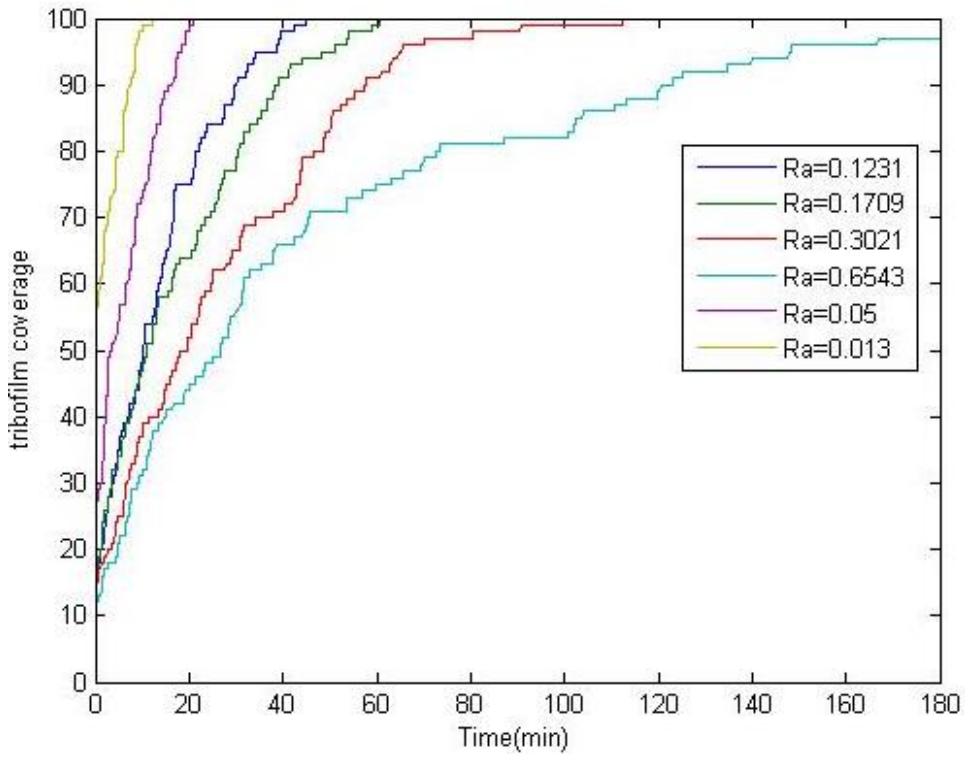

Figure 6-18 The tribofilm area coverage percentage for different Ra values

The results in Figure 6-18 also show that smoother surfaces become covered by the tribofilm faster than rough surfaces. The flattening of the asperities takes longer for rough surfaces, which results in slower coverage compared to smooth surfaces. It also supports the fact that smoother surfaces have a shorter running in period.

There is a very important point that should be noted in this analysis. It is assumed that both smooth and rough surfaces are experiencing boundary lubrication and the λ ratio is small enough for all conditions. One could argue that rough surfaces usually experience faster tribofilm formation and have thicker tribofilm compared to smooth surfaces. This can be true in many cases but if the contact is severe for both cases, the numerical results shown above is valid. The difference observed in experiments comes from the difference in λ ratio and the severity of the contact. Smooth surfaces experience less severe contacts because of bigger λ ratios.

It is logical to say that the real area of contact is greater in the case of smooth surfaces if it is in boundary lubrication. The deformation of asperities then affects the real area of contact faster because asperities are smaller in height.

6.6.7 Effect of Sample Sizes

Sample size is one of the important parameters in the analysis of the surfaces. Hence the effect of sample size on the growth behaviour of the tribofilm is tested numerically. All the working conditions are exactly the same. The roughness of the surfaces is also the same. The only difference between simulations, considered here, is the size of the surface samples in contact. The results are shown in Figure 6-19. Sample sizes vary from 10μm×10μm to 40μm×40μm for simplicity in this analysis.

It is clear from the results of Figure 6-20 that no big difference is observed in terms of tribofilm growth if all the working conditions are the same and different sample sizes are chosen. In many experimental activities, the cut off sample size will affect the analysis results. The reason for this might be the different roughness of different parts of the sample or different distribution of the surface asperities.

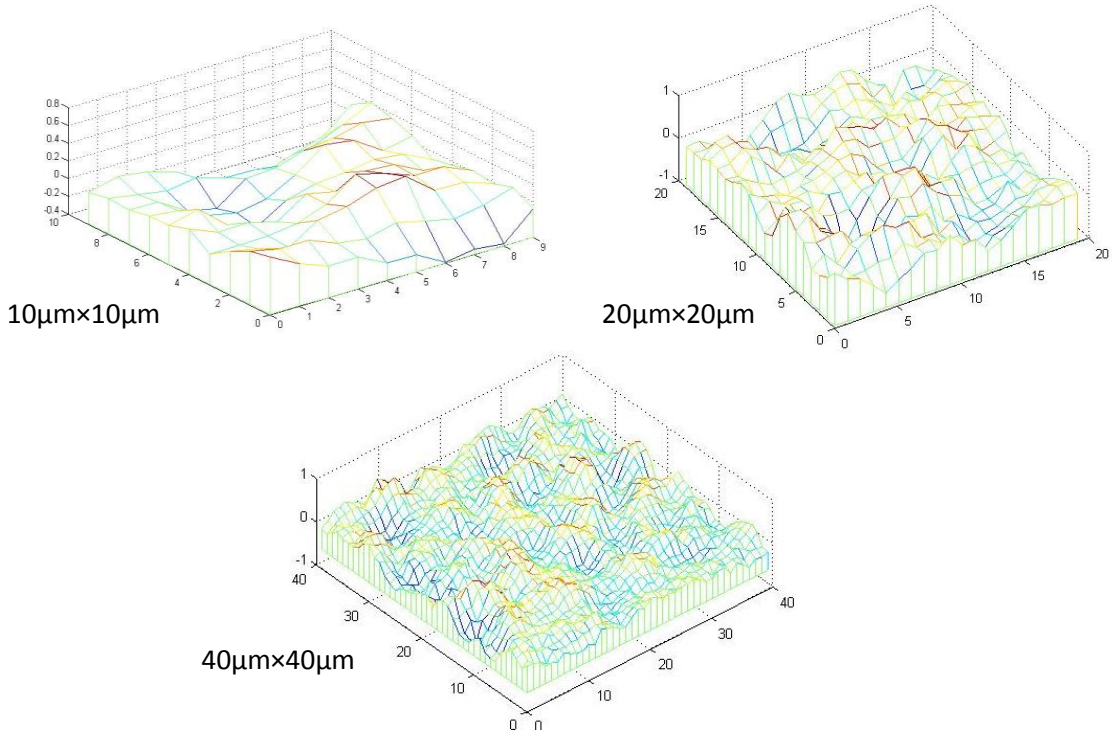

Figure 6-19 Different sample sizes as inputs of the numerical model,

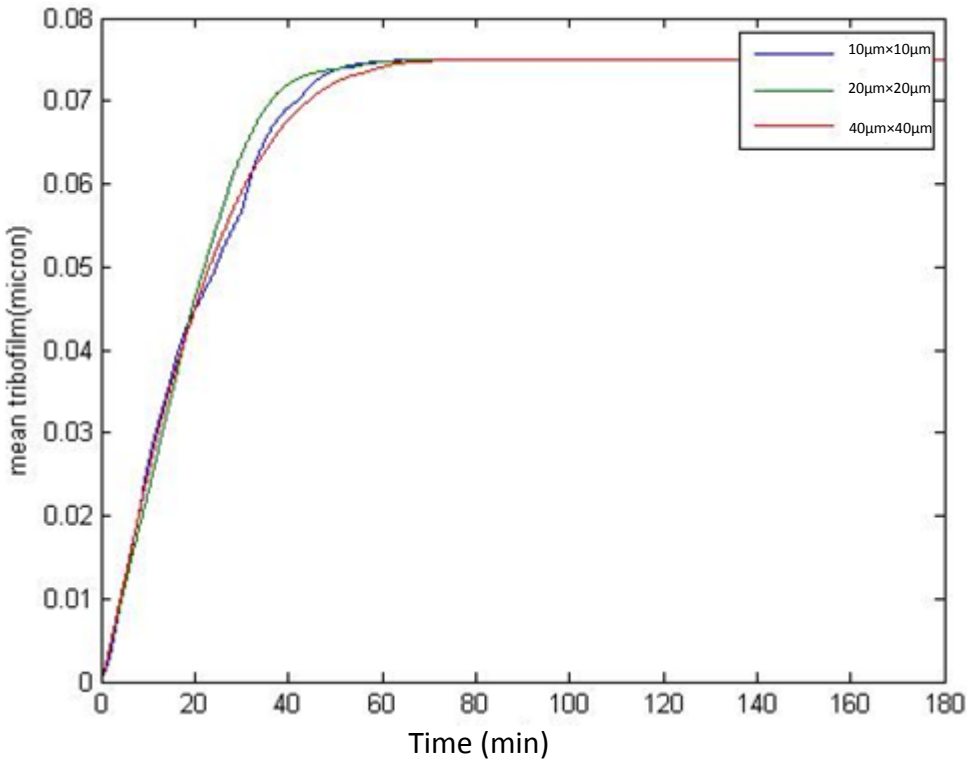

Figure 6-20 Growth of the tribofilm for different sample sizes

The same pattern is observed in Figure 6-21 for the coverage behaviour of the tribofilm on the surfaces. The results suggest that a reasonable size for the sample of the studies is indeed necessary for investigating the tribochemistry. In addition, a comparison between the asperity lateral size and the sample size is essential. A reliable tribochemical study needs a sample to cover at least numbers of asperities. The coverage of the tribofilm or the growth rate might not be affected by the sample size (as suggested by numerical results) but the inhomogeneity of the load, temperature and the tribofilm will be different.

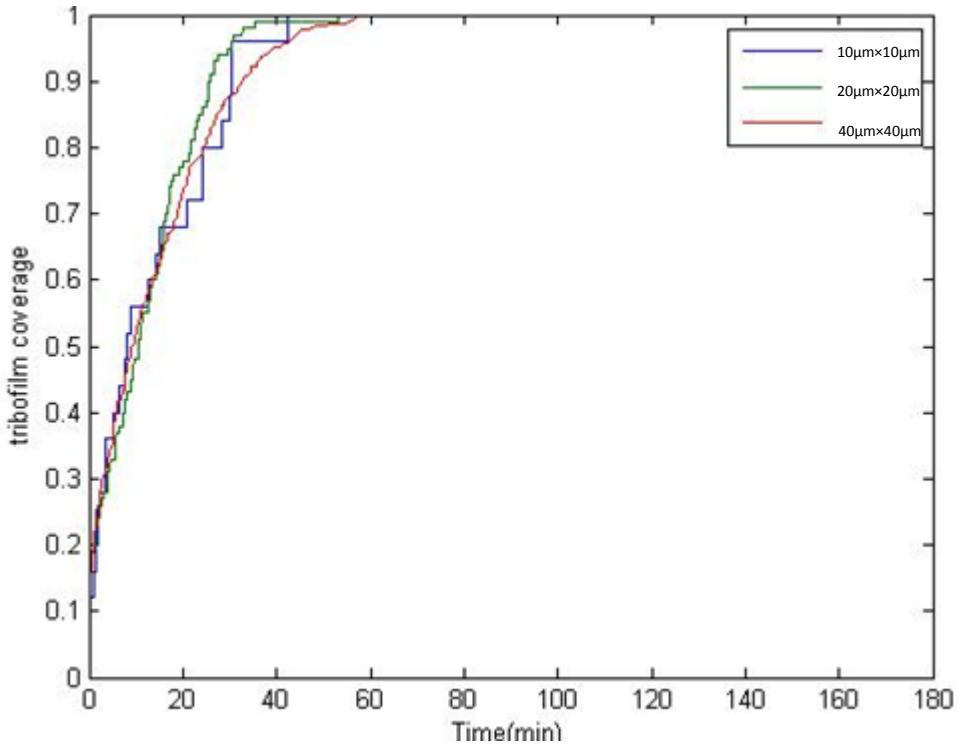

Figure 6-21 Coverage of the surface by tribofilm for different sample sizes

6.7 Discussion and Summary

A robust tribochemical model is an unavoidable part of any boundary lubrication model since the tribofilm properties mainly characterize the frictional and wear behaviour of the tribosystems. This tribochemical model should consider the physical, chemical and mechanical properties of the surfaces in contact as well as the chemical characteristics of the lubricant additives. In this thesis chapter, an attempt to build such a tribochemical model was made based on the thermodynamics of interfaces.

Development of a pure analytical model needs more physical understanding of the real mechanisms in this regime and seems to be very complicated. Therefore a semi-analytical model was developed that is able to capture important physical parameters in the boundary lubrication regime. A very important feature of this semi-analytical model is the capability to be adapted to experimental conditions. This feature helps to extract and involve more physical parameters in the tribochemical model. This feature of the model is investigated further in the next chapter. Another good characteristic which was an important aim of this model is the ability to link macroscale or components scale with microscale or asperity scales. The model is able to use information from experiments and compare it with asperity scale numerical calculations. This feature helps to establish the tribofilm growth model and link it to real tribological applications. The tribofilm thickness experimental results can always be compared or even fitted into the growth model.

This tribofilm growth model is implemented in the contact mechanics model developed and explained in the previous chapter. This combination enables the model to calculate contact properties and predict the formation and removal of the tribofilm. The tribofilm on the surface then changes the mechanical and physical properties of

the interface which eventually affects the frictional and wear behaviour. Details of these influences will be discussed in the next chapter.

The growth model was then calibrated with a set of experimental measurements from a Spacer Layer Interferometer extracted from Ref (1). The model then predicted the growth of the tribofilm on the contacting asperities. The sensitivity of the current model to different important working parameters was also tested in this chapter. It was found that the model also predicts an inhomogeneous growth of the tribofilm on the contacting asperities. The growth model is also sensitive to applied load and higher loads result in faster growth of the tribofilm because of higher contact loads and higher temperatures. The coverage of the tribofilm is also faster for higher loads. That can be because of faster asperity flattening due to the higher loads which leads to faster topography modifications. This will result in more asperities becoming in contact and finally increases the coverage of the tribofilm.

This scenario was also tested for different surface roughnesses. It was found that smoother surfaces are more likely to be covered faster by the tribofilm. This is physically tangible. In severe conditions smooth surfaces experience surface modifications that are close to the roughness of the surface value. This modification influences the real area of contact and therefore surface coverage by the tribofilm increases faster in comparison to rough surfaces. It must be noted that the contact should be severe enough to be in boundary lubrication condition. Otherwise, rough surfaces can experience more severe conditions while the smooth surfaces might be in mixed lubrication regime or less severe contacts.

The sensitivity of the model for different sample sizes (size of surfaces in numerical model) was also tested. It is shown that the size of the samples does not affect the

numerical results if the roughness of the surfaces is exactly the same. It is suggested that the difference observed in the experimental results can be due to differences in the topography of the chosen samples.

The comparison between tribofilm removal and substrate wear, and the ability to isolate each, can help to understand better the true mechanisms of wear. This investigation can help tribologists to relate tribofilm removal to wear of the system. The model is able to calculate tribofilm removal at any time steps and can help to monitor removal during the time. It can be used to compare tribofilm formation and removal rate at any time of the tribosystems runs. Studying the effect of different parameters on tribofilm removal can be carried out in this model which might be a starting point to model film removal based on different factors.

Chapter 7. Wear Modelling

This chapter represents a new proposal for the mechanism of wear in the presence of the ZDDP tribofilm on steel surfaces. The wear model proposal is then validated with the experiments. As explained in Section 5.1, the wear model is then implemented into the numerical framework for wear calculations.

7.1 Introduction

Wear is defined as the material loss that occurs on the surfaces of contacting bodies in relative motion. Wear has a major impact on the reliability of tribosystems and determines the durability of machine elements. Understanding the true mechanisms of this phenomenon can help engineers design more efficient machine parts and also results in the better maintenance of those elements. Predicting wear is one of the most important challenges in the whole engineering field and a lot of attempts have been made to predict material loss on contacting surfaces. Wear of surfaces mostly occurs when solid-solid contact happens between the surfaces and the load is carried by the asperities of the bodies.

One of the first attempts to model wear was made by Archard (25). A wear model was introduced based on the load and rubbing distance of the contacting bodies. This model has been used in a wide range of wear studies and the results show good agreement with experimental observations. The Archard wear model was developed for dry sliding conditions and no effect of the tribofilm was included in the model.

It has been observed widely that the tribofilms change the wear behaviour of the tribosystems. Tribochemistry, e.g. tribofilm formation, removal and associated mechanical properties, highly affect the wear of the system. Including these properties

into wear models is essential if one wants to achieve full prediction of lubricated system wear.

Antiwear additives are generally known to form protective tribofilms on the surface of contacting bodies. The most common such additive is zinc dialkyldithiophosphate (ZDDP) (35), which can form tribofilms on various materials including steel, diamond-like carbon (DLC) and Si/Al alloys (49, 60, 65-73). Though extensively studied, the specific processes involved in formation and removal of tribofilms in these different systems are not yet fully understood. In the case of inert surfaces such as DLCs, tribofilms do form, but some reports indicate that they can be easily removed from the surface (60, 72). The tribofilm has a negligible effect on the wear (72), with wear resistance properties being dominated by those of the DLC itself, and with the type of DLC having an important influence (71). However, it was also reported that the chemistry of the lubricant has significant effect on the removal of the DLCs (216-218). In contrast, ZDDP tribofilms formed on steel surfaces have been shown to contain iron in the bulk (74), indicating a significant interaction between the ZDDP and the substrate. This can be due to several reasons: (i) chemical reaction resulting from cation exchange in the polyphosphate (Fe^{3+} in place of Zn^{2+}); (ii) mechanical mixing in the process of high load and shear stress; and (iii) digestion of the iron oxide abrasive particles in the bulk of the tribofilm. There are different wear reduction scenarios reported for ZDDP but the most accepted one is coverage of the surface, prevention of direct asperity-asperity contact and increasing the load carrying capacity of surfaces.

Previous works have mainly reported contact mechanics simulations for capturing the boundary lubrication regime but the real mechanism in which tribofilm reduces wear

is still unclear. The aim of this chapter is to propose a mechanism by which antiwear additive tribofilms may possibly reduce wear. This mechanism is modelled mathematically and implemented into the deterministic contact mechanics simulations. This wear model takes into account the effect of ZDDP tribofilm and couples it with a localised Archard wear equation. This can be interpreted as a modification to the Archard wear equation taking into account the effect of ZDDP tribofilm. In this chapter, first an introduction to Archard's wear equation and the numerical approach to employ it in different scales will be reported. Then the proposed wear model will be discussed and the modification to Archard's law is reported. Some examples of the numerical results are shown and experiments for validating the model for a set of real tribological systems are shown. The simulation shows good agreement with the experimental measurements.

7.2 Archard's Wear Equation

As explained earlier in this chapter, Archard's wear equation is the most commonly used wear model in the literature. Archard's model was used in different modelling approaches such as Finite Element Method and Boundary Element Method (109, 116, 156, 159) analyses. Archard's model was initially developed for sliding in dry conditions and no effect of lubricant nor chemistry was involved in the model. In this section, a localised version of Archard's wear equation is introduced which is used in the numerical model.

The wear can be calculated using Equation 7-1. This concept was first introduced by Holm (24) in the context of electric contacts. The wear volume can be calculated per sliding distance and proportional to the load.

$$W = K\frac{F_N}{H}S$$ Equation 7-1

in which W is the wear volume and K, F_N, S and H are the wear coefficient, normal load, sliding distance and the hardness of the material respectively. Archard interpreted the wear constant as a probability that collision of an asperity will lead to removal of the material.

The well-known Archard equation can be used at the local (i.e. asperity) scale if all the parameters of Equation 7-1 are adapted to this scale. The sliding distance should be the sliding distance of a single asperity and the load will be the applied pressure of that asperity.

The wear formulation can also be used for wear depth calculations. Both parts of the Equation 7-1 can be divided by the area of a single asperity. The wear depth formulation is as follows:

$$h = K\frac{P}{H}s$$ Equation 7-2

in this case, P is the pressure on the asperity and h is the wear depth on that single asperity.

For the sake of numerical simulations, wear can be calculated for every time step. Considering the time steps and the speed of the movement, the sliding distance can be calculated. If the surface is assumed to contain several contact points in two dimensions, the wear depth calculation is:

$$\Delta h(x,y) = \frac{K}{H}.P(x,y).\Delta t.v$$ Equation 7-3

Equation 7-3 is the same as Equation 7-2 but for two dimensions and includes the speed (v) of surfaces. Δh is the wear depth at each point of the surface. Equation 7-3 will be computed at every time step and the pressure distributions are the pressures calculated at each time step from contact mechanics simulations.

7.3 Tribochemical Wear Calculation

As was explained in the introduction section, a wide range of studies have been conducted to investigate wear in the boundary lubrication regime. Despite the importance of tribofilms in controlling the wear behaviour of such systems, the effect of tribofilms in reducing the wear is not well understood. It is clear that an antiwear additive such as ZDDP can reduce the wear by forming a solid-like tribofilm that protects surfaces from direct solid-solid contact but the real mechanism in which wear of the surfaces happens in presence of the tribofilm is still not clear. It is not clear if this reduction is due to a decrease in the substrate contact pressures, asperity fractures, crack initiations etc. The wear reduction is a complicated process since the numerous complicated physical and chemical phenomena occur at the same time at interfaces. It was reported experimentally that tribochemistry e.g. tribofilm formation and removal in combination play a significant role in this case. It was reported by Spikes (35) that there are three major mechanisms by which ZDDP tribofilm reduces the wear of the system. Firstly it is reported that ZDDP tribofilm acts as a mechanical barrier and prevents the direct asperity-asperity contacts. In this case the adhesion between asperities is decreased and the stresses on the asperities are reduced significantly.

The second mechanism is the ability of the ZDDP tribofilm to digest the hard iron oxide wear particles. These wear particles are very hard and abrasive and digestion of them by glassy polyphosphates can significantly reduce the wear of the system (63). The third antiwear mechanism of ZDDP is the reaction of ZDDP with peroxides that prevent corrosion at metal surfaces (219).

It is clear that the ZDDP tribofilm significantly prevents wear and this is a complicated mechanism. Therefore a new mechanism in which the tribofilm can reduce wear is proposed here. This mechanism is then formulated mathematically and is tested and validated with designed experiments.

The wear modelled in this work is considered to be mild wear which occurs due to the chemical reactions between the substrate and the lubricant additives and this produce thick tribofilm. Note that this mechanism of wear does not apply in the case of inert substrates such as DLC, as mentioned in Section 7.1, but it is reasonable in the case of ZDDP tribofilms on steel surfaces.

It was reported experimentally (35, 48, 59, 220) that even in areas where a tribofilm is fully formed, wear is occurring. It can be interpreted as partial removal of the tribofilm and at the same time formation of the film to restore the balance. Studies show that the concentration of substrate atoms decreases towards the top of the tribofilm produced by ZDDP on steel (18, 74). Therefore if material detaches from the tribofilm due to the contact, some amount of the substrate atoms are removed from the surface. This decrease in the atomic concentration of the substrate as the distance from the substrate/tribofilm interface increases supports the fact that less wear of the substrate occurs if a thicker tribofilm exists. This mechanism was reported by Bosman *et al*. (18), who considered the volumetric percentage of Fe over the depth of the

tribofilm and assumed lower concentration in upper layers of the tribofilm. His formulation was based on the plastic deformation of the tribofilm and that the deformation counts as the removal of the layer. This removal was then combined with an atomic concentration model extracted from the experiments. But in this work, it is assumed that the removal model predicts the amount of tribofilm removed and is independent of the wear model.

The tribofilm can be removed as a result of severe contact of the asperities as sketched in Figure 7-1. In this case a limited number of the substrate atoms present in the uppermost part of the tribofilm are detached from the surface. At the same time, more substrate atoms diffuse into the tribofilm and move towards the upper parts of the film to restore the chemical balance. Replenishment of the tribofilm then might occur due to different surface phenomena including the tribochemical reactions and mechanical mixing due to combined effects of material removal and shear stress.

It was suggested by Ghanbarzadeh *et al*. (117, 221) that the dynamic formation and removal of the tribofilm will lead to the wear of the substrate. It should be noted that this wear is much less than the wear resulting from solid-solid interactions.

The above statement was a starting point to consider the wear of a substrate in the presence of a tribofilm. It is logical to assume that the thicker the tribofilm is, the less the chemical reaction will occur between additives and the substrate. An assumption is made in this work in order to consider the effect of the tribofilm in reducing wear by relating the wear coefficient to the thickness of the tribofilm. It is assumed that in the areas where tribofilm is formed, the coefficient of wear is less than the areas where tribofilm is not formed.

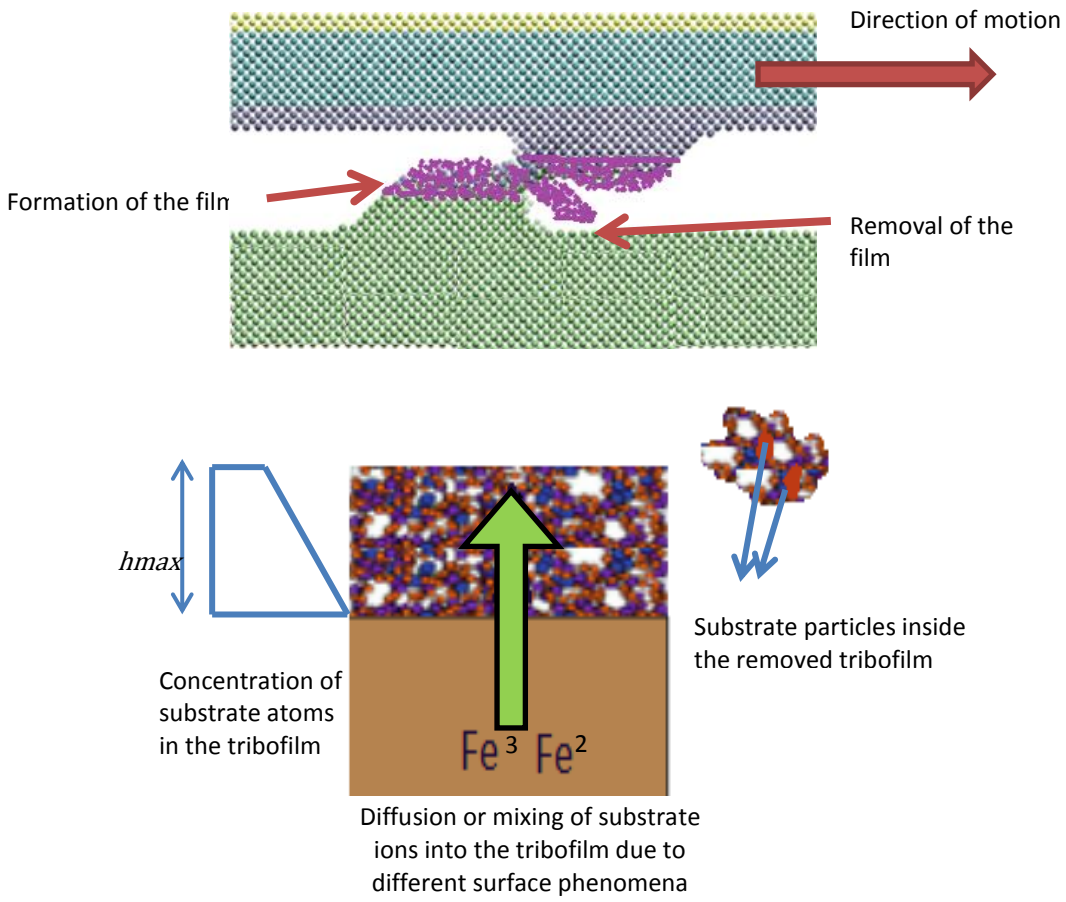

Figure 7-1 Illustration of the wear hypothesis

The coefficient of wear is assumed to change linearly with tribofilm height. Assuming that the coefficient of wear is at its maximum for steel-steel contact and at its minimum when the tribofilm has its maximum thickness, the equation for calculating coefficient of wear is as follows:

$$CoW_{tr} = CoW_{steel} - (CoW_{steel} - CoW_{min}).\frac{h}{h_{max}} \qquad \text{Equation 7-4}$$

CoW_{steel} , CoW_{min} and h_{max} are coefficient of wear for steel and coefficient of wear corresponding to maximum ZDDP tribofilm thickness and maximum film thickness respectively and CoW_{tr} is the coefficient of wear for tribofilm with thickness h.

It should be noted that this model is a local and time-dependant model and is a justification to experimental observation. Linear dependence of the wear to the tribofilm thickness is a simplification in mathematical formulation of the above experimental observations. Regarding this fact, a modification to Archard's wear equation has been made with respect to the thickness of the tribofilm. The Archard's wear coefficient is responsible for characterizing the local wear behaviour of the system. The relationship can be clearly seen in Figure 7-2.

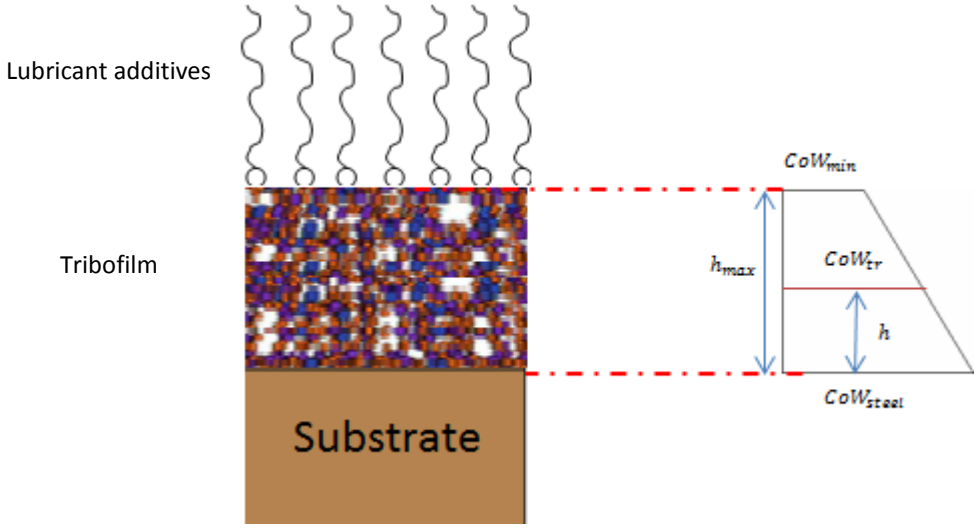

Figure 7-2 Schematic of coefficient of wear variation with tribofilm thickness.

There is no experimental work reported that provides a specific form for the variation of wear rate with tribofilm thickness. The linear form assumed here is the simplest mathematical form that allows for a variation across the tribofilm as a result of the non-uniformity in the concentration of substrate ions across the tribofilm. This could be modified in future iterations of the model, should further experimental results become available, but the comparison with experiments in Section 7.5 indicates that Equation 7-4 is a sufficient representation of the behaviour.

This wear is the wear in the presence of the tribofilm. Therefore it is different from the concept of only fracture and removal of substrates due to mechanical rubbing and is almost similar to what is being observed in steady-state. It should be noted that the formation of the tribofilm takes time and it takes time for the asperities in contact to be covered by tribofilm. In this sense, it takes some time for the coefficient of wear to reduce and the wear and plastic deformations happen severely in the beginning.

It is also important to note that this wear model does not necessarily predict that the thicker tribofilms observed in experiments result in less wear of the substrate. The formation of thicker films on the surfaces may use more substrate as a reactant to produce the tribofilm. The coefficient of wear used in this work is a local coefficient of wear which is changed in time because of changes in tribofilm thickness. The wear results measured in different experiments are shown in experimental Section 7.5.1.3 and the validation of simulation results is reported.

7.4 Effect of Input Parameters on Wear Prediction

In this section the wear model is tested and the sensitivity of the model to variations in the coefficient of wear and load is studied. All the simulations were carried out for one case. The working conditions and calibration parameters are the ones reported in Section 6.6.1 and Table 6-1.

7.4.1 Real Time Wear Calculation

The wear in this work is the wear depth calculated for all surface points at every time step. The wear of the system at each time step is calculated by summation of the wear values for all contacting points. In addition, the wear depth in this work is the summation of wear with plastic deformation at asperities and this is because both wear

and plastic deformation contribute to topographical changes at the asperity scale and the wear depth measured in the experiments is the final depth profile of the surface. Therefore the wear is calculated step by step and a real time calculation of the wear is carried out via the model. An example of the wear calculation which is based on the calibration parameters (Section 6.6.1 and Table 6-1) has been shown here. It can be observed that higher wear occurs in the beginning of the contact. This is likely to be because of higher plastic deformation and less tribofilm formation.

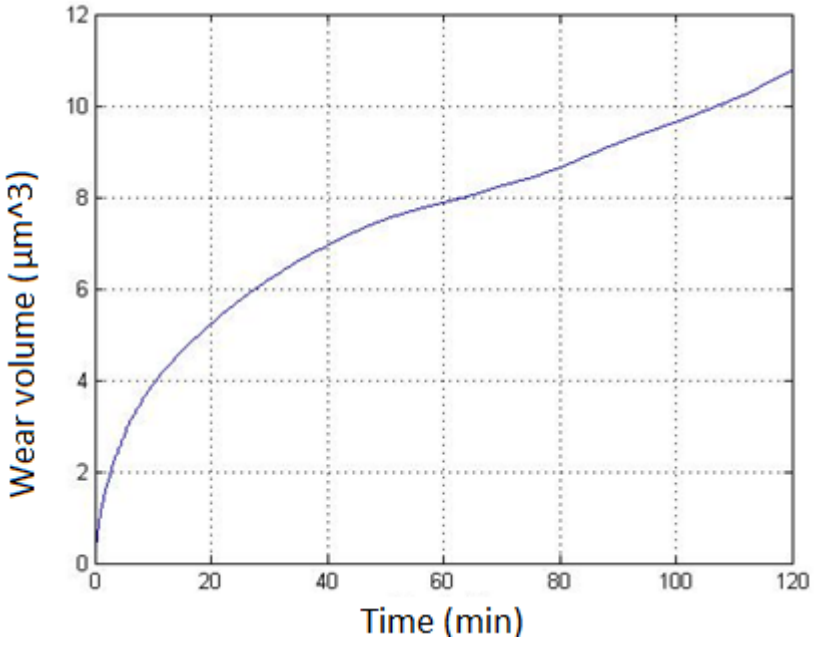

Figure 7-3 Real time wear calculation in the case of ZDDP on steel surfaces for a ball on disk configuration. The tribofilm growth model has been calibrated based on the experimental results from Ref (1). Wear calculation is qualitative because the wear model was not calibrated.

The wear rate shown in Figure 7-3 is high in the beginning and decreases gradually to reach an almost steady state rate. This is observed also experimentally. The means of this behaviour is determined in this model. A greater plastic deformation is calculated in the beginning which is because of high asperities in contact. These asperities will plastically deform and the surface will be flattened over time and the load will be

carried by more asperities. This will lead to smaller contact pressures at the asperities and less plastic deformation will occur. Additionally, the antiwear tribofilm forms and it reduces more wear of the system.

7.4.2 Effect of Coefficient of Wear

The coefficient of wear is an important parameter that defines the wear of tribologically loaded systems. It can be seen in Equation 7-4 that the value of the *initial* coefficient of wear (CoW_{steel}) has direct effect on the predicted wear behaviour of the system. Simulations were conducted with the same working conditions and the parameters are the ones reported in Section 6.6.1. The dimensional *initial* coefficients of wear have been varied from $3.3 \times 10^{-16} ({}^{m^3}/_{Nm})$ to $1.33 \times 10^{-14} ({}^{m^3}/_{Nm})$. The values are reasonable and comparable to the ones reported in the literature. The point of this section is to show the sensitivity of the wear model to the initial coefficient of wear values. Therefore a random but reasonable range of initial coefficient of wear was selected. The wear depth calculation results have been reported in Figure 7-4.

It is clear that the coefficient of wear changes the wear rate of the system. The reason for not choosing a wider range of coefficients of wear is visibility of the wear values in one plot. In this case the difference between real time wear calculations can be clearly observed.

7.4.3 Effect of Load

From the Archard's wear formulation it is expected that load will affect the wear of the system. Simulations were conducted for different loads ranging from 250MPa to 1.2GPa and the real-time wear was calculated.

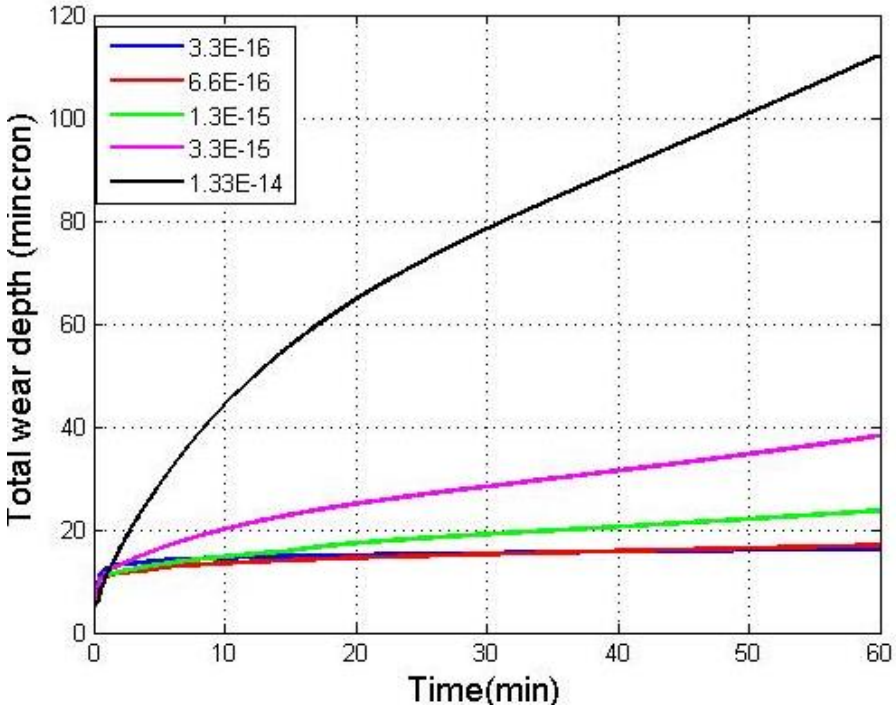

Figure 7-4 Wear depth calculation for different dimensional *initial* coefficients of wear (CoW_{steel})

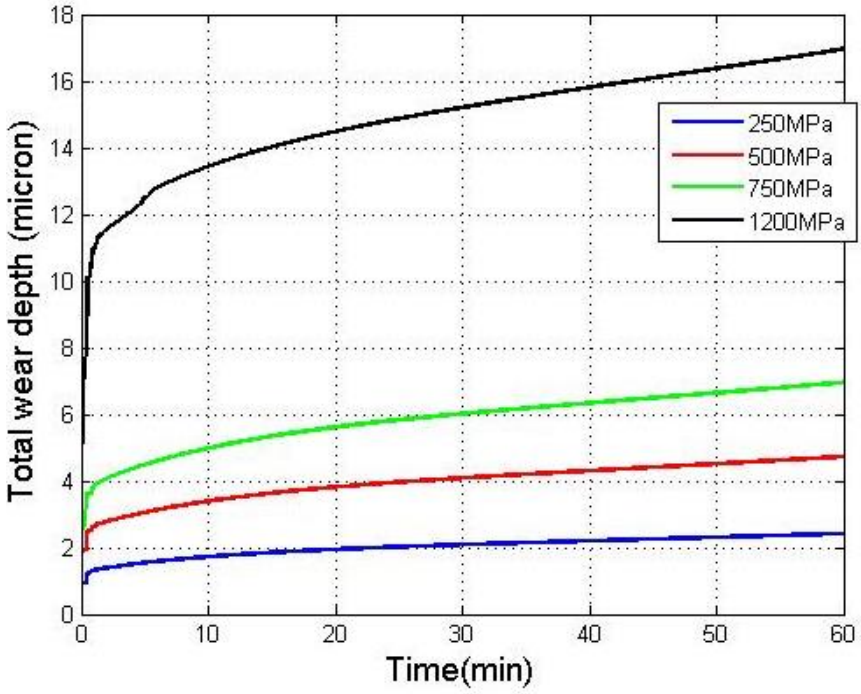

Figure 7-5 Wear depth calculation for different loads

The final wear of the system for different loads is plotted in Figure 7-5. It shows the variation of wear depth with loads. It is expected to observe a linear behaviour based on the Archard's wear equation. Because the wear reported above is the wear calculated via Archard's wear equation and plastic deformation of the contact asperities, there might be a small deviation from the linear behaviour. Especially in the beginning, the difference in plastic deformation is obvious. In addition the Archard's wear equation is applied locally and the tribofilm also affects the coefficient of wear. Despite all these raised points, the wear behaviour is following an almost linear pattern as a function of load. The final predicted wear depth is plotted against load and the results are shown in Figure 7-6.

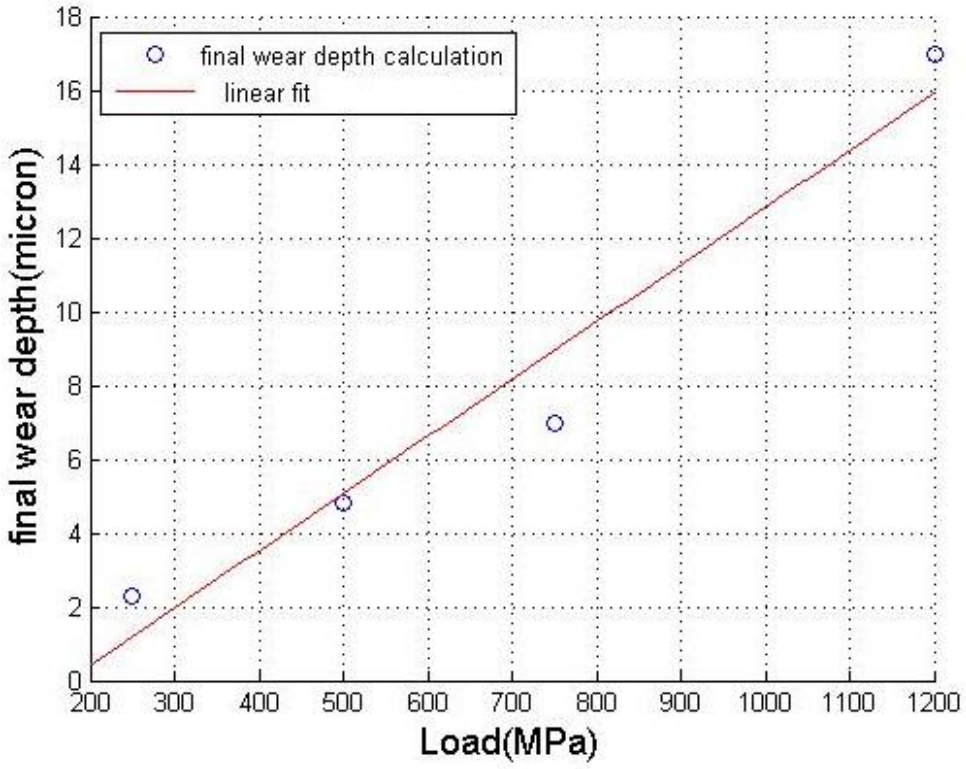

Figure 7-6 Linear behaviour of the final wear depth calculation with respect to the applied load

7.5 Model Validation

7.5.1 Experimental Procedure

Experiments are conducted using a Mini Traction Machine (MTM) to simulate a rolling/sliding condition and a Spacer Layer Interferometry (SLIM) is used to capture the growth of the tribofilm. Wear is measured using a white light interferometer. The aim of experimental part of this chapter is to measure wear and tribofilm thickness and to validate the model with respect to these parameters. Tribotests have been carried out by Pourya Parsaeian and wear measurements have been done by Ali Ghanbarzadeh and Pourya Parsaeian. Experiments were designed by Ali Ghanbarzadeh in order to validate the numerical wear model.

7.5.1.1 Tribo-Test Set-up

The experimental part of this study includes two parts. Firstly, tribotests were conducted to have rolling/sliding contacts in boundary lubrication using a Mini Traction Machine (MTM). The tribofilm thickness was measured using Spacer Layer Interferometry to monitor the growth of the film. MTM-SLIM is capable of measuring tribofilm thickness in the range of 1 to 500 nm thicknesses in both EHL and boundary lubrication regime with an accuracy of ±0.5 nm below 10 nm of thickness and ±2 above this level. The measurements were carried out two times for each experiments and the mean value is reported. As reported in (194), there is no need to have reference film thickness for calibration purposes which can make it significantly important in the case of measuring thin films. The tribometer set-up used in this work is shown schematically in Figure 7-7. One of the key points in using MTM is that the slide-to-roll ratio (SRR) can be changed in the experiments and over a wide range ($0 < SRR < 5$).

In a standard configuration of the MTM, test specimens are a 19.05mm (3/4 inch) steel ball and a 46 mm diameter steel disc. The ball and the disc are loaded and they are connected to two different motors. In a rolling/sliding contact both surfaces (ball and the disc) are moving. The sliding/rolling contact is simulated in the numerical model and both surfaces are moving based on the slide-to-roll Ratio (SRR) defined in the experiments. The frictional force is measured by a force transducer.

7.5.1.2 Materials and Lubricating Oil

The material used in this work was AISI 52100 steel for both ball and disc with a hardness of 6 GPa. The balls and discs are carefully cleaned by immersing in isopropanol and petroleum ether before starting the experiments.

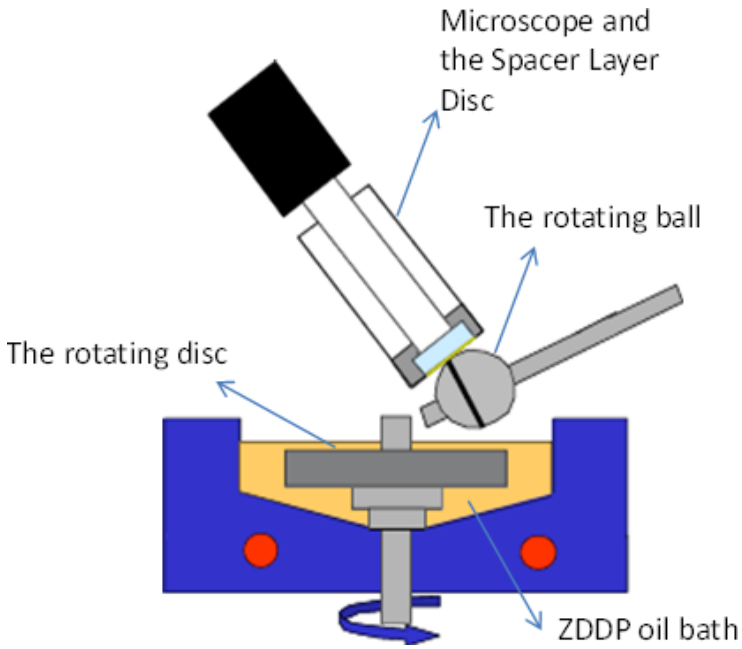

Figure 7-7 Experimental set up for MTM SLIM

All the experiments were conducted at an applied load of 60 N which corresponds to the maximum Hertzian pressure of 1.15 GPa. The materials used in the experiments are shown in Table 7-1.

Table 7-1 Material properties used in the MTM

Material properties	Value
Hardness (GPa)	6
Elastic modulus (GPa)	210
Ball surface roughness (nm)	20
Disc surface roughness (nm)	130

Experiments were carefully designed to study wear in boundary lubricated contact at different ZDDP concentrations and temperatures, and a small entrainment speed was chosen for this purpose. This experimental matrix is chosen to produce several different growth behaviours of ZDDP tribofilm on steel surfaces and at the same time to be able to measure wear at different times corresponding to those growth behaviours. The lubricating oil is selected to be Poly-α-Olefin (PAO) with 0.5% and 1% Wt ZDDP as an antiwear additive. The working conditions and the corresponding λ ratios are reported in Table 7-2.

Table 7-2 Working parameters

Parameters	Value
Maximum contact pressures (GPa)	1.15
Temperature (ºC)	60,80,100
Entrainment speed($\frac{m}{s}$)	0.1
SRR	5%
Test durations (min)	30, 45, 120
λ ratios	Around 0.04
Oil used	PAO+0.5% Wt ZDDP PAO+1% Wt ZDDP

7.5.1.3 Wear Measurement

The samples were analysed after each experiment and wear measurements were carried out by interferometry. Samples were taken out of the experimental set up after the complete tribotests. The tribofilm formed on the surfaces were carefully cleaned. A White Light Interferometer was then used to analyse the profile of the wear track. 2D and 3D images were taken from the wear track and the average wear depth of different areas inside the wear track was calculated. The experiments were repeated 2 times for each working condition and wear was measured in all cases. The reported wear results include the error bars and the variation of the experimental results from the mean value. It should be also noted that the wear depth was measured for 6 different points inside the wear track for each experiment and the average value was reported for the analysis.

Experiments for two different ZDDP concentrations and temperatures were conducted at different times to be able to test the model and the effect of evolution of the ZDDP tribofilm on the wear of the system.

7.5.2 Experimental Results

7.5.2.1 Tribofilm Thickness Results

MTM-SLIM configuration results are shown in this section for two ZDDP concentrations at three temperatures and three times. Thickness measurements for 1 Wt% ZDDP concentrations in oil at two temperatures of 60^0 C and 100^0 C for three different test durations are shown in Figure 7-8 and Figure 7-9. In addition, the measurement results with the same concentration for different temperatures for 2 hours test duration are plotted in Figure 7-10. Spacer layer imaging results are also

plotted for 0.5 Wt% ZDDP concentration in oil at three different temperatures of 60, 80 and 100^{o} C in Figure 7-11.

7.5.2.2 Wear Results

White Light Interferometry was used to measure wear on the discs. An example of wear measurement images is shown in Figure 7-12.

The samples were carefully cleaned by EDTA. Previous works have shown that ZDDP tribofilm on the wear scar can lead to misleading wear measurements when white light interferometry is used because of its transparent characteristics.

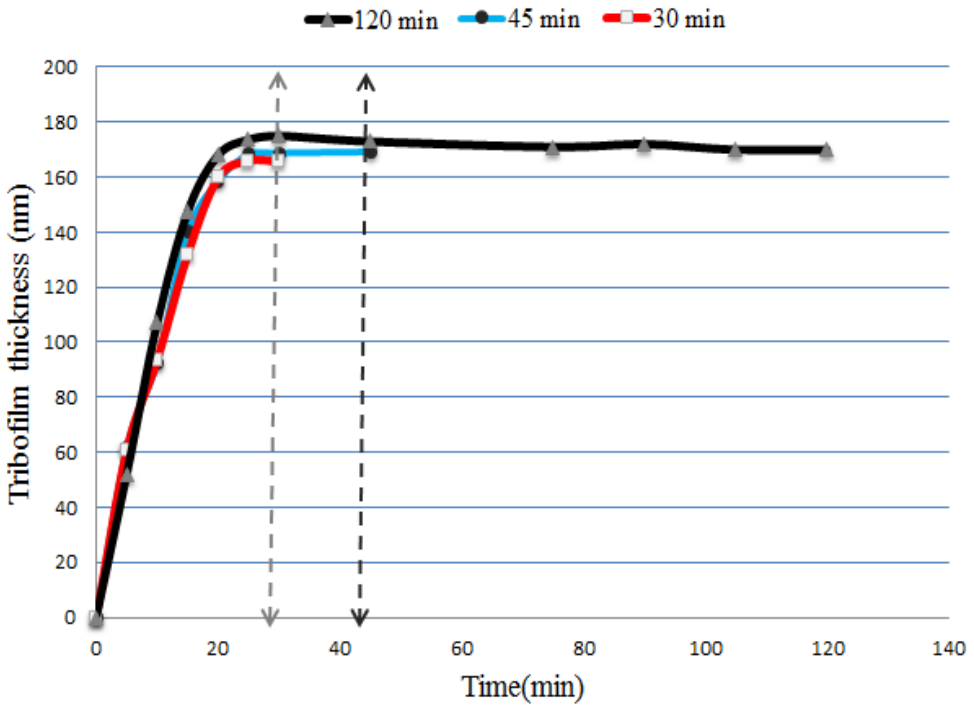

Figure 7-8 Tribofilm thickness measurements for 100° C at different times

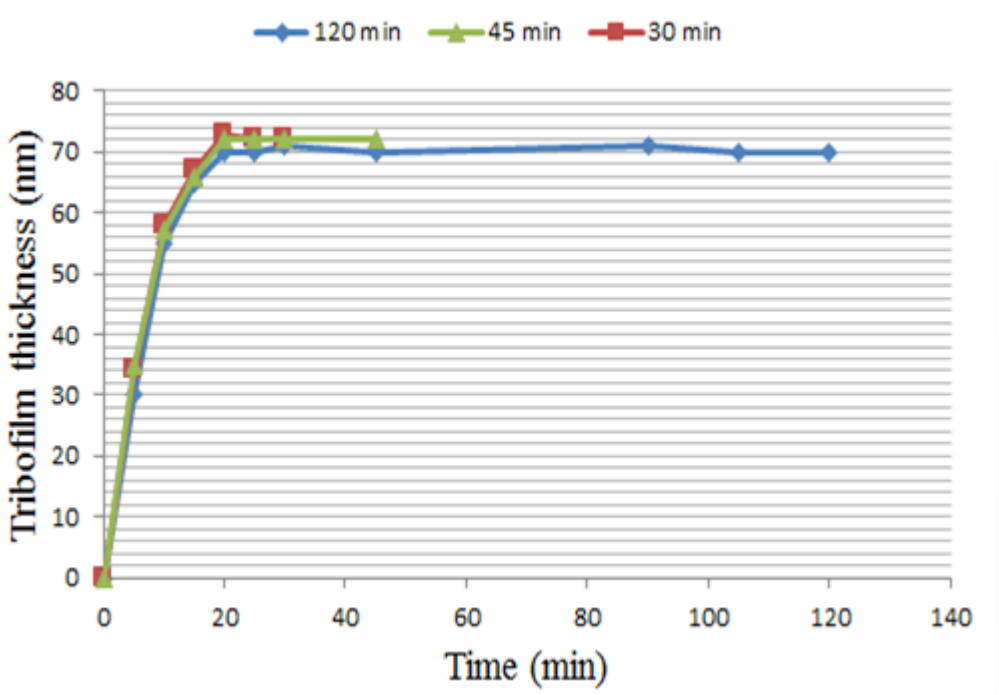

Figure 7-9 Tribofilm thickness measurements for 60° C at different times

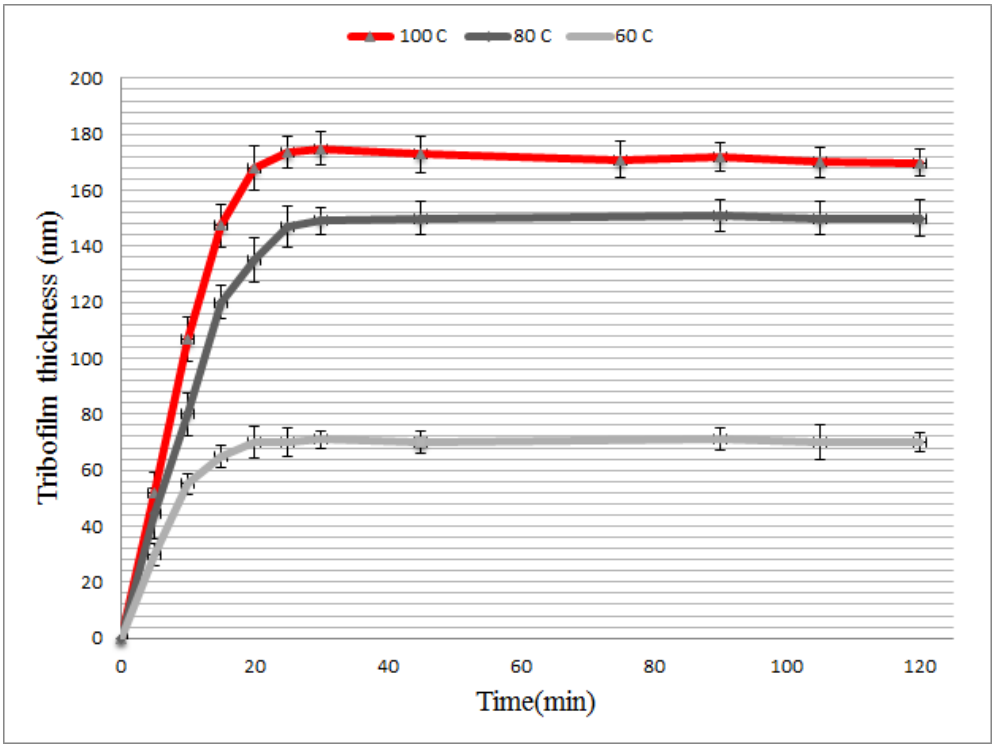

Figure 7-10 Tribofilm thickness measurements at different temperatures for 1Wt% ZDDP in oil

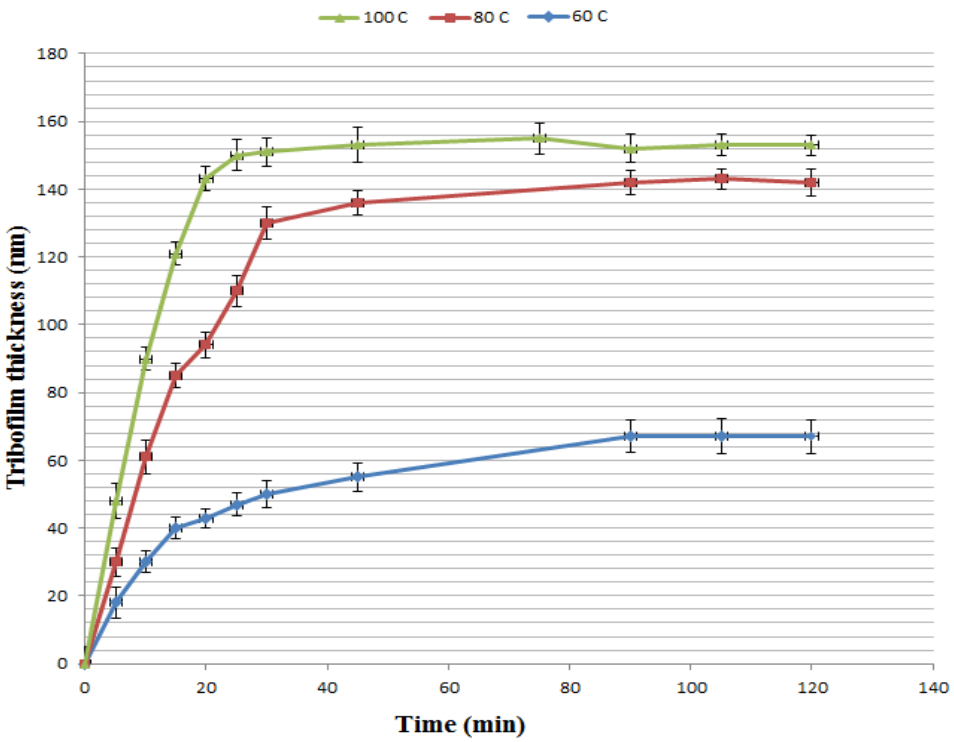

Figure 7-11 Tribofilm thickness measurements at different temperatures for 0.5 Wt% ZDDP in oil

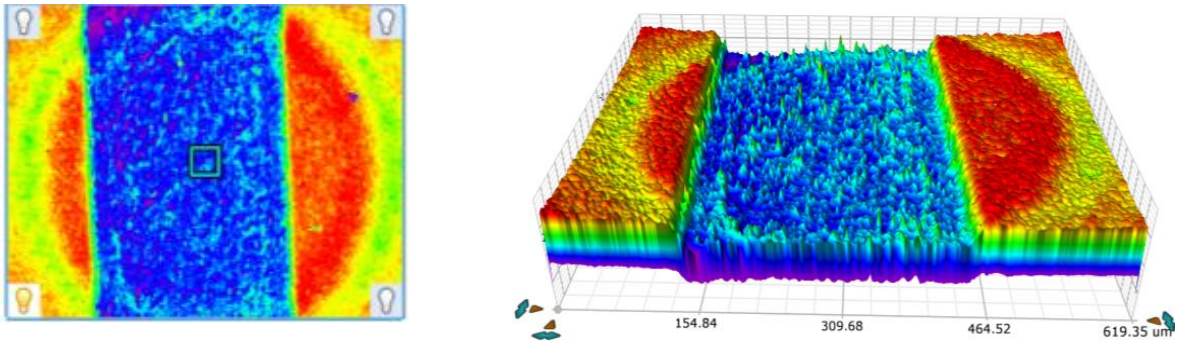

Figure 7-12 2D and 3D images of wear track taken by white light interferometry

The wear analysis in this work is based on the average wear depth. Wear depth is measured by comparing the average heights of points inside and outside the wear track. An example of this comparison is shown in Figure 7-13.

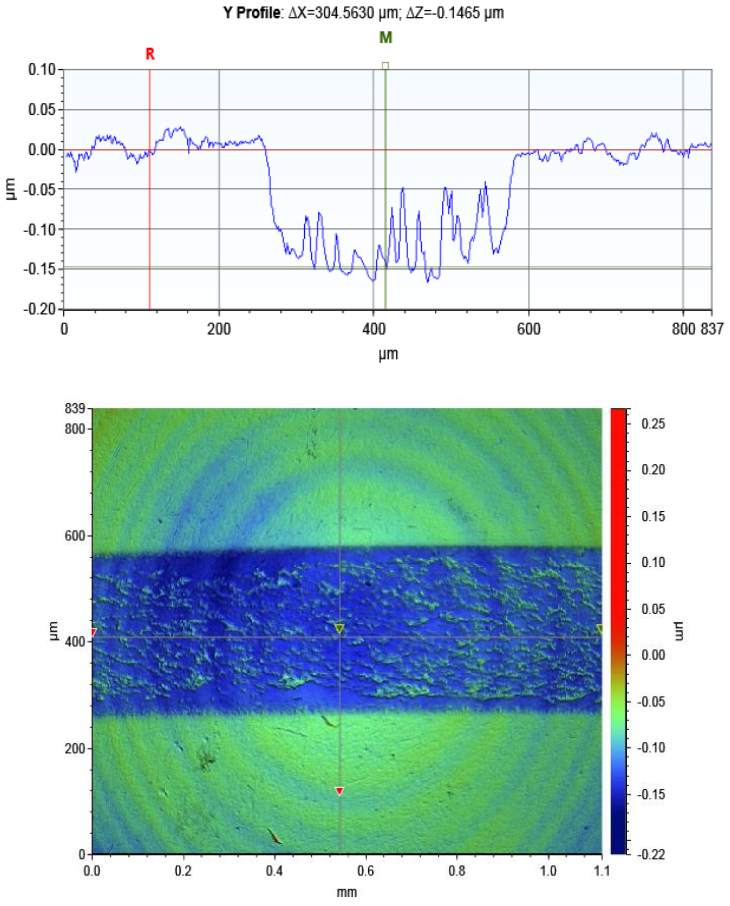

Figure 7-13 2D wear track image and the image profile of the surface after the experiment

The measurement results for different working conditions as reported in Table 7-2 are shown in Figure 7-14 for 1 Wt% ZDDP in oil and Figure 7-15 for 0.5 Wt% ZDDP which give the wear depth measured for different samples. The experiments were conducted for different times for 1 Wt% ZDDP to see the evolution of wear and validating the model but only 2-hour experiments were carried out for 0.5 Wt% ZDDP in the oil.

From the comparison of the experimental results, it can be interpreted that a higher concentration of ZDDP in the oil increases the growth rate of the ZDDP tribofilm. It is also shown that a higher concentration of ZDDP results in less wear in the system.

These conditions are simulated by the model and the results are reported in the next section.

7.5.3 Numerical Results and Discussion

Tribofilm thickness experimental results are used to capture the growth behaviour by setting the simulation values with respect to the experimental results. It is important to notice that once the tribofilm behaviour is captured, the model is able to predict the wear behaviour for the case of ZDDP on steel surfaces.

The parameters used in the tribofilm growth model such as x_{tribo}, h_{max}, C_1 and C_2 for different sets of experiments are reported in Table 7-3. It can be seen from Table 7-3 that the fitting parameters are different for different experiments and this is not surprising due to the different growth behaviour in each experiment.

The calibration results in this work reported in Table 7-3 are in line with the theories explained in Section 6.4. It can be seen that x_{tribo} is the same for different temperatures but otherwise equivalent conditions. It must be noted that the work strongly supports the fact the tribofilm reactions need shear stress to initiate. The temperature dependency of the kinetics is not exponential like conventional Arrhenius type equations. It is also reasonable to have smaller x_{tribo} for lower concentration of

ZDDP in the oil. It shows that concentration of lubricant additives can be considered in the growth modelling of their tribofilm.

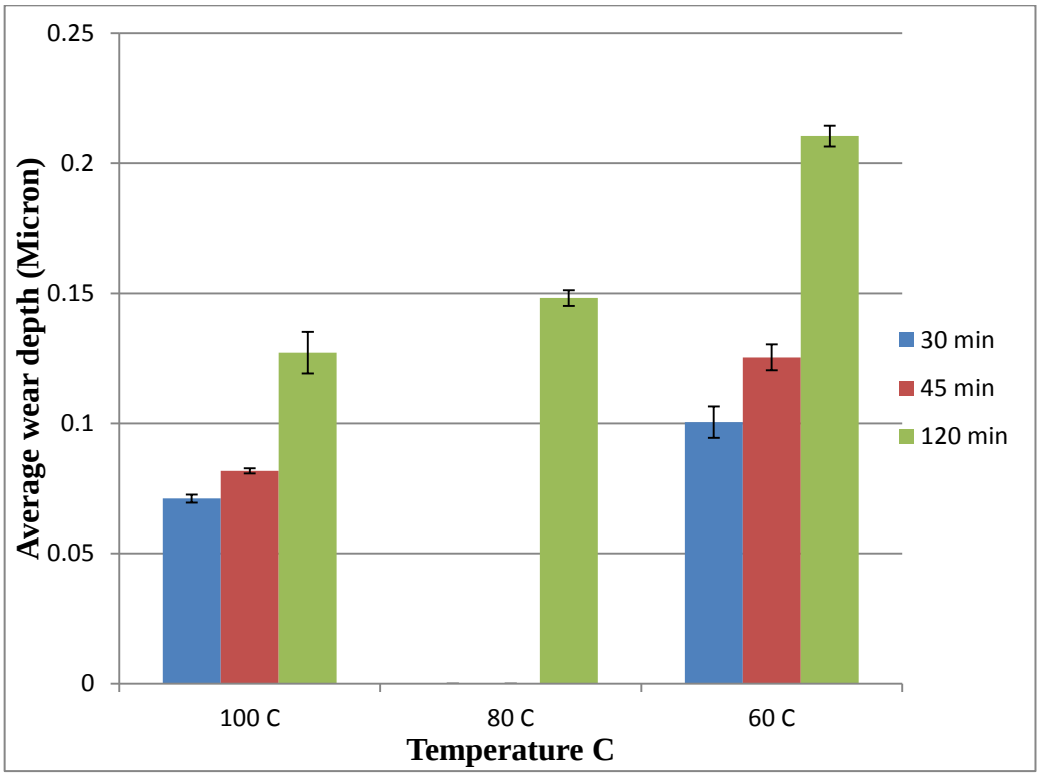

Figure 7-14 Wear measurements for different temperatures and different times for 1 Wt% ZDDP in oil

The tribofilm measurement results are used to calibrate the tribochemical model of Equation 6-14 and the calibrated parameters are reported in Table 7-3. The goodness of the fittings is also shown in the Figure 7-16 for one case of 1 Wt% ZDDP in oil.

Figure 7-16 shows the tribofilm thickness predicted by the simulation and measured experimentally for the three temperatures (60°C, 80°C and 100°C) for 1 Wt% ZDDP.

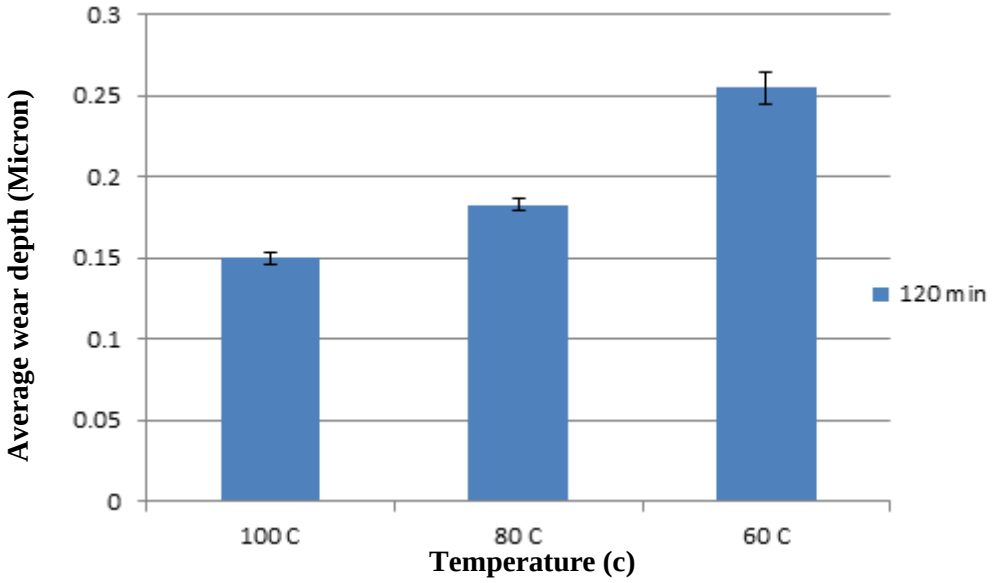

Figure 7-15 Wear measurements for different temperatures for 1 Wt% ZDDP in oil at 2 hours

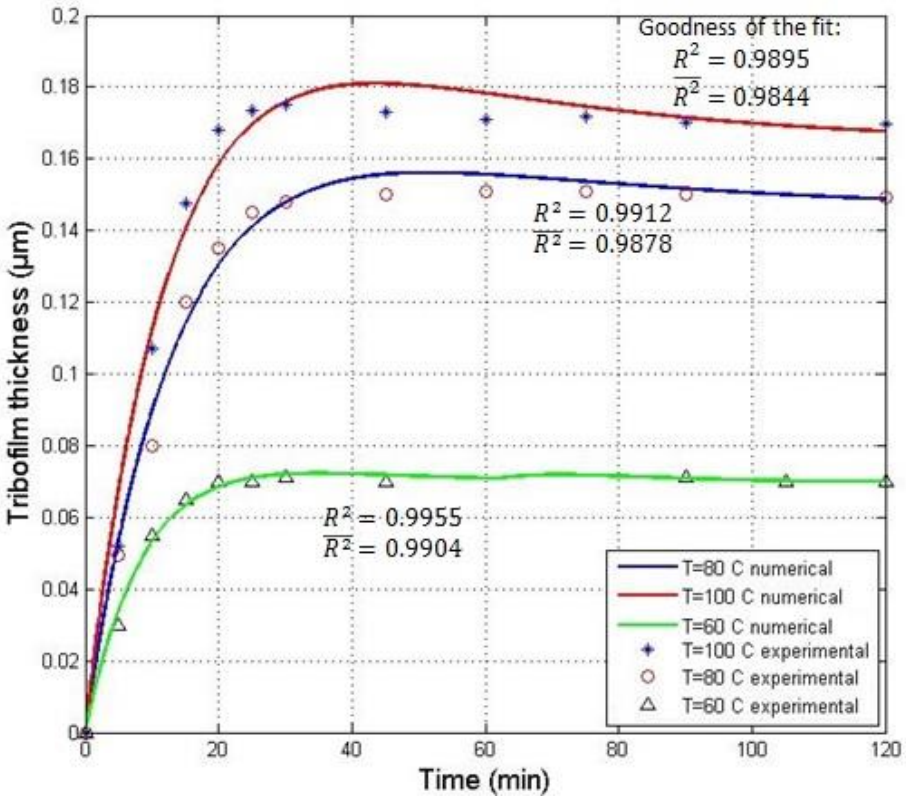

Figure 7-16 Example of numerical and experimental tribofilm growth for 1 Wt% ZDDP in oil at three different temperatures

Table 7-3 Numerical inputs and calibrated parameters

Parameter	1 Wt% ZDDP			0.5 Wt% ZDDP	
	100^0 C	80^0 C	60^0 C	100^0 C	Description
K	5.45×10^{-8}	5.45×10^{-8}	5.45×10^{-8}	5.45×10^{-8}	Initial Dimensionless wear coefficient for steel (m^3/Nm)
COW_{min}	5.45×10^{-9}	5.45×10^{-9}	5.45×10^{-9}	5.45×10^{-9}	Dimensional wear coefficient for maximum film thickness (m^3/Nm)
h_{max}	250 nm	200 nm	150 nm	250 nm	Maximum local tribofilm thickness in the formation process
x_{tribo}	1.66×10^{-16}	1.66×10^{-16}	1.66×10^{-16}	1.30×10^{-16}	Tribofilm formation rate constant
C_3	0.08566	0.05432	0.08052	0.08052	Tribofilm removal constant
C_4	0.000457	0.0004022	0.0004033	0.000406	Tribofilm removal exponential factor
E_1, E_2	209 GPa	209 GPa	209 GPa	209 GPa	Young's modulus of two surfaces
ν_1, ν_2	0.3	0.3	0.3	0.3	Poisson ratio
H_{steel}	6 GPa	6 GPa	6 GPa	6 GPa	Hardness of the steel substrate
H_{tr}	2 GPa	2 GPa	2 GPa	2 GPa	Hardness of the tribofilm at steady state tribofilm thickness

There is very good agreement between simulation and experiment, and both show that the tribofilm formed under these different conditions has a different thickness. The tribochemical model predicts the growth of the tribofilm at the asperity scale. Therefore the next step would be to examine the effect of this formed tribofilm on wear of the system using the proposed wear model. Wear measurement results are shown in the next section and the predicted numerical results are reported afterwards.

Wear is calculated at every time step of the simulation using the wear model described in Section 7.3, and plastic deformation is calculated in the elastic-perfectly plastic

contact model. The amount of wear is accumulated in time at every asperity in contact and the final wear depth can be calculated at the end of the simulation. The experiments reported in Section 7.5.2 were simulated via the model, and the predicted wear depth as a function of time is shown in Figure 7-17 for 1 Wt% ZDDP in oil and Figure 7-18 for 0.5 Wt% ZDDP.

This strategy shows that if the model is able to capture the tribofilm growth on the surface it is also able to capture wear in the systems with this specific mechanism. It is believed that this model in combination with the experiments can open new insights in the mechanisms of wear reduction of ZDDP on steel surfaces and relate it to the tribofilm formation and removal properties.

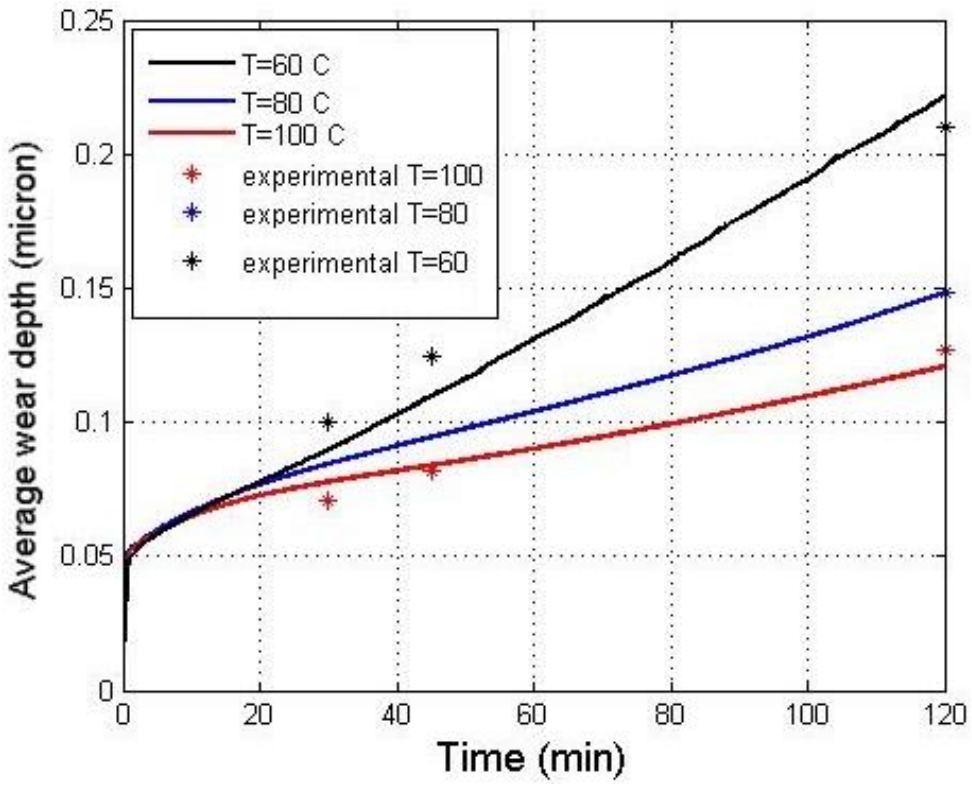

Figure 7-17 Simulation of wear for different temperatures over 2 hours for 1 wt% ZDDP in oil

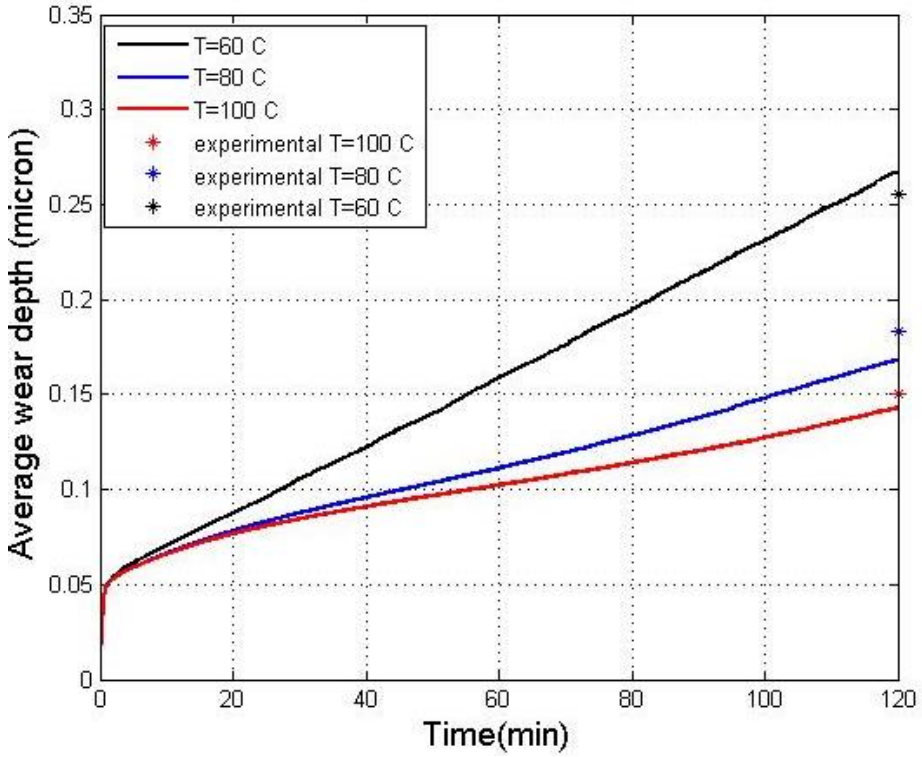

Figure 7-18 Simulation of wear for different temperatures over 2 hours for 0.5wt% ZDDP in oil

It can be extended to systems where tribochemical reactions form reactive layers and these layers offer a physical barrier to the surface.

This would be the case for most P-containing antiwear additives. For comparison with experiments, calculations of wear depth and tribofilm thickness are made by averaging values over the entire computational surface.

As explained in Section 7.3, the coefficient of wear in the simulation is time- and position-dependent. Therefore the average coefficient of wear at each time in the simulation can be obtained by averaging the values for coefficient of wear for all contacting points. The variation of the average coefficient of wear with time for different temperatures in the case of 1Wt% ZDDP in the oil is plotted in Figure 7-19. It can be interpreted from the results that growth of the tribofilm on the contacting

spots can reduce the average wear coefficient and that results in the overall wear reduction. The average wear coefficient tends to stabilize when the tribofilm thickness stabilizes and this is where the steady-state wear is established.

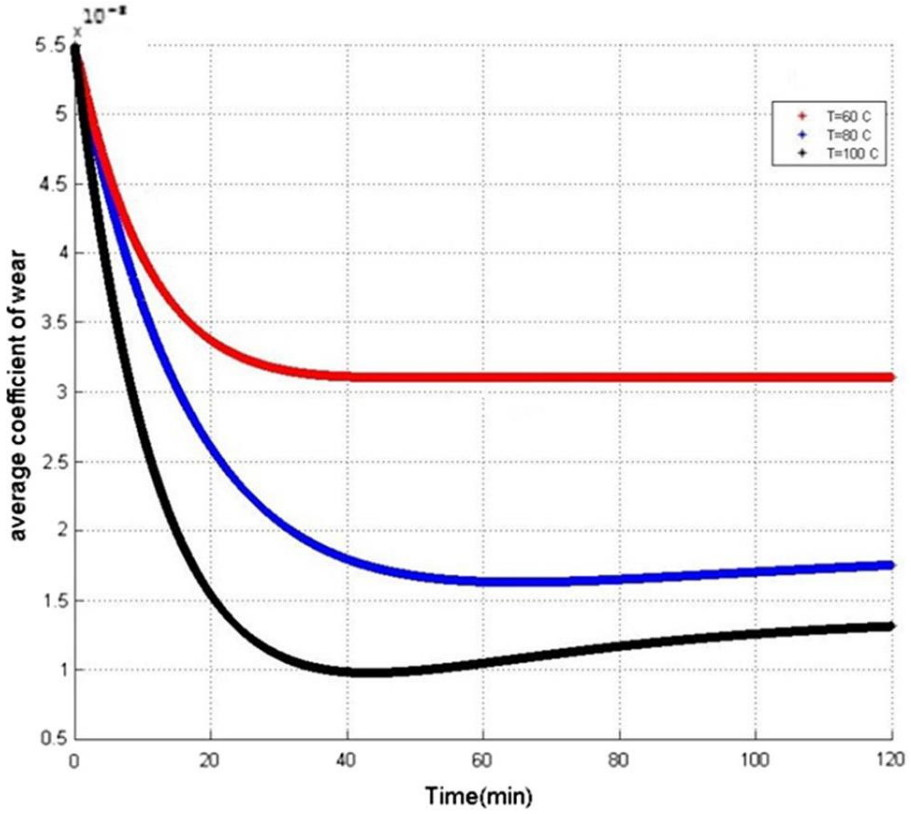

Figure 7-19 Variation of the predicted average coefficient of wear with time for different temperatures for 1 Wt% ZDDP in oil

The predicted pattern of wear depth seen in Figure 7-17 and Figure 7-18 shows that a relatively fast plastic deformation happens in the beginning of the contact and the rate of the wear reduces as the rate of plastic deformation reduces. The wear of material still remains and is responsible for the reduction in depth of the contact. Formation of the tribofilm on the contact spots results in the reduction of wear rate and is responsible for less wear being observed in numerical results. The amount of wear observed experimentally after 30 minutes and 45 minutes at 100°C and 60°C for 1

Wt% ZDDP in oil are also shown as discrete data points in Figure 7-17. The simulation predictions show reasonably good agreement with the experimental measurements; see also Table 7-4 for comparison of the data values.

The tribofilm thickness measurements resulting from spacer layer interferometry were used to calibrate the tribochemical model of Equation 6-14. Simulations were carried out using the calibrated parameters and working conditions. The simulation results show that the assumption of a lower time and spatially-dependent coefficient of wear for thicker tribofilms is reasonable for the case of different temperatures and different concentrations of ZDDP in the oil. It can be seen in Figure 7-17 and Figure 7-18 that at the start of the tribo-contact, simulations show almost the same wear because of high plastic deformation. At some point, when the tribofilm starts to grow, and because of variable reaction rates (indicated by x_{tribo} values), the coefficient of wear starts to decrease and the rate of this decrease depends on temperature and concentration of additive. This fact is also confirmed in Figure 7-19. The experimental results support the model.

The tribochemical wear model tested in this work can be applied to systems similar to the one reported here; where a reacted film with varying chemistry through the thickness is formed. As discussed in Section 7.3, it is possible to have a thick antiwear tribofilm yet a high wear of the surface.

As the tribofilm starts to grow on the surface, the rate of this growth plays a significant role in the rate of reduction of the coefficient of wear. The thickness reported in most experimental studies is the steady-state tribofilm thickness, but the coefficient of wear in this work is a function of time and changes with the gradual changes in the thickness of the tribofilm. Therefore it is very possible to have a thicker tribofilm in the

simulation at steady-state while also having a higher wear. A visual example of this difference is shown in Figure 7-20.

Table 7-4 Comparison between experimental measurements and numerical wear depth calculations

	Test	Experimental wear depth measurements (µm)	Numerical wear depth results (µm)
1 Wt% ZDDP	100^0 C_30 min	0.0712	0.0778
	100^0 C_45 min	0.0818	0.0839
	100^0 C_120 min	0.1272	0.1208
	80^0 C120 min	0.1482	0.1484
	60^0 C_30 min	0.1006	0.0917
	60^0 C_45 min	0.1252	0.1121
	60^0 C_120 min	0.2102	0.2215
0.5 Wt% ZDDP	100^0 C_120 min	0.1505	0.1430
	80^0 C_120 min	0.1830	0.1682
	60^0 C_120 min	0.2550	0.2676

It can be seen in Figure 7-20 that in the case 1 there is a faster growth of the tribofilm at the beginning which can result in faster reduction in the wear coefficient. It is also obvious that tribofilm thickness in the steady-state is thicker for case 2. Wear calculations show that case 2 has a higher wear in comparison to case 1 and the results are shown in Table 7-5. This example highlights the fact that a thicker tribofilm in the steady-state does not guarantee less overall wear of the system. This point is also discussed in Section 7.6.

Table 7-5 Wear depth results for different cases in Figure 7-20

Case	Wear depth (µm)
1	0.1355
2	0.1422

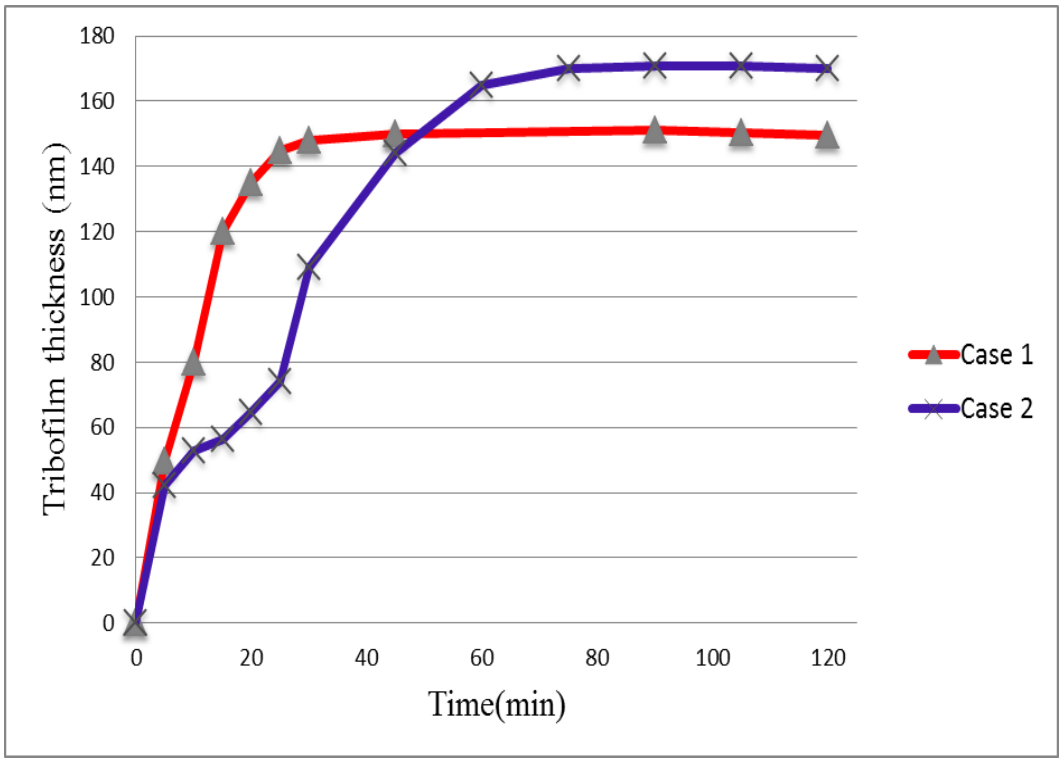

Figure 7-20 An example of two experimental cases with different tribofilm growth rates and different tribofilm steady-state thickness

7.6 Summary

The mechano-chemical model for boundary lubrication developed in this thesis was combined with a newly proposed wear model in the presence of the tribofilm. The wear model is applied locally at the asperity scale, where a local coefficient of wear varies linearly with the current value of the local tribofilm thickness. The model is time-dependent, with the surface topography updated at each time step as a result of plastic deformation and tribofilm formation, and the local wear coefficient changes in response to changes in the thickness of the tribofilm at every time step. Following calibration of the wear model parameters against experiments under one set of conditions, simulations under different conditions are tested against further

experiments. Prediction of both the tribofilm growth and the wear depth as a function of time shows good agreement with experimental observations.

The results support the argument that wear can happen because of the removal of the substrate atoms present in the tribofilm due to different tribochemical phenomena, and the dynamic loss of material within the tribofilm throughout the growth on the contacting asperities. The wear rate under such conditions is much lower than that in the absence of a tribofilm, and the model captures this distinction, predicting faster wear in the early stages of the test where the tribofilm has yet to form.

Although the coefficient of wear in the model decreases with increasing tribofilm thickness, it is seen that having a thicker tribofilm at steady-state does not guarantee lower overall wear. Since the model captures the complete dynamics of the system, from bare surface through to constant average tribofilm thickness, it can be seen how the initial rate of tribofilm formation, influenced by temperature and local surface topography, affects the overall average wear depth seen in tribological tests. Example simulations are shown in which the wear depth is greater for a case with a thicker tribofilm.

The model tested in this work does not necessarily capture the wear mechanisms for all boundary lubrication systems such as DLCs and Al/Si alloys, but the framework can be a good flexible approach to test different mechanisms. There is still a need for more experimental evidence to see how tribofilm formation and/or removal are responsible for the wear of the boundary lubricated systems for ZDDP antiwear additive on steel surfaces. Hence this model will be a foundation for finding the correlation of tribofilm growth and wear and more experiments are currently being

carried out. The study of tribofilm removal and its chemical and physical effects on wear of the boundary lubricated contacts is the subject of the ongoing research.

The model tested shows good agreement with experiments, indicating that, once calibrated, it has predictive capabilities that provide a beneficial tool for further exploration of boundary lubricated systems.

The current hypothesis and model can be explored more in future work both analytically and experimentally. It would help to extend and test this model for more applications and more system configurations in order to be able to predict wear of boundary lubrication contacts in a wider range of applications.

Chapter 8. Surface Topography Prediction

8.1 Introduction

Running-in is an important term used in the field of tribology. Due to the complexity and diversity of the phenomena occurring in this period various definitions of the term can be found in the literature. Based on Blau (222) running-in is a combination of processes that occur prior to the steady-state when two surfaces are brought together under load and with relative motion. He stated that this period is accompanied by changes in friction, wear and physical and chemical properties of surfaces. During the running-in period, surface micro topography is subjected to various changes. In boundary and mixed lubrication conditions, the height of the asperities of rough surfaces normally decrease (223-226). In the case of very smooth surfaces, an increase in the roughness value is observed (28, 227). During the process of change in the roughness of the surfaces, load carrying capacity is increased due to the gradual development of asperity level conformity. The increase in the conformity of the surfaces is significant as peaks and valleys of the surfaces correspond to each other, and the overall performance of the system is improved (228-230).

Predicting changes in the topography of contacting bodies is important for designers to be able to predict the mechanical and chemical behaviour of surfaces in loaded tribological systems. The roughness of operating surfaces influences the efficiency of mechanical parts. In the design of machine elements and selection of materials, the film thickness parameter, known as λ ratio, which is a representation of the severity of the contact is important (231). Its value is inversely proportional to the composite roughness of the two surfaces in contact. It is also widely reported that fatigue life of

bearing components is dependent on their functional surface characteristics such as roughness. Optimization of the surface roughness can help in increasing the life-time of bearings based on their applications (232, 233). Surface roughness can enhance stress concentration that can lead to surface-initiated rolling contact fatigue (234). Therefore, it is important to be able to predict the surface topography changes in a tribologically-loaded system.

The changes in topography can be either due to plastic deformation of the surface asperities or due to removal, loss or damage to the material which is known as wear. Evaluating wear in boundary lubrication has been the subject of many studies. There are almost 300 equations for wear/friction in the literature which are for different conditions and material pairs but none of them can fully represent the physics of the problem and offer a universal prediction (187, 188). Some examples of these models are the Suh's (235) delamination theory of wear, the Rabinowicz (190) model for abrasive wear and the Archard wear equation (24, 25). Wear occurs by different interfacial mechanisms and all these mechanisms can contribute to changes in the topography. It has been widely reported that 3rd body abrasive particles play an important role in changes in the topography of surfaces. There are several parameters that govern the wear behaviour in this situation such as wear debris particle size or shape, configuration of the contact and contact severity etc. (236-238).

It was reported by Godet (239) that a comprehensive mechanical view of the wear should consider the 3rd body abrasive particles and their effect on wear and topography changes. A study of abrasive wear under three-body conditions was carried out by Rabinowicz *et al*. (240). They proposed a simple mathematical model for 3rd body abrasive wear rate and showed that the wear rate in this situation is about ten times

less than 2-body abrasive wear. It was reported by Williams *et al*. (241) that lubricant is used to drag the wear debris inside the interface and the abrasive wear action then depends on the particle size, its shape and the hardness of the materials. They reported that a critical ratio of particle size and film thickness can define the mode of surface damage. Despite the importance of a three-body abrasive wear mechanism there is no comprehensive mechanistic model to describe such a complicated mechanism. In the mild wear regime in lubricated contacts the effect of 3rd body abrasive is often assumed to be insignificant.

Most of the work in the literature has been done using the well-known Archard's wear equation to evaluate wear in both dry and lubricated contacts. Olofsson (242-244) used Archard's wear equation to evaluate wear in bearing applications and observed the same behaviour between model and experiments. One example of the results are shown in Figure 8-1.

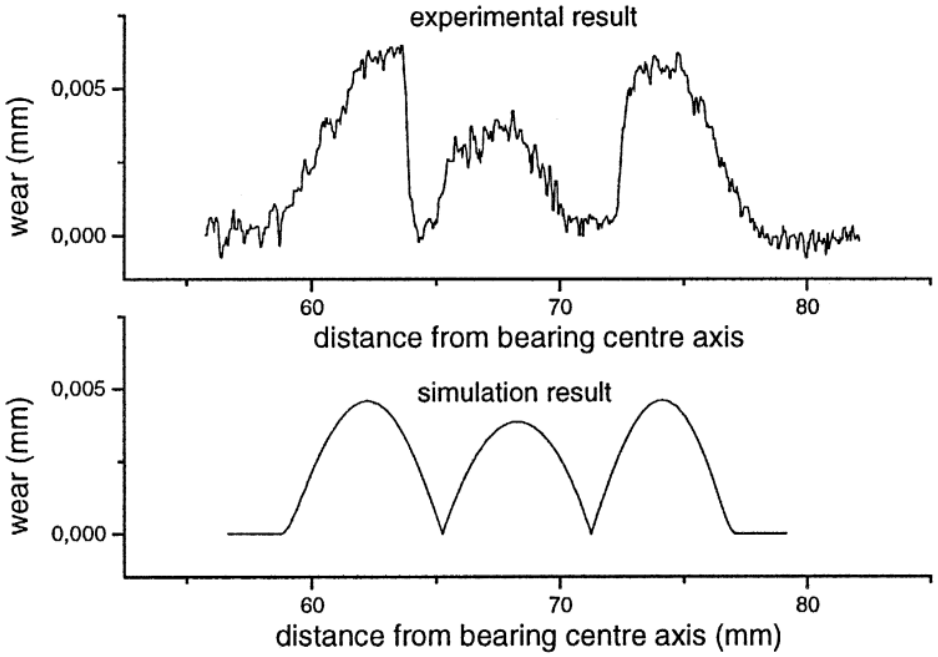

Figure 8-1 Prediction of wear on the bearing using the Archard wear equation. Reprinted from Ref (242)

Flodin (245) showed that Archard's wear equation is good enough to predict wear in spur helical gear applications. Andersson *et al.* (246) tested and reviewed different wear models and reported that Archard's wear model can predict wear of lubricated and unlubricated contacts and is able to predict the surface topography both in macro and micro-scales. They tested their generalized Archard's wear model for random rough surface contact (247). The Archard's wear equation was widely used in numerical studies in order to predict the wear and topography at different scales (56, 80, 109, 113-116, 136, 138, 139, 156, 157, 159, 174).

Recent work was reported by Morales Espejel *et al.* (32) who used a mixed lubrication model to predict the surface roughness evolution of contacting bodies by using a local form of Archard's wear equation. The model results have been compared with experimental data and show good agreement. They used a spatially and time-dependent coefficient of wear that accounts for lubricated and unlubricated parts of the contact. The same modelling framework was used in other works of the authors to predict wear and micropitting (34).

Despite the importance and the attempts in the literature to monitor and predict the roughness evolution of surfaces, there is no reported work that addresses the effect of tribochemistry. The modelling framework developed in this thesis (117, 221) is capable of predicting surface topography evolution in boundary lubrication.

The changes in the surface topography have been widely reported in the literature but the effect of growth of the tribofilm has been neglected. In this work, the topography of surfaces is predicted for surfaces and not only the effect of plastic deformation and

mild wear but the effect of growth of the ZDDP antiwear additive tribofilm on surface topography evolution is investigated.

In this chapter, firstly an introduction to the basics of surface topography definition is included. Then the topography evolution prediction based on the current model is reported. The effect of different parameters on the topography variation is shown and results from a set of experiments for validating the model in boundary lubricated contacts with an antiwear additive (ZDDP) is reported. A comparison between numerical and experimental results is then made. The experimental configuration used to validate the model in this chapter is different from Chapter 7 which included the validation of the wear model.

8.2 Surface Roughness

Almost all engineering surfaces are rough. Roughness of the surface can be defined as the deviation of the surface profile from the flatness (27). The profile of an engineering surface is almost always random unless some features with specific patterns are made on the surface. Roughness of surfaces is characterised using different methods and each of them represents a unique definition of the deviation from flatness. Before introducing these terms, a definition is essential.

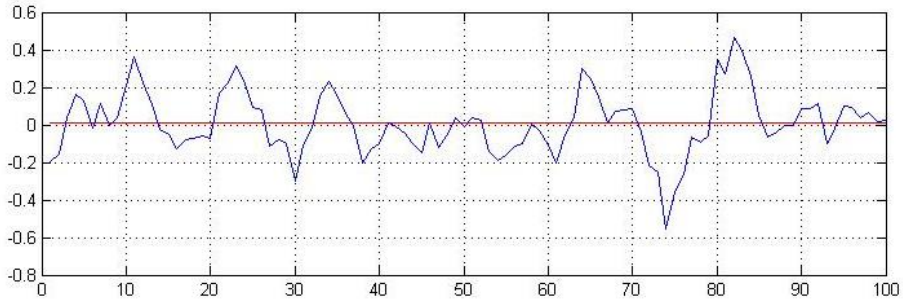

Figure 8-2 Surface profile of a rough surface from numerical simulation

A surface profile of a rough surface is shown in Figure 8-2. The red line in the figure is called the centre line. According to Priest (26) the centre line is defined as: "*A line representing the form of the geometric profile drawn parallel to the general direction of the profile throughout the sampling length such that the sums of the areas contained between it and those parts of the profile which lie on each side of it are equal.*"

In this chapter only two important roughness characterisations are introduced because they are used in the model.

8.2.1 Centre Line Average Roughness

The centre line average roughness is the average value of the difference of the profile above and below the centre line through the whole sampling length. The centre line average roughness is often indicated by R_a value and is formulated as following:

$$R_a = \frac{1}{L}\int_0^L |Z| dx \qquad \text{Equation 8-1}$$

in which L is the length of the sampling and $|Z|$ is the magnitude of the departure from the centre line.

8.2.2 Root Mean Square Roughness

The root mean square value of the difference of the profile above and below the centre line in the whole sampling profile is called root mean square roughness and is often indicated by R_q and is formulated as following:

$$R_q = \left[\frac{1}{L}\int_0^L Z^2 dx\right]^{1/2} \qquad \text{Equation 8-2}$$

This root mean square roughness is the most commonly used roughness parameter in theoretical tribology (26). If the surface profile follows a Gaussian distribution, the relationship between R_a and R_q would be as follows:

$$R_q \approx 1.25R_a \qquad \text{Equation 8-3}$$

It should be noted that the roughness of the surfaces is characterized by a reasonably large area of the surfaces. Using such large areas as input into numerical model makes it computationally expensive to simulate, especially for high values of loading cycles that result in the evolution of surface topography. In principle, the study area should cover at least several wavelengths of the surface in order to be reasonable. For the surfaces used in this work, an average wavelength of 15 to 20 μm was identified. Therefore the computational domain is selected to be a 64μm×64μm area consisting of 64 nodes of one micron size in every dimension.

8.3 Effect of Parameters on Topography of Surfaces

It is important to see what parameters are affecting the topography evolution of the surfaces. These evolutions can have different patterns because so many parameters are involved. Therefore a study on the effect of different parameters on changing the topography of surfaces during the time is carried out. The effect of load, coefficient of wear and the initial surface roughness is studied. The roughness of surfaces is calculated throughout the simulations thus a real time calculation of roughness evolution is reported. The parameters used for the simulation are reported in Table 8-1 and the values of varying parameters are reported in each section. The contact configuration is for a ball-on-disc rig with the specifications reported in Table 8-2.

The calibration parameters in the model, are the ones used previously in Section 7.4 to investigate the effect of different parameters on the wear prediction of the model and are reported in Table 6-1. The results in this section are purely numerical to see the effect of different parameters on the predicted evolution of surface topography. The approach is very similar to the one used in Section 7.4. The model used in this section is the full numerical model including the contact mechanics, tribofilm growth and the wear model.

Table 8-1 Working conditions

Parameter	Value
T	100 C
Load	750 MPa
Entrainment Speed (U_e)	1 m/s
Slide-to Roll Ratio ($\frac{U_s}{U_e}$)	5%

Table 8-2 Material properties

Material properties	Value
Hardness	6 GPa
Elastic modulus	210 GPa
Ball surface roughness	85nm
Disc surface roughness	240 nm

8.3.1 Effect of Wear Coefficient

It is reasonable that the *initial* wear coefficient (CoW_{steel}) will affect the topography of the surfaces as wear is one of the most important causes of topography changes. Wear happens at the asperities that are in contact. Higher asperities are more likely to

experience contact and this will result in the deformation and wear at higher asperities. Higher coefficient of wear will lead to more wear at surface asperities thus more modification to topography of the surfaces. The effect of wear coefficient in the evolution of surface topography is shown in Figure 8-3. The figures are based on the R_q value.

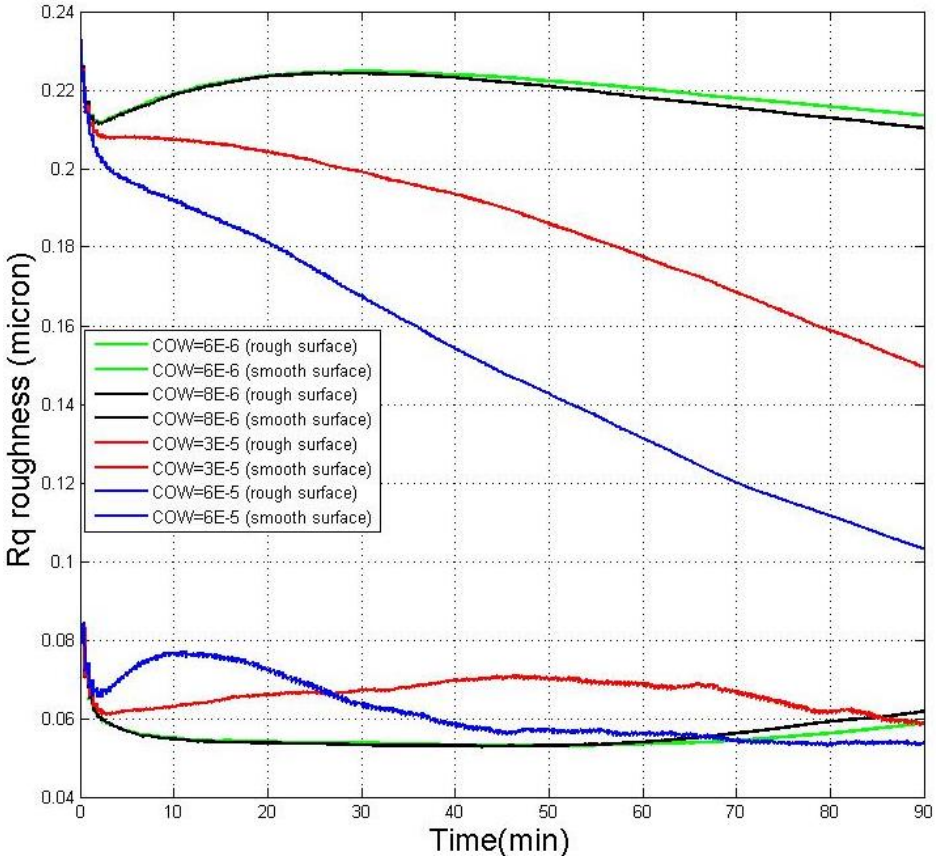

Figure 8-3 Surface roughness evolution for rough and smooth surface at different *initial* wear coefficients

It can be seen that a higher *initial* coefficient of wear results in faster and larger modifications of topography on the rougher surface. The pattern of topography evolution for smoother surface is not repetitive. It can be attributed to the complex

physical process happening at the contact. Plastic deformation is occurring as well as the wear of the system and also tribofilm growth on the contacting asperities. It is very interesting to see how the behaviour of topography evolution of the surfaces can be different.

8.3.2 Effect of Load

Higher loads in general will lead to higher surface modification as the surfaces are experiencing higher plastic deformations and wear. An example of the surface roughness evolution for different loads is illustrated in Figure 8-4. The evolution is only plotted for the rougher surface. The load is varied from 250MPa up to 1GPa.

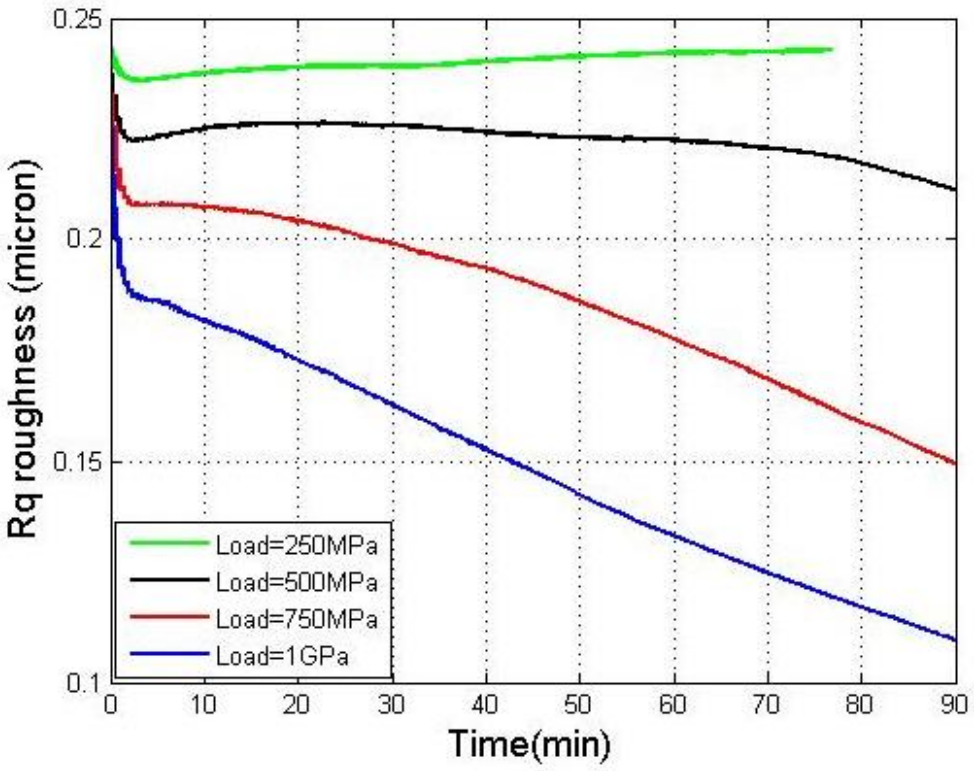

Figure 8-4 Surface roughness evolution for rough surface at different loads

It is clear that higher load leads to more smoothing of the surface. At the beginning more plastic deformation occurs and this is followed by higher wear at the contacting asperities.

The final surfaces after 5 minutes of contact for different loads are shown in Figure 8-5.

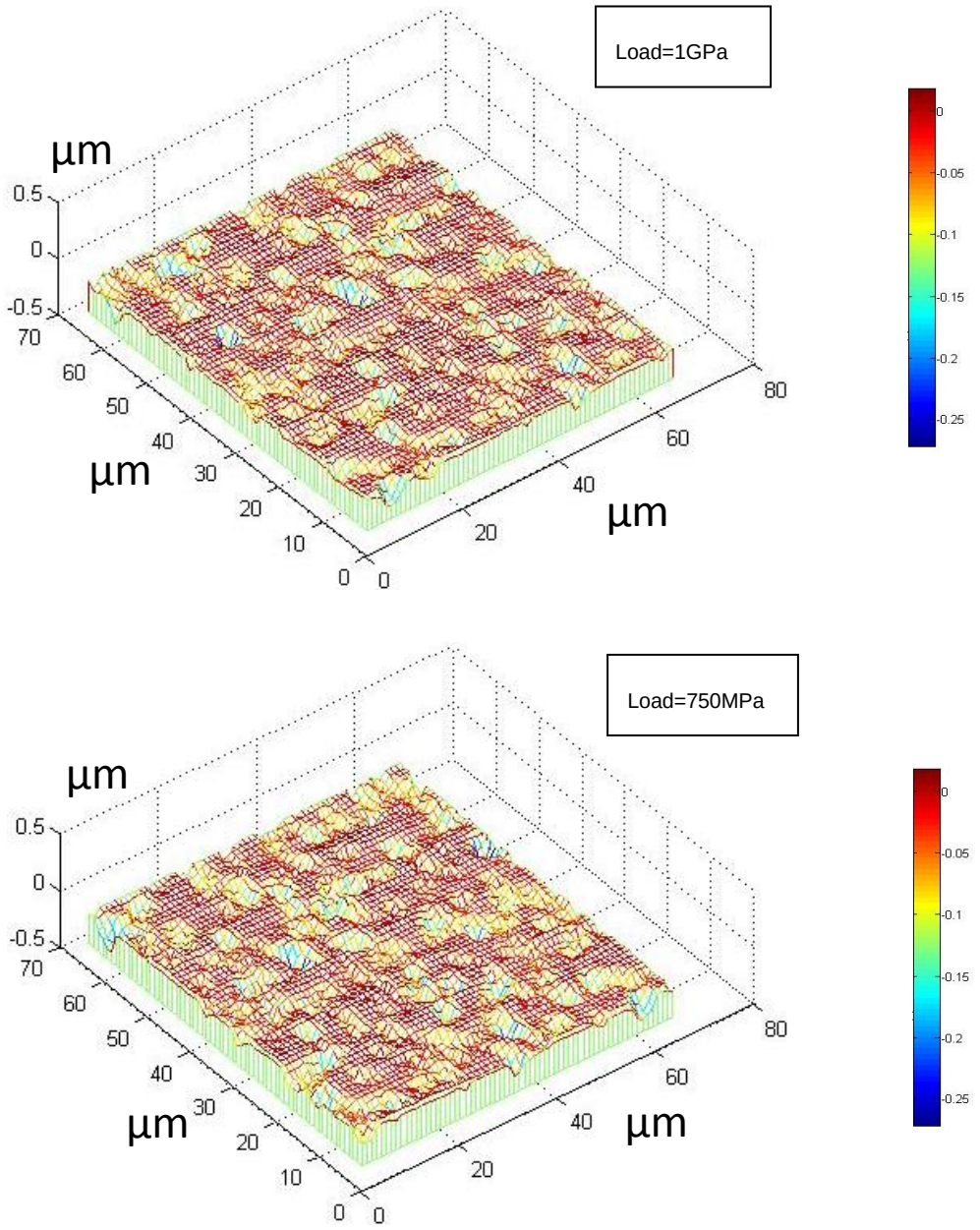

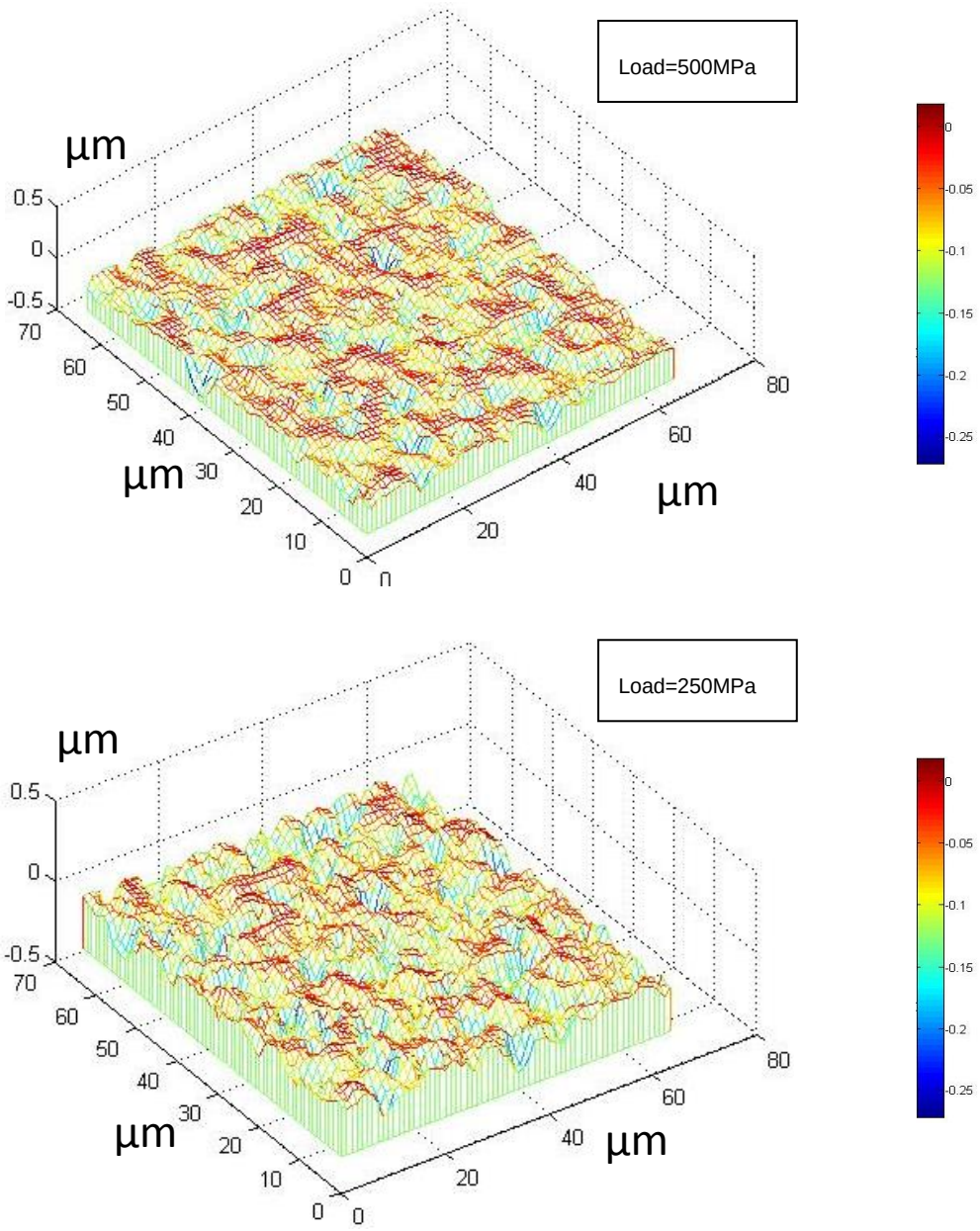

Figure 8-5 Final surface topography after 5 minutes at different loads

8.3.3 Effect of the Initial Surface Roughness

It is widely observed experimentally that initial roughness combination of both contacting surfaces can affect the topography evolution. For this reason, a set of simulations with different initial R_q values of the rougher surface were carried out to

see this effect in the simulation. The values were selected as $R_q = 100\ \text{nm}, 254\ \text{nm}, 500\ \text{nm}$ for the rougher surface.

It can be seen from Figure 8-6 that rougher surfaces experience more topography evolution. This higher topography changes start even from the beginning of the contact which is due to larger plastic deformations. The difference between final and initial R_q values are reported in Figure 8-7. Figure 8-7 also supports the fact that rougher surface might experience higher wear due to higher surface topography modification.

It should be noted that different surface roughness of surfaces might experience different lubrication regimes. The above analysis is true, when all the surfaces are in boundary lubrication regime.

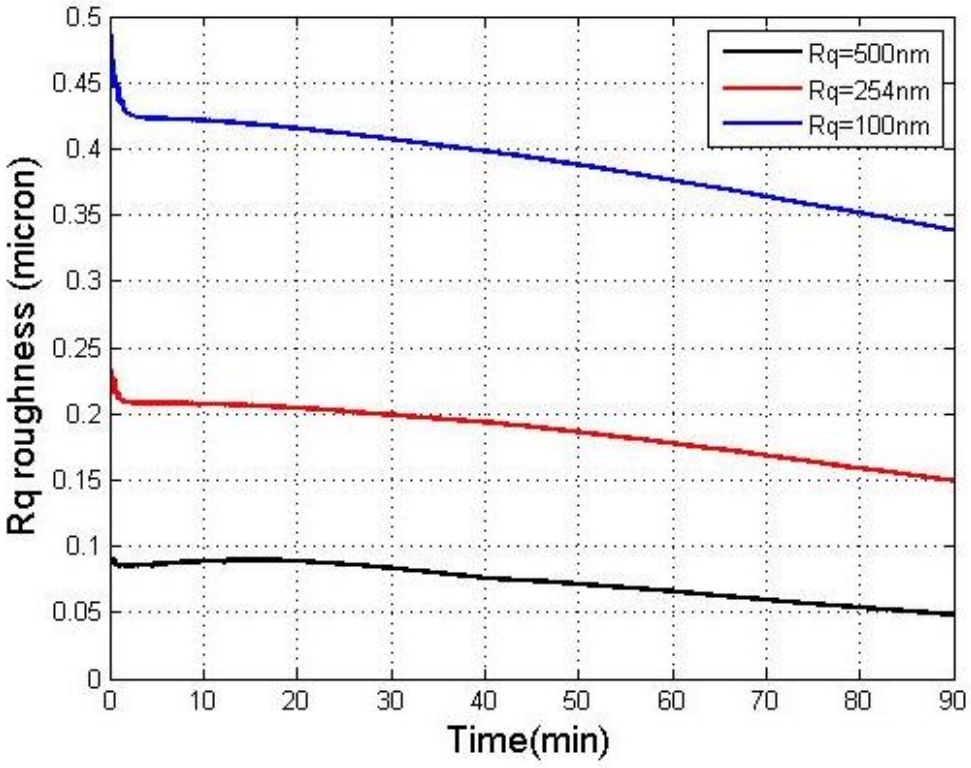

Figure 8-6 Effect of initial roughness on the Surface topography evolution of the rougher surface

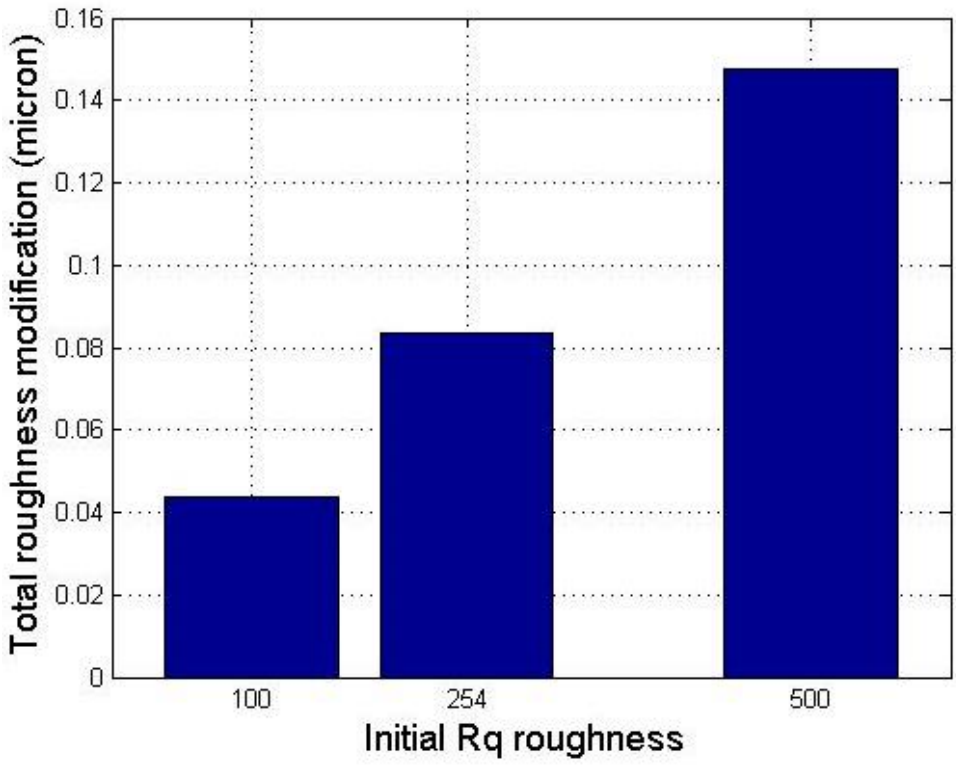

Figure 8-7 Total roughness modification for different initial R_q values

8.3.4 Effect of Material Hardness

Simulations were carried out with the same configuration and working condition and only the hardness of the materials have been changed. The results are shown in Figure 8-8.

It can be clearly seen that harder materials are less likely to be modified. These phenomena can be because of two reasons. Firstly the amount of wear due to Archard wear formulation is less for harder materials and secondly, the plastic deformation is lower because of higher hardness of the surface asperities.

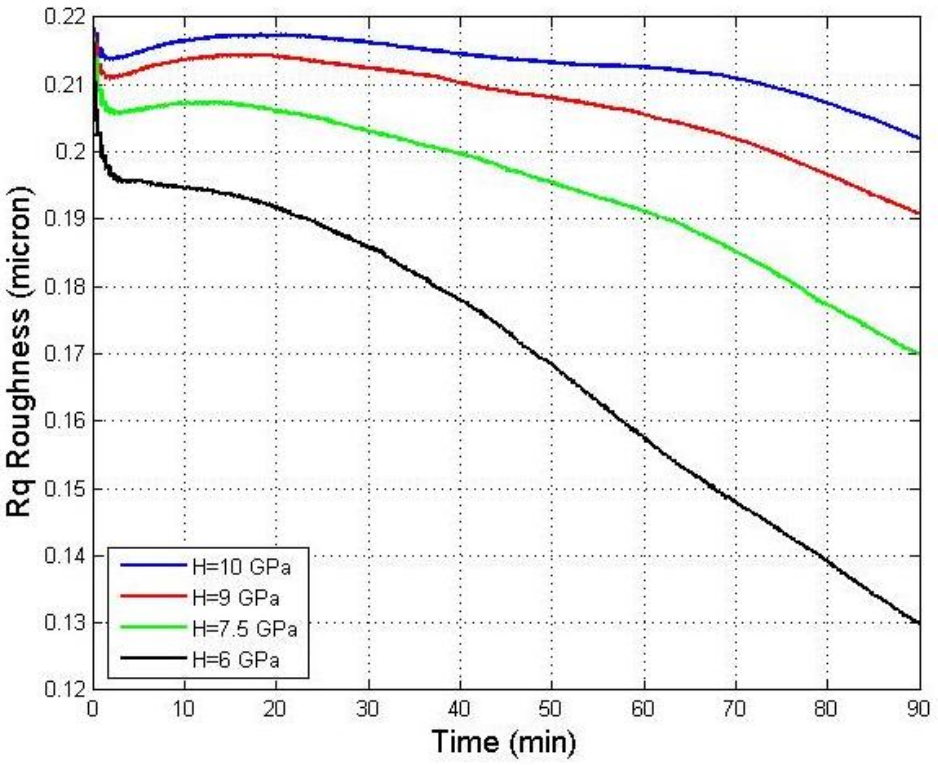

Figure 8-8 Roughness evolution of rings for different material hardness

8.4 Model Validation

The numerical results presented above demonstrate that the model is capable of predicting the roughness evolution of the surfaces. To validate these predictions, a set of experiments were designed for a sliding-rolling contact lubricated with ZDDP containing oil. The experiments were carried out by Elio Piras at SKF Engineering and Research Centre in the Netherlands. The numerical model was then adapted to the experimental configuration and the comparison between results has been made.

8.4.1 Experimental Setup

The tests were carried out using a MicroPitting Rig (MPR) which is shown schematically in Figure 8-9.

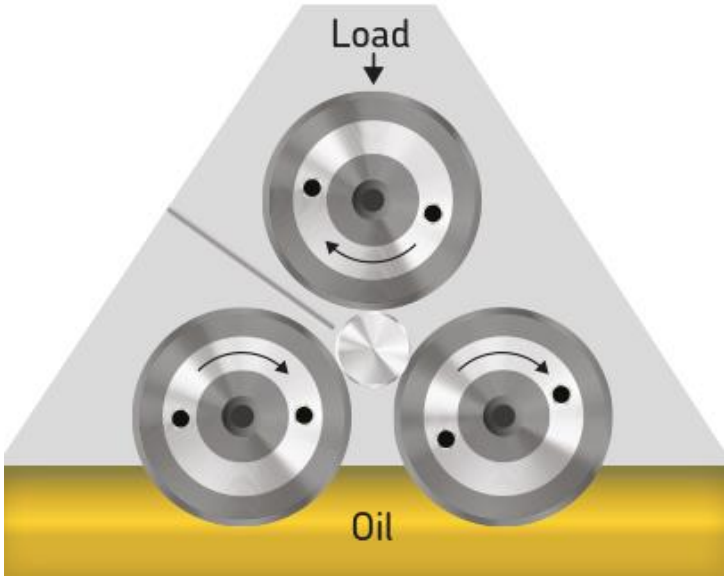

Figure 8-9 The load unit of the MicroPitting Rig (MPR)

The principal part of the load unit of the micropitting rig is the load unit which includes a spherical roller bearing of 12 mm in diameter (taken from a spherical roller bearing), which comes into contact with three larger counter bodies (which are in fact inner rings of a cylindrical roller bearing). The roller and the rings can be ground and/or honed and finished to any desired roughness on the surface. With this configuration, the roller accumulates loading cycles 13.5 times faster than any of the three rings during a test. The oil is carried into the contact by the two bottom rings which are creating the conditions of fully lubricated contact, depending, of course, on the desired lubrication regime.

The maximum load that can be applied on the machine is 1250 N corresponding to a maximum Hertzian pressure of 2.75 GPa which is high enough for bearing studies. The temperature can be controlled up to 135ºC and the maximum tangential speed can be 4 m/s.

Temperature	90°C
Entrainment Speed (U_e)	1 m/s
Slide-to Roll Ratio ($\frac{U_s}{U_e}$)	2%
Hertzian Contact Pressure	1.5 GPa
Lubricants	PAO + ZDDP 1%
Number of Cycles for roller	20, 50, 100 KCycles
Number of Cycles for rings	1, 2, 7 KCycles
R.M.S. Roughness Roller	50 nm
R.M.S. Roughness Rings	100, 200, 600 nm

Table 8-3. List of experimental test conditions for MicroPitting Rig

The roller and discs are driven by two independent motors, which means that a controlled slide-to-roll ratio of ±200% can be reached. The size of the Hertzian contact varies with the load and the transverse radius of the roller, but the typical values are around 0.244 × 1.016 mm (in the rolling and transverse direction, respectively) corresponding to the maximum Hertzian contact pressure of 1.5 GPa. The operating conditions used in the present work are listed in Table 8-3. The oil temperature, load, speed and slide-to-roll ratio have been maintained constant during the experiments. The roughness has been changed only for the rings. For each roughness value, tests with different running times have been carried out in order to have a complete view of the roughness evolution during the running-in period.

The numbers of rolling cycles are different for roller and rings; in fact each cycle of the rings correspond to 13.5 cycles of the roller. This is why the roller and ring have different cycles while the running time is the same.

The lubricant used is a synthetic model oil (Poly-alpha-Olefine) mixed with 1% weight of primary zinc dialkyldithiophosphate (ZDDP). The properties of oil and additives are listed in the following table:

Code	Kinematic viscosity 40°C (mm^2/s)	Kinematic viscosity 100°C (mm^2/s)	Sulphur content (wt%)	Phosphorus content (wt%)
Mineral Oil	56.2	9.84	0.01	**0.00**
Primary ZDDP (C_8)	**---**	**---**	**23.4**	**11.3**

Table 8-4 Properties of base oil and additive used for experiments.

To avoid the effect of a new running-in at the beginning of each test, it was decided not to use the same rings and roller for more than one time (interrupted test) but to run a new set of specimens with nearly identical roughness for every time step of the experiment.

After each test, the samples were cleaned in an ultrasonic bath with petroleum ether for 5 minutes and then the roughness was measured using white light interferometry (Wyko NT1100). As shown in other work (32), the presence of a tribofilm can interfere with the measurements of the roughness using white light interferometry. The roughness of interest is the roughness of the steel surface and to be able to measure it, the tribofilm has to be removed. The technique consists of covering the wear track with a drop of ethylene diamine tetra acetic acid (EDTA). The EDTA dissolves the tribofilm and then it is removed with a tissue after 20 seconds by just

rubbing the wear track. The roughness of each roller sample was accurately measured at 5 different circumferential locations along the contact track. The same process for roughness measurements was repeated for each of the rings and then the r.m.s. value was obtained by averaging all the measured R_q values.

Changes in R_q values for the roller and the three rings were monitored with time (see Figure 8-10).

The morphology of ZDDP-derived reaction layers was observed with a Zeiss Supra 55 Scanning Electron Microscope (SEM) using 5 kV electron beam voltage in the secondary electron mode.

Analysis of the chemical composition of the ZDDP-derived tribolayer was made by means of X-ray Photoelectron Spectroscopy (XPS) using a PHI 5000 Versa Probe Spectrometer (Ulva-PHI Inc, Chanchassen, MN, USA) equipped with a monochromatic Al kα source (1486.6 eV). The data were collected with a beam size of 100 μm and a power of 25W in the FAT analyzer mode. The pass energy was 117.0 eV with energy step size of 1 eV for Survey scan and 46.95 eV with an energy step of 0.1 eV for high resolution spectra. During all the measurements the pressure was always below 10^{-7} Pa.

The identification of the wear track was performed by Scanning X-ray Images (SXI) collected in an area of 1x1 mm^2, allowing the identification of the different analysis locations inside the tribological wear track. XPS data were processed using CASA XPS software (version 2.3.16, Casa Software Ltd, UK). The detailed spectra were fitted with Gaussian/Lorentzian curves after linear background subtraction. Charge effect is taken into account by referring to C 1s Binding Energy at 285.0 eV.

Roller	
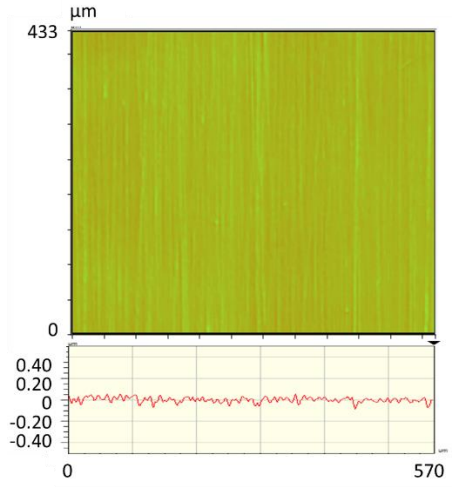	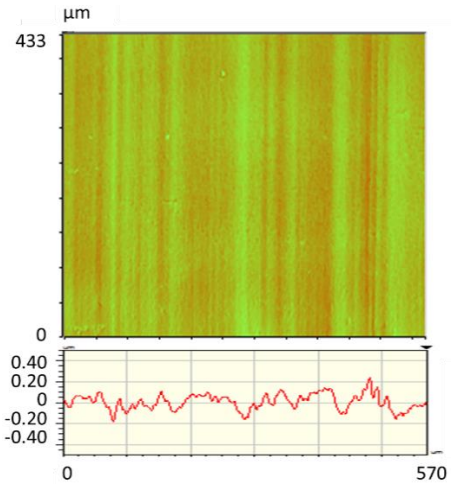
Initial Surface	100 KCycles
Rings	
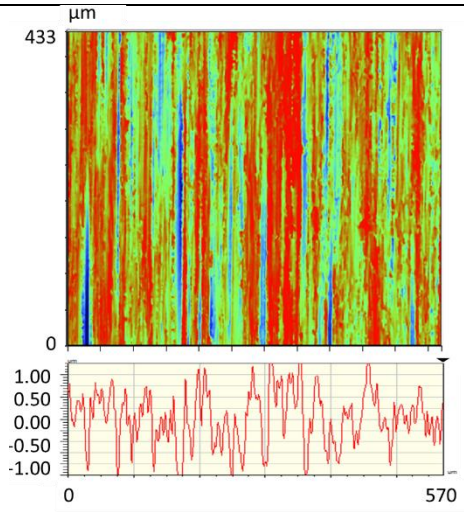	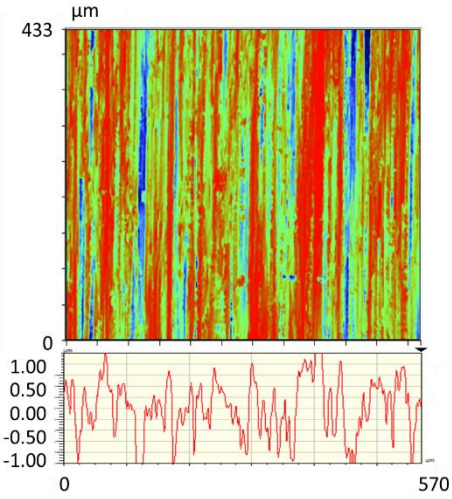
Initial Surface	7 KCycles

Figure 8-10. Example of Wyko roughness measurements (all values are in microns).

The profile of the chemical composition of the ZDDP-derived tribolayer were obtained by using an Ar^+ ion gun source with an energy of 2 KeV, 2x2 mm^2 area, 10 µA sputter current and 60s of waiting time before spectra acquisition. The sputtering

rate for the tribofilm was found to be 4.5 nm/min using optical profilometry and measuring the wear depth after 10 min of sputtering. Sputtering depth profiles were processed by using MultiPack™ Software (version 8.3, ULVAC-PHI Chanchassen, MN, USA), and the reaction layer thickness was defined as the thickness where the atomic concentration of O1s signal is less than 5% for steel samples. The sputtering time provides the measures of layer thickness.

The surface composition and morphology was analyzed by X-ray photoelectron spectroscopy (XPS) and Secondary Electron microscopy (SEM) coupled with Energy-dispersive X-ray spectroscopy (EDX) before roughness measurements.

The experiments have been run with different initial roughness values of rings to simulate different lubrication conditions. The values of initial roughness of the rings were: R_q= 100±20 nm, 200±20 nm, and 600±50 nm while the roughness of rollers was kept nearly constant with values of R_q= 50±10 nm.

The specimens used were made of steel AISI 52100 (Chemical composition shown in Table 8-5), with Elastic Modulus of 210 GPa and a Poisson's ratio of 0.27.

Table 8-5 Chemical properties of steel AISI 52100 in %

	Cr	Ni	Mn	Mo	Si	C	S	Cu
AISI 52100	**1.350**	**0.250**	**0.450**	**0.100**	**0.350**	**1.050**	**0.015**	**0.030**

8.4.2 Numerical Results and Discussion

The MicroPitting Rig (MPR) experiments which was discussed in the experimental section was simulated with the numerical model. The numerical model was adapted to the same configuration as the MPR. The numerical model follows a semi-deterministic approach so that some parameters in the model should be calibrated

prior to any predictions. One important calibration parameter is the *initial* coefficients of wear used in the wear model. Simulations have been run with different *initial* coefficient of wear and the calculated wear was compared with one single experimental wear measurement. The true *initial* coefficient of wear was then used for the rest of the simulations.

The other important parameters in the model are the tribofilm growth model parameters of Equation 6-14. These parameters (x_{tribo}, h_{max}, C_3 and C_4) are obtained by fitting the mathematical expression of Equation 6-14 to the experimental tribofilm thickness results. In this part, the calibration parameters are the ones reported previously in Ref (117) and reported in Section 6.6.1 and Table 6-1. The experimental results used to calibrate the model in the previous work were the tribofilm thickness measurement results reported in Naveira-Suarez *et al*. (57). The material used in that work was Steel AISI 52100 and the oil was Poly-α-Olephin (PAO) with ZDDP antiwear additive. Since the materials and lubricated oil were similar, the same calibration parameters (presented again in Table 8-6) were used in this work for simplicity.

The growth of the tribofilm is assumed to occur only at the contacting asperities. Therefore the local contact properties calculated from the contact model are responsible for the formation of the tribofilm at the asperity scale. It is observed experimentally that the formation of the tribofilm on asperities can lead to change in the mechanical properties of interfaces and also results in an increase in load-carrying capacities of the contacting bodies (16). Once the tribofilm, which is a solid–like material, forms on the contact asperities, the topography of the surfaces is changed and the contact condition between surfaces may change as a result. This change in the

contact conditions can lead to a different topographical evolution at the interface in comparison to the case when no such tribofilm is formed. This effect can be seen in the numerical results.

One example of the model results is shown in Figure 8-11. It can be seen that the rougher surface (Figure 8-11 (a) left) starts to become smoother in the beginning of the contact then gradually becomes rougher over time. It can be interpreted that in the beginning of the contact the dominant plastic deformation can lead to relatively fast surface deformations. The tribofilm formed on the surfaces will change the local mechanical properties of the surfaces as well as their micro-geometry. An increase in the roughness of the rougher surface can occur because of the growth of the tribofilm. The tribofilm growth on the surfaces which are solid-like material will change the contact behaviour of the interface and will eventually roughen the surface. After some time, the surface becomes gradually smoother because of the mild wear occurring at the contacting asperities.

Different points of the simulation are numbered in Figure 8-11. Point 0 is the beginning of the simulation where the initial surfaces are not in contact yet. Point 1 is the time after 20 Kcycles for the roller. It is the time that highest asperities of surfaces are plastically deformed. Point 2 is selected to be the end of the experiments (after 100 Kcycles of the roller). These points are selected and schematically shown in Figure 8-11 in order to be referred in this thesis. Points are used in Figure 8-13 and Figure 8-14 to study the difference in the surface topography and tribofilm formation at different times of the simulation.

In the beginning of the contact, the highest asperities of the rough surface experience high levels of plastic deformation. This plastic deformation results in the smoothening

of the rough surface. Simulation results to confirm this are reported in Figure 8-13. It can be seen in the figure that the asperities of the initial surface (Figure 8-13-a) are smoothened (Figure 8-13-b) after 20 Kcycles of the roller. The asperities are then made smoother due to mild wear (Figure 8-13-c). The smooth surface come into contact with highest asperities of the rough surface and it produces grooves on the smooth surface (Figure 8-13 d-f). Growth of the tribofilm on the contacting asperities then results in roughening of the rough surface. The simulation results of the inhomogeneous tribofilm formed on the surface confirms this and the results are shown in Figure 8-14. It can be seen that the tribofilm grows on the contacting asperities both in thickness and coverage. Fast growth of the tribofilm in the running-in stage on highest asperities changes the geometry of that asperity in the contact. The new asperity consists of a substrate (steel) and the glassy polyphosphates tribofilm on top which is a solid-like material. It can come into contact with the counter body and increase the average peak-to-valley height difference. The counter body also consists of a tribofilm on top but in the running-in stage, there are numerous asperities that are not covered by the tribofilm yet. This will lead to the contact of the high asperities consisting tribofilm into the asperities of the counter body that are not yet covered by the tribofilm. Different simulations have been run with and without considering the growth of the tribofilm. Interestingly, in the latter case, there was no increase in the surface roughness value in the computational results. The topography evolution in the case that no tribofilm was formed on the surfaces has been plotted in Figure 8-12 and the results have been compared to the case that tribofilm growth was considered in the numerical model.

This growth of the tribofilm is responsible for the increase in the roughness of the ring. The growth of the tribofilm on both rough (ring) and smooth (roller) surfaces are

shown in Figure 8-14. It can be seen that the growth on the roller (smooth surface) is faster in comparison to the ring (rough surface) and it is due to higher number of loading cycles (13.5 times higher) on the roller. The growth of the tribofilm on the surfaces is directly proportional to the time of rubbing. The roller is exposed to rubbing 13.5 times more than the ring and this is the reason that there is a faster growth of tribofilm observed on the roller. It should be noted that the number of cycles for ring and the roller are different and the scale of the x axis in Figure 8-11-a is different from Figure 8-11-b.

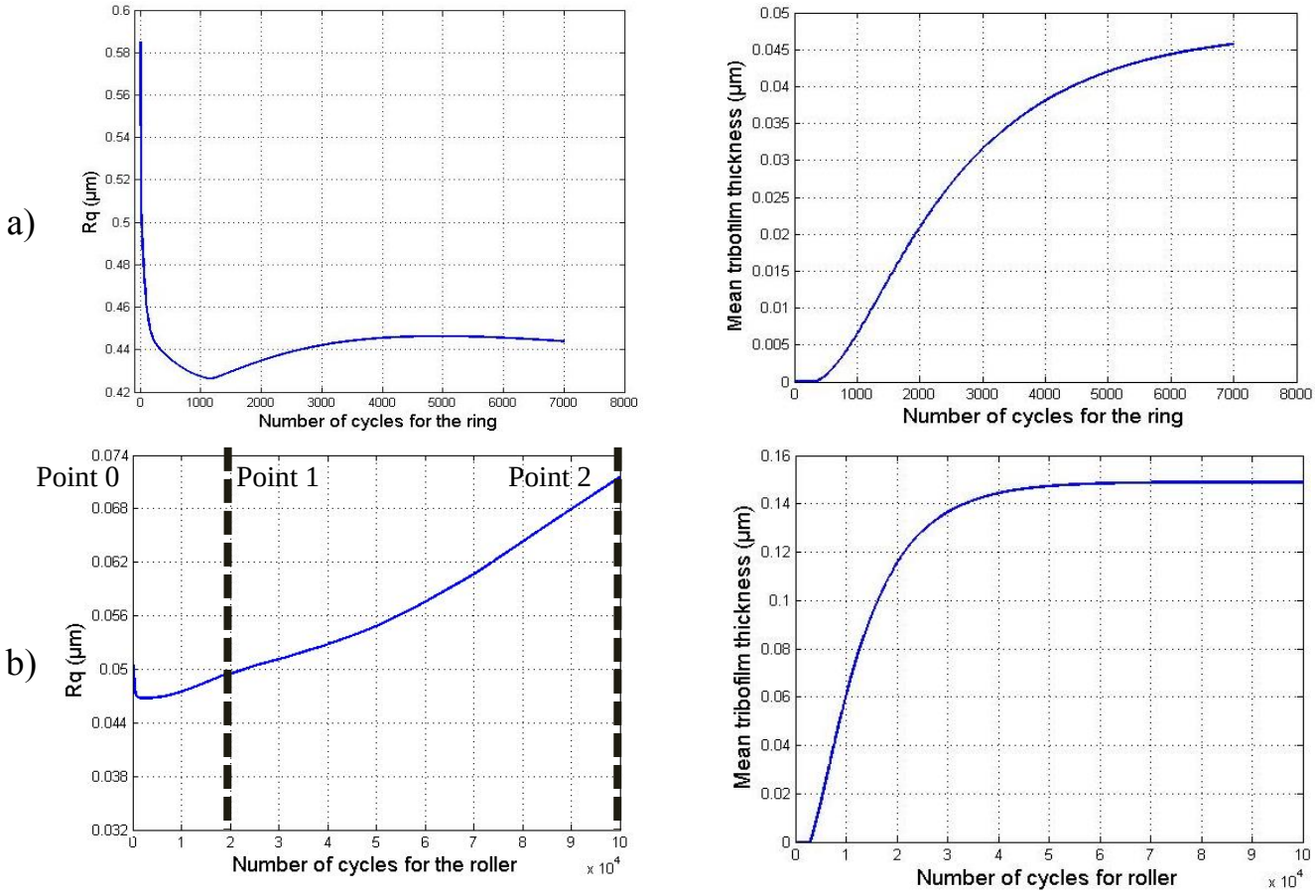

Figure 8-11 (Left) roughness evolutions and (Right) tribofilm growth for the (a) rougher (ring) (b) smoother (roller) body as predicted by the model

The smoother body (roller) experiences a relatively fast decrease in the roughness value because of plastic deformation (See Figure 8-13 d-f). The root mean square

sharply decreases from 0.05 µm to 0.047 µm; this is because of high plastic deformation calculated via the model in comparison to small surface roughness of the roller. Then an overall increase in the roughness of the smoother surface is observed because of contact with a rougher surface. Similar results were obtained in (32). It should be noted that the tribofilm is formed on both surfaces and the corresponding average tribofilm thickness is shown in Figure 8-11 parallel to the roughness evolution of both surfaces for comparison purposes.

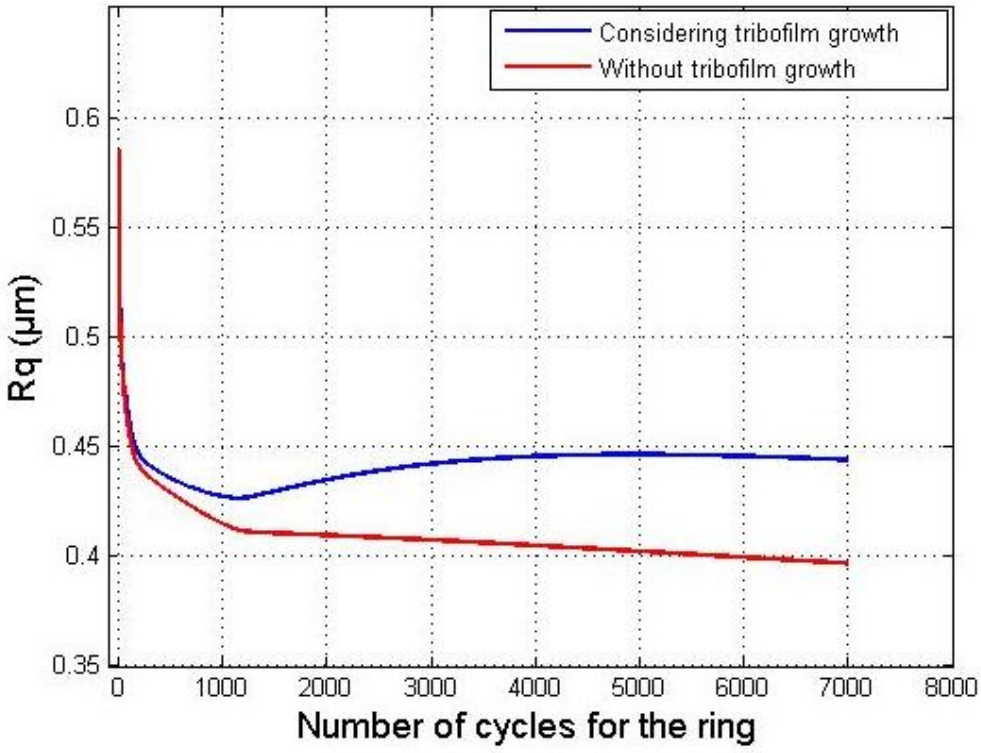

Figure 8-12 The comparison of the topography evolution between the cases when a tribofilm growth is considered in the model and the case that there is no tribofilm being formed on the surfaces.

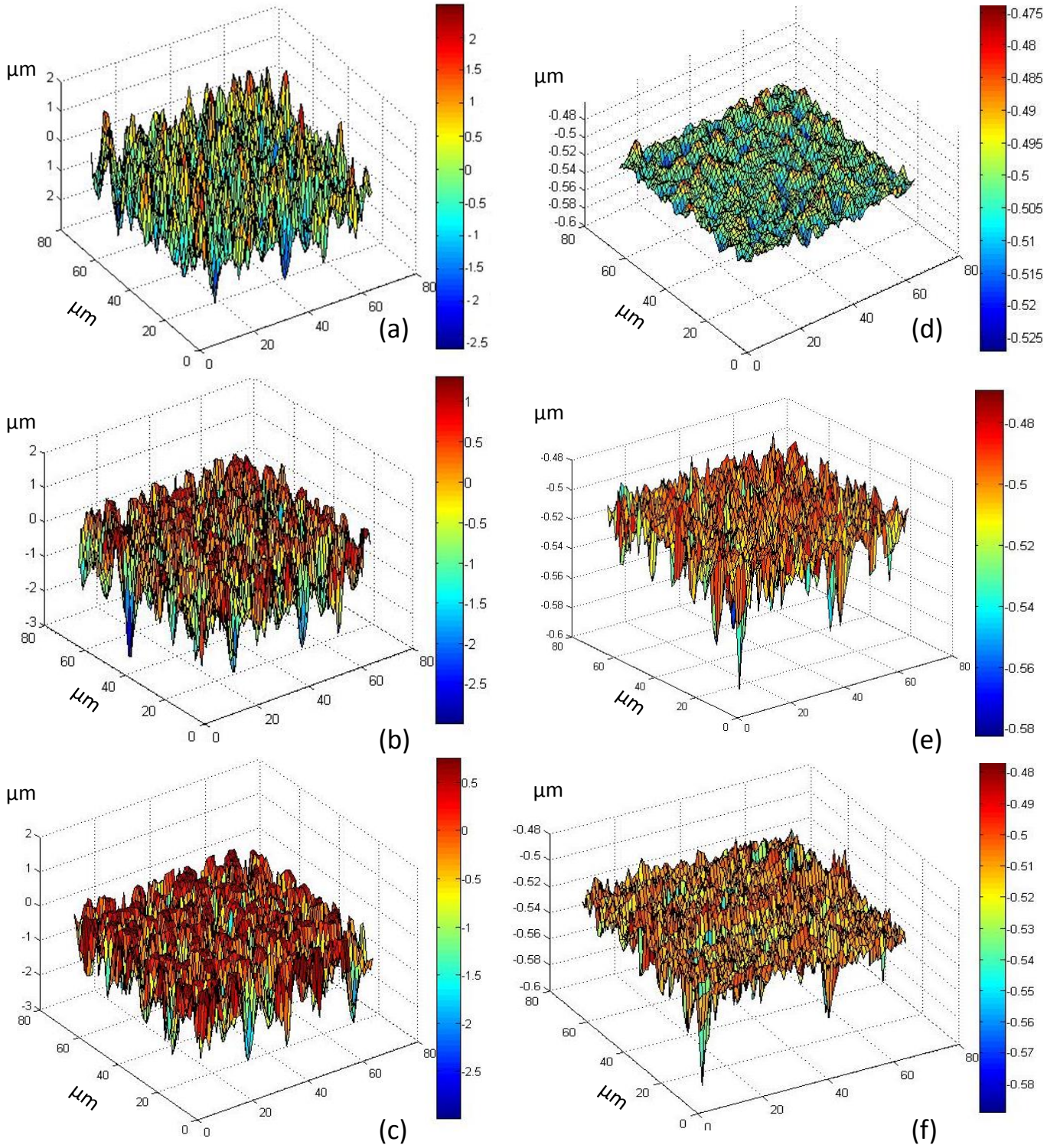

Figure 8-13 Surface topography evolution predicted by the model (a) surface of the ring before the experiment point 0 (b) surface of the ring at point 1 (c) surface of the ring at point 2 (d) surface of the roller before the experiment point 0 (e) surface of the roller at point 1 (f) surface of the roller at point 2

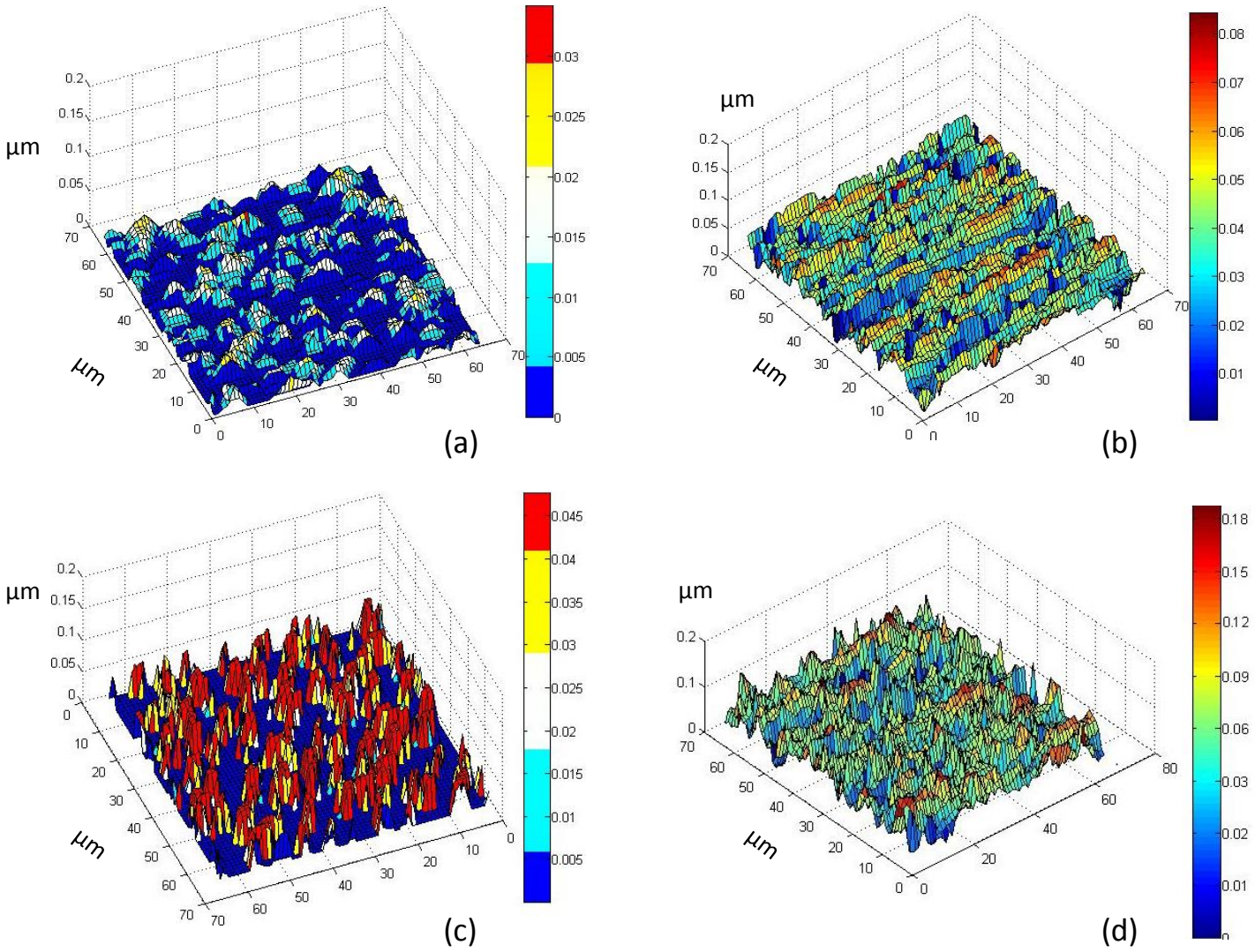

Figure 8-14 Tribofilm growth on the contacting asperities (a) at point 1 for rough surface (ring) (b) at point 2 for rough surface (ring) (c) at point 1 for smooth surface (d) at point 2 for smooth surface

The experimental part of this work is then carried out to validate the model and to confirm the proposed mechanism for changing the topography of surfaces by means of experiments.

8.4.3 Experimental Results

The roughness evolution of MPR roller and three different rings obtained by the method described above is shown in Figure 8-15. The figure shows that when the roughness of the rings is higher, longer running-in will occur which delays the

tribofilm build up and the surface modifications are at the beginning very similar to those found without the presence of additives. With smoother surfaces, the roughness modifications decrease because of the formation of a tribofilm. When the contact is in the EHL regime ($R_{q\,\mathrm{rings}}$=100 nm), the process is mainly governed by the coverage of the contacting asperities in with ZDDP tribofilm. The asperities of the bodies covered with a tribofilm promote the roughening of the ring's surface until it reaches the steady state. This can be noticed because the differences in roughness are not visible during the initial cycles on the smoother body. It is clear that, when the contact is in the boundary or mixed lubrication regimes ($R_{q\,\mathrm{rings}}$=600 nm and $R_{q\,\mathrm{rings}}$=200 nm), the first process which occurs on the surface is the plastic deformation of asperities, leading to a smoothening of the surface and it is in agreement with the numerical results. In complete boundary lubricated contact ($R_{q\,\mathrm{rings}}$=600 nm), after the plastic deformation process, the tribofilm can increase the roughness of the surfaces.

The numerical model is only valid for boundary lubrication conditions. Therefore, for validation purposes, it was necessary to compare numerical results with the experiments in the boundary lubrication regime. Although this is one of the shortcomings of the numerical framework, it is important to develop robust models in boundary lubrication that able to capture tribochemistry phenomena. The experimental topography measurements for the case of boundary lubrication regime ($R_{q\,\mathrm{rings}}$=600 nm), are shown in Figure 8-16 for comparison purposes. Good qualitative agreement between the experimental and the model results is shown in Figure 8-11.

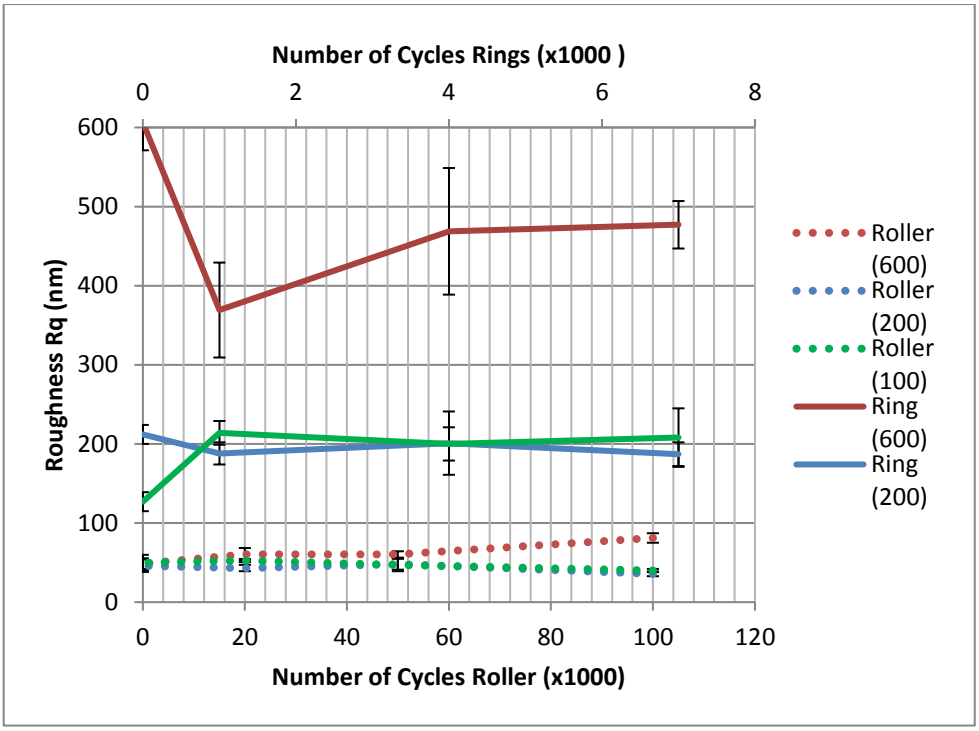

Figure 8-15 Experimental results on different roughness of rings

It is demonstrated in the model that the roughness of both smooth and rough contacting surfaces will converge to specific values but they will never reach the same number (see also (32)). It was also shown that different surface roughness configurations would have different topography behaviour. The initial roughnesses of both contacting surfaces are the key parameters which govern the further roughness evolution. It was assumed in the numerical results that the tribofilm growth on the contacting asperities is responsible for the roughening of the rings. The numerical results for tribofilm growth were then presented in the same section. To confirm this by means of experimental data, surface analysis results of the tribofilm formed on the surface are reported here.

Table 8-6 The calibration parameters

Parameter	Value	Description
K/H	1.25×10^{-17}	Dimensional wear coefficient for steel (m^3/Nm)
COW_{min}	1.25×10^{-18}	Dimensional wear coefficient for maximum film thickness (m^3/Nm)
h_{max}	176	Maximum local tribofilm thickness in the formation process (nm)
x_{tribo}	4.13×10^{-16}	Tribofilm formation rate constant
C_3	0.1125	Tribofilm removal constant
C_4	0.0006799	Tribofilm removal exponential factor
E_1, E_2	209	Young's modulus of two surfaces (GPa)
ν_1, ν_2	0.3	Poisson ratio
H_{steel}	8	Hardness of the steel substrate (GPa)
H_{tr}	2	Hardness of the tribofilm at steady state tribofilm thickness (GPa)

Figure 8-17 shows an SEM image of the tribofilm in the middle of the wear track formed on the roller. It can be seen from the image how the tribofilm is formed on the wear track due to severe conditions. It can be compared to the numerical results of Figure 8-14 and a similar pattern can be observed. The image is taken at the end of the experiment for the case of boundary lubrication regime when the initial roughness of the ring was $R_{q\,\text{rings}}$=600 nm.

XPS analysis performed on the tribolayer showed the oxygen signal with two different peaks. According to the literature, these peaks belong to two different Oxygen types: the main peak at 531.6 eV is assigned to the Non-Bridging Oxygen (NBO) in poly(thio)-phosphate chains and also to other oxygen-containing groups such as sulphates, carbonates or hydroxides (248); the second peak at 532.8 eV can be

assigned to the presence of the Bridging Oxygen (BO) which corresponds to P-O-P and P-O-C bonds (248).

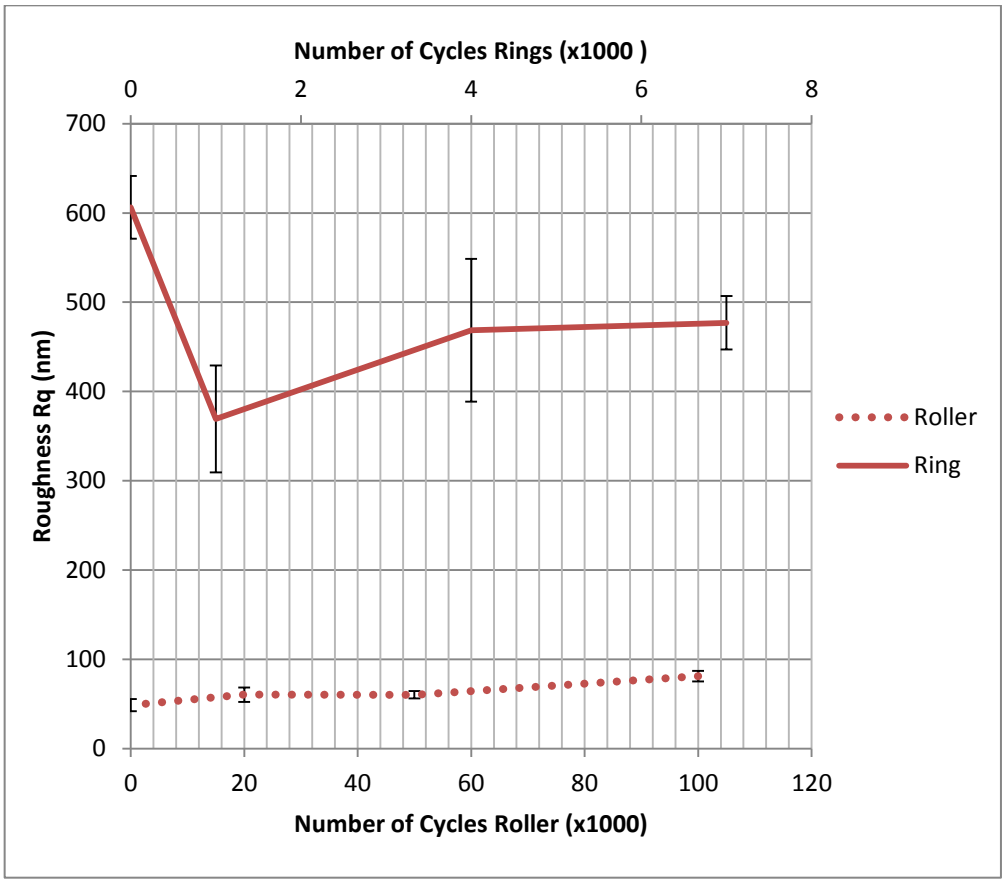

Figure 8-16 Roughness measurement experimental results for both ring and roller

The P 2p signal has been detected at 133.4 eV while the Zn 3s at 140.0 eV. S 2p signal has been found on the surface at 161.8 eV which is attributed to the oxidation state of -2 as found in sulphides (249) and thiolates (250) or when sulphur is substituting oxygen atoms in a phosphate (248). Iron signal has not been found on the surface of the tribolayer indicating that the layer was uniformly covering the entire surface.

Figure 8-18 shows the XPS depth profile of the tribolayer formed on the surface of the ring in boundary lubrication regime. The thickness of the tribolayer has been found to be of around 55 nm; this means that a uniform tribolayer is covering all the asperities of the surface and hence giving a completely different pattern when

compared to a surface without any tribolayer. The composition of the tribolayer, according to previous studies (35) is composed by chains of polyphosphate which determine the hardness and the strength of the tribolayer. The length of the polyphosphate present on the surface can be determined by the ratio between Bridging Oxygen (BO) and Non-Bridging Oxygen (NBO) as it is shown in Figure 8-19 (251).

In this case, the ratio is equal to 0.3 which corresponds to the presence of a polyphosphate chain (252). The same results have been obtained for mixed lubrication indicating that the tribolayer formed on the surface is the same as shown in Figure 8-19. It was reported that chain length of the polyphosphate tribofilm is important for local mechanical properties of the film on the surface and different mechanical behaviour such as the durability of the films (16, 46, 48, 50). For this reason, chemical characteristics of the film are important parameters in defining the physical and mechanical behaviour of the film and the corresponding changes in the topography of the surfaces.

Surface analysis results shown in Figure 8-17 and Figure 8-18 indicate that the tribofilm covers the surface asperities of the roller. This tribofilm which consists of polyphosphates (confirmed with XPS) is reported to be a solid-like material. In the numerical simulation results of Section 4, growth of such a tribofilm was reported to be the reason for the increase of roughness of the ring surface. The thickness of the tribofilm demonstrated by XPS was about 55nm which is close to the numerical results (see Figure 8-11 (a), right).

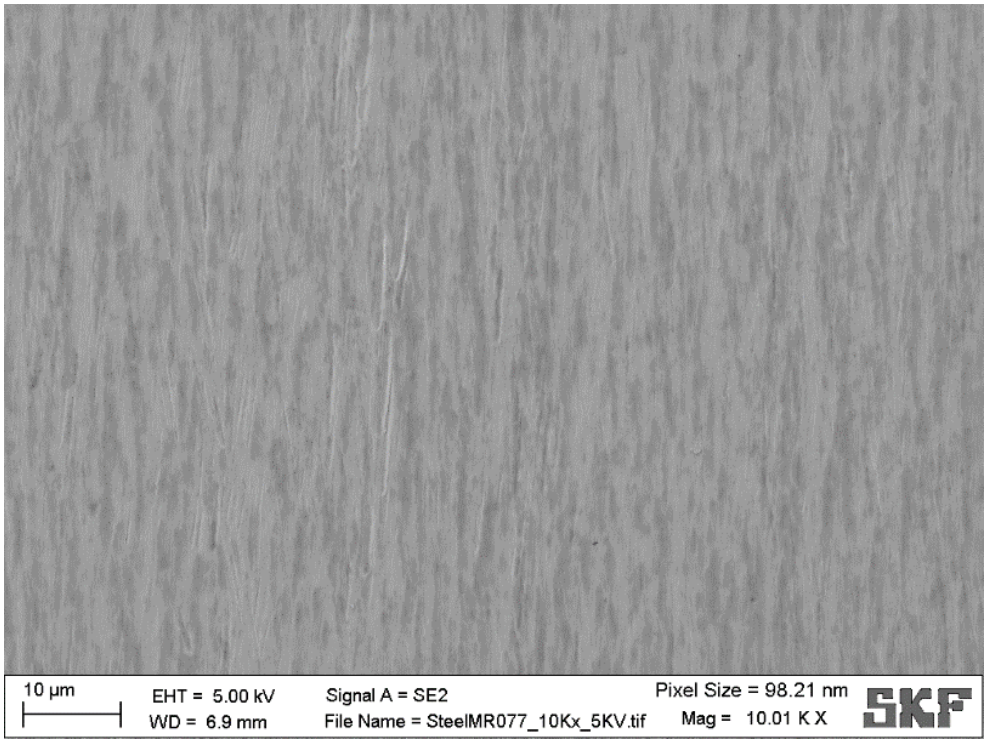

Figure 8-17 SEM image of the tribofilm uniformly formed on the wear track

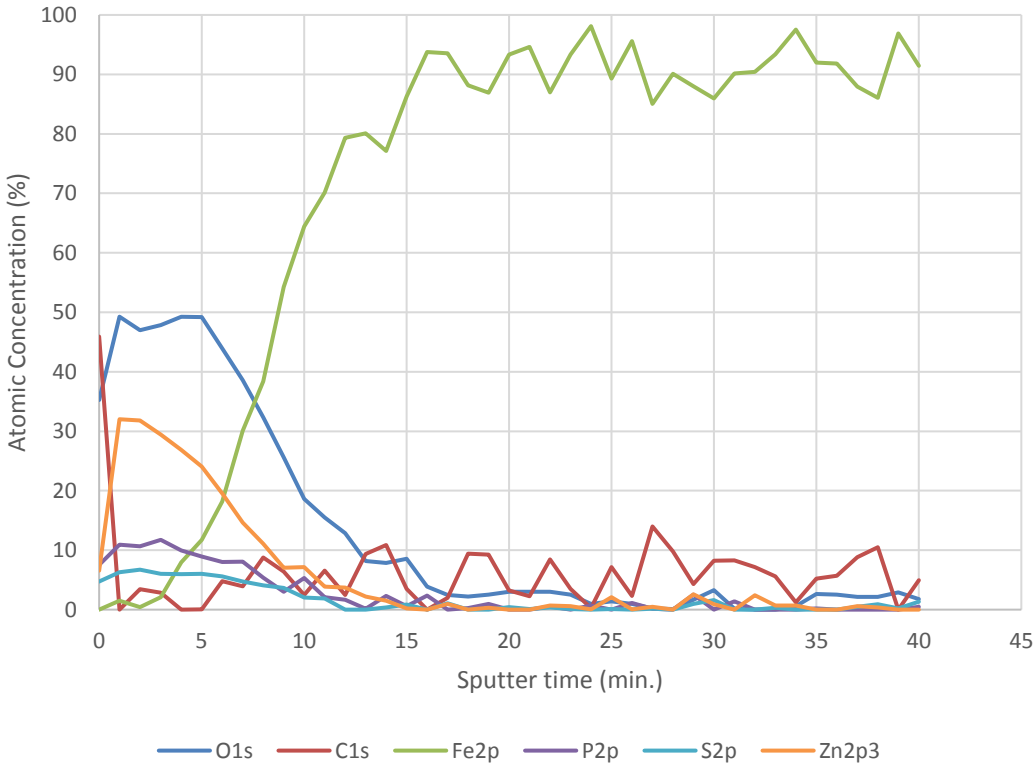

Figure 8-18 XPS depth profile of the tribofilm formed on the surface of the ring

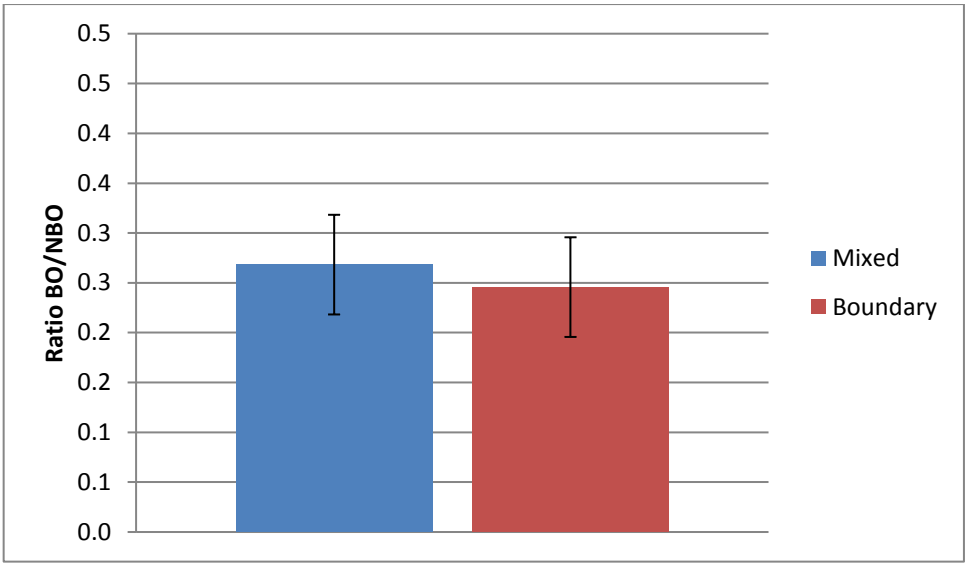

Figure 8-19. Ratio of BO/NBO for the two lubricating conditions

8.5 Summary

The tribochemistry model integrated into the contact mechanics simulation has been shown to be capable of predicting the development of topography of the contacting bodies. The predictions of emerging topography were validated against experiments which were carried out using a micro pitting rig. The surface topography is affected by surface plastic deformations, tribofilm formation and wear. It is shown that during initial contact, high plastic deformations on the surfaces are responsible for changes in the topography. It is also reported that formation of a tribofilm can change the local mechanical properties at interfaces which can influence the further roughness evolution of surfaces. One interesting conclusion from an analysis of the pool of numerical simulations is that the roughness evolution of both contacting bodies is significantly influenced by the initial roughness patterns. It means that the initial roughness of both surfaces in combination will determine the mode of topography evolution and hence a proper finishing of both contacting surfaces is required to obtain a better tribological performance in the steady-state.

It was shown that the growth of polyphosphate tribofilm formed on the contacting asperities is responsible for an increase in the topography of surfaces in contact. This was shown numerically and was verified with experiments by means of surface analysis. The surface analysis results show that a uniform tribofilm was formed on the surface with a thickness very close to the predicted values.

In addition, the effects of load, material hardness, coefficient of wear and the initial surface roughness on the roughness evolution have been studied. It was observed that the applied load is important in topography evolution and higher load will result in higher plastic deformations and bigger changes in surface roughness. Regarding the hardness effect, the harder materials are less likely to deform plastically and therefore they will experience less topography variations.

Chapter 9. Discussions

In this chapter, the main point of the literature review of the boundary lubrication modelling is discussed first. Then the gap in the literature is highlighted and important parameters that should be considered in boundary lubrication models are presented. All individual parts of the boundary lubrication model developed in this thesis is then summarised and the main points are discussed. Finally, the limitations of this model is highlighted and the possible approaches to overcome these limitations are proposed.

9.1 Overall Discussion

Different numerical approaches applicable in modelling of boundary lubrication were introduced in the literature review of Chapter 4. The survey of the literature has demonstrated that the Finite Element Methods can be a good approach in the calculation of contact mechanics simulations due to their robust solid mechanics calculation abilities (111, 112, 159). On the other hand, it has several disadvantages in modelling boundary lubrication. It is very difficult to capture the nano and micro scale properties of roughness in the FEM due to complex mesh requirements. In addition, wear changes the local geometry of the rough surfaces and these changes are difficult to capture by FEM due to the need for remeshing. These are only the complexities allocated with capturing wear and the moving boundaries allocated with that. Furthermore, growth of the tribofilm on the contacting asperities (which is a combination of formation and removal) also occurs in boundary lubrication, which results in changes to the geometry of surfaces with different mechanical properties.

It has also been shown that Molecular Dynamics (MD) might answer fundamental questions at the atomic scale (81) (nano-scale) and might be able to capture the interactions between lubricant additives molecules and the substrate (89). On the other

hand it has difficulties in dealing with larger scales (at least asperity scale) and it is unable to cover the longer time scales of tribological systems. Another complexity in molecular dynamics simulations in tribology is considering the non-equilibrium thermodynamics with its complex formulations.

Examples of the Discrete Element Method modelling approach applicable in boundary lubrication was also presented in literature review. It has been shown that DEM has the advantage of small scale calculation of contact force and deformations (124). It can model the roughness of surfaces with high precision and wear of material can be directly calculated by detachment of particles (253). But, like molecular dynamics, it is limited with time and length scales. Calibration of particles' bonding to simulate a solid material is also complex.

The best and most suitable numerical approach to model boundary lubrication found in this survey was the Boundary Element Method (BEM). BEM is very efficient in solving the contact mechanics problems due to its simple discretising properties (151). Changes in geometries due to wear (139), plastic deformation (141) and tribochemical changes (17) can be modelled by means of BEM.

It was discussed earlier in this thesis that contact mechanics, chemistry and thermodynamics are the three most important components of boundary lubrication. Therefore a robust modelling approach for boundary lubricated systems considering all of the mentioned characteristics is very difficult and at the start of the present research, was still lacking in the literature. Such an approach should consider contact between rough surfaces and be able to analyse the load and deformations as well as temperature at interfaces. The model also should consider chemistry of the lubricant additives that can possibly react with the substrate to form the protective tribofilm.

Consideration of the tribofilm should not be limited only to the reaction kinetics but also to the chemical characterization of the tribofilm and its mechanical properties which overall define the durability and behaviour of the tribofilm.

Considering the above mentioned complexities in modelling boundary lubrication, this thesis presents the development of a numerical framework that combines tribochemistry with contact mechanics of rough surfaces as well as a wear model that accounts for the effect of tribofilm in reducing wear.

9.1.1 Contact Mechanics Model

The contact mechanics model developed in this work is flexible to any contact configuration and sliding/rolling condition. The model is able to calculate elastic-perfectly plastic contact of rough surfaces. Digitized rough surfaces with different asperity areas and roughness values can be generated and used in the contact mechanics simulation. The complementary potential energy method with variational principle was the base of the contact mechanics simulations. Fast Fourier Transforms (FFTs) were used for numerical calculations of contact pressure and surface deformations. Two numerical approaches were used to move the contacting surfaces in the sliding direction. The first method was the conventional matrix shifting method which has been used widely in the literature. The second approach was using the influence matrix and extracting the necessary elements to reduce the computational time. The elastic-perfectly plastic model used hardness as the limiting parameter for plastic pressure. Only pressures below the hardness of the material were used for rigid body deformations and the plastic deformation was calculated by subtracting elastic deformation from the body interference. Flash temperature was calculated using Blok's theory assuming square contact area.

The contact mechanics simulation is then the base of the numerical framework and is able to calculate the local asperity pressure, temperature and deformations.

9.1.2 Tribofilm Growth Model

It has been shown in this thesis that tribological processes should be studied through non-equilibrium thermodynamics of interfaces. This is due to the non-equilibrium processes occurring during the transfer of mass and energy which consequently change the entropy of the system. Therefore studying the kinetics of the tribochemical reactions should consider entropy as an important parameter in inducing the chemical reactions.

A mathematical model is developed for the formation of the tribofilm on the contacting asperities. The model is based on the kinetics of tribochemical reaction. Tribochemical reactions are assumed to occur in two general steps. Firstly, the substrate is mechanically activated by rubbing on the counter face. This stage is called mechanical activation. This process leads to formation of a surface with high reactivity and this surface will react with the lubricant additive to form the tribofilm in a thermomechanical process.

The rate of the tribochemical reaction is mathematically formulated as:

$$k_{tribo-thermo} = \frac{x_{tribo}}{x_{thermo}} k_{thermo}$$

In which x_{tribo} and x_{thermo} are the population of the transition states for tribochemical and thermal reactions respectively.

It is known from the thermodynamics that:

$$k_{thermo} = \frac{k_1 T}{h'} exp\left(\frac{\Delta E}{RT}\right)$$

$$x_{thermo} = exp\left(\frac{\Delta E}{RT}\right)$$

k_1 and h' are the Boltzmann and Plank's constant and ΔE, R and T are activation energy, gas universal constant and the temperature respectively.

The above formulation is then used to develop the tribofilm formation model. The mathematical expression for the tribofilm formation is the following:

$$h = h_{max}\left(1 - e^{\left(-\frac{k_1 T}{h'}.x_{tribo}.t\right)}\right)$$

The removal of the tribofilm was also considered in this thesis and a mathematical formulation is included to capture this in local scale. It was assumed that tribofilm is being formed and removed at the same time and this dynamic process in combination results in the growth of the tribofilm. The overall formulation for the growth of the tribofilm will be as the following:

$$h = h_{max}\left(1 - e^{\left(-\frac{k_1 T}{h'}.x_{tribo}.t\right)}\right) - C_3(1 - e^{-C_4 t})$$

Tribofilm thickness experimental results are used to capture the growth behaviour by setting the simulation values with respect to the experimental results. So far in this research, capturing the tribofilm behaviour was dependent on the experimental results due to the lack of comprehensive analytical understanding of the real mechanisms of tribofilm formation and removal. Despite all the complexities, such simplified semi-analytical models for tribofilm growth can be good starting points for the problem. As explained in detail in Section 6.7, there is more need for experimentation to develop the proposed tribofilm growth even further.

The tribofilm growth model was then calibrated with the existing experimental results in the literature (15) to study the effect of different additive concentrations and

temperature on the tribofilm growth. It was shown that the term x_{tribo} can change linearly with the concentration of the ZDDP in the oil and is independent of the temperature as expected. This is a good starting point for further investigation of the effect of such parameters on the kinetics of tribochemical reactions and the formation of the tribofilm on the contacting asperities.

There found to be similarities between the empirical tribofilm growth model reported by Fujita and Spikes (61) with the developed model in this thesis. Both models capture the experimentally-observed tribofilm growth behaviour. In both models, the formation of the tribofilm follows an exponential form. There are also important differences in the nature of the models that should be pointed out. The model of Fujita and spikes was an empirical model for the global (macroscopic) tribofilm thickness growth over the time but the current model of this thesis is a local tribofilm growth model based on the local properties of the contact of rough surfaces.

Unlike the work of Fujita and Spikes, the effect of mechanical rubbing was considered in the parameter x_{tribo} in this work. In addition, in the current model, a phenomenological model is developed to account for the removal of the tribofilm. This removal model can help to further develop the understanding of the removal process and the durability of the tribofilm.

9.1.3 Coupling Growth Model with Contact Mechanics

The tribofilm growth model is implemented into the contact mechanics simulation and the result is the inhomogeneous tribofilm growth on the contacting asperities due to the inhomogeneous nature of the load and temperature distribution. The model is capable of capturing the tribofilm thickness and coverage at any time of the simulation.

It was shown by the simulations that higher loads will result in a faster coverage rate of the surface by the tribofilm and it is because of the faster flattening of the surfaces. More asperities come into contact when asperities are flattened and it results in greater coverage of the tribofilm.

The numerical results suggest that smooth surfaces are covered by the tribofilm faster than rough surfaces. It is due to the longer time for flattening of the asperities in the rough surface. It is also in line with the experimental observations that smoother surfaces have shorter running-in times.

It must be noted that both surfaces should experience severe contact and should be in the boundary lubrication for the above statement to be valid. It could be debated that rough surfaces experience faster tribofilm coverage and it is observed experimentally. This can be true in many cases but if the contact is severe for both cases, the numerical results shown above is valid. The difference observed in experiments comes from the difference in λ ratio and the severity of the contact. Smooth surfaces experience less severe contacts because of bigger λ ratios.

The effect of sample sizes was also investigated by means of the numerical simulations and no significant differences were observed for tribofilm coverage and tribofilm thickness on the contacting asperities.

9.1.4 Wear Model

In Chapter 7, a wear model was proposed which takes into account the thickness of the ZDDP tribofilm and modifies Archard's wear equation. A brief summary of the wear model is explained in this section.

It was observed extensively in the literature that even in the areas where tribofilm is formed on the surface, wear occurs (48, 59, 220). It is believed that this tribochemical

wear is due to partial removal of the tribofilm. Therefore the dynamic process of formation and removal of the tribofilm leads to mild wear of the system.

However this wear is much less than the wear resulting from solid-solid interactions. Note that this mechanism of wear does not apply in the case of inert substrates such as DLC, as mentioned in Chapter 7, but it is reasonable in the case of ZDDP tribofilms on steel surfaces.

Studies show that the concentration of substrate atoms decreases towards the top of the tribofilm produced by ZDDP [29,33] on steel. If material detaches from the tribofilm due to the contact, some amount of the substrate atoms are removed from the surface. This decrease in the atomic concentration of the substrate as the distance from the substrate/tribofilm interface increases suggests that less wear of the substrate occurs if a thicker tribofilm exists. At the same time of the tribofilm removal, more substrate atoms diffuse into the tribofilm and move towards the upper parts of the film to restore the chemical balance. This movement can be due to different mechanisms. Replenishment of the tribofilm then might occur due to different surface phenomena including the tribochemical reactions and mechanical mixing due to combined effects of material removal and shear stress.

Therefore the wear model used in this work modifies Archard's wear equation and takes into account the thickness of the antiwear tribofilm. Assuming that the coefficient of wear is at its maximum for steel-steel contact and at its minimum when the tribofilm has its maximum thickness, the equation for calculating coefficient of wear is as follows:

$$CoW_{tr} = CoW_{steel} - (CoW_{steel} - CoW_{min}).\frac{h}{h_{max}}$$

CoW_{tr} is the coefficient of wear for tribofilm with thickness h.

CoW_{steel} , CoW_{min} and h_{max} are the coefficient of wear for steel and the coefficient of wear corresponding to maximum ZDDP tribofilm thickness and maximum film thickness respectively.

There is no experimental work reported in the literature presented thus far that provides a specific form for the variation of wear rate with local tribofilm thickness. The linear form assumed here is the simplest mathematical form that allows for a variation across the tribofilm as a result of the non-uniformity in the concentration of substrate ions across the tribofilm. This could be modified in future iterations of the model, should further experimental results become available, but the comparison with experiments in Chapter 7 indicates that Equation 7-4 is a sufficient representation of the behaviour.

The wear discussed is the tribochemical wear that is wear in the presence of a tribofilm. It is therefore different from the concept of only fracture and removal of substrate due to mechanical rubbing. It should be noted that the formation of the tribofilm takes time as it takes time for the asperities in contact to be covered by a tribofilm. It is also shown in the simulation results that the tribofilm gradually covers the surface in time and the inhomogeneous tribofilm is formed on the contacting asperities due to inhomogeneity of local properties of surfaces. In this sense, it takes some time for the coefficient of wear to reduce. The wear and plastic deformation happen severely at the beginning.

The model is capable of capturing wear at all times of experiments in real time and the wear prediction pattern was shown to be very similar to the ones reported in the literature. The effect of different parameters was studied on the wear and it was

confirmed numerically that the *initial* coefficient of wear plays an important role in the final wear of the system. It was observed that different simulations with different *initial* coefficients of wear have shown different wear rates (Figure 7-4). The effect of load was also studied. The results show that the main difference between wear behaviours at different loads is the plastic deformation occurring at the initial stages. The wear rate is also higher for higher loads (Figure 7-5).

To validate the wear model, experiments were carefully designed to monitor tribofilm thickness and measure wear. The experimental wear measurements were based on the average wear depth and were compared with the numerical results. A good agreement was found between numerical and experimental results.

9.1.5 Prediction of Surface Topography

The developed model is able to calculate the surface roughness parameters such as R_q and R_a at any time of the simulation. This characteristic of the model was explained in detail in Chapter 8. It was found that a combination of the roughness of both surfaces in contact may characterize the evolution of the topographies.

It was found that the wear coefficient can significantly affect the topography evolution of both contacting surfaces. This effect is more for the rough surface in comparison to smooth surface (Figure 8-3). It was shown that load is also an important parameter in changing the topography of surfaces. Higher load will result in higher changes in roughness values of the surfaces (Figure 8-4). It was also reported that initial surface roughness plays an important role in the behaviour of the topography evolution (Figure 8-6). Material hardness and its effect were investigated on the roughness evolution of surfaces. It was presented that harder materials are less likely to get modified in topography (see Figure 8-8).

The topography prediction capability of the model was then validated against experimental results. Experiments were conducted using a Micro Pitting Rig (MPR) and the topography of the surfaces was measured at different times of the experiment. Numerical model results showed a good agreement with the experimental measurements. Both experiments and the model indicated a fast change in the roughness of the surfaces in the beginning of the experiment which was due to high plastic deformations. Then an increase in the roughness was observed which was interpreted to be the effect of ZDDP tribofilm formed on the surfaces. Then the mild wear of the system becomes dominant and the decrease in the asperity heights and the corresponding decrease in the roughness value of the surfaces were observed.

9.2 Limitations of This Study

Although in this work, a new numerical framework was developed that considers contact mechanics as well as tribofilm growth on contacting asperities and a modification to Archard's wear equation that accounts for the thickness of the ZDDP tribofilm, there are still some limitations that should be addressed.

- The contact mechanics simulation uses an elastic-perfectly plastic model in which the hardness of the material is used as a criterion for the plastic flow. This assumption neglects the work hardening behaviour of the asperities as they deform. Although this method gives a realistic contact pressure estimation, the deformations due to the pressure are highly underestimated as the influence coefficients of an elastic material are used neglecting the non-linear behaviour of the yielding subsurface material. Future work could overcome this problem using a more robust elasto-plastic contact model considering the non-linear behaviour of the material.

- The contact mechanics simulation can potentially consider the tangential tractions and consider the effect of frictional contact on the contact pressure and surface deformations. Due to expensive computational cost, this was not studied in this work. A robust mathematical solution to the frictional contact can be a potential path for developing the model in further.
- Sub-surface stresses are important in studying the plastic deformation of materials and predicting the life-time of the machine elements. It can be added to the existing numerical model for further analysis.
- The heat partitioning and calculation of the flash temperature is simplified in this work. A robust thermal calculation is needed to develop the boundary lubrication model further. The thermal model can consider the heat partitioning between different materials and using heat source geometries for better estimation of contact temperature.
- The tribofilm growth model includes two major parts; tribofilm formation and removal. The term x_{tribo} which is responsible for the rate of tribochemical reaction and is an indication of mechanical activation of the tribochemical reaction can be studied in further detail by designing experiments to see the effect of different physical and chemical parameters on this term.
- The tribofilm removal part is a simple mathematical formulation for capturing an important physics in the growth behaviour. This simple mathematical formulation can be developed further by designing careful experiments to monitor the removal of the tribofilm. Developing a mechanistic model for tribofilm removal can be a starting point.

Chapter 10. Conclusions and Future Work

10.1 Conclusions

A new model for boundary lubrication in real tribosystems has been developed. This model considers tribochemistry and its effects on wear as well as mechanical properties of surfaces. Local tribofilm growth considering both formation and removal, can be calculated in this model and it is possible to monitor the global tribofilm formation on the surfaces. It was shown that the global average tribofilm thickness shows a very similar trend to macroscale experimental studies of tribofilm growth. It therefore represents a good start in implementing tribochemistry into predictive boundary lubrication models. The tribofilm removal model can help tribologists to compare tribofilm removal with an amount of wear and will give a good insight for real mechanisms of wear. The tribofilm removal model was a starting point to further explore the durability of the ZDDP tribofilm. The model initiated an experimental investigation into the physical and chemical concept of the durability of the tribofilm. This can be later related to the wear of the tribosystem in the presence of a protective antiwear tribofilm.

The effect of this tribofilm on local wear of the system is considered in the model leading to a framework for predicting wear in boundary lubricated contacts. The model is applicable to a wide range of experimental observations and is able to be adapted to different experimental configurations.

The wear model is applied locally at the asperity scale, where a local coefficient of wear varies linearly with the current value of the local tribofilm thickness. The model is time-dependent, with the surface topography updated at each time step as a result of plastic deformation and tribofilm formation, and the local wear coefficient changes

in response to changes in the thickness of the tribofilm at every time step. Following calibration of the wear model parameters against experiments under one set of conditions, simulations under different conditions are tested against further experiments. Prediction of both the tribofilm growth and the wear depth as a function of time shows good agreement with experimental observations.

The results support the argument that wear can happen because of the removal of the substrate atoms present in the tribofilm due to different tribochemical phenomena, and the dynamic loss of material within the tribofilm throughout the growth on the contacting asperities. The wear rate under such conditions is much lower than that in the absence of a tribofilm, and the model captures this distinction, predicting faster wear in the early stages of the test where the tribofilm has yet to form.

Although the coefficient of wear in the model decreases with increasing tribofilm thickness, it is seen that having a thicker tribofilm at steady-state does not guarantee lower overall wear. Since the model captures the complete dynamics of the system, from bare surface through to constant average tribofilm thickness, it can be seen how the initial rate of tribofilm formation, influenced by temperature and local surface topography, affects the overall average wear depth seen in tribological tests. Example simulations are shown in which the wear depth is greater for a case with a thicker tribofilm.

The model tested in this work does not necessarily capture the wear mechanisms for all boundary lubrication systems such as DLCs and Al/Si alloys, but the framework can be a good flexible approach to test different mechanisms. There is still a need for more experimental evidence to see how tribofilm formation and/or removal are responsible for the wear of the boundary lubricated systems for ZDDP antiwear

additive on steel surfaces. Hence this model will be a foundation for finding the correlation of tribofilm growth and wear and more experiments are currently being carried out. The study of tribofilm removal and its chemical and physical effects on wear of the boundary lubricated contacts is the subject of ongoing research.

The model tested shows good agreement with experiments, indicating that, once calibrated, it has predictive capabilities that provide a beneficial tool for further exploration of boundary lubricated systems.

10.2 Future Work

Based on the limitations pointed in Section 9.2, a plan for extensions of this study is as follows:

- Incorporating a more robust contact mechanics simulation using an elastic-plastic contact model
- Extending the model for the case of dissolved water in the oil and different humidity by measuring the tribofilm thickness and incorporating that into the tribofilm growth model. Then predicting wear in these conditions.
- Considering tangential forces in the contact mechanics model and studying the stick/slip of the rough surfaces by calculations of the tangential displacements.
- Including sub-surface stress calculations in the contact mechanics model and relating that to the plastic deformation of half the bodies. Extensions to surface fatigue and crack propagations could be possible.
- Developing a heat partitioning model of contact of similar and dissimilar materials in order to fortify the tribochemistry model.

- A thorough investigation of the physical and chemical aspects of the removal of the tribofilm and the effect of different parameters. Adding more physical parameters to the removal model would be possible.
- Experimentation to extract more links between physical parameters and the term x_{tribo}. This will lead to a more robust tribofilm formation model. This model can be extended to various lubricant additives.
- Extending the model to predict friction in the boundary lubrication using the stick/slip of rough surfaces. The effect of tribofilm in local reduction of friction will be studied.
- Extending the model to the tribocorrosion condition and studying the repassivation/depassivation of the oxide layer and the current density. The contact mechanics model can calculate the evolution of the real area of contact which can be potentially important in the current density measurements and the tribocorrosive wear in the boundary lubrication contacts.

Chapter 11. References

1. Suárez AN. The Behaviour of Antiwear Additives in Lubricated Rolling-Sliding Contacts: Luleå University of Technology; 2011.
2. Studt P. Boundary lubrication: adsorption of oil additives on steel and ceramic surfaces and its influence on friction and wear. Tribology international. 1989;22(2):111-9.
3. Morina A, Neville A. Tribofilms: aspects of formation, stability and removal. Journal of Physics D: Applied Physics. 2007;40(18):54-76.
4. Bhushan B. Encyclopedia of nanotechnology: Springer; 2012.
5. Beeck O, Givens J, Williams E, editors. On the mechanism of boundary lubrication. II. Wear prevention by addition agents. Proceedings of the Royal Society of London A: Mathematical, Physical and Engineering Sciences; 1940: The Royal Society.
6. Tonck A, Martin J, Kapsa P, Georges J. Boundary lubrication with anti-wear additives: study of interface film formation by electrical contact resistance. Tribology international. 1979;12(5):209-13.
7. Blok H. Fundamental mechanical aspects of boundary lubrication. SAE Technical Paper, 1940 0148-7191.
8. Godfrey D. Boundary lubrication. 1968.
9. Klaus EE. Effect of Some Physical and Chemical Properties of Lubricants on Boundary Lubrication. 1964.
10. Ling FF, Klaus EE, Fein R. BOUNDARY LUBRICATION. AN APPRAISAL OF WORLD LITERATURE. 1969.
11. Persson B. Theory of friction and boundary lubrication. Physical Review B. 1993;48(24):18140.
12. Tabor D. Mechanism of boundary lubrication. Proceedings of the Royal Society of London Series A, Mathematical and Physical Sciences. 1952:498-505.
13. Jean Michel Martin TO, Clotilde Minfray,, Miyamotoc FDA. The origin of anti-wear chemistry of ZDDP. Faraday Discussions. 2012;156(1):311-23.
14. Pawlak Z. Tribochemistry of lubricating oils: Elsevier; 2003.
15. Fujita h, Glovnea R, Spikes H. Study of zinc dialkydithiophosphate antiwear film formation and removal processes, part I: experimental. Tribology transactions. 2005;48(4):558-66.
16. Aktary M, McDermott MT, McAlpine GA. Morphology and nanomechanical properties of ZDDP antiwear films as a function of tribological contact time. Tribology letters. 2002;12(3):155-62.
17. Joel Andersson, Roland Larsson, Andreas Almqvist, Grahnb M, Minami I. Semi-deterministic chemo-mechanical model of boundary lubrication. faraday Discussions. 2012;156(1):343-60.
18. Bosman R, Schipper DJ. Mild Wear Prediction of Boundary-Lubricated Contacts. Tribology Letters. 2011;42(2):169-78.
19. hydrodynamic lubrication 2015. Available from: http://www.synlube.com/SynLube_Magic2.htm.

20. EHL lubrication. Available from: http://www.slideshare.net/Sentientscience/modeling-tribological-contacts-in-wind-turbine-gearboxes.
21. Hamrock BJ, Dowson D. Isothermal elastohydrodynamic lubrication of point contacts: Part III—fully flooded results. Journal of Tribology. 1977;99(2):264-75.
22. stribeck curve [cited 2015 01/09/2015]. Available from: http://www.intechopen.com/books/ionic-liquids-new-aspects-for-the-future/tribological-properties-of-ionic-liquids.
23. lubrication regimes. Available from: http://www.kewengineering.co.uk/content/lubrication-explained.
24. Holm R, Holm EA. Electric contacts. 1967.
25. Archard J. Contact and rubbing of flat surfaces. Journal of applied physics. 1953;24(8):981-8.
26. M.Priest. Introduction to tribology.
27. Gwidon W. Stachowiak AWB. Engineering tribology. 2000.
28. Karpinska A. Running-in and the evolution of metallic surfaces subjected to sliding and rolling contact: Imperial College London; 2010.
29. Blau PJ. A model for run-in and other transitions in sliding friction. Journal of tribology. 1987;109(3):537-43.
30. Blau PJ. On the nature of running-in. Tribology International. 2006;38(11):1007-12.
31. Jamari J. Running-in of rolling contacts: University of Twente; 2006.
32. Morales-Espejel G, Brizmer V, Piras E. Roughness evolution in mixed lubrication condition due to mild wear. Proceedings of the Institution of Mechanical Engineers, Part J: Journal of Engineering Tribology. 2015:1350650115577404.
33. Boucly V. Semi-analytical modeling of the transient thermal-elastic-plastic contact and its application to asperity collision, wear and running-in of surfaces 2008.
34. Morales-Espejel GE, Brizmer V. Micropitting modelling in rolling–sliding contacts: Application to rolling bearings. tribology transactions. 2011;54(4):625-43.
35. Spikes H. The history and mechanisms of ZDDP. Tribology Letters. 2004;17(3):469-89.
36. Dacre B, Bovington C. The adsorption and desorption of zinc di-isopropyldithiophosphate on steel. ASLE TRANSACTIONS. 1982;25(4):546-54.
37. Piras FM, Rossi A, Spencer ND. Combined in situ (ATR FT-IR) and ex situ (XPS) study of the ZnDTP-iron surface interaction. Tribology Letters. 2003;15(3):181-91.
38. Taylor L, Dratva A, Spikes H. Friction and wear behavior of zinc dialkyldithiophosphate additive. Tribology transactions. 2000;43(3):469-79.
39. Fujita H, Spikes H. The formation of zinc dithiophosphate antiwear films. Proceedings of the Institution of Mechanical Engineers, Part J: Journal of Engineering Tribology. 2004;218(4):265-78.
40. Fuller MS, Fernandez LR, Massoumi G, Lennard W, Kasrai M, Bancroft G. The use of X-ray absorption spectroscopy for monitoring the thickness of antiwear films from ZDDP. Tribology Letters. 2000;8(4):187-92.

41. Yin Z, Kasrai M, Fuller M, Bancroft GM, Fyfe K, Tan KH. Application of soft X-ray absorption spectroscopy in chemical characterization of antiwear films generated by ZDDP Part I: the effects of physical parameters. Wear. 1997;202(2):172-91.
42. Minfray JMMTOC. Antiwear mechanisms of zinc dithiophosphate: a chemical hardness approach. Tribology Letters. 1999;6(1):1-8.
43. Taylor L, Spikes H. Friction-enhancing properties of ZDDP antiwear additive: part I—friction and morphology of ZDDP reaction films. Tribology transactions. 2003;46(3):303-9.
44. Taylor LJ, Spikes HA. Friction-enhancing properties of ZDDP antiwear additive: part II—influence of ZDDP reaction films on EHD lubrication. Tribology transactions. 2003;46(3):310-4.
45. S. Bec AT, J. M. Georges, R. C. Coy, J. C. Bell and G. W. Roper. Relationship between mechanical properties and structures of zinc dithiophosphate anti-wear films. Proceedings of the Royal Society A: Mathematical, Physical and Engineering Science. 1999;445(1992):4181-203.
46. Gabi Nehme RM, Pranesh B. Aswath,. Effect of contact load and lubricant volume on the properties of tribofilms formed under boundary lubrication in a fully formulated oil under extreme load conditions. Wear. 2010;268(9):1129-47.
47. M.A. Nicholls PRN, G.M. Bancroft, M. Kasrai, T. Dob, B.H. Frazerc and G. De Stasio. Nanometer scale chemomechanical characterization of antiwear films. Tribology Letters. 2004;17(2):205-16.
48. Nicholls MA, Do T, Norton PR, Kasrai M, Bancroft GM. Review of the lubrication of metallic surfaces by zinc dialkyl-dithiophosphates. Tribology international. 2005;38(1):15-39.
49. G. Pereira AL, M.A. Nicholls, M. Kasrai, P.R. Norton, and G. De Stasio. Chemical characterization and nanomechanical properties of antiwear films fabricated from ZDDP on a near hypereutectic Al–Si alloy. Tribology Letters. 2005;18(4):411-27.
50. Ramoun Mourhatch PA. Tribological behavior and nature of tribofilms generated from fluorinated ZDDP in comparison to ZDDP under extreme pressure conditions—Part II: Morphology and nanoscale properties of tribofilms. tribology international. 2011;44(3):201-10.
51. N.J. Mosey TKW, M. Kasrai, P.R. Norton, G.M. Bancroft and M.H. Muser. Interpretation of experiments on ZDDP anti-wear films through pressure-induced cross-linking. Tribology Letters. 2006;24(2):105-14.
52. Demmou K, Bec S, Loubet J-L, Martin J-M. Temperature effects on mechanical properties of zinc dithiophosphate tribofilms. Tribology international. 2006;39(12):1558-63.
53. Martin JM, Grossiord C, Le Mogne T, Bec S, Tonck A. The two-layer structure of Zndtp tribofilms: Part I: AES, XPS and XANES analyses. Tribology international. 2001;34(8):523-30.
54. Crobu M, Rossi A, Mangolini F, Spencer ND. Tribochemistry of bulk zinc metaphosphate glasses. Tribology letters. 2010;39(2):121-34.
55. J.F. Graham CMaPRN. Topography and nanomechanical properties of tribochemical films derived from zinc dialkyl and diaryl dithiophosphates. Tribology Letters. 1999;6(3-4):149-57.

56. Bosman R, Schipper DJ. Running-in of systems protected by additive-rich oils. Tribology Letters. 2011;41(1):263-82.
57. Naveira-Suarez A, Tomala A, Pasaribu R, Larsson R, Gebeshuber IC. Evolution of ZDDP-derived reaction layer morphology with rubbing time. Scanning. 2010;32(5):294-303.
58. Gunsel S, Spikes HA, Aderin M. In-Situ Measurement of ZDDP Films in Concentrated Contacts. Tribology transactions. 1993 1993/01/01;36(2):276-82.
59. Z. Zhang ESY, M. Kasrai and G.M. Bancrofta. Tribofilms generated from ZDDP and DDP on steel surfaces: Part 1, growth, wear and morphology. Tribology Letters. 2005;19(3):211-20.
60. Gosvami N, Bares J, Mangolini F, Konicek A, Yablon D, Carpick R. Mechanisms of antiwear tribofilm growth revealed in situ by single-asperity sliding contacts. Science. 2015;348(6230):102-6.
61. H. FUJITA HAS. Study of Zinc Dialkyldithiophosphate Antiwear Film Formation and Removal Processes, Part II: Kinetic Model. Tribology transactions. 2007;48(4):567-75.
62. M L S Fuller MK, G. Michael Bancroft, Kim Fyfe and Kim H. Tan. Solution decomposition of zinc dialkyl dithiophosphate and its effect on antiwear and thermal film formation studied by X-ray absorption spectroscopy. Tribology international. 1998;31(10):627-44.
63. Clotilde Minfray TLM, Jean-Michel Martin, Tasuku Onodera, Sayaka Nara, Shuko Takahashi, Hideyuki Tsuboi, Michihisa Koyama, Akira Endou, Hiromitsu Takaba, Momoji Kubo, Carlos A. Del Carpio, Akira Miyamoto. Experimental and Molecular Dynamics Simulations of Tribochemical Reactions with ZDDP: Zinc Phosphate–Iron Oxide Reaction. Tribology transactions. 2008;51(5):589-601.
64. Lin Y, So H. Limitations on use of ZDDP as an antiwear additive in boundary lubrication. Tribology international. 2004;37(1):25-33.
65. Nicholls MA, Norton PR, Bancroft GM, Kasrai M. X-ray absorption spectroscopy of tribofilms produced from zinc dialkyl dithiophosphates on Al–Si alloys. Wear. 2004;257(3):311-28.
66. Xia X, Morina A, Neville A, Priest M, Roshan R, Warrens C, et al. Tribological performance of an Al—Si alloy lubricated in the boundary regime with zinc dialkyldithiophosphate and molybdenum dithiocarbamate additives. Proceedings of the Institution of Mechanical Engineers, Part J: Journal of Engineering Tribology. 2008;222(3):305-14.
67. Pereira G, Lachenwitzer A, Kasrai M, Norton PR, Capehart TW, Perry TA, et al. A multi-technique characterization of ZDDP antiwear films formed on Al (Si) alloy (A383) under various conditions. Tribology Letters. 2007;26(2):103-17.
68. Vengudusamy B, Green JH, Lamb GD, Spikes HA. Tribological properties of tribofilms formed from ZDDP in DLC/DLC and DLC/steel contacts. Tribology International. 2011;44(2):165-74.
69. Haque T, Morina A, Neville A, Kapadia R, Arrowsmith S. Study of the ZDDP antiwear tribofilm formed on the DLC coating using AFM and XPS techniques. J ASTM Int. 2007;4(7):1-7.

70. de Barros' Bouchet M, Martin J, Le-Mogne T, Vacher B. Boundary lubrication mechanisms of carbon coatings by MoDTC and ZDDP additives. Tribology International. 2005;38(3):257-64.
71. Vengudusamy B, Green JH, Lamb GD, Spikes HA. Influence of hydrogen and tungsten concentration on the tribological properties of DLC/DLC contacts with ZDDP. Wear. 2013;298:109-19.
72. Vengudusamy B, Green JH, Lamb GD, Spikes HA. Durability of ZDDP tribofilms formed in DLC/DLC contacts. Tribology Letters. 2013;51(3):469-78.
73. Kosarieh S, Morina A, Lainé E, Flemming J, Neville A. Tribological performance and tribochemical processes in a DLC/steel system when lubricated in a fully formulated oil and base oil. Surface and Coatings Technology. 2013;217:1-12.
74. Minfray C, Martin J, De Barros M, Le Mogne T, Kersting R, Hagenhoff B. Chemistry of ZDDP tribofilm by ToF-SIMS. Tribology Letters. 2004;17(3):351-7.
75. Morina A, Neville A, Priest M, Green J. ZDDP and MoDTC interactions in boundary lubrication—the effect of temperature and ZDDP/MoDTC ratio. Tribology international. 2006;39(12):1545-57.
76. Sullivan JL. Boundary lubrication and oxidational wear. Journal of Physics D: Applied Physics. 1986;19(10):1999.
77. Stolarski TA. A System for Wear Prediction in Lubricated Sliding Contacts. Lubrication Science. 1996;8(4):315-51.
78. Williamson JAGaJBP. Contact of Nominally Flat Surfaces. Proceedings of the Royal Society of London A Mathematical and Physical Sciences. 1966;295(1442).
79. H. Zhang LC. A Micro-Contact Model for Boundary Lubrication With Lubricant/Surface Physiochemistry. Journal of tribology. 2003;125(1):8-15.
80. V. Hegadekatte J. Hilgertb OKNH. Multi time scale simulations for wear prediction in micro-gears. Wear. 2010;268(1):316-24.
81. Dong Y, Li Q, Martini A. Molecular dynamics simulation of atomic friction: A review and guide. Journal of Vacuum Science & Technology A: Vacuum, Surfaces, and Films. 2013;31(3):030801--24.
82. Li Q, Dong Y, Perez D, Martini A, Carpick RW. Speed dependence of atomic stick-slip friction in optimally matched experiments and molecular dynamics simulations. Physical review letters. 2011;106(12):126101.
83. Harrison J, White C, Colton R, Brenner D. Molecular-dynamics simulations of atomic-scale friction of diamond surfaces. Physical Review B. 1992;46(15):9700.
84. Zhu P-z, Hu Y-z, Ma T-b, Wang H. Molecular dynamics study on friction due to ploughing and adhesion in nanometric scratching process. Tribology Letters. 2011;41(1):41-6.
85. Solar M, Meyer H, Gauthier C, Benzerara O, Schirrer R, Baschnagel J. Molecular dynamics simulations of the scratch test on linear amorphous polymer surfaces: A study of the local friction coefficient. Wear. 2011;271(11):2751-8.
86. Berro H, Fillot N, Vergne P. Molecular dynamics simulation of surface energy and ZDDP effects on friction in nano-scale lubricated contacts. Tribology international. 2010;43(10):1811-22.

87. Lin E-Q, Niu L-S, Shi H-J, Duan Z. Molecular dynamics simulation of nano-scale interfacial friction characteristic for different tribopair systems. Applied Surface Science. 2012;258(6):2022-8.
88. Gao H, Stone D, Mohseni H, Aouadi S, Scharf T, Martini A. Mechanistic studies of high temperature friction reduction in silver tantalate. Applied Physics Letters. 2013;102(12):121603.
89. Bai S, Onodera T, Nagumo R, Miura R, Suzuki A, Tsuboi H, et al. Friction Reduction Mechanism of Hydrogen-and Fluorine-Terminated Diamond-Like Carbon Films Investigated by Molecular Dynamics and Quantum Chemical Calculation. The Journal of Physical Chemistry C. 2012;116(23):12559-65.
90. Landman U, Luedtke WD, Ringer EM. Atomistic mechanisms of adhesive contact formation and interfacial processes. Wear. 1992;153(1):3-30.
91. Zheng X, Zhu H, Kosasih B, Kiet Tieu A. A molecular dynamics simulation of boundary lubrication: The effect of n-alkanes chain length and normal load. Wear. 2013;301(1):62-9.
92. Onodera T, Morita Y, Suzuki A, Koyama M, Tsuboi H, Hatakeyama N, et al. A computational chemistry study on friction of h-MoS2. Part I. Mechanism of single sheet lubrication. The Journal of Physical Chemistry B. 2009;113(52):16526-36.
93. Heyes D, Smith E, Dini D, Spikes H, Zaki T. Pressure dependence of confined liquid behavior subjected to boundary-driven shear. The Journal of chemical physics. 2012;136(13):134705.
94. Solar M, Meyer H, Gauthier C, Benzerara O, Pelletier H, Schirrer R, et al. Molecular dynamics simulations as a way to investigate the local physics of contact mechanics: a comparison between experimental data and numerical results. Journal of Physics D: Applied Physics. 2010;43(45):455406.
95. Zheng X, Zhu H, Kiet Tieu A, Kosasih B. A molecular dynamics simulation of 3D rough lubricated contact. Tribology international. 2013;67:217-21.
96. Anciaux G, Molinari JF. Contact mechanics at the nanoscale, a 3D multiscale approach. International journal for numerical methods in engineering. 2009;79(9):1041-67.
97. Yang C, Tartaglino U, Persson B. A multiscale molecular dynamics approach to contact mechanics. The European Physical Journal E. 2006;19(1):47-58.
98. Medina S, Dini D. A numerical model for the deterministic analysis of adhesive rough contacts down to the nano-scale. International Journal of Solids and Structures. 2014;51(14):2620-32.
99. Onodera T, Martin JM, Minfray C, Dassenoy F, Miyamoto A. Antiwear chemistry of ZDDP: coupling classical MD and tight-binding quantum chemical MD methods (TB-QCMD). Tribology Letters. 2012:1-9.
100. Onodera T, Morita Y, Suzuki A, Sahnoun R, Koyama M, Tsuboi H, et al. A theoretical investigation on the abrasive wear prevention mechanism of ZDDP and ZP tribofilms. Applied Surface Science. 2008;254(23):7976-9.
101. Martin JM, Onodera T, Bouchet M-IDB, Hatakeyama N, Miyamoto A. Anti-wear Chemistry of ZDDP and Calcium Borate Nano-additive. Coupling

Experiments, Chemical Hardness Predictions, and MD Calculations. Tribology Letters.1-10.
102. Martin JM, Onodera T, Minfray C, Dassenoy F, Miyamoto A. The origin of anti-wear chemistry of ZDDP. Faraday Discussions. 2012.
103. Yue D-C, Ma T-B, Hu Y-Z, Yeon J, van Duin AC, Wang H, et al. Tribochemistry of Phosphoric Acid Sheared between Quartz Surfaces: A Reactive Molecular Dynamics Study. The Journal of Physical Chemistry C. 2013;117(48):25604-14.
104. Hayashi K, Tezuka K, Ozawa N, Shimazaki T, Adachi K, Kubo M. Tribochemical reaction dynamics simulation of hydrogen on a diamond-like carbon surface based on tight-binding quantum chemical molecular dynamics. The Journal of Physical Chemistry C. 2011;115(46):22981-6.
105. Salib J, Kligerman Y, Etsion I. A model for potential adhesive wear particle at sliding inception of a spherical contact. Tribology Letters. 2008;30(3):225-33.
106. Aghdam A, Khonsari M. On the correlation between wear and entropy in dry sliding contact. Wear. 2011;270(11):781-90.
107. Jourdan F. A numerical model of wear taking account of multidirectional effects. Modélisation du contact et de l'usure. 2013.
108. McColl I, Ding J, Leen S. Finite element simulation and experimental validation of fretting wear. Wear. 2004;256(11):1114-27.
109. Priit Podra SA. Simulating sliding wear with finite element method. Tribology international. 1999;32(2):71-81.
110. Pei L, Hyun S, Molinari JF, Robbins MO. Finite element modeling of elasto-plastic contact between rough surfaces. Journal of the Mechanics and Physics of Solids. 2005;53(11):2385-409.
111. Molinari J, Ortiz M, Radovitzky R, Repetto E. Finite-element modeling of dry sliding wear in metals. Engineering Computations. 2001;18(3/4):592-610.
112. Kim NH, Won D, Burris D, Holtkamp B, Gessel GR, Swanson P, et al. Finite element analysis and experiments of metal/metal wear in oscillatory contacts. Wear. 2005;258(11):1787-93.
113. E.M. Bortoleto ACR, V.Seriacopi,F.J.Profito,D.C.Zachariadis,I.F.Machado,, A. Sinatora RMS. Experimental and numerical analysis of dry contact in the pin on disc test. Wear. 2012;301(1):19-26.
114. V Hegadekatte NHaOK. Finite element based simulation of dry sliding wear. modelling and simulation in materials science and engineering. 2005;13(1):57.
115. V. Hegadekatte S. Kurzenha NH, O. Kraft. A predictive modeling scheme for wear in tribometers. Tribology international. 2008;41(11):1020-31.
116. Öqvist M. Numerical simulations of mild wear using updated geometry with different step size approaches. wear. 2001;249(1):6-11.
117. Ghanbarzadeh A, Wilson M, Morina A, Dowson D, Neville A. Development of a New Mechano-Chemical Model in Boundary Lubrication. Tribology International. 2016;93:573-82.
118. Cundall PA, Strack ODL. A discrete numerical model for granular assemblies. Géotechnique. 1979;29(1):47-65.

119. Zhu H, Zhou Z, Yang R, Yu A. Discrete particle simulation of particulate systems: theoretical developments. Chemical Engineering Science. 2007;62(13):3378-96.
120. Zhu H, Zhou Z, Yang R, Yu A. Discrete particle simulation of particulate systems: A review of major applications and findings. Chemical Engineering Science. 2008;63(23):5728-70.
121. Jerier J, Molinari J. Normal contact between rough surfaces by the Discrete Element Method. Tribology international. 2012;47:1-8.
122. Iliescu D, Gehin D, Iordanoff I, Girot F, Gutiérrez M. A discrete element method for the simulation of CFRP cutting. Composites Science and Technology. 2010;70(1):73-80.
123. Tan Y, Yang D, Sheng Y. Discrete element method (DEM) modeling of fracture and damage in the machining process of polycrystalline SiC. Journal of the European Ceramic Society. 2009;29(6):1029-37.
124. Brown NJ. Discrete element modelling of cementitious materials 2013.
125. Rojek J, Oñate E, Labra C, Kargl H. Discrete element simulation of rock cutting. International journal of rock mechanics and mining sciences. 2011;48(6):996-1010.
126. Raje N, Sadeghi F, Rateick RG, Hoeprich MR. Evaluation of stresses around inclusions in hertzian contacts using the discrete element method. Journal of tribology. 2007;129(2):283-91.
127. Huang H, Detournay E. Intrinsic Length Scales in Tool-Rock Interaction 1. International Journal of Geomechanics. 2008;8(1):39-44.
128. Fillot N, Iordanoff I, Berthier Y, editors. Simulation of wear through mass balance in a dry contact. ASME/STLE 2004 International Joint Tribology Conference; 2004: American Society of Mechanical Engineers.
129. Obermayr M, Dressler K, Vrettos C, Eberhard P. A bonded-particle model for cemented sand. Computers and Geotechnics. 2013;49:299-313.
130. Potyondy D, Cundall P. A bonded-particle model for rock. International journal of rock mechanics and mining sciences. 2004;41(8):1329-64.
131. Le Bouteiller C, Naaïm M, editors. Dynamic Breakage of Agglomerates under Normal Impact and Tangential Friction. POWDERS AND GRAINS 2009: PROCEEDINGS OF THE 6TH INTERNATIONAL CONFERENCE ON MICROMECHANICS OF GRANULAR MEDIA; 2009: AIP Publishing.
132. Wang Y, Mora P. Macroscopic elastic properties of regular lattices. Journal of the Mechanics and Physics of Solids. 2008;56(12):3459-74.
133. Jerier J-F, Richefeu V, Imbault D, Donzé F-V. Packing spherical discrete elements for large scale simulations. Computer Methods in Applied Mechanics and Engineering. 2010;199(25):1668-76.
134. Rousseau J, Frangin E, Marin P, Daudeville L. Damage prediction in the vicinity of an impact on a concrete structure: a combined FEM/DEM approach. Computers and Concrete. 2008;5(4):343-58.
135. G.K. Sfantos MHA. Application of BEM and optimization technique to wear problems. International journal of solids and structures. 2006;43(11):3626-42.
136. G.K. Sfantos MHA. Wear simulation using an incremental sliding Boundary Element Method. Wear. 2006;260(9):1119-28.

137. Sfantos G, Aliabadi M. Application of BEM and optimization technique to wear problems. International journal of solids and structures. 2006;43(11):3626-42.
138. Sfantos G, Aliabadi M. A boundary element formulation for three-dimensional sliding wear simulation. Wear. 2007;262(5):672-83.
139. J. Andersson AA, R. Larsson. Numerical simulation of a wear experiment. Wear. 2011;271(11):2947-52.
140. A. Almqvist FS, R. Larsson, S. Glavatskih. On the dry elasto-plastic contact of nominally flat surfaces. Tribology international. 2007;40(4):574-9.
141. F Sahlin RL, A Almqvist, P M Lugt and P Marklund. A mixed lubrication model incorporating measured surface topography. Part 1: theory of flow factors. Proceedings of the Institution of Mechanical Engineers, Part J: Journal of Engineering Tribology. 2009;224(4):335-51.
142. Polonsky I, Keer L. A numerical method for solving rough contact problems based on the multi-level multi-summation and conjugate gradient techniques. Wear. 1999;231(2):206-19.
143. Webster M, Sayles R. A numerical model for the elastic frictionless contact of real rough surfaces. Journal of tribology. 1986;108(3):314-20.
144. Karpenko YA, Akay A. A numerical model of friction between rough surfaces. Tribology international. 2001;34(8):531-45.
145. Xuefeng Tian BB. A Numerical Three-Dimensional Model for the Contact of Rough Surfaces by Variational Principle. 1996.
146. Liu G, Zhu J, Yu L, Wang QJ. Elasto-Plastic Contact of Rough Surfaces. Tribology transactions. 2001 2001/01/01;44(3):437-43.
147. Liu S, Wang Q. A three-dimensional thermomechanical model of contact between non-conforming rough surfaces. Journal of tribology. 2001;123(1):17-26.
148. Liu S, Wang Q, Liu G. A versatile method of discrete convolution and FFT (DC-FFT) for contact analyses. Wear. 2000;243(1–2):101-11.
149. Man K, Aliabadi M, Rooke D. BEM frictional contact analysis: load incremental technique. Computers & structures. 1993;47(6):893-905.
150. Lai W, Cheng H. Computer simulation of elastic rough contacts. ASLE transactions. 1985;28(2):172-80.
151. Bhushan B. Contact mechanics of rough surfaces in tribology: multiple asperity contact. Tribology Letters. 1998;4(1):1-35.
152. Bhushan B. Contact mechanics of rough surfaces in tribology: single asperity contact. Applied mechanics reviews. 1996;49:275.
153. Yu MM-H, Bhushan B. Contact analysis of three-dimensional rough surfaces under frictionless and frictional contact. Wear. 1996;200(1-2):265-80.
154. Poon C, Sayles R. Numerical contact model of a smooth ball on an anisotropic rough surface. Journal of tribology. 1994;116(2):194-201.
155. Ren N, Lee SC. Contact simulation of three-dimensional rough surfaces using moving grid method. Journal of tribology. 1993;115(4):597-601.
156. Ilincic S, Vorlaufer G, Fotiu P, Vernes A, Franek F. Combined finite element-boundary element method modelling of elastic multi-asperity contacts. Proceedings of the Institution of Mechanical Engineers, Part J: Journal of Engineering Tribology. 2009;223(5):767-76.

157. Ilincic S, Vernes A, Vorlaufer G, Hunger H, Dörr N, Franek F. Numerical estimation of wear in reciprocating tribological experiments. Proceedings of the Institution of Mechanical Engineers, Part J: Journal of Engineering Tribology. 2013;227(5):510-9.
158. Medina S, Olver AV, Dini D. The influence of surface topography on energy dissipation and compliance in tangentially loaded elastic contacts. Journal of Tribology. 2012;134(1):011401.
159. Ilincic S, Tungkunagorn N, Vernes A, Vorlaufer G, Fotiu P, Franek F. Finite and boundary element method contact mechanics on rough, artificial hip joints. Proceedings of the Institution of Mechanical Engineers, Part J: Journal of Engineering Tribology. 2011;225(11):1081-91.
160. Tonder YZHaK. Simulation of 3-D random rough surface by 2-D digital filter and Fourier analysis. International journal of machine tools and manufacture. 1992;32(1):83-90.
161. Nayak PR. Random process model of rough surfaces. Journal of Lubrication Technology. 1971;93(3):398-407.
162. Thompson M, Thompson J, editors. Methods for generating probabilistic rough surfaces in ANSYS. Proceedings of the 20th Korea ANSYS User's Conference, Gyeongju, South Korea; 2010.
163. Thompson MKTaJM. Methods for Generating Probabilistic Rough Surfaces in ANSYS. proceedings of the 20th korea ANSYS user's conference 2010.
164. Thompson MK. Geometric Primitive Surface Roughness in Finite Element Models.
165. Wu J-J. Simulation of rough surfaces with FFT. Tribology international. 2000;33(1):47-58.
166. Hertz H. On the contact of elastic solids. J reine angew Math. 1881;92(156-171):110.
167. Williamson J, editor Paper 17: Microtopography of Surfaces. Proceedings of the Institution of Mechanical Engineers, Conference Proceedings; 1967: SAGE Publications.
168. Francis H. The accuracy of plane strain models for the elastic contact of three-dimensional rough surfaces. Wear. 1983;85(2):239-56.
169. Conry TF, Seireg A. A mathematical programming method for design of elastic bodies in contact. Journal of Applied Mechanics. 1971;38:387.
170. Kalker J, Van Randen Y. A minimum principle for frictionless elastic contact with application to non-Hertzian half-space contact problems. Journal of engineering mathematics. 1972;6(2):193-206.
171. Richards TH. Energy Methods in Stress Analysis: with an introduction to finite element techniques: Ellis Horwood; 1977.
172. Timoshenko SP, Gere JM. Theory of elastic stability: Tata McGraw-Hill Education; 1961.
173. K.L.Johnson. Contact Mechanics.
174. Andersson J. Modelling of wear and tribofilm growth. 2012.
175. Love AEH. A treatise on the mathematical theory of elasticity: Cambridge University Press; 2013.
176. Joel F. Semi-deterministic numerical simulations of wear on various scales : From chemo-mechanical effects to the wear of components in orbital type hydraulic motors: Lulea University of technology; 2014.

177. H. M. Stanley TK. An FFT-Based Method for Rough Surface Contact. Journal of tribology. 1997;119(3):481-5.
178. Liu S, Hua D, Chen WW, Wang QJ. Tribological modeling: application of fast Fourier transform. Tribology international. 2007;40(8):1284-93.
179. Kennedy F. Frictional heating and contact temperatures. Modern tribology handbook. 2001;1:235-59.
180. Blok H. The flash temperature concept. Wear. 1963;6(6):483-94.
181. Carslaw H, Jaeger J. Heat in solids: Clarendon Press, Oxford; 1959.
182. Archard J. The temperature of rubbing surfaces. wear. 1959;2(6):438-55.
183. Kuhlmann-Wilsdorf D. Temperatures at interfacial contact spots: dependence on velocity and on role reversal of two materials in sliding contact. Journal of tribology. 1987;109(2):321-9.
184. Greenwood J. An interpolation formula for flash temperatures. Wear. 1991;150(1):153-8.
185. Tian X, Kennedy FE. Maximum and average flash temperatures in sliding contacts. Journal of Tribology. 1994;116(1):167-74.
186. Bos J, Moes H. Frictional heating of tribological contacts. Journal of tribology. 1995;117(1):171-7.
187. Meng H-C. Wear modeling: evaluation and categorization of wear models. 1994.
188. Meng H, Ludema K. Wear models and predictive equations: their form and content. Wear. 1995;181:443-57.
189. Ashby M, Lim S. Wear-mechanism maps. Scripta Metallurgica et Materialia. 1990;24(5):805-10.
190. Rabinowicz E. Friction and wear of materials. 1965.
191. MacGinley T, Monaghan J. Modelling the orthogonal machining process using coated cemented carbide cutting tools. Journal of materials processing technology. 2001;118(1):293-300.
192. Maxian TA, Brown TD, Pedersen DR, Callaghan JJ. 3-Dimensional sliding/contact computational simulation of total hip wear. Clinical orthopaedics and related research. 1996;333:41-50.
193. Yen Y-C, Söhner J, Lilly B, Altan T. Estimation of tool wear in orthogonal cutting using the finite element analysis. Journal of Materials Processing Technology. 2004;146(1):82-91.
194. Spikes H, Cann P. The development and application of the spacer layer imaging method for measuring lubricant film thickness. Proceedings of the Institution of Mechanical Engineers, Part J: Journal of Engineering Tribology. 2001;215(3):261-77.
195. Ji H, Nicholls MA, Norton PR, Kasrai M, Capehart TW, Perry TA, et al. Zinc-dialkyl-dithiophosphate antiwear films: dependence on contact pressure and sliding speed. Wear. 2005;258(5):789-99.
196. H.Fujita HAS. Study of Zinc Dialkyldithiophosphate Antiwear Film Formation and Removal Processes, Part II: Kinetic Model. Tribology transactions. 2005;48:567-75.
197. H. So YCL. The theory of antiwear for ZDDP at elevated temperature in boundary lubrication condition. Wear. 1994;177(2):105-15.
198. Crank J. The mathematics of diffusion: Oxford university press; 1979.

199. Mortazavi V, Nosonovsky M. Friction-Induced Pattern Formation and Turing Systems. Langmuir. 2011;27(8):4772-9.
200. Fox-Rabinovich GS, Gershman IS, Yamamoto K, Biksa A, Veldhuis SC, Beake BD, et al. Self-organization during friction in complex surface engineered tribosystems. Entropy. 2010;12(2):275-88.
201. Gershman IS, Bushe N. Elements of Thermodynamics of Self-Organization during Friction. Self-Organization during Friction Advanced Surface-Engineered Materials and Systems Design. 2006:13-58.
202. Nosonovsky M. Entropy in tribology: in the search for applications. Entropy. 2010;12(6):1345-90.
203. Prigogine I. Introduction to thermodynamics of irreversible processes. New York: Interscience, 1967, 3rd ed. 1967;1.
204. Kuzharov A, Bulgarevich S, Burlakova V, Kuzharov A, Akimova E. Molecular mechanisms of self-organization at friction. Part VI. Analysis of thermodynamic features of tribochemical reactions. Journal of Friction and Wear. 2007;28(2):218-23.
205. Bulgarevich S, Boiko M, Kolesnikov V, Feizova V. Thermodynamic and kinetic analyses of probable chemical reactions in the tribocontact zone and the effect of heavy pressure on evolution of adsorption processes. Journal of Friction and Wear. 2011;32(4):301-9.
206. Bulgarevich S, Boiko M, Kolesnikov V, Korets K. Population of transition states of triboactivated chemical processes. Journal of Friction and Wear. 2010;31(4):288-93.
207. b RATaWB. A Model for Asperity Load Sharing in Lubricated Contacts. ASLE transactions. 1972;15(1):67-79.
208. Borri-Brunetto M, Chiaia B, Ciavarella M. Incipient sliding of rough surfaces in contact: a multiscale numerical analysis. Computer Methods in Applied Mechanics and Engineering. 2001;190(46–47):6053-73.
209. Sellgren U, Björklund S, Andersson S. A finite element-based model of normal contact between rough surfaces. Wear. 2003;254(11):1180-8.
210. Persson BN. Contact mechanics for randomly rough surfaces. Surface Science Reports. 2006;61(4):201-27.
211. Willner K. Fully coupled frictional contact using elastic halfspace theory. Journal of Tribology. 2008;130(3):031405.
212. Mirwais Aktary MTMaGAM. Morphology and nanomechanical properties of ZDDP antiwear films as a function of tribological contact time. Tribology Letters. 2002;12(3):155-62.
213. Bosman R, de Rooij M. Transient thermal effects and heat partition in sliding contacts. Journal of Tribology. 2010;132(2):021401.
214. Bulgarevich S, Boiko M, Tarasova E, Feizova V, Lebedinskii K. Kinetics of mechanoactivation of tribochemical processes. Journal of Friction and Wear. 2012;33(5):345-53.
215. Bennett PA. A surface effect associated with the use of oils containing zinc dialkyl dithiophosphate. ASLE Transactions. 1959;2(1):78-90.
216. Haque T, Morina A, Neville A. Influence of friction modifier and antiwear additives on the tribological performance of a non-hydrogenated DLC coating. Surface and Coatings Technology. 2010;204(24):4001-11.

217. Haque T, Morina A, Neville A, Kapadia R, Arrowsmith S. Effect of oil additives on the durability of hydrogenated DLC coating under boundary lubrication conditions. Wear. 2009;266(1):147-57.
218. Haque T, Morina A, Neville A, Kapadia R, Arrowsmith S. Non-ferrous coating/lubricant interactions in tribological contacts: assessment of tribofilms. Tribology International. 2007;40(10):1603-12.
219. Rounds F. Effects of hydroperoxides on wear as measured in four-ball wear tests. Tribology transactions. 1993;36(2):297-303.
220. McQueen J, Gao H, Black E, Gangopadhyay A, Jensen R. Friction and wear of tribofilms formed by zinc dialkyl dithiophosphate antiwear additive in low viscosity engine oils. Tribology international. 2005;38(3):289-97.
221. Ghanbarzadeh A, Parsaeian P, Morina A, Wilson MC, van Eijk MC, Nedelcu I, et al. A Semi-deterministic Wear Model Considering the Effect of Zinc Dialkyl Dithiophosphate Tribofilm. Tribology Letters. 2016;61(1):1-15.
222. Blau PJ. Running-in: Art or engineering? Journal of materials engineering. 1991;13(1):47-53.
223. Atala H, Rowe G. Surface roughness changes during rolling. Wear. 1975;32(2):249-68.
224. Masouros G, Dimarogonas A, Lefas K. A model for wear and surface roughness transients during the running-in of bearings. Wear. 1977;45(3):375-82.
225. Dong W, Stout K. An integrated approach to the characterization of surface wear i: Qualitative characterization. Wear. 1995;181:700-16.
226. Jeng YR, Lin ZW, Shyu SH. Changes of surface topography during running-in process. Journal of tribology. 2004;126(3):620-5.
227. Chou C, Lin J. Tribological effects of roughness and running-in on oil-lubricated line contacts. Proceedings of the Institution of Mechanical Engineers, Part J: Journal of Engineering Tribology. 1997;211(3):209-22.
228. Tyagi MR, Sethuramiah A. Asperity level conformity in partial EHL. Part I: Its characterization. Wear. 1996;1(197):89-97.
229. Sreenath A, Raman N. Mechanism of smoothing of cylinder liner surface during running-in. TRIBOLOGY international. 1976;9(2):55-62.
230. Sreenath A, Raman N. Running-in wear of a compression ignition engine: factors influencing the conformance between cylinder liner and piston rings. Wear. 1976;38(2):271-89.
231. Neale MJ. The tribology handbook: Butterworth-Heinemann; 1995.
232. Goepfert O, Ampuero J, Pahud P, Boving H. Surface roughness evolution of ball bearing components. Tribology transactions. 2000;43(2):275-80.
233. Tripp J, Ioannides E, editors. Effects of surface roughness on rolling bearing life. Japan International Tribology Conference II; 1990.
234. Nélias D, Dumont M, Champiot F, Vincent A, Girodin D, Fougeres R, et al. Role of inclusions, surface roughness and operating conditions on rolling contact fatigue. Journal of tribology. 1999;121(2):240-51.
235. Suh NP. An overview of the delamination theory of wear. Wear. 1977;44(1):1-16.
236. Stachowiak G, Stachowiak G. The effects of particle characteristics on three-body abrasive wear. Wear. 2001;249(3):201-7.

237. Dwyer-Joyce R. Predicting the abrasive wear of ball bearings by lubricant debris. Wear. 1999;233:692-701.
238. Dwyer-Joyce R, Sayles R, Ioannides E. An investigation into the mechanisms of closed three-body abrasive wear. Wear. 1994;175(1):133-42.
239. Godet M. The third-body approach: a mechanical view of wear. Wear. 1984;100(1):437-52.
240. Rabinowicz E, Dunn L, Russell P. A study of abrasive wear under three-body conditions. Wear. 1961;4(5):345-55.
241. Williams J, Hyncica A. Mechanisms of abrasive wear in lubricated contacts. Wear. 1992;152(1):57-74.
242. Olofsson UA, Sören Björklund, Stefan. Simulation of mild wear in boundary lubricated spherical roller thrust bearings. Wear. 2000;241(2):180-5.
243. Olofsson U, Dizdar S. Surface analysis of boundary-lubricated spherical roller thrust bearings. Wear. 1998;215(1):156-64.
244. Ulf Olofsson SrA, Stefan Bjorklund. Simulation of mild wear in boundary lubricated spherical roller thrust bearings. Wear. 2000;241(2):180-5.
245. Flodin A. Wear of spur and helical gears. Royal Institute of Technology, Stockholm, Doctoral Thesis. 2000.
246. Andersson S, Olofsson U, editors. Towards a general model for wear simulation. IRG-OECD Meeting, Uppsala, Sweden; 2005.
247. Andersson S, Söderberg A, Olofsson U. A random wear model for the interaction between a rough and a smooth surface. Wear. 2008;264(9):763-9.
248. Rossi A, Piras F, Kim D, Gellman A, Spencer N. Surface reactivity of tributyl thiophosphate: effects of temperature and mechanical stress. Tribology Letters. 2006;23(3):197-208.
249. De Donato P, Mustin C, Benoit R, Erre R. Spatial distribution of iron and sulphur species on the surface of pyrite. Applied Surface Science. 1993;68(1):81-93.
250. Zerulla D, Mayer D, Hallmeier K, Chassé T. Angular-resolved XANES measurements of the polar and azimuthal orientation of alkanethiols on InP (110). Chemical physics letters. 1999;311(1):8-12.
251. Heuberger RC. Combinatorial study of the tribochemistry of anti-wear lubricant additives: Diss., Eidgenössische Technische Hochschule ETH Zürich, Nr. 17207, 2007; 2007.
252. Brow RK, Tallant DR, Myers ST, Phifer CC. The short-range structure of zinc polyphosphate glass. Journal of Non-Crystalline Solids. 1995;191(1):45-55.
253. Fillot N, Iordanoff I, Berthier Y. Modelling third body flows with a discrete element method—a tool for understanding wear with adhesive particles. Tribology International. 2007;40(6):973-81.